The Performance of Soil Reinforcement in Bending and Shear

' by

Martin John Pedley

Thesis submitted for the
degree of Doctor of Philosophy
at the University of Oxford

Wolfson College   Michaelmas Term, 1990.

The Performance of Soil Reinforcement in Bending and Shear

Martin Pedley
Wolfson College, University of Oxford

A Thesis submitted for the Degree of Doctor of Philosophy.
Michaelmas Term, 1990.

ABSTRACT

Previous experimental studies of soil-reinforcement interaction have generally concentrated on the effect of reinforcement working in axial tension; this study looks at reinforcement working in bending and shear.

The experimental programme was carried out in a large scale direct shear apparatus able to contain a cubic soil sample of side $1m$. A previous study showed that the apparatus required improvements to its boundaries. Modifications to the apparatus resulted in a significant improvement in the performance of the apparatus. The data being comparable with those from direct shearboxes with similar symmetrical boundary conditions.

The effect of reinforcement in shear and bending was studied by varying the reinforcement cross section, reinforcement orientation, method of installation, and the relative soil-reinforcement stiffness and strength. All tests were carried out on a well graded and uniform quartz sand. The reinforcement was typically mild steel circular bar. Data from tests on instrumented reinforcement bars allowed the distribution of lateral loading to be observed. This led to the development of a mathematical model for predicting the shear force available from reinforcement in soil. A comparison of this model with the test data and from data in the literature revealed it to provide an accurate upper estimate of reinforcement shear force.

The overriding conclusion from this study, both experimental and theoretical, is that reinforcement used in shear is much less efficient than that used in axial tension, and that the displacements required to mobilise the available reinforcement shear force are much greater than those required for axial force. The conclusions in this dissertation address much of the ambiguity over the use of soil reinforcement in shear and bending for soil nailing and dowelling design.

CONTENTS

ACKNOWLEDGEMENTS

NOMENCLATURE

α, β	Angles as defined
δ	Reinforcement resultant displacement
δ_{ax}	Reinforcement axial displacement
δ_s	Reinforcement shear displacement
ε_{ax}	Reinforcement axial strain
ε_b	Reinforcement bending strain
ε_s	Reinforcement surface strain
ε_y	Reinforcement yield strain
$d\varepsilon_1$	Major principal strain increment
$d\varepsilon_3$	Minor principal strain increment
$d\varepsilon_{yy}$	Volumetric strain increment
γ_d	Unit weight of soil
γ_{yx}	Shear strain in x direction
$d\gamma_{yx}$	Shear increment strain in x direction
λ	Ratio of steel strength to grout strength in compression (σ_p / σ_{cu})
μ	Poisson's ratio
ψ	Dilation angle
ϕ'	Friction angle
ϕ'_{cv}	Critical state friction angle
ϕ'_{ds}	Direct shear friction angle
ϕ'_i	Interface friction angle
ϕ'_{ps}	Plane strain friction angle
ϕ'_{triax}	Triaxial strain friction angle
σ'_1	Major principal stress
σ'_2	Intermediate principal stress
σ'_3	Minor principal stress
σ'_b	Limiting bearing stress
σ'_l	Lateral stress on reinforcement
σ'_n	Normal stress governing bearing failure
σ'_r	Radial stress around reinforcement
σ'_v	Vertical stress
σ'_{yy}	Stress acting normal central plane of shearbox

σ'_{cu}	Grout cube strength
σ	Maximum reinforcement stress
σ_{ax}	Mean reinforcement axial stress
σ_{bend}	Maximum stress in reinforcement due to bending
σ_p	Reinforcement yield stress
(σ_p/σ'_b)	Strength ratio
τ	Shear stress
τ_{yx}	Shear stress parallel to central plane of shearbox
τ_{po}	Mean shear stress mobilised by pullout
θ	Reinforcement orientation
e	Voids ratio
h	Thickness of zone of simple shear
l_1, l_2	Lengths defining plastic reinforcement deformation
l_b	bearing length of reinforcement
l_o	Elastic transfer length
l_p	Pullout length
l_s	Shear width
(l_s/D)	Normalised shear width
m	Constant equal to critical state shearing resistance
m_e	Elastic portion of reinforcement bending moment
m_p	Plastic portion of reinforcement bending moment
p_n	Load in vertical loading jack n, $(n = 1, 2, 3, 4)$
p'	Mean stress
p_l	Menard limit pressure
p_f	Menard creep pressure
s'	Mean stress in plane strain
t'	Deviatoric stress in plane strain
t	Reinforcement thickness
y_n	Vertical displacement measured by LVDT $(n = 1, 2, 3, 4)$
x, y	Coordinate axes for shearbox
y	Distance from neutral axis to point of maximum stress in reinforcement cross section
y_p	Lever arm of plastically yielded area of cross section
z	Distance measured along reinforcement

A_{ax}	Area of reinforcement cross section yielding in axial tension
A_b	Area of reinforcement cross section yielding in bending
A_c	Circumferential area per unit length of reinforcement
A_e	Area of reinforcement cross section in elastic stress state
A_p	Area of reinforcement cross section in plastic stress state
A_r	Reinforcement cross sectional area
A_s	Plan area of shearbox
B	Laterally loaded width of reinforcement
C_u	Coefficient of uniformity
D	Reinforcement bar diameter
D_g	Grouted bar diameter
D_i	Tubular bar internal diameter
D_o	Menard pressuremeter reference diameter
D_{50}	Mean particle size
(E/K_sD)	Stiffness ratio
E	Young's modulus of reinforcement
E_m	Menard pressuremeter modulus
E_s	Elastic soil modulus
(G/p')	Shear modulus normalised by mean stress
G_s	Specific gravity
I	2nd moment of area of reinforcement
I'	2nd moment of area of reinforcement in elastic stress state
I_d	Relative density
K_a	Active earth pressure coefficient
K_o	At rest earth pressure coefficient
K_p	Passive earth pressure coefficient
K_s	Modulus of subgrade reaction
L	Reinforcement length
L_a	Anchorage length of reinforcement
M	Bending moment
M_e	Elastic yield moment
M_p	Fully plastic moment
M_R	Moment of resistance of grouted bar reinforcement
N_q	Bearing capacity factor

P_{ax}	Reinforcement axial force
(P_{ax}/P_p)	Normalised axial force
P_d	Pole for directions in Mohr's circle
P_{po}	Pullout force
P_p	Plastic reinforcement axial capacity
P_s	Reinforcement shear force
(P_s/P_p)	Normalised shear force
P_v	Vertical load applied to soil
Q	Mineralogy constant
S	Shear force applied to soil
ΔS	Additional soil strength attributed to reinforcement
W_{box}	Weight of top half of shearbox
W_{soil}	Weight of soil in top half of shearbox
X	Shear displacement in X direction
dX	Incremental displacement in X direction
X_i	Shear displacement when reinforcement installed
Y	Vertical displacement or dilation in Y direction
dY	Incremental displacement in Y direction
dY/dX	Dilation rate

Subscripts and Superscripts

axial	Axial interaction mechanism
bear	Bearing interaction mechanism
bm	From bending moment
def	From deformation
e	Elastic analysis
lim	Limiting value
max	Minimum value
min	Maximum value
mob	Mobilised
p	Plastic analysis
test	Test value

CHAPTER 1: INTRODUCTION

Many laboratory studies of soil-reinforcement interaction are reported in the literature, and the vast majority of these are concerned with the use of reinforcement in axial tension. The objective of the research reported in this dissertation was to study the effect of reinforcement in shear and bending and the relative importance of shear force to axial force in improving the shearing resistance of soil.

For the vast majority of reinforced soil structures the major reinforcement force is axial tension. However, for the specific techniques of soil nailing and soil dowelling there is still much confusion with respect to the forces leading to stability and their magnitudes. Indeed, for soil nailing there is a great deal of debate over the possible conservatism of ignoring the contribution of the reinforcement shear force. It is apparent therefore that research is required in this particular area in order that a general consensus may be reached on the magnitude of reinforcement shear force and when it is appropriate to consider it.

A concise review of the techniques of soil nailing and soil dowelling is presented in Chapter 2, where the mechanisms leading to soil stabilisation are outlined along with the various methods by which soil-reinforcement interaction may be investigated.

This study of soil-reinforcement interaction was carried out using a modified version of the Oxford University large direct shear apparatus, originally reported in Palmeira (1987). This apparatus allows reinforced soil samples of one cubic metre to be tested and is described fully in Chapter 3. The details of a smaller direct shear apparatus used in this experimental study are also described.

Chapters 4 and 5 are concerned with the analysis of unreinforced test data from the large direct shear apparatus. The data obtained are compared with those from a smaller shearbox in order to establish the effectiveness of the modifications carried out.

A description of reinforced tests to investigate reinforcement shear force is given in Chapter 6. Specific details of the reinforcement used in each test are presented along with both boundary and internal strain gauge data. The data are grouped into categories depending on sample density and the particular facet influencing the interaction between soil and reinforcement to be studied: reinforcement orientation, bending stiffness, soil strength and method of installation.

Chapter 7 is essentially a review of the existing theoretical analyses for determining reinforcement shear force and the parameters used in them. A mathematical model for determining the limiting reinforcement shear force is developed from the data presented in Chapter 6. An amended multi-criteria analysis defining the limiting combination of shear and axial reinforcement force is proposed, based on that of Schlosser (1983). The potential benefit of reinforcement shear force on soil shearing resistance is also investigated and compared with that of axial force.

Using the theoretical model for reinforcement shear force described in Chapter 7 the data from tests given in Chapter 6 are analysed in Chapter 8. In particular the measured shear and axial forces are compared with the predicted values. These are then substituted into a limit equilibrium analysis allowing comparison with the measured boundary forces. Data from the literature, laboratory and field are also compared with the proposed model to provide an independent check.

Finally, a resume of the overall conclusions and suggestions for further research into soil-reinforcement interaction are given in Chapter 9.

CHAPTER 2:

SOIL-REINFORCEMENT INTERACTION

The term *reinforced soil* describes any soil mass which has had its shear strength improved by combining it with resisting elements; these resisting elements, or reinforcements may take the form of bars, strips, tubes, grids or sheets. Reinforcement can be used as either a permanent component of a reinforced soil structure or simply to provide a temporary increase in soil strength to allow the construction of an adjacent structure. The observed increase in soil shear strength of a reinforced soil is always a direct result of relative soil-reinforcement displacements.

The roots of reinforced soil go back as far as biblical times and therefore it cannot be considered as a modern technique. However, it was not until the patenting in France of the Reinforced Earth system for retaining structures, Vidal (1969), that reinforced soil became a widely used technique in geotechnical engineering. This is considered by many as the catalyst which led to a rapid expansion in the use and development of reinforced soil structures. A concise history of the development of reinforced soil and a review of the different systems are given in Jones (1985).

The objective of this chapter is to introduce the mechanisms of interaction between soil and reinforcement and to highlight the various aspects of reinforced soil to which the findings of this dissertation may be applicable. A brief description of the alternative techniques and methods available for investigating soil-reinforcement interaction is given.

2.1 Classification of Soil Reinforcement Systems and Interaction Mechanisms

(a) Reinforced Embankments   (b) Reinforced abutments

(c) Dowelling unstable slopes   (d) Soil nailing
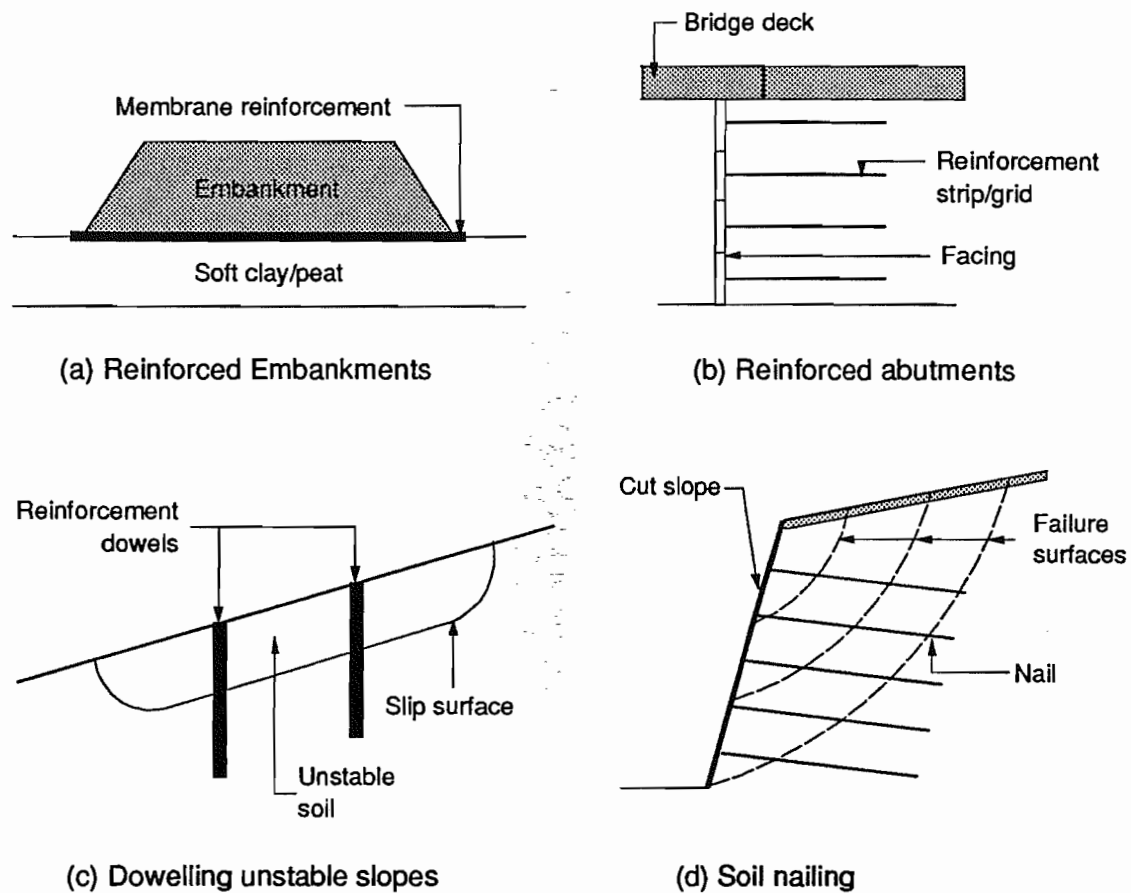
Figure 2.1 - Examples of reinforced soil systems.

Soil reinforcement systems can be divided into two major categories: *in-situ* and *constructed.* The former category covers techniques where the reinforcement is placed into virgin soil to form a reinforced soil structure; this includes the techniques of soil nailing and soil dowelling. The latter category describes techniques where the reinforcement is placed at the same time as an imported and remoulded soil. Such techniques are often referred to as bottom up processes, as they involve the placement of a fill and include structures such as reinforced soil embankments and bridge abutments. The reinforcement used for in-situ structures is usually linear owing to the method of installation, whereas reinforcement used
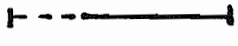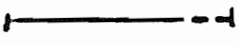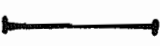
for the constructed category can be much more varied in form and often consists of strips, mats or grids. Typical applications of in-situ and constructed reinforced soil are given in Figure 2.1.

The enhancement in shear strength induced by the presence of reinforcement is a function of the forces in the reinforcement; these forces are a direct result of soil-reinforcement interaction. There are two modes of interaction between soil and reinforcement: *reinforcement bearing* leading to bending moments and shear forces, and *reinforcement friction* leading to axial tension or compression. The magnitudes of the induced reinforcement forces are principally dependent on the relative soil-reinforcement stiffnesses and strengths, and the soil deformations occurring in the structure. The mechanisms of bearing and friction are illustrated in Figure 2.2. Table 2.1 gives the predominant interaction mechanisms and reinforcement forces for different soil-reinforcement systems.
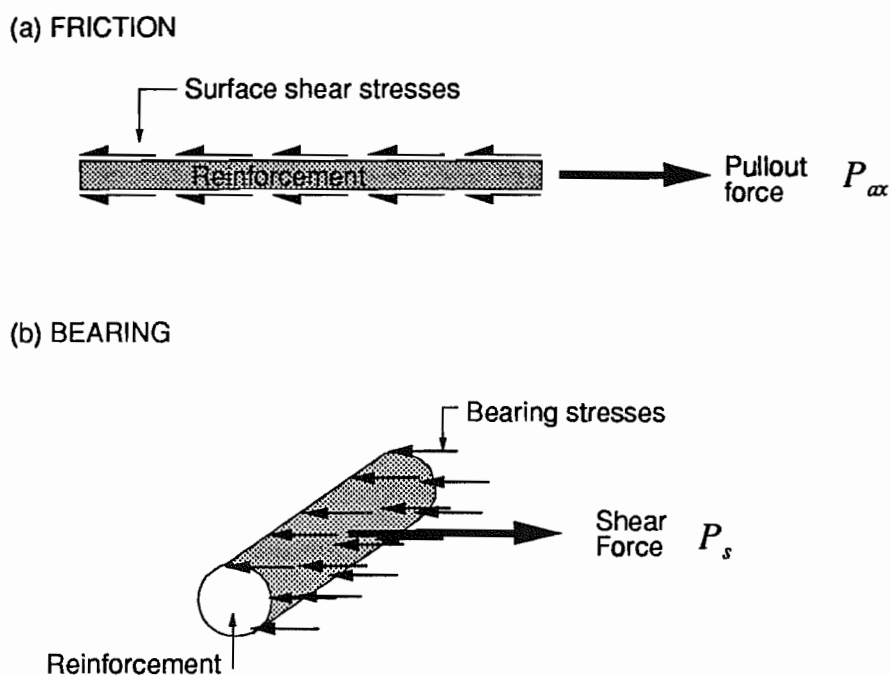
Figure 2.2 - Mechanisms of soil reinforcement interaction: (a) friction and (b) bearing.

Table 2.1 shows that whilst many of the reinforcement systems exhibit both bearing and frictional interaction mechanisms it is only for soil dowelling that shear force is the major reinforcement force; all of the other techniques rely predominantly on axial tension. Why, therefore, despite the similarities between soil nailing and constructed reinforced soil walls is there so much debate over the use of shear force in soil nailing design and its magnitude?

SYSTEM	INTERACTION MECHANISM		MAJOR REINFORCEMENT FORCE	
	Bearing	Friction	Tension	Shear
Soil Nailing (in-situ)	⊢ ‒ ‒ ▬▬▬▬⊣		⊢▬▬▬▬ ‒ ‒ ‒ ⊣	
Soil Dowelling (in-situ)	⊢▬▬▬▬▬ ‒ ‒ ⊣			⊢ ‒ ‒ ▬▬▬▬⊣
Constructed Walls & Embankments		⊢▬▬▬▬▬⊣	⊢▬▬▬▬⊣	
Embankments with membrane reinforcement		⊢▬▬▬▬⊣	⊢▬▬▬▬⊣	

Table 2.1 - Interaction mechanisms and predominant reinforcement forces for different reinforced soil systems.

Possible explanations may be associated with the reinforcement cross sections and orientations commonly found in soil nailed structures. Typically, round bar or angle reinforcement is used for soil nailing; these cross sections exhibit much higher second moments of area than the strip or sheet reinforcement used in constructed soil walls, therefore giving a greater resistance in shear and bending. Soil nailing also differs from most reinforced soil systems in that the reinforcement often crosses the potential failure planes in the soil at angles close to right angles, allowing the reinforcement to work as a dowel. Typical reinforcement orientations in other reinforced soil systems are such that the reinforcement lies close to the direction of the principal tensile strain increment in the soil leading to tensile reinforcement forces.

The objective of this dissertation is to investigate the role of reinforcement shear force and its effect on soil shear strength when compared with axial force. For this reason further reference to reinforced soil systems will be confined to the in-situ techniques of soil nailing and soil dowelling. Subsequent sections discuss typical in-situ reinforcement types and their methods of installation along with current design recommendations pertinent to this study.

2.2 In-situ Soil Reinforcement Systems

2.2.1 Soil nailing

The technique of soil nailing is used for stabilising either vertical or steep cut slopes and is executed incrementally; after each stage of excavation the reinforcements, or nails are installed. It has typically been used for stabilising cuts in soils varying from soft rocks to medium stiff clays and sands and gravels, Gassler and Gudehus (1981). Detailed descriptions of soil nailing construction techniques are given in Bruce and Jewell (1986/7), Mitchell and Villet (1987) and Gassler (1990).

The most common form of reinforcement used for soil nailing is that of a circular steel bar, typically of diameter $20mm - 30mm$; however, angle sections have been used (*Hurpinoise* system, Rabejac and Toudic, 1974) as have tubular sections, Louis (1984). Mild and high yield steel reinforcement are both commonly used although the former is preferred owing to its more ductile behaviour.

There exist essentially two methods of nail installation, with many small variations to each: drilling and grouting, where the reinforcement is grouted into a pre-drilled hole, and driving by hammering, vibration or firing which is sometimes followed by grouting. The action of grouting the reinforcement leads to the advantage of greatly enhanced pullout resistance because of the increased surface area and roughness. The presence of grout may also provide increased corrosion protection, although, both the German and the French codes of practice require additional protection for reinforcement in permanent structures.

The small displacements that occur during the construction of soil nailed structures result in axial reinforcement forces being mobilised. For typical *serviceability* crest displacements of between 0.1% to 0.3% of the height of the structure, the major reinforcement force is axial tension, with bending moments and shear forces being of secondary importance. Test walls loaded to failure have shown that large bending moments occur in the reinforcement as the structure reaches collapse, at which point the observed displacements are large and the structure cannot be considered serviceable, Gassler (1987) and Plumelle et al. (1990). Observed shear forces, even at this stage have been shown to be limited when compared with the mobilised axial forces.

Soil nailing design methods appear to exhibit a general consensus regarding the design of soil nails for pullout. Most existing design methods suggest that the unit reinforcement pullout force should be obtained from pullout tests on test nails. This is because there appear to be no sound analytical techniques which provide unit pullout resistances comparable with those obtained from pullout tests. On obtaining the unit pullout resistance, the limiting reinforcement axial force is simply a factored value of unit pullout force multiplied by the length of reinforcement anchored beyond the most critical failure surface in the soil.

Schlosser and Guilloux (1981) proposed an empirical solution for an apparent friction coefficient between granular soil and steel reinforcement for the design of Reinforced Earth; this empirical correlation showed reasonable agreement with friction coefficients obtained by Cartier and Gigan (1983) for driven bars pulled out of a full scale soil nailed wall.

In contrast to a consensus of opinion over the calculation of reinforcement axial force there is much discussion on the use of reinforcement shear force in design.

The German code of practice for soil nailing, Institut fur Bautechnik (1986), takes into account reinforcement axial force only, this is also the case with stability calculations proposed by Shen et al. (1981) (*Davis* method), Stocker and Reidinger (1990) and Kakurai and Hori (1990). However, the French design method proposed by Schlosser (1983) considers both shear and axial force in stability calculations, as do design methods proposed by Juran et al. (1988) and Bridle (1989). In all of the latter methods it is assumed that there

is one unique failure surface passing through the nailed structure; reinforcement spanning this surface is subjected to bearing stresses as a result of the relative movement of the soil on either side, Figure 2.3. The magnitude of the shear force at the failure surface is a function of the lateral stress distribution on the reinforcement and is a maximum at this point, provided the reinforcement extends a sufficient distance either side. It is also assumed in the above analyses that the interaction between the reinforcement and soil can be characterised by elastic parameters.

At A $P_s = 0$

At B $M = 0$
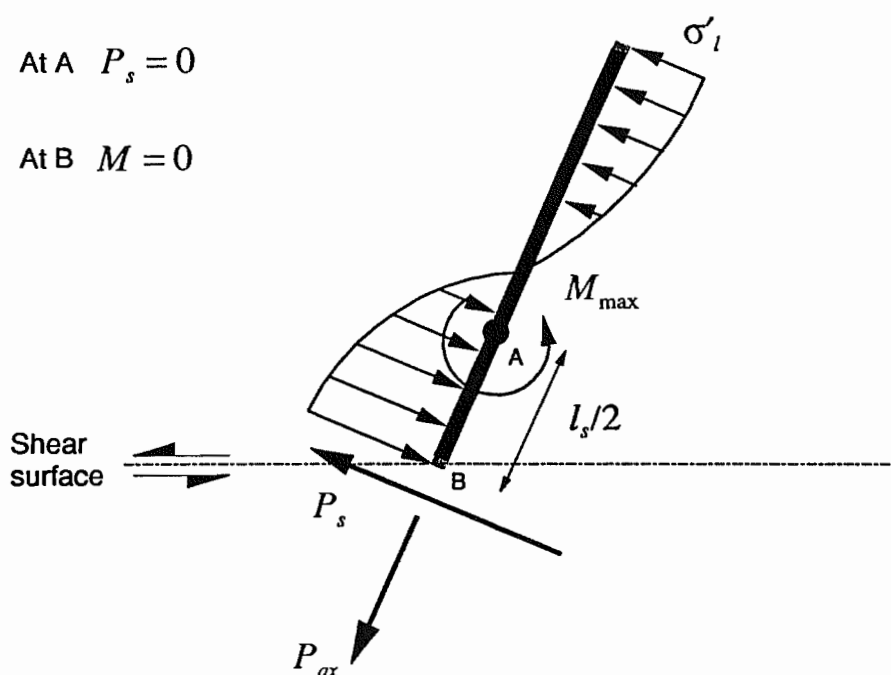
Figure 2.3 - Bearing stresses acting on reinforcement on one side of a slip surface.

The model usually adopted to calculate the reinforcement shear force is that originally developed for laterally loaded piles in an elastic subgrade. The major problems with this theory concern firstly the inherent underprediction of the maximum reinforcement shear force owing to the condition of no plasticity in the reinforcement, and secondly the validity of the assumption that soil can be characterised by a single elastic constant K_s, the modulus of subgrade reaction.

A finite element study of nailed structures by Shafiée (1986) suggests that relative displacements occur throughout the active zone, and are not just concentrated along a small band in the soil, even when taking into account the inability of failure planes to form within individual finite elements. If these results are applicable, such a deformation of the soil and reinforcement would lead to a much lower rate of change of bending moment in the reinforcement and consequently lower shear forces than theoretically predicted. Also, the incremental nature of soil nailing construction leads to a whole series of failure surfaces being formed in the soil giving rise to a zone of deformation.

Delmas et al. (1986) observed that axial forces calculated using the finite element method compared well with those using the programme *Prosper* (elastic analysis, unique failure surface). However, the reinforcement shear forces were found to be much lower and negligible when compared with the axial force; this may well be owing to the assumption of a single discrete failure surface.

A comparative study of the effect of reinforcement shear force on the global factor of safety of soil nailed walls by Gigan and Delmas (1987) found that including the reinforcement shear force in the calculation led to a maximum increase in factor of safety of about 10%, but the effect of shear force diminished rapidly as the density of reinforcement increased to typical quantities.

The evidence presented would suggest that whilst there is no doubt over the presence of both axial and shear force in soil nails, there is still a great deal of uncertainty with respect to the magnitude of the shear force and what its effect is on the stability of nailed walls; it is for this reason that many designers conservatively choose to ignore the influence of reinforcement shear force.

2.2.2 Soil dowelling

The technique of soil dowelling is used for the stabilisation of shallow, unstable or creeping slopes. Many case histories of soil dowelling are cited in the literature, including Sommer (1979), Winter et al. (1983), Cartier et al. (1984) and Gudehus and Schwarz (1985).

In most cases of soil dowelling the reinforcement is placed so that maximum benefit can be obtained from the reinforcement shear force, i.e. the reinforcement is placed near normal to the failure surface. Various types of reinforcement have been reported in the literature ranging from small diameter micro-piles, tubular steel piles, H-piles and reinforced concrete piles of large diameter, Cartier (1986).

Installation of the reinforcement may be by drilling or driving, and is dependent on the type of soil and reinforcement. Generally two or three rows of dowels are placed in the ground, and may be linked at the surface by a ground beam. The dowels should be long enough to pass through the creeping zone of soil and into the stable soil or rock located below the failure surface, which provides resistance.

Stabilisation of creeping slopes by dowels is usually a result of bearing interaction. In the case where the surface area of the pile is large compared with the area for bending the axial force may play a significant role. Stability of the creeping soil occurs when sufficient bearing stresses have been mobilised on the dowels above and below the failure surface such that the shear force induced in the dowel is equal to the net sliding force of the creeping soil. Owing to the large displacements required to mobilise bearing stresses, stabilisation requires further creep of the slope to occur and is therefore not instantaneous upon reinforcement installation.

The major difference between design methods for the stabilisation of creeping slopes concerns the calculation of the gross force required to stabilise the slope. The load which each pile can resist is generally calculated using an elastic model for lateral pile loading (see for example Poulos and Davis, 1980) or using the rigid-plastic model of pile-soil interaction proposed by Brinch Hansen and Lundgren (1960). Further methods of calculating the net load taken by each dowel in a group of dowels have been proposed by Wang and Yen (1974) and Ito and Matsui (1975), and are based on the phenomenon of soil arching.

The elastic and plastic models of soil-dowel interaction are shown diagrammatically in Figure 2.4. As with soil nailing an elastic model is less appropriate than a plastic model as it results in an under prediction of the limiting reinforcement shear force. More

importantly, it is dependent the use of the modulus of subgrade reaction K_s which is an ill defined parameter and normally deduced from empirical correlations, whereas a plastic model requires an estimate of the limiting lateral stress. However, one advantage that the elastic model does offer is the ability to estimate the additional deformations after reinforcement installation for stability to occur.
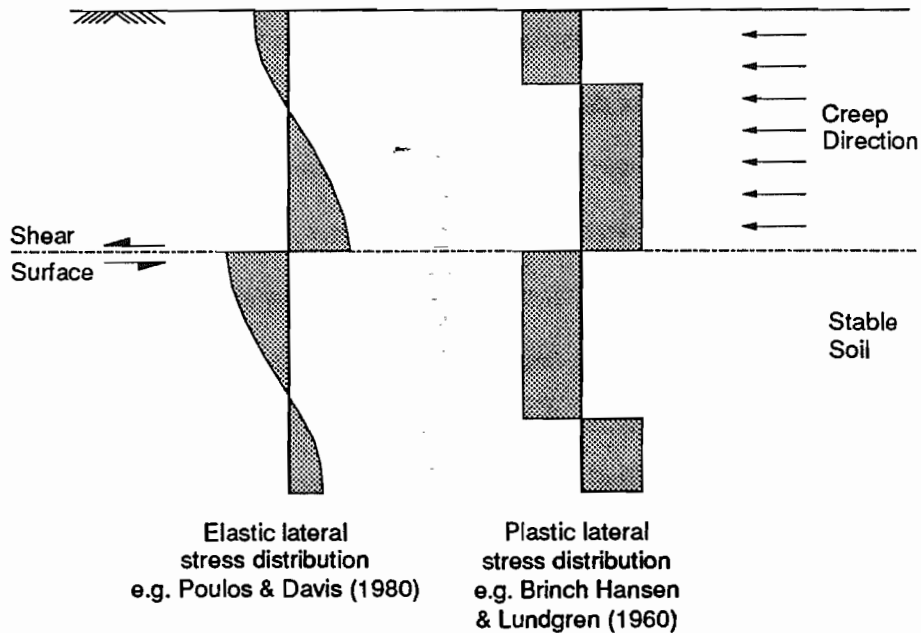
Figure 2.4 - Elastic and plastic soil-dowel loading models.

Unlike soil nailing, there is little doubt that the major reinforcement force leading to soil stabilisation is that of shear, however, there is very little guidance in the form of design methods or codes of practice for practising engineers on the magnitude of this shear force. Despite many case histories of soil dowelling in the literature there are very few cases of fully instrumented reinforcement where shear forces have been measured allowing comparison with design methods.

2.3 Investigating Soil-Reinforcement Interaction

There are numerous methods and techniques which may be used for the investigation of soil-reinforcement interaction. They can be divided into three broad categories: field, model and unit cell tests. A brief review of each category is now given.

2.3.1 Field tests

Full scale field testing of reinforced structures has many advantages, not only allowing direct observation of the failure mechanisms, but also calibration of design methods and predictions. However, full scale testing is not only expensive but can also lead to inadequate and erroneous conclusions if the planning and execution of the test is ill managed. In order that this does not occur it is necessary to ensure that a thorough site investigation is performed and that there is sufficient and appropriate instrumentation. Care must always be taken when interpreting field test results as generally it is not possible to replicate them and often they may only be applicable to the particular site tested. Recent full scale field tests on soil nailed structures are reported in Gassler (1987) and Plumelle et al. (1990).

2.3.2 Model tests

Generally, model tests are more attractive than field tests. Not only are they cheaper but a larger number of tests can be performed allowing full parametric studies to be undertaken under controlled boundary and loading conditions. One major advantage with model testing is that both internal and external measurements of soil and reinforcement displacements can be made. For the case of model tests from which results are extrapolated to full scale structures it is important that dimensional similitude is observed. The centrifuge apparatus can in some cases be used to overcome the problems of testing small scale models e.g. Bolton and Pang (1982).

Examples of model tests are given in Haussmann and Lee (1978), who studied the pullout of reinforcement in reinforced soil retaining walls, and Gassler (1987) who used models for the investigation of failure modes in soil nailed structures.

2.3.3 Unit cell tests

Although the two previous categories of methods of investigating soil-reinforcement interaction can provide much information on the mechanisms occurring within a specific structure, particular aspects of soil-reinforcement interaction such as bearing or friction are best studied with unit cell tests. The majority of fundamental soil-reinforcement interaction studies to date appear to have been performed under plane strain conditions, although triaxial tests on reinforced soil have been reported in the literature (e.g. Long et al. 1983); perhaps this is owing to the common use of soil reinforcement in applications where the boundary conditions approximate to plane strain.

Some of the earliest reinforced unit cell tests were performed by McGown et al. (1978) in a biaxial stress cell to study the effects of reinforcement on sand. Probably the most common piece of laboratory apparatus for investigating soil-reinforcement interaction is the direct shear apparatus; first used by Jewell (1980) who predominantly studied the influence of reinforcement axial force on soil shear strength. Further studies in the direct shear apparatus have been performed Juran et al. (1981) and Marchal (1984) to examine reinforcement shear force, and Dyer (1985) and Palmeira (1987) to look at other aspects of soil reinforcement interaction. The advantage of the direct shear apparatus is that the boundary conditions force a failure surface in the soil which can be studied both with and without reinforcement crossing it, allowing quantification of the effects of reinforcement. A large scale direct shear apparatus was used for the tests described in this dissertation.

Finally, pullout tests can be performed to investigate the limiting bond between soil and reinforcement, although caution should be exercised when interpreting and comparing data owing to potentially significant boundary effects, Palmeira and Milligan (1989). Interface tests can also provide data on the limiting shear between soil and reinforcement.

CHAPTER 3:

LABORATORY APPARATUS

To investigate the interaction between soil and reinforcement two forms of the direct shear apparatus were used; the first, a medium sized apparatus similar to that used by Jewell (1980), and the second a modified version of the large direct shear apparatus described in Palmeira (1987) which will be referred to as the LDSA. The main features of these shearboxes are described below, along with details of instrumentation, data acquisition and methods of sample preparation.

3.1 Large Direct Shear Apparatus

3.1.1 Mechanical layout

A previous study of direct shear testing and soil-reinforcement interaction by Palmeira (1987) using the original form of the LDSA highlighted areas in which improvements could be made to the apparatus. Problems associated with the original design led to a rotation of the soil sample within the shearbox, resulting in a non uniform stress distribution across the central plane, and to difficulties in measuring the dilation from the boundaries. The arrangement used for applying the vertical load also prevented installation of reinforcement after application of this force. In order to tackle the above shortcomings a series of modifications was undertaken leading to the form of the LDSA now described. Figure 3.1 illustrates schematically the mechanical layout of the LDSA.
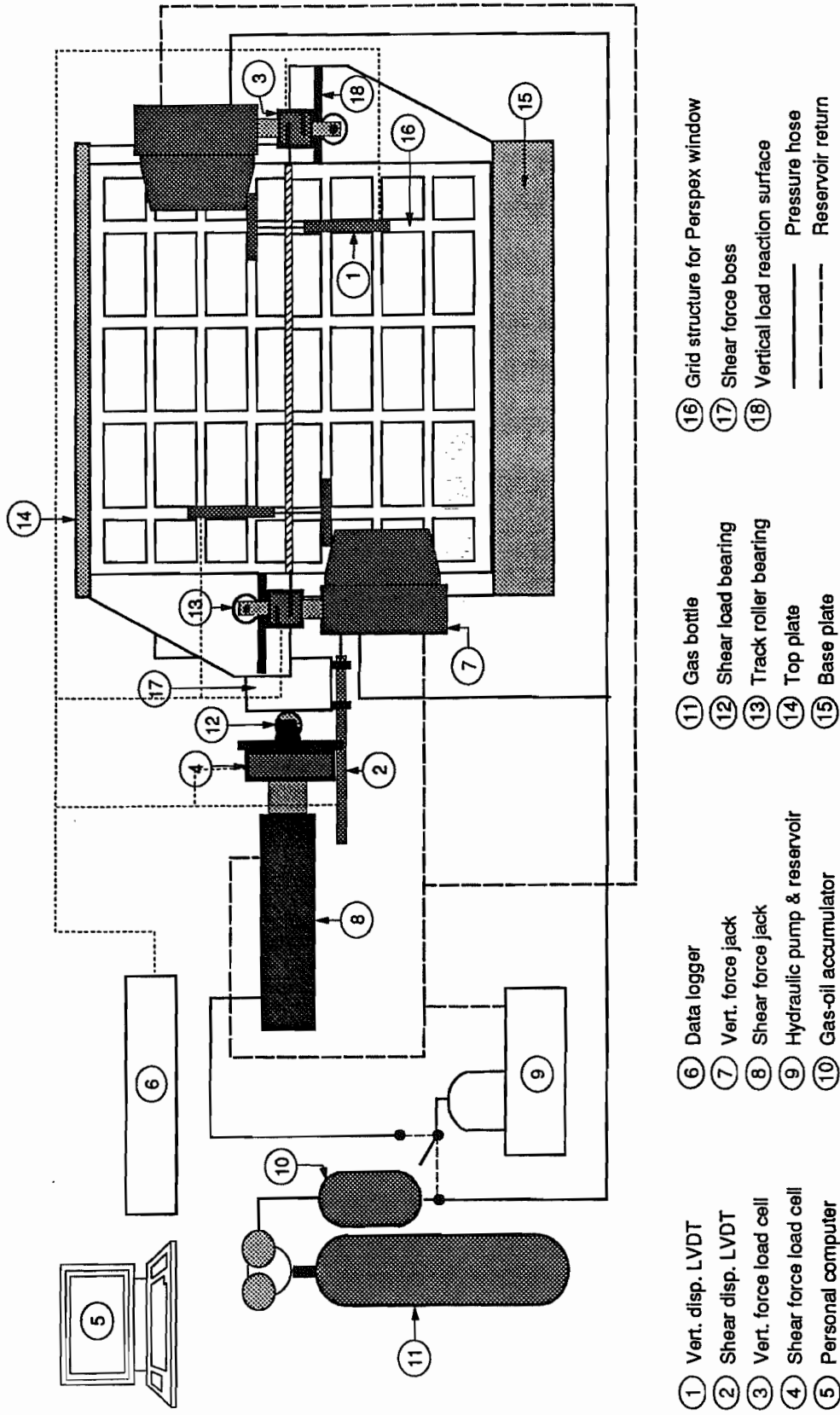
Figure 3.1 - Schematic side elevation of the Large Direct Shear Apparatus giving details of the instrumentation and mechanical layout.

① Vert. disp. LVDT
② Shear disp. LVDT
③ Vert. force load cell
④ Shear force load cell
⑤ Personal computer

⑥ Data logger
⑦ Vert. force jack
⑧ Shear force jack
⑨ Hydraulic pump & reservoir
⑩ Gas-oil accumulator

⑪ Gas bottle
⑫ Shear load bearing
⑬ Track roller bearing
⑭ Top plate
⑮ Base plate

⑯ Grid structure for Perspex window
⑰ Shear force boss
⑱ Vertical load reaction surface

——— Pressure hose
‒ ‒ ‒ Reservoir return

The structure of the LDSA consists of a cube of internal side $1m$ containing the soil sample, and split at mid-height in the horizontal direction. The upper and lower halves of the shearbox may be separated vertically by the means of four screw jacks. The sides of the cube are of $25mm$ thick mild steel plate supported by a steel grid structure, except for one of the sides which is of *Perspex* sheet to allow observation of the sample inside the shearbox. The top of the shearbox consists of a rigid $40mm$ thick mild steel plate, and the bottom a reinforced concrete slab, both of which are bolted securely to the sides of the shearbox. The top half of the shearbox is free to move relative to the lower half, which is fixed securely to a reaction structure.

A vertical load is applied to the soil by means of four $80kN$ hydraulic jacks, one at each corner of the shearbox and disposed symmetrically about the shear plane so as not to induce a moment on the sample. The body of each jack is fixed to one half of the shearbox and the piston to the other by means of a track roller bearing to allow relative horizontal movement. The jacks apply the load to the sample by pulling the upper and lower halves of the box together after the top plate has been fixed in position. The jacks are pressurised using an oil-gas interface accumulator.

The shear load is applied to the upper half of the shearbox by a $600kN$ hydraulic jack pressurised by an electric pump, the reaction being provided by a frame attached to the lower half of the shearbox. The shear load is transmitted from the piston of the jack via a single roller bearing onto a boss welded to the top half of the shearbox; the boss allows the shear load to be applied at the level of the shear plane. The rate of displacement between the two halves of the shearbox is controlled by varying the applied shear load by means of flow control and dump valves.

Palmeira (1987) designed the original shearbox to withstand a maximum shear load of $140kN$; this limited the maximum vertical load to about $150kN$ for the types of soil and

reinforcement used during the test programme. Although the loading arrangement for the LDSA allows a higher vertical load to be applied this is not recommended without a significant stiffening of the structure.

3.1.2 Instrumentation

During testing, data readings of loads and displacements were taken using a number of different types of transducer: linear variable differential transformers (LVDT), load cells and electrical resistance strain gauges. Data acquisition was accomplished using an RDP Electronics E500 Translog datalogger controlled by an Ollivetti M21 personal computer. Software supplied by RDP Electronics Ltd. was used to record the test data at set intervals of time, convert it into engineering units and to format it for analysis using spreadsheets. In general data were recorded every 10 seconds.

The shear force S was measured by a $200 \pm 0.01 kN$ load cell (Type TCLM-20A) manufactured by Tokyo Sokki Kenkyujo Co. Ltd. attached to the piston of the shear loading jack. To avoid a moment acting on the load cell a single roller bearing transferred the load through to the top half of the shearbox.

The force applied by each vertical loading jack p_n was monitored by a Maywood Instruments Ltd. U5000 tension/compression load cell of capacity $50 \pm 0.01 kN$. Special attention was paid to the piston–load cell–bearing connection used to transfer the load between the two halves of the shearbox; any eccentricity of this load with respect to the axis of the jack would have resulted in a reduction in the accuracy of the measured loads. During testing constant checks to ensure the roller bearings were running freely were made.

The relative shear displacement X of the two halves of the shearbox was measured using a long stroke ($\pm 150 mm$) LVDT supplied by RDP Electronics Ltd. This was mounted between the two halves of the box and directly below the point of shear load application. Although the LVDT was calibrated to an accuracy of $\pm 0.01 mm$ it is unlikely that the true accuracy was much greater than $\pm 0.5 mm$ owing to elastic deformation of the shearbox. The

vertical displacement y_n at each corner of the shearbox and the rotation of the shearbox were monitored using 4 N° ±50*mm* stroke LVDTs, one placed at each corner of the shearbox. These transducers were also calibrated to an accuracy of ±0.01*mm* with a measured accuracy in the region ±0.1*mm*.

In many tests, electrical resistance strain gauges were used for measuring reinforcement surface strains. Details of these are discussed in Chapter 6.

In all cases, calibration was carried out in the laboratory to obtain calibration factors in the working range of the transducers, taking due regard of the mounting of the transducer and the specific system into which they were wired. The calibration procedure also confirmed the accuracy of the transducers.

Also fitted into the front wall of the shearbox is a row of total pressure cells which were not used during the research project; details of these can be found in Palmeira (1987).

3.1.3 Sample preparation

The method of sample preparation is described below and the main stages are summarised diagrammatically in Figure 3.2.

The first stage of sample preparation involved locating the upper half of the shearbox directly above the lower half, and then separating them vertically using the screw jacks mounted at each corner of the shearbox. The vertical gap formed, measured by the LVDTs principally used to monitor dilation, was sealed with masking tape to prevent soil escaping from the chamber during sample preparation. An initial gap of 6.0*mm* proved to be suitable for the particular sand used (Leighton Buzzard 14/25 sand); allowing initial contraction of the sample to be accommodated, but preventing loss of sand through the gap towards the end of the test when the masking tape had sheared. The two halves of the box were then fixed in position by the application of a small vertical load ($\approx 1-2kN$).

A uniform soil sample was prepared using the technique of raining which involves pluviating the soil (Leighton Buzzard 14/25 sand) through a series of grids into the test chamber. This technique has been used by many researchers; Cole (1967) observed from

X-radiographs that a homogeneous sample can be obtained with this method and Kolbuszewski (1965) found that the density obtained by raining is a function of the height and rate of fall of the soil being pluviated.

A hopper of dimension $1050mm \times 1050mm \times 250mm$ located above the shearbox by means of a support frame was used for sample preparation. The hopper was open at the top, but its base consisted of two identical perforated plates; the lower of which could be displaced so that the perforations became aligned allowing the sand to pluviate through.

During the course of the test programme the sample density was changed from medium dense to dense and this involved changing the perforated plates located in the base of the hopper. Using a similar system of shutter plates to Palmeira (1987), with a pattern of $6.4mm$ diameter holes on a triangular pitch of $11.3mm$ and a minimum height of fall of $540mm$, a mean relative density of $I_d \approx 55\%$ was attained. On changing the shutter plates so that the sand pluviated through holes of the same diameter, but with a triangular pitch of $80mm$ underneath which two layers of $6mm$ dispersal meshes were situated, it was found that the mean relative density was increased to $I_d \approx 90\%$. The dispersal meshes were placed at a depths of $100mm$ and $200mm$ below the shutter plates leaving a minimum height of fall of $340mm$. Cole (1967) recommends the use of a minimum height of fall of approximately $600mm$ for the preparation of dense and uniform samples of sand. To check the implications of a smaller drop height a series of density checks at various depths throughout the shearbox was instigated. This was performed by raining sand into a $200mm$ cube placed at different heights z, where z is the depth of the base of the cube relative to the top of the shearbox. The cube was placed at the centre of the shearbox and the results obtained are shown in Table 3.1.

The results obtained agree well with calculated values of the mean relative density of the sample from the total mass of sand in the shearbox and an estimate of the initial volume of the sample. The values obtained by this method were in the range $87.6\% < I_d < 92.4\%$,
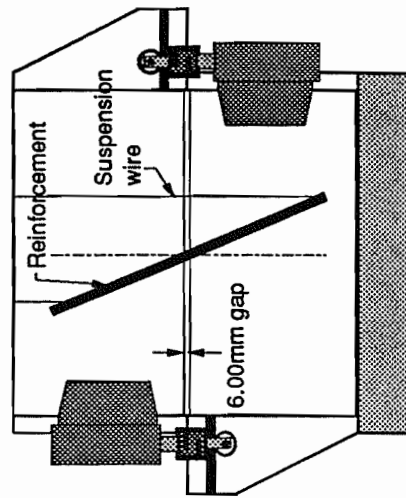
Figure 3.2(a) - Gap formed and sealed between upper and lower sections of shearbox and reinforcement suspended in correct position by wires.
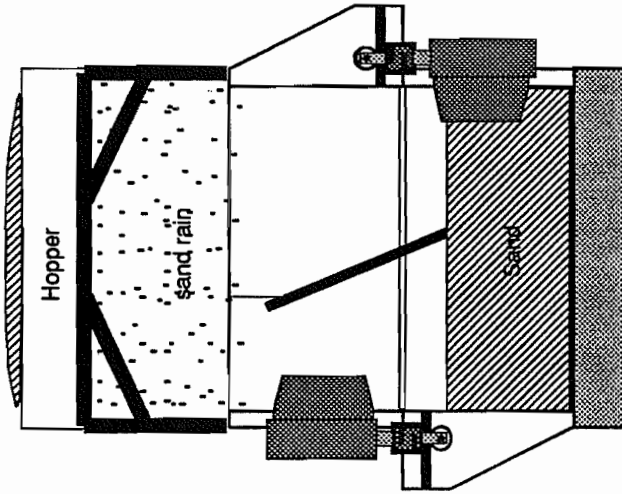
Figure 3.2(b) - Hopper placed above shearbox and sample is rained in, as depth of sand increases the suspending wires are removed. Sand is rained to a level just above the top of the shearbox.
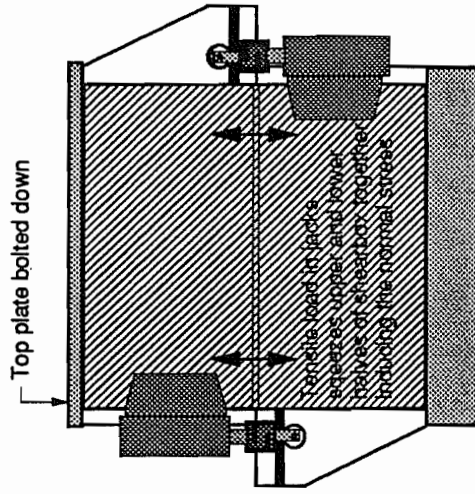
Figure 3.2(c) - After removing surplus sand from top of shearbox the top plate is bolted down and a tensile load in the jacks pulls the two halves of the shearbox together.

Figure 3.2 - Diagrammatic representation of sample preparation in the Large Direct Shear Apparatus.

with a mean of $I_d = 89.3\%$. The conclusion drawn from the data is that the method of sample preparation for the particular sand used produced a repeatable and uniform sample with respect to depth, ignoring small deviations at the upper and lower boundaries of the shearbox.

Depth of cube z (*mm*)	Relative density I_d (%) (±1%)
820	93.4
665	89.3
405	89.7
205	89.3
20	86.9

Table 3.1 - Variation of measured relative density with depth in the Large Direct Shear Apparatus.

As the hopper's capacity was approximately $0.2m^3$, for the majority of tests it was possible to prepare the soil sample only stopping the raining process four times. As any suspension of the raining process was likely to lead to a thin band of soil of lower density and lower shear strength, ceasing raining at the height of the central plane of the shearbox was avoided when possible. However, in tests where photographic markers were used this was unavoidable and it is likely that these samples are less homogeneous.

In most of the reinforced tests the reinforcement was placed in the shearbox before raining the sand. To locate the reinforcement at the required height and inclination the simplest method proved to be hanging the reinforcement from a tensioned steel wire suspended over the top of the shearbox. After a sufficient depth of sand had been deposited and the reinforcement firmly embedded the suspending wires were removed and the sample preparation continued as normal.

Plate 3.1
Right: **Arrangement for applying the vertical load and instrumentation for measuring dilation.**
Below: **View of shearbox before testing showing datalogger and computer in background.**
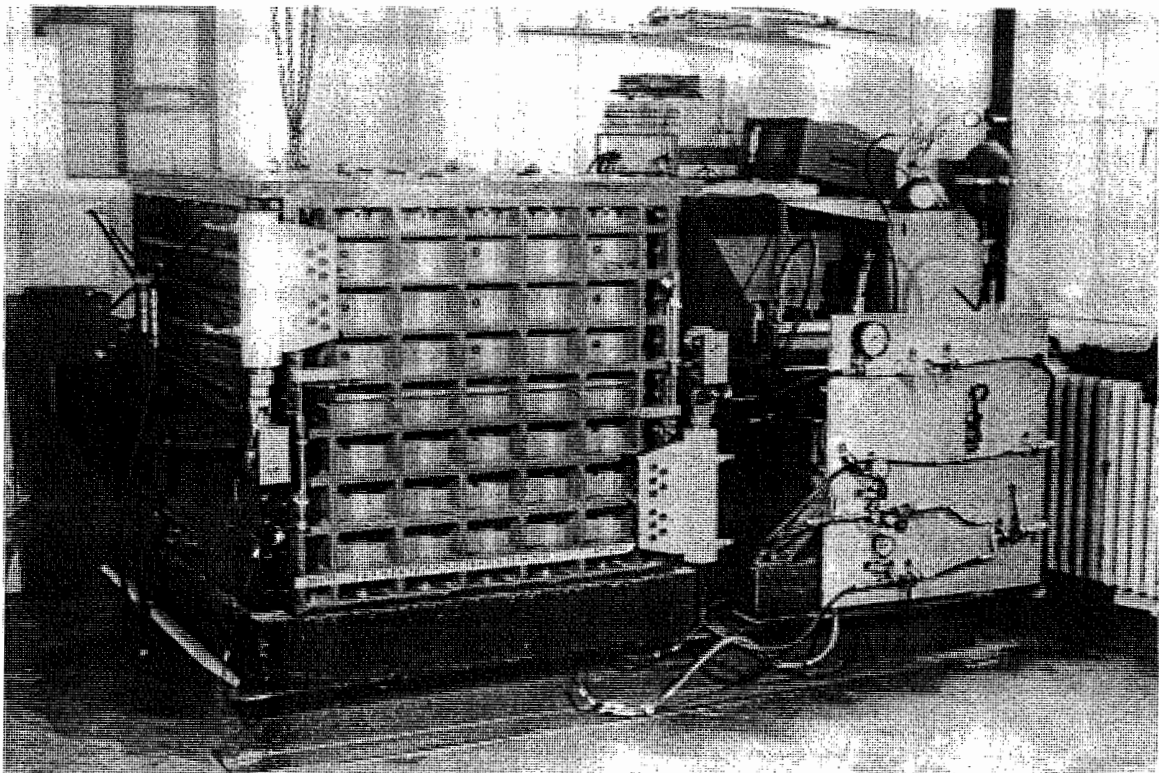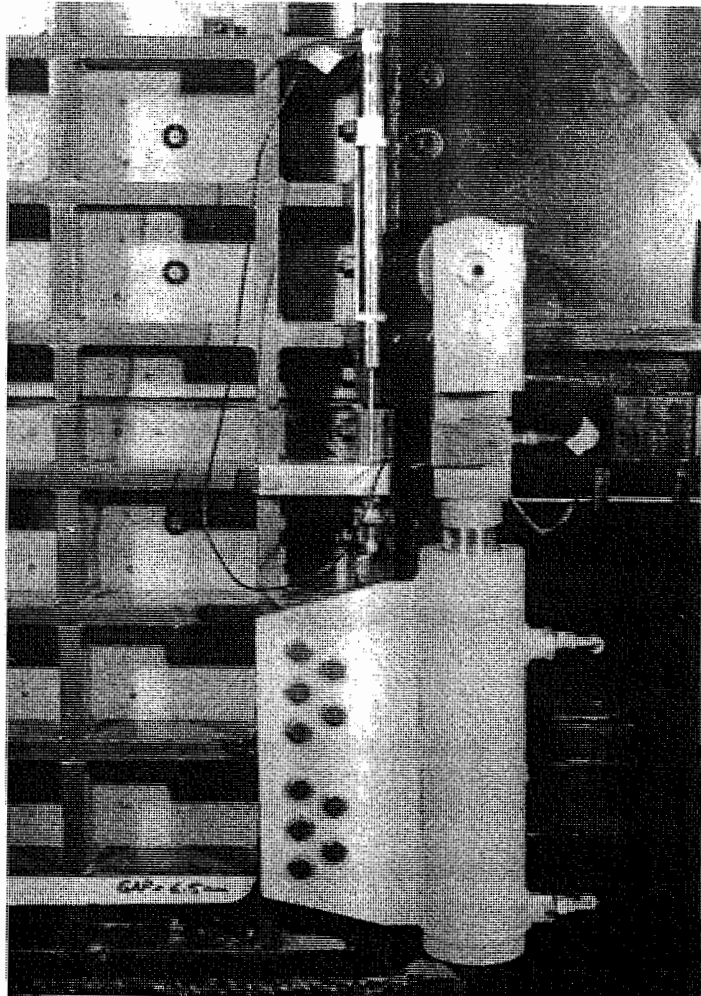
The final volume of sand to be poured was always greater than that required to fill the shearbox, resulting in a surplus of sand. The hopper was lifted away at this stage and a smooth surface formed by scraping away the surplus with a blade, using the top of the shearbox as a guide. The top plate was then lifted carefully into position and firmly bolted down to complete the sample preparation.

At this stage, the four screw jacks separating the two halves of the box were retracted and the vertical load slowly applied with the vertical loading jacks. The vertical displacement and load in the jacks were monitored at all stages during this process until the required vertical stress in the sample was attained. After allowing all pressures and readings to stabilise the sample was ready for testing. Plate 3.1 shows details of the LDSA before testing.

During the course of some tests reinforcement was introduced after application of the vertical load; the exact methods of installation and the displacement at which this took place are discussed further in Chapter 6.

3.1.4 Test procedure

Before starting a test the initial loads and displacements measured by the various transducers were recorded to provide a datum, or reset to zero using the data acquisition control software as necessary.

The test proper was then started by instructing the data acquisition system to record. The piston of the shear load jack was then advanced causing a relative displacement between the upper and lower halves of the shearbox, further displacements being induced by increasing the shear load. The rate of displacement, controlled by increasing or decreasing the shear load, was monitored by both the data logger output on the screen of the personal computer and by a dial gauge spanning between the two halves of the shearbox.

For most tests the rate of displacement was held as constant as possible at around $0.5mm/$ min until a total displacement X of between $60mm$ and $70mm$ had been attained. At this point the data acquisition was stopped, the shear loading ram retracted to its original position and the vertical load removed from the sample.

To provide additional interpretation of some unreinforced tests photographic measurements of markers in the sand were taken in order to estimate the soil strains during shearing; details of this technique are described briefly below.

Photographs of markers during a test were taken with an *Olympus* OM10 camera fitted with a *Vivitar* 135mm telescopic lens and placed perpendicular, and at a distance of approximately 5.5m to the *Perspex* front wall of the shearbox. The camera was fitted with a colour 200 ASA print film and the aperture settings were adjusted according to the light conditions. Photographs of the markers were taken at different intervals of shear displacement X during the test, with an initial photograph being taken before any shear load had been applied to provide a datum.

By digitising these photographs (a Summagraphics digitising pad interfaced with an IBM compatible computer was used for this purpose) it was possible to relate the position of the markers placed in the sand to reference points of known coordinate attached to the *Perspex* front wall of the shearbox. The digitised data were then analysed using a Fortran 77 program entitled *BIT.FOR*, described in Palmeira (1987), which calculated the relative displacement of the markers. From the relative displacement between the markers and the reference points the horizontal, vertical, principal, shear and volumetric strains could be calculated along with their respective orientations.

After completion of a test the acquired data was stored and backed up. The top plate of the apparatus was then removed and the shearbox emptied by shovelling; any markers in the sand were recovered for further use. Once empty, the upper half of the shear box was moved back to its original position by placing rollers between the two halves. It was then cleaned ready for a subsequent test. In reinforced tests the reinforcement was retrieved, labelled and observations made of any permanent deformation.

3.2 Medium Shearbox

3.2.1 Description of apparatus

The medium shearbox has a plan area of $254mm \times 153mm$ and a sample depth of about $150mm$ and was originally designed and used by Jewell (1980). The side panels of the shearbox are of *Perspex* and all other panels of aluminium alloy including the base and top platen. This shearbox is similar to the LDSA in that the top platen is fixed to the top half of the shearbox, i.e. it has symmetrical upper and lower boundary conditions. A diagram of the Medium shearbox is given in Figure 3.3.
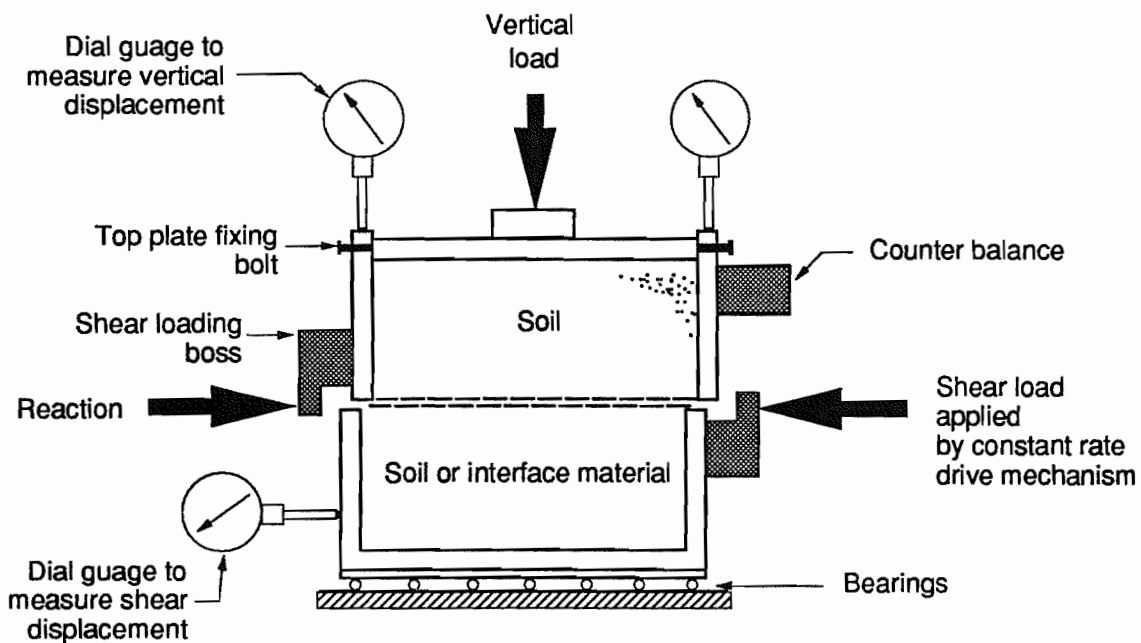
Figure 3.3 - Elevation of the Medium shearbox apparatus.

The shear load S is applied by a ram driven at constant speed by an electric motor. The ram pushes the bottom half of the shearbox which is free to run on bearings; the top half providing resistance to movement by reacting against a deflector bar. The deflection at the middle of the deflector bar is measured with a dial gauge and is directly proportional to the shear load transmitted through the soil.

The vertical load P_v is applied to the soil by weights supported on a hanger and resting on the top platen of the shearbox. As the top platen is fixed to the upper half of the shearbox it is essential that there is a gap between the upper and lower halves so that the load is transferred through the soil. Because of the relatively large cross sectional area of the Medium shearbox and the use of a hanger system to apply the vertical load, the vertical stress was limited to a maximum of about $\sigma'_v \approx 60 \, kN/m^2$.

The shear displacement X and the dilation Y during testing are measured by means of dial gauges with a sensitivity of $\pm 0.002mm$. A more detailed description of this apparatus is given in Jewell (1980).

3.2.2 Sample preparation and test procedure

The method of sample preparation is similar to that used in the LDSA, namely the upper and lower halves of the shearbox are separated vertically by inserting aluminium packing strips and then clamping them so that an even gap of approximately $1.5mm$ is formed.

The sand sample is then prepared by raining, using a hopper with an identical arrangement of shutter plates to that described in Section 3.1.3 and also covering the full plan area of the shearbox. As no reinforced tests were performed in the Medium shearbox the sample was prepared in one pour. The sand was rained to a level slightly above that required and the surplus removed by a compressed air vacuum device to form a level sand surface. This method gave a mean relative density of $I_d = 95.9\%$ for the sand used.

The top platen is then placed onto the sample and the vertical load applied, it is then fastened to the top half of the shearbox. The clamps fixing the two halves of the shearbox together and the packing strips are then removed to leave a clear gap between upper and lower halves. All of the required dial gauges are then positioned, leaving the sample ready for testing.

Testing a sample involves starting the constant drive shear loading ram, after taking the initial readings of the dial gauges and selecting the gear to give the required shear rate. For the tests undertaken a rate of $0.08mm/$ min was used as this allowed sufficient time to read and record the measurements from the dial gauges. Generally, the sample was sheared to a displacement of $8mm$ with readings being taken at regular intervals.

The Medium shearbox apparatus was also used to perform interface shear tests by installing the interface to be investigated at the level of the shear plane, in the lower half of the shearbox. The sample preparation was otherwise identical to that described previously. Details of the interfaces tested are given in Chapter 6.

CHAPTER 4:

RESULTS OF UNREINFORCED DIRECT SHEAR TESTS

A description of the direct shear apparatus and test procedure was presented in Chapter 3. The particular shearboxes used differ from the typical apparatus not only in size, but also because the top platen is fixed to the upper half of the shearbox leading to symmetrical boundary conditions about the central plane. The objectives of this chapter are to introduce suitable methods of analysing shearbox data, to describe the behaviour and mechanical properties of the standard test soil (which are fundamental to an understanding of its behaviour when reinforced) and to discuss data obtained from the Large Direct Shear Apparatus.

4.1 Observation and Interpretation of Direct Shear Test Data

4.1.1 Experimental observations

The experimental observations made during a direct shear test consist of four principal quantities, all of which are required for a proper analysis of the test, they are:-

(i)   the shear load S which is applied to the shearbox in the horizontal direction and is transferred to the soil by the rigid end boundaries of the apparatus, Dyer (1985), inducing a relative shear displacement between the upper and lower halves of the shearbox.

(ii)   the relative shear displacement X, measured in the horizontal direction, between the two halves of the shearbox.

(iii)   the vertical load P_v acting perpendicular to the central plane of the shearbox. This

force comprises the self weight of the soil, the dead load associated with the

shearbox structure and the applied load. For most shearboxes this load is constant

throughout a test, however, owing to friction within the hydraulic vertical loading

system of the LDSA small fluctuations in this load are observed as the sample

dilates during shear. These fluctuations are measured during testing and can be

minimised by reducing the rate of shear displacement.

(iv)   and finally, the vertical displacement Y of the sample caused by contraction or

dilation of the soil. The vertical displacement of the sample should be measured

at two or more points to enable rotation of the shearbox to be detected. The rotation

occurring during shearbox tests has been investigated by Airey (1987), and Jewell

(1980) who found that by fixing the top loading platen to the upper half of the

shearbox rotation could more or less be eliminated. This point is discussed further

in Section 4.3.1.
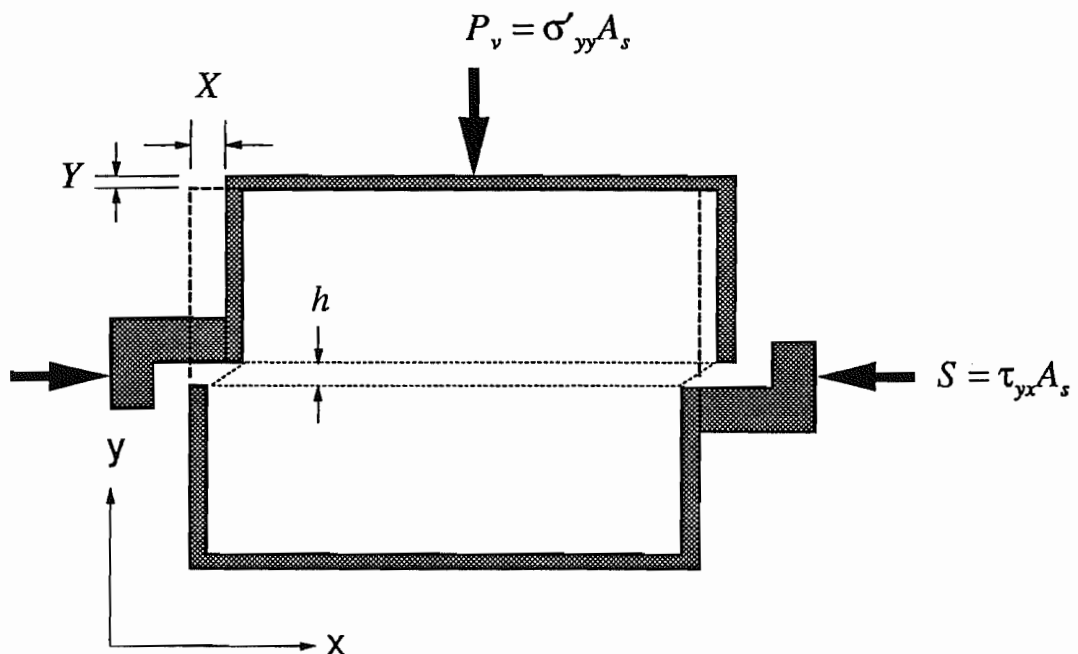
Figure 4.1 - Principal measured quantities in a shearbox test.

Figure 4.1 illustrates the principal measured quantities. These quantities are generally measured at set increments of shear displacement X or time during a test. The interval used should be sufficiently small to allow a more or less continuous record of shear load, vertical load and vertical displacement to be plotted with respect to the shear displacement.

4.1.2 Interpretation of boundary data

There are various methods which may be used to interpret direct shear test data; the particular method used is dependent on the number and quality of measurements made during a test.

The simplest interpretation of the direct shear test uses the shear stress τ_{yx} and normal stress σ_{yy} applied to the central plane. Often the normal stress acting on this plane is referred to as the vertical stress σ_v, owing to the y direction being vertical for most shearboxes, Figure 4.1. It is assumed that the friction angle mobilised on the central plane is equal to the plane strain friction angle of the soil ϕ'_{ps} and is given by

$$\tan \phi'_{ps} = \frac{S/A_s}{P_v/A_s} = \frac{\tau_{yx}}{\sigma_{yy}} \qquad ...(4.1)$$

where S and P_v are defined in Figure 4.1 and A_s is the plan area of the shearbox.

Equation (4.1) leads to an underprediction of the plane strain friction angle in many cases. This is explained by the experimental observations of Jewell (1980) and Dyer (1985), and from a finite element analysis by Potts et al. (1987). They all observed that the soil in the central region of the shearbox consisted of a series of horizontal planes along which there was no linear incremental strain. This implies that the soil in this region deforms in simple shear and the mobilised friction angle is in fact the *direct shear* friction angle ϕ'_{ds}. In order to be more precise equation (4.1) should strictly be written as

$$\tan \phi'_{ds} = \frac{\tau_{yx}}{\sigma_{yy}} \qquad ...(4.2)$$

If boundary measurements of sample dilation Y are taken with respect to shear displacement X it is possible to calculate the angle of dilation of the soil ψ. Provided the horizontal direction in the shearbox is one of zero extension, the angle of dilation is deduced from the Mohr's circle of strain increment, Figure 4.2, as

$$\tan \psi = \frac{d\varepsilon_{yy}}{d\gamma_{yx}} = \frac{dY}{dX} \qquad \ldots(4.3)$$

where $d\varepsilon_{yy}$ and $d\gamma_{yx}$ are increments of vertical and horizontal shear strain in the soil.
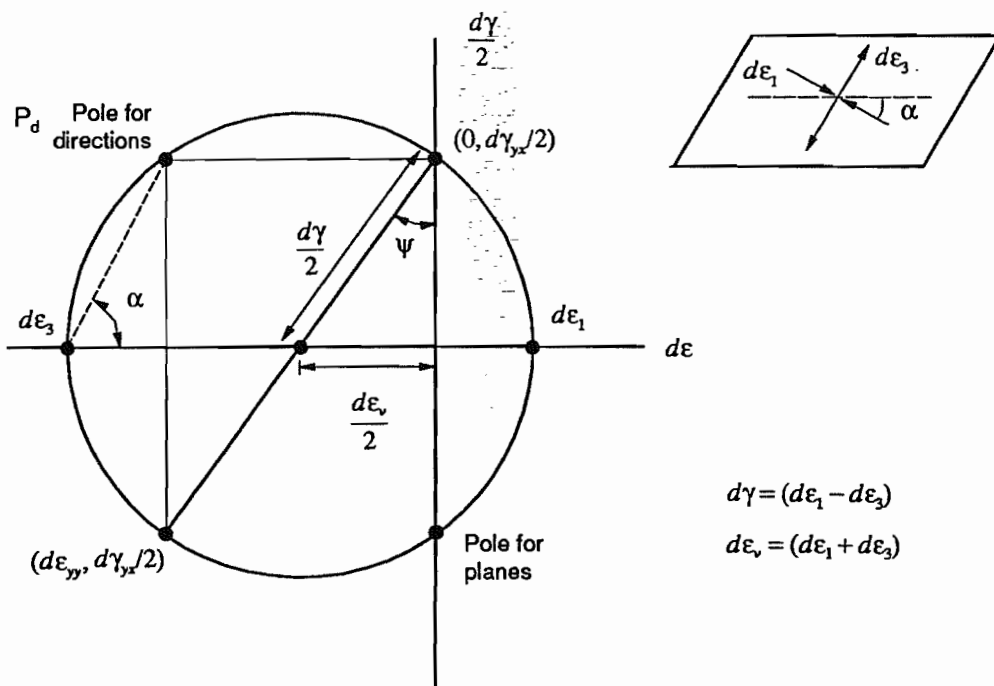
Figure 4.2 - Mohr's circle of incremental strain

Experimental evidence exists in the literature (Roscoe, 1970 and Dyer, 1985) which suggests that the behaviour of a granular soil can be idealised to that of a perfectly plastic isotropic material, as defined by Hill (1950). Therefore, it is possible to combine measured boundary stresses and the Mohr's circle of strain increment to construct a Mohr's circle of

stress, Figure 4.3, giving the true plane strain friction angle of the soil. An analytical expression relating ϕ'_{ps} to ϕ'_{ds} and ψ can be derived from the geometry of the Mohr's circle and is of the form

$$\sin \phi'_{ps} = \left\{ \frac{\sigma_1 - \sigma_3}{\sigma_1 + \sigma_3} \right\} = \frac{\tau_{yx}/\sigma_{yy}}{\cos \psi (1 + \tau_{yx}/\sigma_{yy} \tan \psi)} \qquad ...(4.4)$$

This method of interpretation is often referred to as the coaxiality analysis.
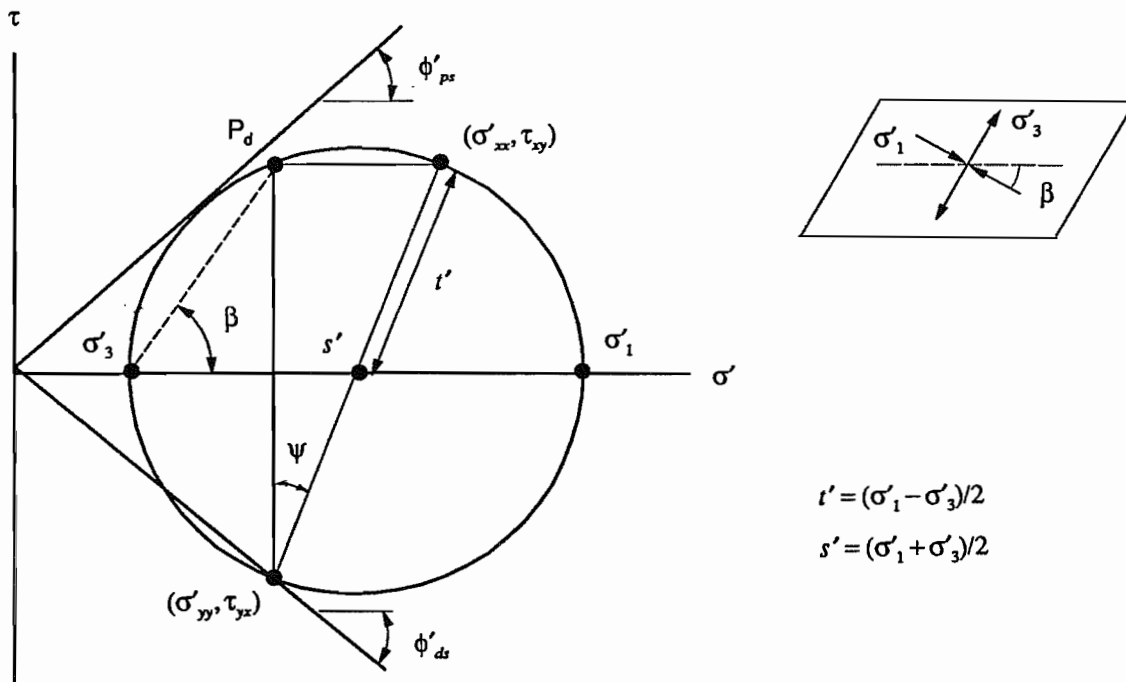
Figure 4.3 - Mohr's circle of stress

Alternatively, instead of using Mohr's circles to interpret the direct shear test flow rules may be used. These relate the state of stress in a plastically deforming soil to the incremental strains and a material constant, usually taken as equal to the critical state shearing resistance of the soil ϕ'_{cv}. Several flow rules are now presented.

Taylor (1948) suggested that a boundary energy correction should be applied to the maximum measured shear stress from direct shear tests in which the normal load is constant. Jewell (1980) presents this correction in the form of the flow rule

$$\frac{\tau_{yx}}{\sigma_{yy}} + \frac{dY}{dX} = m \qquad \qquad \dots(4.5)$$

for use with the direct shear test. Stroud (1971) has shown that Rowe's (1962) flow rule successfully describes the stress-dilatancy behaviour of sands and can be presented for plane strain in the form

$$\sin \phi'_{ps} = \frac{(K-1)+(K+1)\tan \psi}{(K+1)+(K-1)\tan \psi} \qquad \qquad \dots(4.6)$$

where $K = \tan^2(45 + \phi'_{cv}/2)$. Equation (4.6) has also been demonstrated to be valid for the case of non coincidence of principal axes, De Josselin de Jong (1976). Based on the above flow rule, Rowe (1969) developed a simple relationship between the direct shear angle of friction ϕ'_{ds} and the plane strain angle of friction ϕ'_{ps} to explain the difference in strength measured in biaxial compression and direct shear tests. The relationship is

$$\tan \phi'_{ps} = \frac{\tan \phi'_{ds}}{\cos \phi'_{cv}} \qquad \qquad \dots(4.7)$$

and has been shown to provide an excellent correlation with experimental data. However, it is important to note that this is not a flow rule as it does not contain a term dependent on the incremental strains. Finally, Bolton (1986) found the following empirical fit to Rowe's (1962) flow rule

$$\phi'_{ps} = \phi'_{cv} + 0.8\psi \qquad \qquad \dots(4.8)$$

Jewell (1989) observed that the predicted plane strain friction angles given by equations (4.6) and (4.8) correlated well for values of the angle of dilation in the range $0° \leq \psi \leq 25°$, Figure 4.4. He also found that the plane strain friction angle deduced from a modified form of Taylor's energy correction, and given in Stroud (1971), also showed good agreement.

To be able to analyse direct shear test data using flow rules a knowledge of the critical state shearing resistance ϕ'_{cv} is required; this can be estimated from test data, the mineralogy
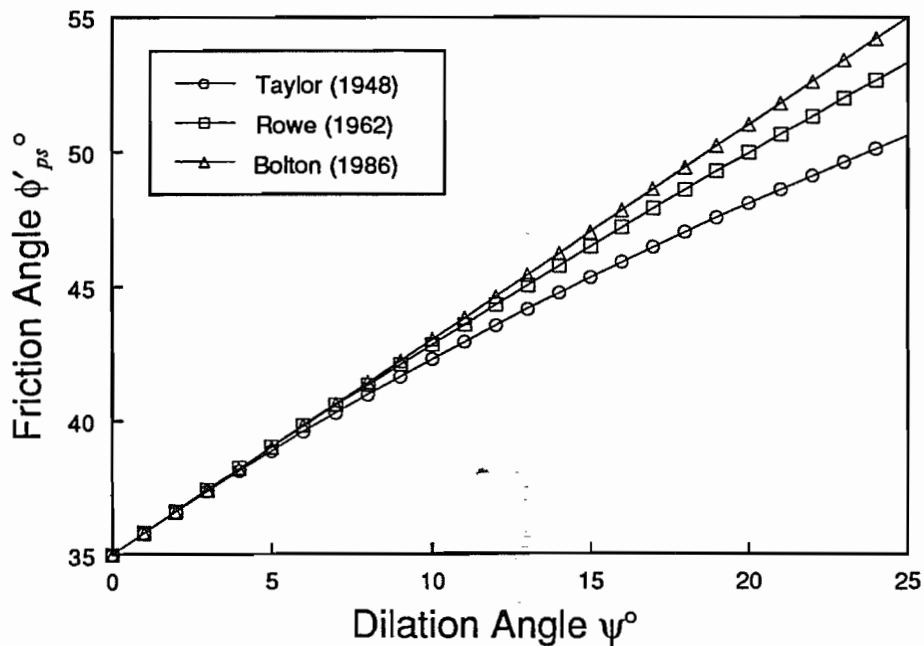
Figure 4.4 - Prediction of ϕ'_{ps} from flow rules for a range of dilation angle ψ. (After Jewell, 1989).

of the soil (Bolton, 1986) or from the angle of repose of a loosely tipped heap of the soil excavated at its toe, Jewell (1989). The accuracy of the results deduced using the flow rule analysis are affected to some extent by the choice of critical state friction angle.

The interpretation of direct shear test data is carried out and discussed further in Chapter 5. More details on the use of flow rules for interpreting direct shear tests, and the likely factors which lead to misinterpretation of data can be found in Jewell and Wroth (1987) and Jewell (1989).

In conjunction with the Mohr's circle analysis, flow rules provide a separate method which may be used to assess the suitability of a particular test set-up to provide repeatable and reliable data. Good agreement between the separate methods of analysis gives confidence in the results.

4.2 Standard Test Sand

The standard test soil used throughout the test programme was Leighton Buzzard 14/25 sand. This is a commonly used quartz laboratory sand composed of sub-angular particles passing the N° 14 sieve (1.40*mm*) but retained on the N° 25 sieve (0.60*mm*).

The particular batch of Leighton Buzzard 14/25 sand adopted as the standard test soil had differing physical properties to previous batches; the particles were slightly less angular in shape and whiter in colour, the darker colour of previous batches being attributed to iron staining. The standard test soil will be referred to as *white* Leighton Buzzard sand and the previous batch as *yellow* Leighton Buzzard. Jewell (1980) observed small differences in the mechanical behaviour between batches of a similar sand, which is an observation also made in the current work and subsequently discussed in Chapter 5.

Table 4.1 compares the properties of the *white* sand with those of the *yellow* sand, as used by Palmeira (1987), and for some comparative tests in the current work. The standard procedures to obtain some of the properties in the table are described in BS1377 (1975).

A series of 12 dense unreinforced direct shear tests was performed in the Medium sized apparatus on both batches of sand to provide a datum with which to assess the effectiveness of modifications to the LDSA. This test series also allowed the mechanical differences between the white and yellow sands to be investigated. Previous research conducted in the Medium shear apparatus by Jewell (1980), Dyer (1985) and Palmeira (1987) has shown that it can be used to give reliable results.

Sand	Spec. Gravity	Voids ratio		Max. Unit Weight	Mean Particle Size	Coeff. Uniformity	Particle size range
	G_s	e_{max}	e_{min}	γ_d (kN/m^3)	$D_{50}(mm)$	C_u	(mm)
White	2.654	0.77	0.47	17.71	0.70	1.25	0.6-1.18
Yellow	2.65	0.79	0.49	17.51	0.80	1.30	0.6-1.18

Table 4.1 - Summary of the properties of the standard test sand compared with those of yellow sand.

4.8

Shearbox	Sand type	Density	Test voids ratio e_{test}	Relative density $I_d = \dfrac{e_{max} - e_{test}}{e_{max} - e_{min}} \times 100\%$
Medium	White	Dense	0.48 ± 0.01	95%
	Yellow	Dense	0.50 ± 0.01	93%
Large	White	Med.dense	0.60	55%
	White	Dense	0.50 ± 0.01	90%

Table 4.2 - Summary of approximate sample densities for unreinforced direct shear tests.

Figure 4.5 compares the behaviour of the white and yellow sands in the Medium shear apparatus. The data presented are from five dense direct shear tests with a range of applied vertical stress from $\sigma'_v = 31kN/m^2$ to $\sigma'_v = 52kN/m^2$. The normalised shear stress (τ_{yx}/σ'_v) shown on the left hand axis, and plotted against shear displacement X, clearly shows that despite the similarities between the two sands (Table 4.1) the yellow sand has a significantly greater strength. The measurement of dilation Y shown on the right hand axis confirms this finding by illustrating the tendency of the yellow sand to dilate more strongly than the white sand.

The measured peak shearing resistance for the tests on white sand with $\sigma'_v \approx 30kN/m^2$ was $(\tau_{yx}/\sigma'_v)_{max} \approx 0.85$ and the corresponding rate of dilation was $(dY/dX) \approx 0.26$, giving a direct shear angle of friction of $\phi_{ds} \approx 40°$, equation (4.2), and an angle of dilation $\psi \approx 14.5°$ from equation (4.3). Using the Mohr's circle analysis, equation (4.4), gives a plane strain angle of friction of $\phi_{ps} \approx 46°$ for white sand.

For the yellow sand the direct shear angle of friction was $\phi_{ds} \approx 47°$ and the dilation angle $\psi \approx 26°$, corresponding to a plane strain friction angle of $\phi_{ps} \approx 52°$, confirming the greater strength of the yellow sand compared with the white.

Although not shown for all tests in Figure 4.5 a high degree of repeatability was observed.
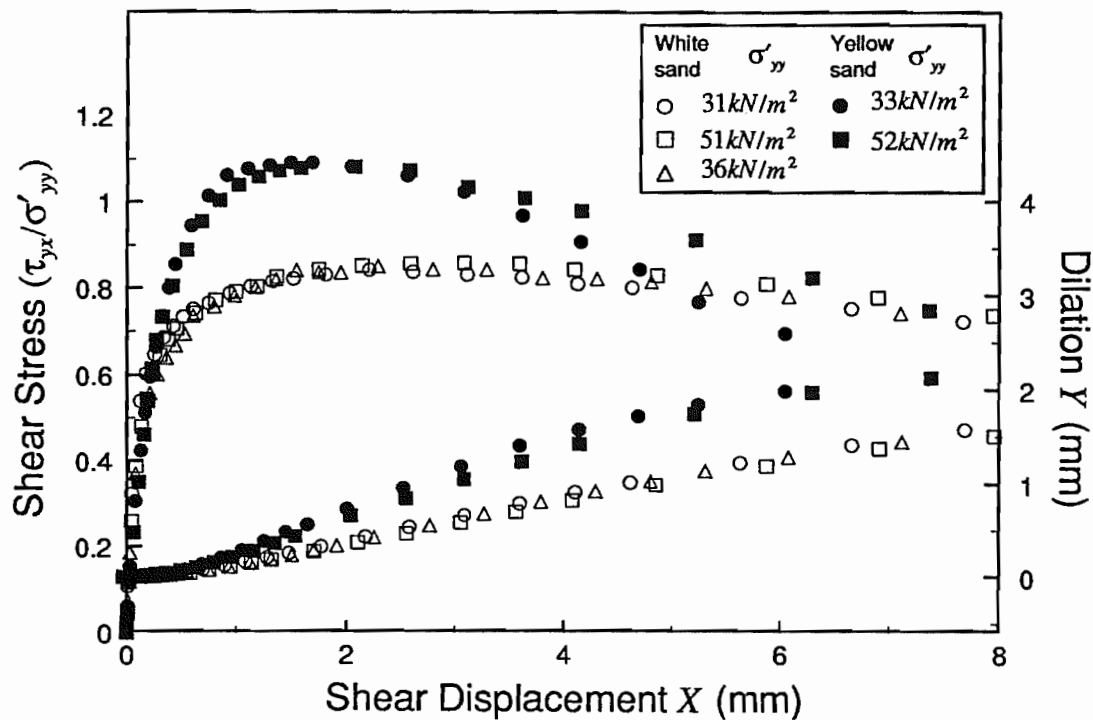
Figure 4.5 - Direct shear test data for white and yellow Leighton Buzzard 14/25 sand. Shear displacement versus normalised shear stress (left hand axis) and dilation (right hand axis).

4.3 Large Unreinforced Direct Shear Tests

Two series of unreinforced direct shear tests were performed in the LDSA, both of which used white Leighton Buzzard 14/25 sand; the first test series was with medium dense sand and a vertical stress σ'_v in the range $45kN/m^2 - 145kN/m^2$ comprising 6 tests, the second with dense sand and σ'_v in the range $30kN/m^2 - 160kN/m^2$ comprising 9 tests (see Table 4.2). The boundary data from these test series are now presented and discussed.

4.3.1 Boundary measurements

As described in Section 4.1, there are four principal measurements required to interpret the direct shear test, and all of these quantities are boundary measurements. Typical boundary data from a dense direct shear test with a vertical stress, $\sigma'_v \approx 100kN/m^2$ are presented in

Figure 4.6 as a function of the shear displacement X. Figure 4.6(a) shows the measured shear force S and the vertical load p_n applied by the jacks mounted at each corner of the shearbox. The total load applied perpendicular to the shear plane is

$$P_v = W_{box} + W_{soil} + p_1 + p_2 + p_3 + p_4$$

where $W_{box}(= 12.27kN)$ and W_{soil} are the dead load of the top half of the shear box and of the soil respectively acting on the shear plane, and p_1 to p_4 are the loads applied by the vertical loading jacks.

Figure 4.6(b) shows the relative vertical displacement between the upper and lower halves of the shearbox measured at each corner. The mean vertical displacement is

$$Y = \frac{1}{4}(y_1 + y_2 + y_3 + y_4)$$

where y_1 to y_4 are the vertical displacements measured at each corner of the shearbox.

The following trends are shown in the figure and are in agreement with those observed by Jewell and Wroth (1987):

(i)   between O and A, the shear load S increases linearly with shear displacement, at the same time a decrease in vertical displacement at each corner of the shearbox y_n is observed, with a minimum value being reached at A. The vertical load applied by each jack is constant during this period.

(ii)   after point A has been reached the shear load continues to increase with shear displacement, but at a decreasing rate until a maximum is reached at point B. From point A it is also observed that the vertical displacement at each corner of the shearbox starts to increase as a result of dilation of the soil, this being more or less linear with shear displacement. However, there is a slight difference in vertical displacement between the front (circles) and rear (squares) of the shearbox. This difference corresponds to a tilt of approximately 1:1000, comparing well with the worst tilt observed in any test of 3:1000. Also noted is a fluctuation in the applied vertical loads; this is explained by the dilation of the sample requiring the piston
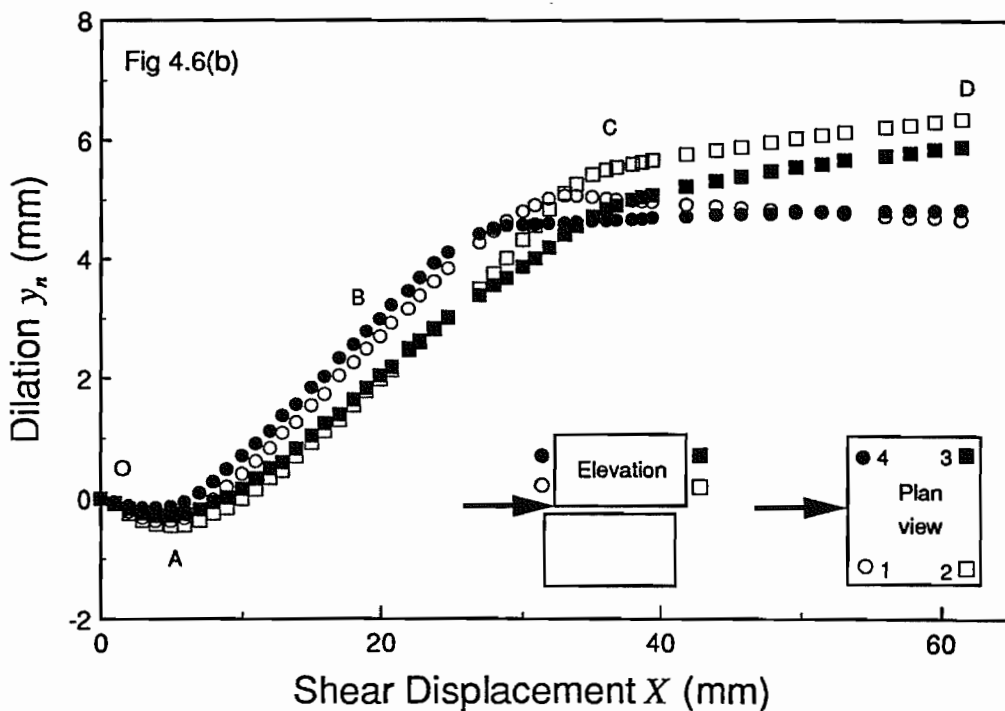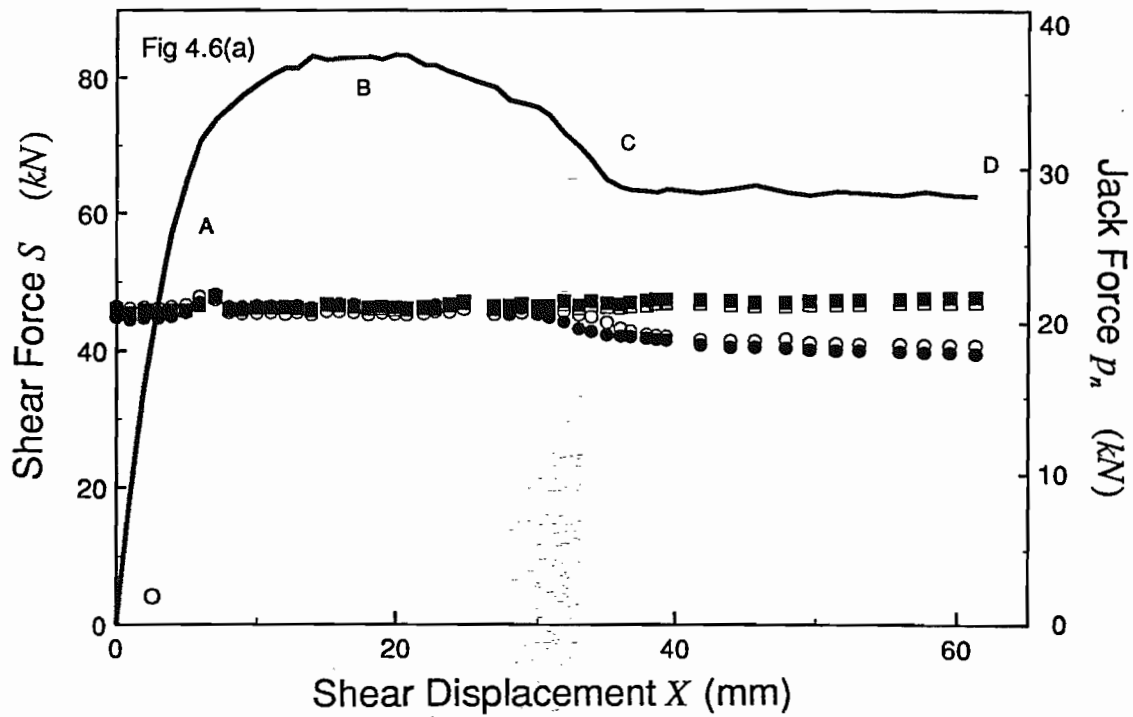
Figure 4.6 - Typical boundary data from a large direct shear test with $\sigma'_v \approx 100 kN/m^2$ **plotted against the shear displacement** X. **(a) Shear load** S **and load measured in each of the vertical loading jacks** p_n **and (b) the vertical displacement** y_n **at each corner of the shearbox.**

in each jack to move out suddenly. Any movement of a piston within a jack requires firstly a flow a hydraulic fluid, resulting in viscous forces being mobilised and secondly a mobilisation of the friction between the piston and jack body. Until these forces have come into equilibrium a temporarily high force in the jacks is observed, such forces are reduced to a minimum by slowing down the rate of shear displacement and consequently the rate at which vertical displacements occur.

(iii)   between points B and C it is observed that the shear load starts to decrease, as does the rate of dilation. At point C a sharp change of gradient is observed in both the shear load and vertical displacement curves which corresponds to the cessation of dilation.

(iv)   following point C, the shear load remains constant until point D, the end of the test. It is observed that the load applied in the front two vertical loading jacks drops at point C, whereas the load in the rear two increases slightly. This can be explained by the vertical jack loads adjusting themselves to compensate for the counter clockwise moment acting on the sample as a result of the eccentricity between the shear load S and the centroid of the sample. This eccentricity occurs as a result of sample dilation moving the centre of gravity of the sample relative to the point of application of the shear load. The moment applied to the sample in turn leads to the observed rotation of the top half of the shearbox at large shear displacements. The relative displacement of the top half of the shearbox is seen to increase with shear displacement, the vertical displacement falling at the front of the shearbox relative to that at the rear, with a final relative displacement in the range 3mm to 6mm at the end of the test.

Although tilting of the top half of the shearbox is observed in the LDSA, the magnitude of the rotations is of the order 5 to 10 times less than those noted by Airey (1987) in the standard Casagrande shearbox. The problem of tilt has been partly cured by fixing the top platen to the top half of the shearbox to give symmetrical boundary conditions. Further reductions in rotation may be possible with modifications to the system used to apply shear

and vertical loads. Such changes would involve a shear load jack which can compensate for eccentricity of the shear force and a separate control of the load in each vertical loading jack.

In order to overcome small fluctuations in the vertical load the mobilised shear stress should be normalised with respect to the vertical stress acting on the central plane. Data normalised in this way from the LDSA are presented in Figure 4.7 for dense sand ($I_d = 88\%$) and in Figure 4.8 for medium dense sand ($I_d = 55\%$), for a range of vertical stresses. In both of the figures typical trends are observed, such as decreasing initial stiffness, reduced peak strength and reduced dilation with increasing vertical stress. These phenomena have been observed by other researchers including Jewell (1980), Dyer (1985) and Palmeira (1987). Also observed in the figures is a degree of repeatability consistent with a reliable method of sample preparation and test procedure.
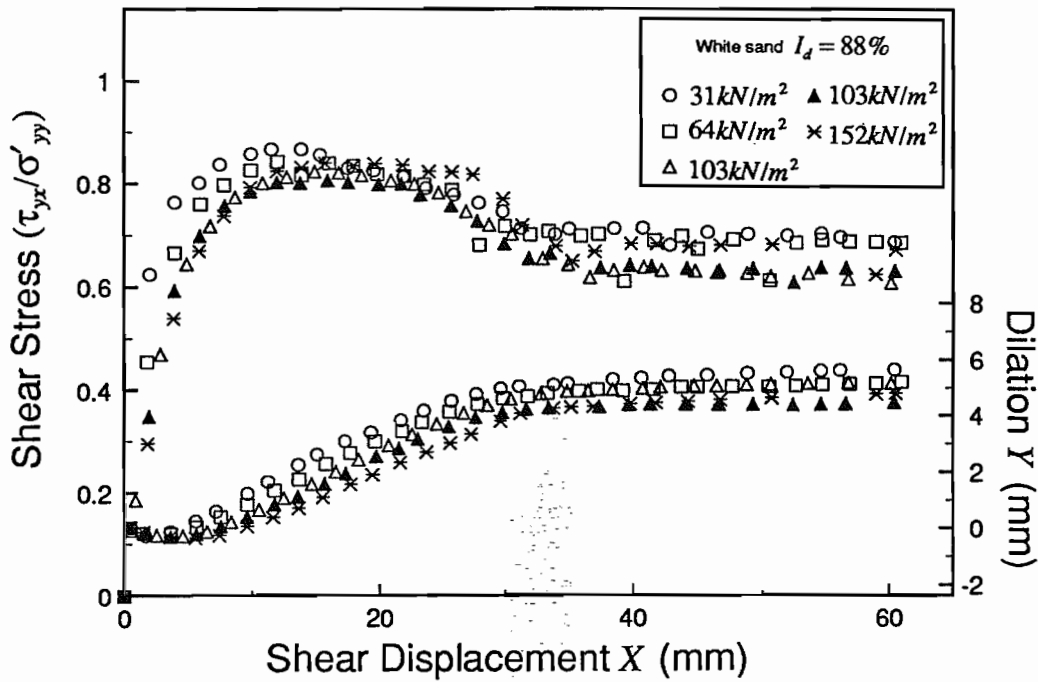
Figure 4.7 - Boundary data for tests in the LDSA on dense Leighton Buzzard 14/25 sand at various values of σ'_v.
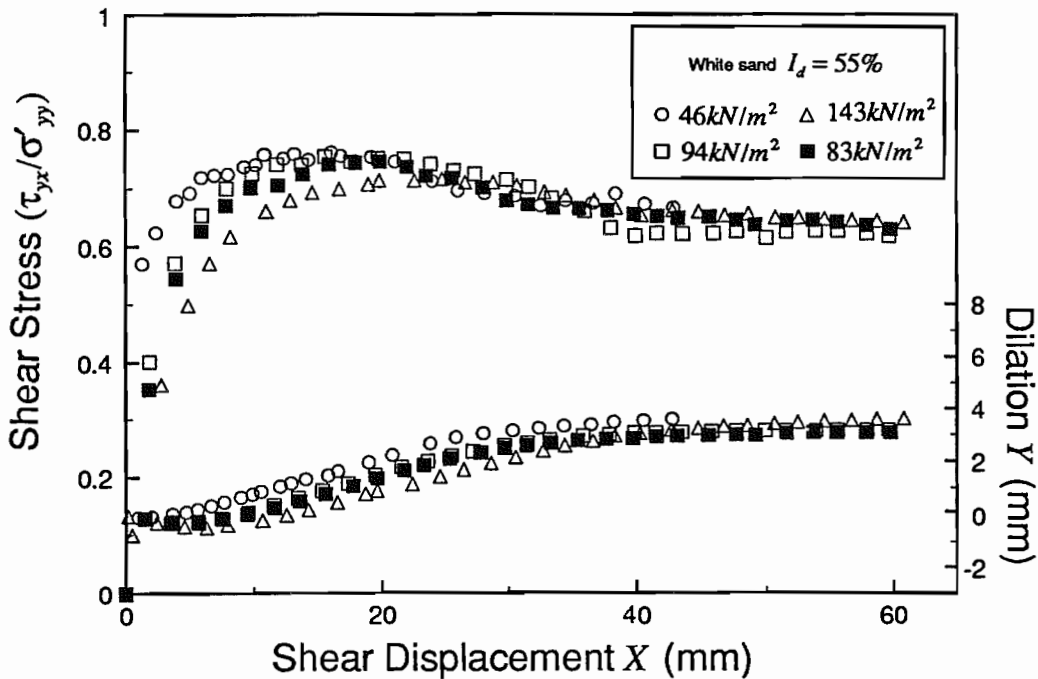
Figure 4.8 - Boundary data for tests in the LDSA on medium dense Leighton Buzzard 14/25 sand at various values of σ'_v.

4.3.2 Internal photographic measurements
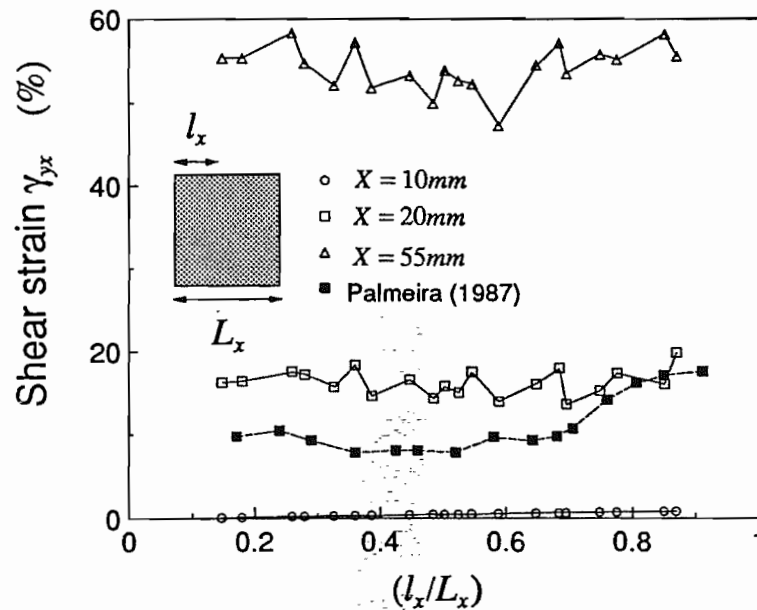
Figure 4.9 - Variation of shear strain γ_{yx} across the central plane of the LDSA at different stages during a test. Also shown are data from Palmeira (1987) at peak stress ratio.

As described in Section 3.1.3, during some of the unreinforced direct shear tests photographic measurements of the displacement of markers placed in the sand were taken, from which estimates of the soil strains were obtained. Several factors influence the accuracy of the measurements; these include the relative size of the markers to the size of the photographic image, the physical size of the markers and the photographic hardware and digitising apparatus used.

Observations of the calculated volumetric and shear strains indicated a great deal more scatter in the values of volumetric strain compared with the shear strain. This results from the large relative horizontal displacement of markers on either side of the shear plane compared with their vertical displacements. The distribution of shear strain γ_{yx} across the shear plane is shown in Figure 4.9 at different stages during a test in which $\sigma'_v \approx 100 kN/m^2$. It is seen that a good uniformity of shear strain is exhibited throughout the test. Similar data at peak shear stress from Palmeira (1987) before modification of the apparatus are shown, where it can be seen that the previous arrangement exhibited slightly less uniformity.
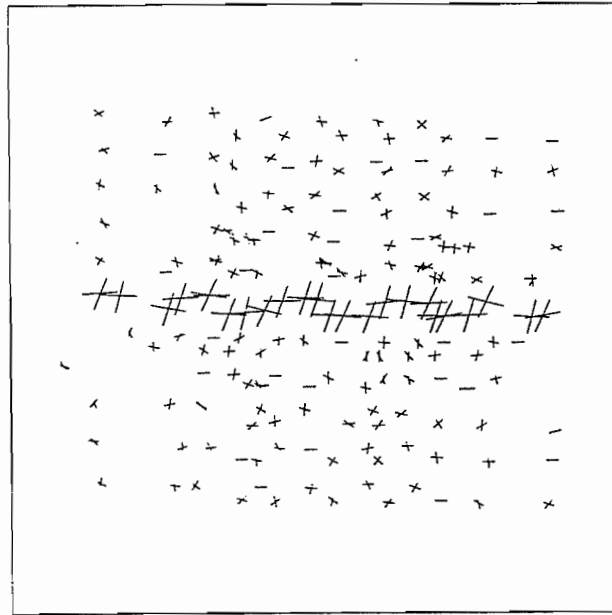
Figure 4.10 - Plot of zero extension directions for a test with $\sigma'_v \approx 100\text{kN/m}^2$ at peak stress ratio.

From data on the incremental strains, a plot of zero extension directions at peak stress ratio ($X \approx 20mm$) is shown in Figure 4.10 for the same data as presented in Figure 4.9. This data supports, allowing for experimental scatter, the observations of Jewell (1980) and Dyer (1985) that the horizontal direction in the shearbox is one of no linear incremental strain.

4.3.3 Comparison of test data from the LDSA with the medium shearbox

The mobilised shear stress τ_{yx} can be normalised by the normal stress σ_{yy} as shown above. However, it is not possible to find a parameter with which to normalise the shear displacement X or the vertical displacement Y, allowing comparison between shearboxes of different size. Of course, if the dimensionless quantities of shear strain γ_{yx} and volumetric (vertical) strain ε_{yy} have been measured, comparison between different shearboxes is relatively straightforward.

Palmeira (1987), normalised shear and vertical displacement data by the observed shear band thickness h (i.e. giving estimates of the shear and volumetric strains) from three

different shearboxes with limited success. There are several criticisms with this method of normalisation; firstly it is difficult to estimate the shear band thickness h with any degree of accuracy (it also be increases throughout a test), and secondly the shear band thickness h is only really relevant when the soil is behaving plastically. Therefore, it is unlikely that this parameter will fit the data at the beginning of the test when some elastic behaviour exists.
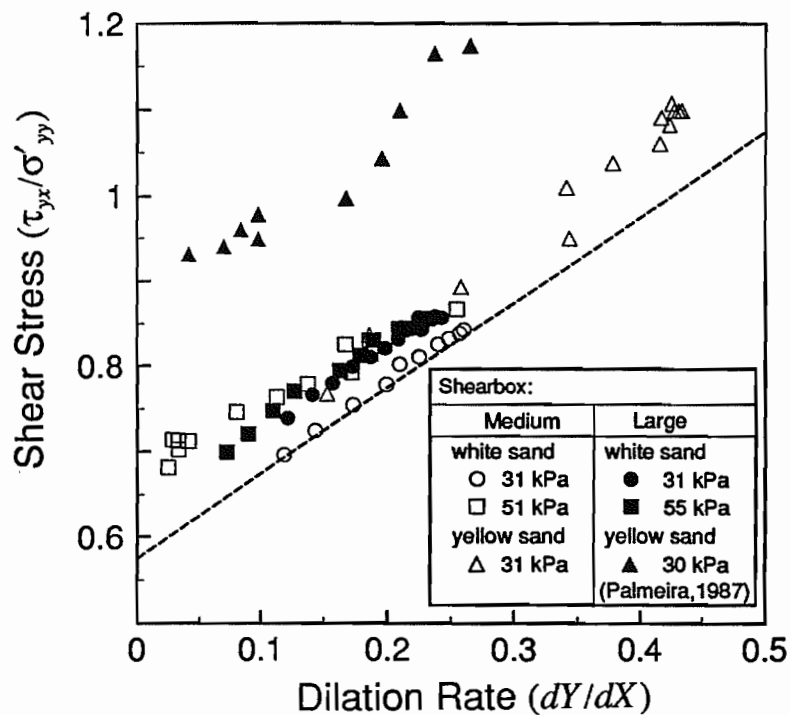
Figure 4.11 - (τ_{yx}/σ_{yy}) versus (dY/dX) for data from the medium and large direct shearboxes for dense white Leighton Buzzard 14/25 sand.

Utilising the idea presented by Jewell (1989) of plotting data from direct shear tests in the form (τ_{yx}/σ_{yy}) versus (dY/dX), one has a non-dimensional plot encompassing both the shearing resistance and dilation of the soil. This method can be used to compare data from direct shear apparatus of different dimensions and soil samples of different densities.

Such a plot is an alternative presentation of Taylor's (1948) energy correction and is discussed further in Section 5.1. Jewell (1989) observed that data presented in this way lay

on a slope of 45°, provided that the sample was not free to rotate. Any rotation resulted in the data lying on a steeper slope as rotation resulted in the underestimation of the rate of dilation dY/dX.

Figure 4.11 presents data for dense white and yellow sand from both the Medium apparatus and LDSA before and after modification. The agreement exhibited for white sand in both shearboxes is very good, with the data lying on a slope very close to 1:1. Comparing the previous arrangement of the LDSA with the medium shear apparatus (Yellow sand, open and solid triangles) it is observed that the LDSA overestimated the shear strength of the soil by a significant factor. From the data it is apparent that by modifying the boundary conditions to a symmetrical form the performance of the LDSA has been enhanced.

4.4 Summary of Conclusions Regarding the Large Direct Shear Apparatus

The following conclusions have been formed with respect to the modified LDSA and the test soil:

(i)   boundary data from the Medium direct shear apparatus highlighted a difference in the mechanical properties of different batches of Leighton Buzzard sand. The data obtained provided a datum by which the modified LDSA could be assessed.

(ii)   a comprehensive series of tests in the LDSA was presented for two sample densities, illustrating a good degree of repeatability, therefore giving confidence in the method of sample preparation and test procedure.

(iii)   boundary data from the LDSA agreed well with data from the Medium direct shear apparatus. Tilting of the top half of the apparatus was observed and attributed to an eccentricity of the applied shear force. This resulted in some asymmetry of the applied vertical load about the central plane. However, this phenomenon was not apparent until large relative shear displacements and the cessation of dilation, indicating that the modifications to the boundaries of the LDSA were successful. This conclusion is supported by data from photographic measurements of markers placed in the sand, which indicated good uniformity of shear strain across the central

plane. It was also observed that the central plane of the shearbox approximated to a direction of no linear incremental strain supporting the observations of other researchers.

(iv)   improvements were suggested to the method of applying the vertical and shear loads in order to enhance the performance of the LDSA.

CHAPTER 5:

ANALYSIS OF UNREINFORCED DIRECT SHEAR TESTS

In the previous chapter a framework for the interpretation of the direct shear test was presented along with boundary data from the Medium and Large Direct Shear Apparatus. The objective of this chapter is to use this data to investigate the various methods of interpretation and to compare the parameters obtained with data from the literature, and those predicted with Bolton's (1986) stress-dilatancy index. Comments are also made with respect to the mechanical behaviour of white and yellow Leighton Buzzard sand.

5.1 Friction Angles Deduced from Direct Shear Test Data

In Chapter 4 it was explained that only the direct shear angle of friction ϕ'_{ds} can be obtained directly from boundary data from the direct shear test, and that if the true plane strain strength of the soil is required then assumptions about the stress and strain in the soil have to be made. The data from direct shear tests in the LDSA and Medium apparatus are now analysed using the various interpretive analyses described earlier.

5.1.1 Deduced plane strain friction angle ϕ'_{ps}

Mobilised plane strain angles of friction $(\phi'_{ps})_m$ deduced from test data for the white sand in the LDSA at $\sigma'_v \approx 100 kN/m^2$ are plotted in Figure 5.1, for all stages during the test. The mobilised friction angles are obtained from the following analyses: Mohr's circle

analysis, equation (4.4), Rowe's flow rule in the form of equation (4.6), Rowe's relationship between ϕ'_{ps} and ϕ'_{ds}, equation (4.7), Bolton's flow rule, equation (4.8), and the plane strain strength based on the direct shear strength obtained from Taylor's energy correction, Stroud (1971). For the analyses requiring the critical state shearing resistance of the soil it is assumed $\phi'_{cv} = 34°$, as this is within the typical range $33° \leq \phi'_{cv} \leq 35°$ usually associated with quartz sands.
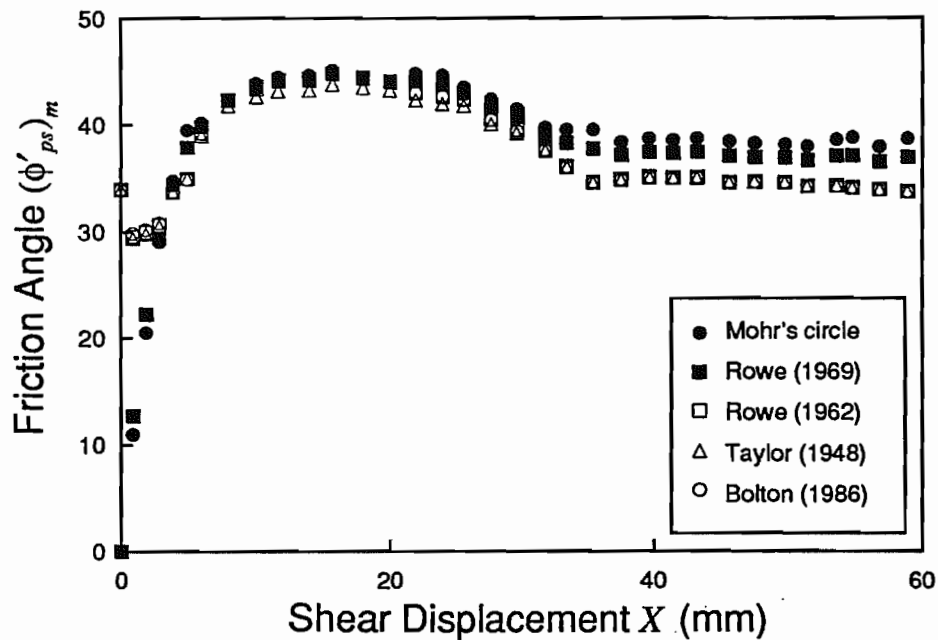
Figure 5.1 - Comparison between the mobilised plane strain angle of friction $(\phi'_{ps})_m$ deduced from different methods of analysis.

The various methods of analysing the plane strain strength appear to exhibit very good agreement over a large range of the test. In the initial loading stage it is observed that the analyses based on flow rules are unable to provide any useful information. The mobilised plane strain strength from the other two analyses should also be treated with some caution owing to the effect of non-coincidence of stress and strain rates on the calculation. Between a shear displacement of $X = 10mm$ to $X = 30mm$ the agreement between all of the analyses can be described as excellent, and gives a great deal of confidence in the test set up and the measurement of sample dilation.

As might be expected from Figure 4.4 the flow rule analyses predict almost identical values throughout the test. Owing to the complicated nature of Rowe's flow rule and that based on Taylor's energy correction there appears to be a very good case for adopting the simple flow rule proposed by Bolton (1986), equation (4.8). Similarly, although giving a slightly higher shearing resistance than the flow rules, equation (4.7) also provides a simple method for deducing the plane strain strength. This method also has the distinct advantage that it is much less sensitive to the assumed critical state friction angle than the flow rule analyses, and will not lead to gross errors in predicted strengths provided a sensible estimate of ϕ'_{cv} is made.

Relative Density I_d (%)	Vertical Stress σ'_{yy} (kN/m^2)	Dilation Angle ψ°	Direct Shear $\phi'_{ds}{}^\circ$	Peak plane strain friction angle $(\phi'_{ps})_{peak}{}^\circ$		
				Mohr's circle eq^n(4.3)	Rowe eq^n(4.7)	Bolton eq^n(4.8)
55	46	9.1	37.5	43.7	42.7	41.3
	73	8.4	35.5	40.7	40.7	40.7
	83	7.8	36.7	43.1	42.0	40.2
	94	8.5	37.1	43.3	42.3	40.8
	143	7.7	35.6	41.2	40.8	40.2
88	31	14.6	40.9	46.9	46.3	45.7
	55	12.9	40.4	46.9	45.7	44.3
	64	12.9	40.0	46.2	45.3	44.3
	76	13.1	40.5	46.9	45.8	44.5
	103	13.4	39.5	45.1	44.8	44.8
	103	12.8	39.9	46.2	45.3	44.2
	152	11.5	39.9	46.7	45.2	43.2
	158	11.9	38.6	44.3	43.9	43.5

Table 5.1 - Comparison between methods of predicting peak plane strain friction angles from direct shear test data.

Of interest is that if one examines the difference in deduced plane strain strengths towards the end of the test, when dilation has ceased, it is clear that the measured shearing resistance is greater than the expected simple shear strength. This highlights the problem of using the Mohr's circle analysis alone for the prediction of the plane strain strength.

Typically the shear stress on the central plane is an overestimate and the dilation, depending on the boundary conditions, an underestimate leading to an overprediction of ϕ'_{ps} with this method.

Table 5.1 presents the analysis of the peak plain strain strength $(\phi'_{ps})_{peak}$ deduced from the boundary measurements of all tests carried out in the LDSA.

The data in Table 5.1 generally show good agreement between the three methods of calculating the plane strain friction angle. The flow rule analysis tends to give a lower strength whereas the Mohr's circle analysis gives an upper strength, with that from Rowe's relationship falling between the two. By increasing the value of the critical state shearing resistance the disparity between the strengths becomes less, however, it is not until the critical state strength is well outside the typical range of $33° \leq \phi'_{cv} \leq 35°$ that the difference becomes nominal. From the data it appears the LDSA may slightly underpredict the dilation angle from boundary measurements, or that it marginally overestimates the shear stress ratio on the central plane, or possibly a combination of these factors exists which leads to an overprediction of strength with the Mohr's circle analysis, but an under prediction with Bolton's flow rule.

Rowe's relationship between direct shear and plane strain is therefore preferred as it is relatively insensitive to the choice of ϕ'_{cv}, and the strength predicted is not dependent on measurements of dilation, which appears to be a major source of error in direct shear testing and can lead to conservatism with flow rules. The most significant source of error in the analysis of direct shear test results with this method is with the typical overestimate of the shear stress ratio on the central plane in the direct shear test.

5.1.2 Deduced critical state friction angle ϕ'_{cv}

The critical state friction angle is that mobilised when a sample shears at constant volume and represents the minimum shear strength that a soil can display, it is therefore a useful design parameter. There are several ways of interpreting direct shear test data which

lead to the critical state shearing resistance and these are now described.
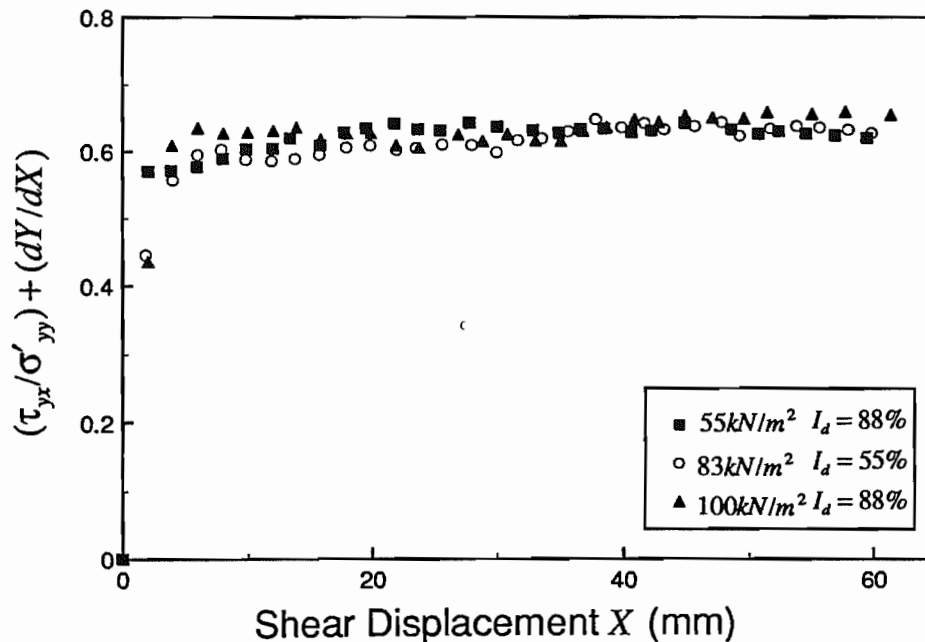
Figure 5.2 - Taylor's (1948) energy correction plotted as a function of shear displacement for data from three large direct shear tests.

Data from three tests in the LDSA are presented in Figure 5.2 by plotting Taylor's (1948) energy correction ($\tau_{yx}/\sigma_{yy} + dY/dX$) against shear displacement X. It is seen, ignoring the initial data, that the function does not assume a constant value, but one rising very slightly with shear displacement. Theoretically, equation (4.5) plots as a line parallel to the horizontal axis of shear displacement and intercepts the vertical axis at a value m

$$\sin(\phi'_{cv})_{ps} = m = \tan(\phi'_{cv})_{ds} \qquad \qquad \ldots(5.1)$$

This comes from comparing equations (4.2) and (4.4) with equation (4.5) for the case when the rate of dilation dY/dX is zero, that is, when constant volume shear is occurring in the soil.

The data in Figure 5.2 intercepts the vertical axis in the range $m = 0.60 - 0.62$, which is slightly less than found by Jewell (1980) and Palmeira (1987), but greater than $m = 0.575$ observed by Stroud (1971) in the simple shear apparatus. Along with the data presented in Section 5.1.1 this would lead one to conclude that the LDSA, and indeed the direct shear

apparatus in general measures a slightly higher shear strength on the central plane than the simple shear apparatus, by between 5% and 10%. Airey (1987) who performed tests on two modified versions of the standard Casagrande direct shear apparatus noted that the measured strength was sensitive to the boundary conditions and any sample rotation occurring during a test.
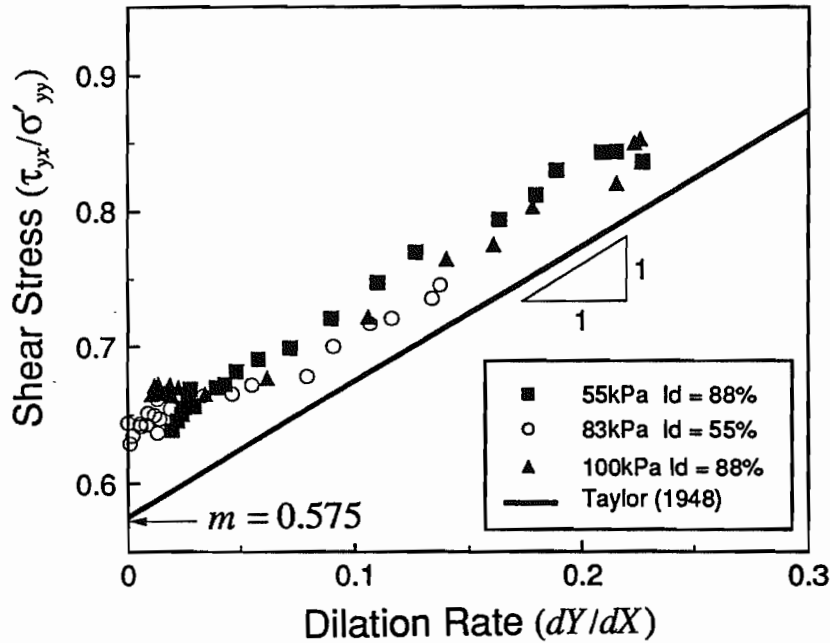
Figure 5.3 - Alternative representation of Taylor's (1948) energy correction which may be used to estimate the critical state shearing resistance.

An alternative method of plotting Taylor's energy correction was shown in Figure 4.11, where it was used to compare data from different shearboxes and sand batches. By rearranging equation (4.9) to

$$\frac{\tau_{yx}}{\sigma_{yy}} = m - \frac{dY}{dX} \qquad \qquad ...(5.2)$$

and comparing it with data plotted in this way the critical state friction angle can be deduced by extrapolating the data back to the vertical axis to give a value of m which can be substituted into equation (5.1). The data from Figure 5.2 are replotted in this way in Figure 5.3, with post peak data being excluded.

The data in the figure are compared with the theoretical relationship assuming that at the critical state $m = 0.575$, after Stroud (1971). As might be expected from Figure 5.2 the data lie at a slope close to 1:1, and more or less parallel to the theoretical relationship passing through $m = 0.575$. The fact that the data lie close to such a slope is encouraging as this implies that the measurements of dilation are not underpredicted with respect to the shear displacement, Jewell (1989). However, as the data lies above the line passing through $m = 0.575$ it is again apparent that the mobilised shearing resistance is greater than that expected in simple shear, indicating that the direct shear test overestimates the shear stress on the central plane.

Extrapolating the data back to the vertical axis, and ignoring data at low values of dY/dX a range for m of between 0.60 and 0.65 is attained, which is an even greater range than that obtained from Figure 5.2. This range for m when analysed using equation (5.1) leads to a value of $(\phi'_{cv})_{ps}$ from 37° to 41° and $(\phi'_{cv})_{ds}$ of between 31° and 33°.

The major disadvantage with plotting data from the shearbox with this particular method is that any *stick-slip* behaviour tends to increase the scatter of the data making any estimation of the critical state friction angle ϕ'_{cv} less accurate.

By plotting the peak strengths and dilation rates from a series of tests an alternative method for estimating ϕ'_{cv} is found, this is shown in Figure 5.4 for data from white Leighton Buzzard sand in the Medium and Large Direct Shear Apparatus. Also plotted on Figure 5.4 are the ranges of m for $(\phi'_{cv})_{ps} = 33°$ to 35°, or alternatively $(\phi'_{cv})_{ds} = 33°$ to 35°. It is commonly assumed that ϕ'_{cv} for quartz sand is close to 34°, Bolton (1986). It can be seen from the figure that the value of m calculated from $(\phi'_{cv})_{ps}$ is in fact slightly higher than this value and that calculated from $(\phi'_{cv})_{ds}$ is slightly lower.

To recap, plotting data using this form of Taylor's energy correction is very useful as it not only provides a method of estimating ϕ'_{cv}, but also a way of checking the measurement of dilation, comparing different sands, different density samples and data from different shearboxes.
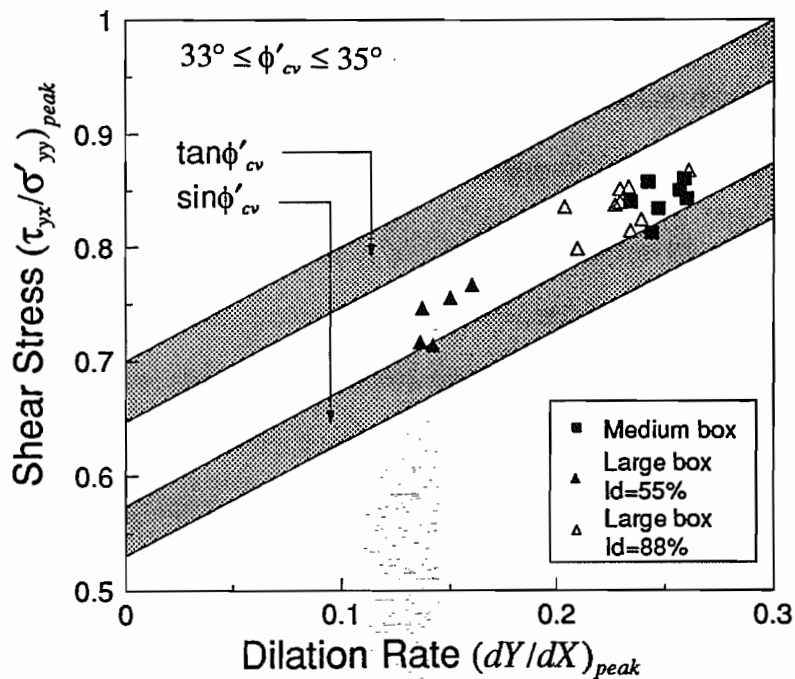
Figure 5.4 - Peak values of $(\tau_{yx}/\sigma_{yy})_{peak}$ versus $(dY/dX)_{peak}$ for direct shear tests on dense and medium dense sand in the medium and large apparatus.

If satisfactory results have been obtained using the Mohr's circle analysis it is possible to substitute the plane strain angle of friction ϕ'_{ps} into Bolton's flow rule along with the corresponding angle of dilation ψ and obtain a value for critical state friction angle from

$$\phi'_{cv} = (\phi'_{ps})_{Mohr} - 0.8\psi \qquad \ldots(5.3)$$

or, alternatively one can use Rowe's relationship between direct shear and plane strain expressed as

$$\phi'_{cv} = \cos^{-1}\left(\frac{\tan\phi'_{ds}}{\tan(\phi'_{ps})_{Mohr}}\right) \qquad \ldots(5.4)$$

Using either of these two methods for calculating the shear strength at the critical state requires care, and it must be borne in mind from the above evidence that the direct shear resistance of the soil appears typically to be overpredicted by 5% to 10% in the direct shear

apparatus, and depending on the boundary conditions, the rate of dilation may also be underestimated. In which case equation (5.3) will lead to a double error as ϕ'_{ps} will be an overestimate from equation (4.4) and ψ an underestimate.

Finally a useful, but quick and crude method of estimating ϕ'_{cv} is to tip a loose heap of sand into a parallel sided container and excavate the soil at its toe, the angle of repose of the soil being considered equal to ϕ'_{cv}.

The methods described above for estimating the critical state angle of friction were used to interpret the data from the LDSA for both dense and medium dense sand and for a range of vertical stresses (Table 5.1). The mean value and standard deviation obtained for each method are presented in Figure 5.5, and details of the calculation given in Table 5.2.

Method	Description of technique
A	ϕ'_{ps} from measured ϕ'_{ds} and ψ, equation (4.4), then equation (5.3) for ϕ'_{cv}.
B	ϕ'_{ps} from measured ϕ'_{ds} and ψ, equation (4.4), then equation (5.4) for ϕ'_{cv}.
C	Plot $\tau/\sigma + dY/dX$ against X, then $\phi'_{cv} = \sin^{-1}($ intercept at $X = 0)$
D	Plot τ/σ against dY/dX, then $\phi'_{cv} = \sin^{-1}($ intercept at $dY/dX = 0$ for best fit 1:1 slope)
E	Plot $(\tau/\sigma)_{peak}$ against $(dY/dX)_{peak}$, then $\phi'_{cv} = \sin^{-1}($ intercept at $dY/dX = 0$ for best fit 1:1 slope)
F	Angle of repose of loose heap of soil

Table 5.2 - Details of the methods used to predict ϕ'_{cv} from LDSA data.

Figure 5.5 provides an interesting comparison of six different methods of analysing the critical state shearing resistance of the soil. It is observed that there is a large variation in the interpreted strengths indicating that even using one particular method no definitive answer is obtained. Using Taylor's energy correction (Methods D and E) provided the best fit to the expected range of values when plotted in the form suggested by Jewell (1989). However, a large range of values was still observed with the strength lying between the critical state strength in simple shear and the critical state strength in direct shear. Using a combination of the Mohr's circle analysis and then a flow rule (Methods A and B) produced

values which were well outside of the expected range, this is probably best attributed to the measurement of a slightly higher strength on the central plane than the direct shear strength, which in Method B leads to a double error in the calculation of ϕ'_{cv}.
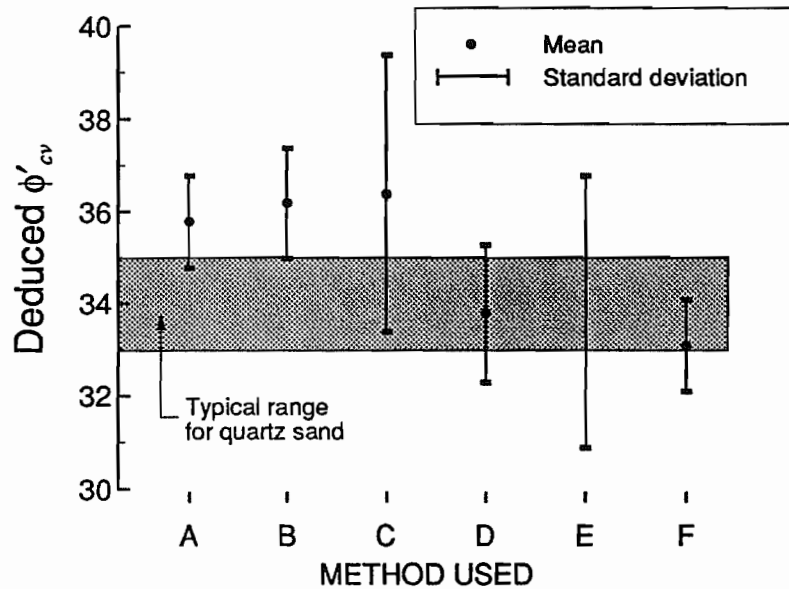
Figure 5.5 - Comparison of methods to estimate the critical state shearing resistance of soil from direct shear test data from the LDSA.

To conclude, the above data indicates that using Taylor's energy correction in the form of equation (5.2) is most likely to give a range for ϕ'_{cv} of the correct magnitude; alternatively the loose heap test gives a quick and simple method which is unlikely to be in gross error. The major problem of estimating ϕ'_{cv} from the direct shear test results stems from the measured shearing resistance being higher than the simple shear resistance of the soil, leading to a small overestimate of ϕ'_{cv}.

5.2 Measured and Predicted Shear Strengths

5.2.1 The strength of white and yellow Leighton Buzzard sand at low stresses

The data presented in Figure 4.5 clearly identified a difference in strength between white and yellow Leighton Buzzard sand. Figure 5.6 presents the measured peak strength

data from tests on white and yellow Leighton Buzzard sand carried out in the Casagrande, Medium and Large shearboxes. In all cases the data are from tests where the relative density of the sample was in the range $85\% < I_d < 95\%$.
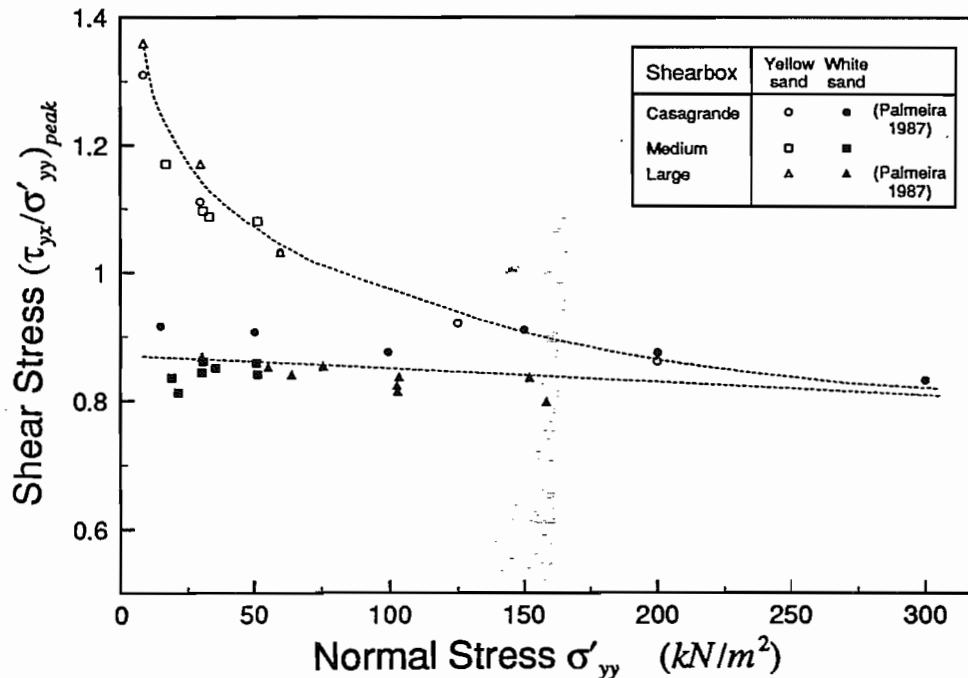
Figure 5.6 - Comparison between measured peak shearing resistances of the white and yellow batches of Leighton Buzzard sand as a function of applied vertical stress.

The most striking feature between the two sands is that at vertical stresses below $\sigma'_v \approx 100kN/m^2$ a large discrepancy arises between the mobilised peak shearing resistances, above this vertical stress the difference is much less discernible and can be wholly attributed to variation in the sample densities.

It was noted in Section 4.2 that the white sand was slightly more rounded than the yellow sand. This leads the Author to hypothesize that the additional strength of the yellow sand at low stresses may be attributed to the extra energy required to dilate the more angular soil particles and to allow shearing of the sample, whereas at higher stresses crushing of the sand occurs allowing it to shear with a lower relative input of energy. This assumption can

also be used to explain the slightly lower minimum and maximum voids ratios of the white sand compared with those of the yellow sand (Table 4.1); the more rounded particles of the white sand are able to move into a denser packing configuration much more freely.

Tatsuoka (1986) has also observed that at low stress levels the shear strength of Toyoura sand appeared almost to exhibit a cut off strength, which is similar to that demonstrated by white Leighton Buzzard sand.

5.2.2 Predicted and observed plane strain shear strengths

Bolton (1986) presents an empirically derived stress-dilatancy function which may be used to predict the peak strength of a granular soil at a given relative density I_d and mean stress $p' = (\sigma'_1 + \sigma'_2 + \sigma'_3)/3$ and is of the form

$$\phi'_{peak} = \phi'_{cv} + k\{I_d(Q - \ln p') - 1\} \qquad \ldots(5.5)$$

where ϕ'_{peak} is the maximum friction angle of the soil, Q is a constant related to the mineralogy of the soil and is given as 10 for quartz sand, and k is a constant set equal to 5 for plane strain and 3 for triaxial compression.

For plane strain it will be assumed that $p' \approx s'$, which results from substituting the mean stress in plane strain, $s' = (\sigma_1 + \sigma_3)/2$, and $\sigma'_2 \approx 0.75s'$, (Stroud, 1971), into the expression given above for p'. With the assumption of coincidence of principal axes and zero extension in the horizontal direction, the mean stress s' can be obtained from the Mohr's circle of stress as

$$s' = \sigma_{yy} + \tau_{yx} \tan \psi \qquad \ldots(5.6)$$

Bolton (1987) suggests that at mean stresses lower than $p' = 150kN/m^2$ the tendency for particles to crush is reduced and that an appreciable change in soil strength may be observed, see Figure 5.6. He therefore advocates using a minimum mean stress of $p' = 150kN/m^2$ in equation (5.5) to avoid over prediction of strength.
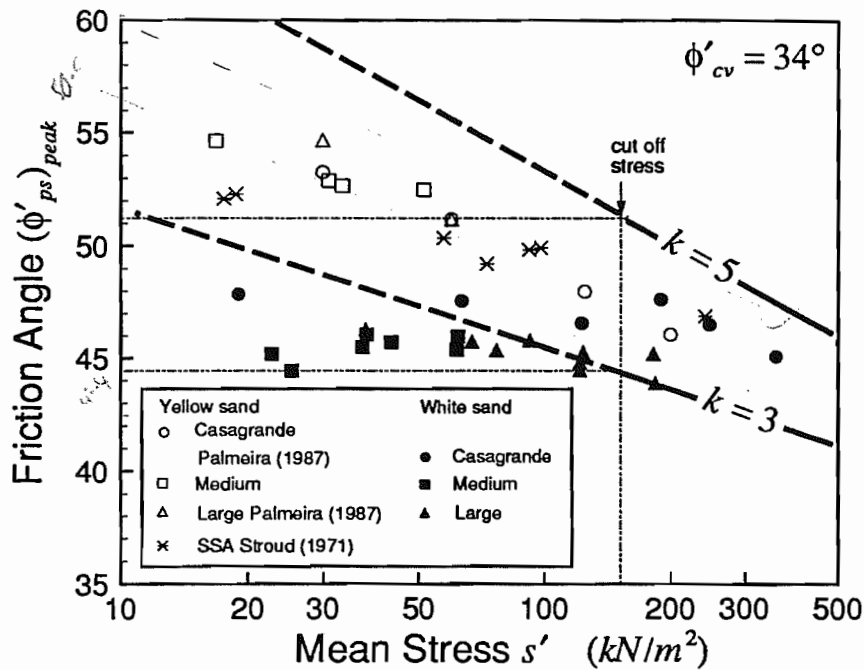
Figure 5.7 - Comparison between measured and predicted plane strain strengths of Leighton Buzzard sand using Bolton's stress-dilatancy index.

The peak strength data in plane strain from the current work (interpreted with equation (4.7) and $\phi'_{cv} = 34°$) and data from the literature are plotted against the mean stress s' in Figure 5.7, along with the theoretical predictions of plane strain and triaxial compression strengths from equation (5.5).

From the figure it is clear that equation (5.5) for $I_d \approx 90\%$ and plane strain overpredicts the strengths exhibited by all of the data . Even when employing the suggested minimum cut off stress of $p' = 150 kN/m^2$ to limit the predicted strength the data are still overestimated by equation (5.5), illustrating that the stress-dilatancy function is non conservative for plane strain strengths. It appears that setting k equal to 3 (corresponding to triaxial compression), and invoking a cut off stress provides a conservative and safe prediction of the plane strain strength. Why therefore, does an empirical fit of this type provide non conservative strengths in plane strain? An examination of the data to which equation (5.5) was fitted, and shown in Figure 5.8, provides some possible explanations to this question:

(i)   the number of plane strain data presented in Bolton (1986) is extremely limited compared with the triaxial compression data, and appears to assume that the equation for both sets of data is identical in form except for the value of k, and that both triaxial and plane strain data share a common intercept on a plot of $\phi' - \phi'_{cv}$ versus I_d. This is clearly illustrated not to be the case, Figure 5.8.
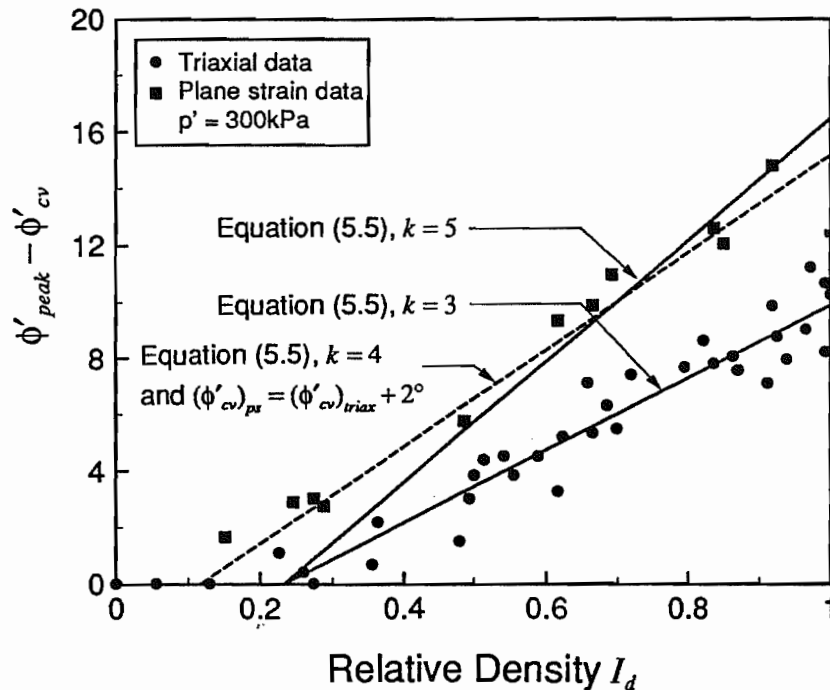
Figure 5.8 - Plane strain and triaxial data used to derive Bolton's stress dilatancy index. (After Bolton, 1986).

(ii)   although it is commonly assumed that the critical state friction angle is a material property and not a function of the test configuration used, the data in Bolton (1986) would perhaps suggest otherwise; a 2° difference between the plane strain and triaxial compression critical state shearing resistance would lead to a common intercept in Figure 5.8.   Bolton (1987) comments on an observed difference between triaxial friction and plane strain critical state strengths.   The author's observations also point to the fact that critical state strengths are influenced by the particular test set-up; this point obviously requires further research.

Although the constant Q may have some effect on the predicted plane strain strength it can be shown that it merely changes the slope of the empirical correlation, but does not improve its fit with respect to the plane strain data.

In Figure 5.8 it is shown that if k has a value of 4 and if the critical state friction angle is 2° greater in plane strain than in triaxial compression a much better fit is obtained to the plane strain data (dashed line). Therefore, it is recommended that such an approach be taken when using Bolton's stress dilatancy function for the prediction of plane strain strengths, otherwise the triaxial strength prediction should be adopted, especially for design purposes as this is both safe and not overtly conservative for plane strain.

5.3 Conclusions Concerning Analysis of Direct Shear Test Data

Several different methods were used to interpret the unreinforced direct shear test data from the LDSA, from which the following conclusions have been formed:

(i)   data from the LDSA indicates that the shear stress mobilised on the central plane of the shearbox is higher than that for a soil deforming in simple shear, it appears that this is indigenous to the direct shear test. However, if Taylor's energy correction is valid, and the measurement of the dilation occurring during shear is not underestimated it is possible to bypass the measured stress ratio to obtain the true plane strain soil strength.

(ii)   the use of the Mohr's circle analysis in conjunction with flow rule analyses provides a method by which deduced plane strain strengths can be compared and anomalies highlighted. If there is a large discrepancy between the deduced strengths then it is apparent that the boundary measurements are in error.

(iii)   the direct shear test can be used to estimate the critical state friction angle ϕ'_{cv}.

However, because the measured shearing resistance on the central plane is greater than the resistance in simple shear the value of ϕ'_{cv} is an overestimate, therefore

caution should be exercised. It was found that the method giving predicted values closest to the expected range for a quartz sand was Taylor's energy correction in the form of equation (5.2).

The difference between the measured strengths exhibited by the white and yellow Leighton Buzzard sand was attributed to the angularity of the yellow sand compared with the white and to the applied vertical stress, which can lead to particle crushing at higher stresses.

The method proposed by Bolton (1986) to predict the plane strain strength of granular soil was found to overestimate the plane strain strength of quartz sand from tests in the LDSA and from data in the literature. It is concluded that the predicted strength in triaxial compression provides a conservative estimate to the observed behaviour and is therefore more suitable for design.

Finally, it is suggested that further research is required to investigate whether the critical state shearing resistance can be considered a true material property of the soil, and how to overcome the problem of different critical state strengths in triaxial and plane strain.

CHAPTER 6:

RESULTS OF REINFORCED DIRECT SHEAR TESTS

The direct shear apparatus has been used before to investigate soil-reinforcement interaction and the potential benefits to soil shear strength derived from the presence of reinforcement. Jewell (1980) was the first to test reinforced soil in the direct shear apparatus and performed a systematic study of soil-reinforcement interaction by testing grid and bar type reinforcements. Juran et al. (1981) carried out shearbox tests on instrumented circular bar reinforcement; these tests were later modelled by Shaffiée (1986) using the finite element technique. Marchal (1984,1986) reports data from similar tests using both circular and rectangular section reinforcement. Studies in the direct shear apparatus were advanced by Dyer (1985) who used a photoelastic technique to investigate the stresses acting between an artificial granular soil (crushed glass) and reinforcement.

All of the above studies suffered from a potential problem of scale, for example that which might arise from the relative size of the soil particles to the reinforcement, however, Palmeira (1987) demonstrated that scale was not a problem by repeating the tests in a large direct shear apparatus. It is this apparatus that was modified by the Author to carry out the study of soil-reinforcement interaction described in this dissertation.

The experimental programme concentrated on the use of soil-reinforcement in shear, and comprised several series of tests to investigate:

(i)   reinforcement orientation.

(ii)   reinforcement bending stiffness and plastic moment capacity.

(iii)   soil density and bearing strength.

(iv)   methods of reinforcement installation and surface texture.

General details of the test programme are given, followed by a description of the reinforcement materials and properties. Specific details of each test series and the results of the tests are then presented.

6.1 General Comments

A total of 29 tests on reinforced white Leighton Buzzard 14/25 sand were performed in the LDSA. Most of these tests were carried out using mild steel bar reinforcement of total length $L = 920mm$ placed symmetrically in the shearbox, both in plan and in elevation, Figure 6.1. Two reinforcement bars per test were used and placed at an angle θ to the vertical, where θ is defined positive as shown in Figure 6.1. Three methods of installing the reinforcement were used, they were: (i) placing the reinforcement at the time of sample preparation, (ii) forming a void in the soil sample and grouting in the reinforcement, and (iii) driving the reinforcement into the sample. The last two of these techniques were aimed at simulating common methods of installing soil nails in practice.

In approximately half of the tests one of the reinforcing bars was instrumented with resistance strain gauges in order to measure the axial force P_{ax} and the bending moment M. The R.D.P. Translog system described in Chapter 3 was only able to monitor up to 10 strain gauges in 1/4 bridge formation. For tests where the number of strain gauges exceeded 10 additional capacity was provided by a Mowlem Microsystems ADU datalogger.

Boundary data from two typical reinforced tests are shown in Figure 6.2 with the corresponding unreinforced tests at the same relative density I_d and applied vertical stress $\sigma'_v (\approx 100kN/m^2)$. The data are from tests on samples reinforced with 2N° mild steel bars of diameter $D = 25mm$; one sample was prepared with a relative density $I_d = 55\%$ and the other with $I_d = 90\%$. The left hand axis in Figure 6.2 gives normalised shear stress (τ/σ'_v) and the right hand axis the sample dilation Y, both as a function of shear displacement X.
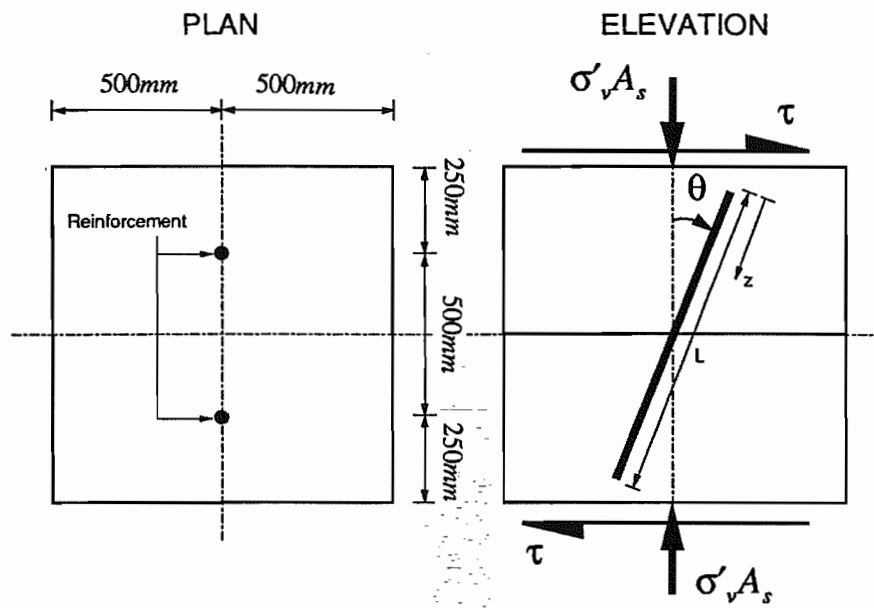
Figure 6.1 - Illustration of the positioning of reinforcement in the LDSA.
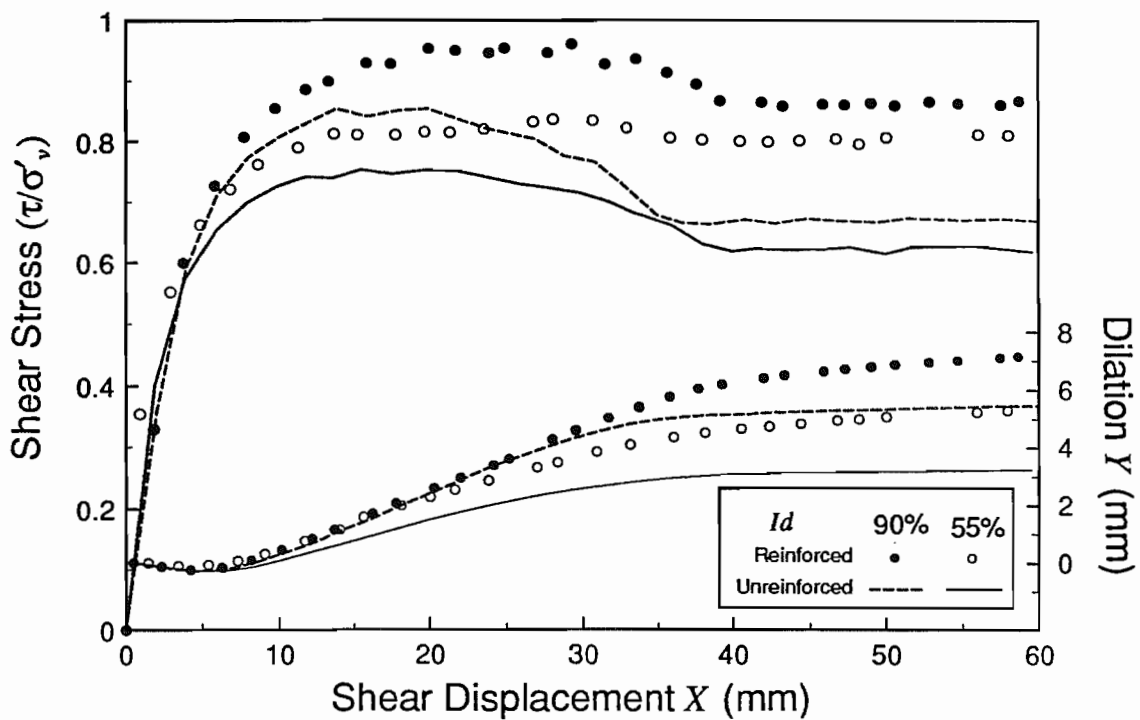
Figure 6.2 - Comparison between typical reinforced and unreinforced direct shear test data in the LDSA.

For both soil densities the reinforced sample demonstrates a similar behaviour to that of the unreinforced sample. Initially, as the shear displacement increases there is very little difference in the mobilised shear strength (τ/σ'_v) and dilation Y between the reinforced and unreinforced samples, although marginally less contraction Y occurs when reinforced. With continued shearing the measured strength and dilation of the reinforced samples rise above those of the respective unreinforced samples. For the dense reinforced sample ($I_d = 90\%$) the strength increases to a maximum, at a shear displacement X greater than that at which it occurs for the unreinforced sample, it is then followed by a period of strain softening until a residual strength is mobilised. This residual strength, greater than that of the unreinforced soil, is constant for the remainder of the test.

For the medium dense sample ($I_d = 55\%$) the behaviour is slightly different; the strength increases to a maximum with no strain softening occurring thereafter (as with the unreinforced test). The mobilised strength is less than that observed for the denser sample for all stages of the test. For both reinforced tests the measured dilation is greater than for the respective unreinforced test.

The additional shearing resistance of the soil is a resultant of the axial and shear force in the reinforcement, P_{ax} and P_s respectively, which are induced by relative soil-reinforcement displacements. The additional dilation results from the increased volume of soil being sheared due to the presence of the reinforcement.

6.2 Reinforcement Materials and Properties

Descriptions of the reinforcement form, material and surface properties are now given below. Details of the soil used in this research were given in Chapters 4 and 5.

6.2.1 Section types

Reinforcement of circular cross section was used for all of the reinforced direct shear tests. Three different types of circular cross section were tested and can be described as *solid bar, tube* and *grouted bar*. The various sections that have been defined are illustrated in Figure 6.3. The solid bars were all of mild steel and the tubes were either mild steel or brass. Grouted bars were formed from a mild steel bar of diameter D placed centrally in a column of grout of external diameter D_g. The overall length of the reinforcement is L, and the anchor length L_a is the distance between the point where the reinforcement crosses the central shear plane and the end of the reinforcement.
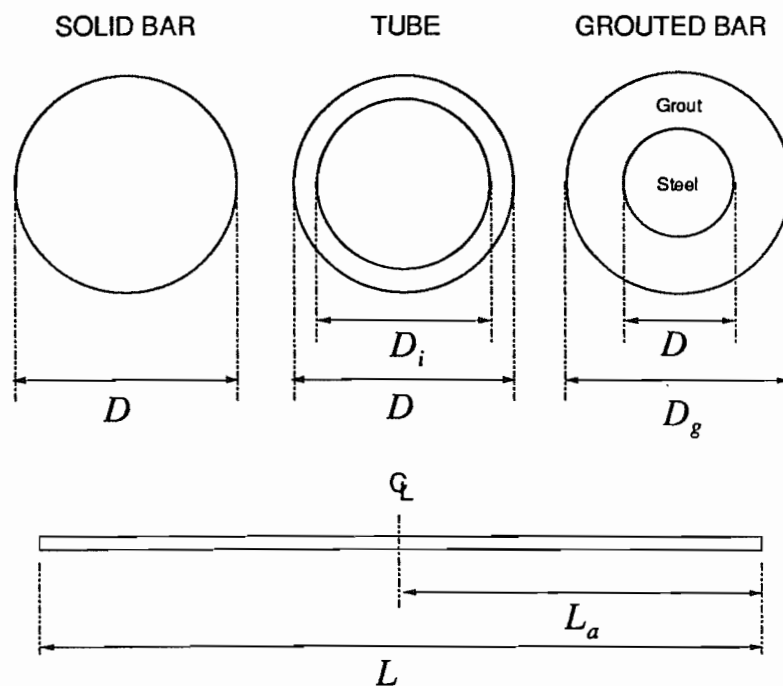
Figure 6.3 - Definition of reinforcement dimensions and section types.

6.2.2 Material types

Table 6.1 summarises the mechanical properties of the reinforcement materials. The mechanical properties of the mild steel: elastic modulus E, yield stress σ_p and yield strain ε_y were measured in tensile tests on samples of the steel machined from a piece of reinforcing bar. These agree well with the expected values for mild steel.

The mechanical properties of the brass were assumed equal to those values quoted in tables by Beer and Johnston (1981).

The yield strength of the cement grout was taken as equal to the cube strength σ_{cu} of 50mm cubes. The elastic modulus E was deduced from σ_{cu}, utilising the empirical correlation given in Neville (1973). The mix for the cement grout was approximately 8.9 parts Ordinary Portland Cement to 1 part High Alumina Cement, and a water cement ratio $W/C = 0.43$. This mixture provided a flash set of the order 17 minutes, whilst still achieving a reasonable cube strength. The method of forming grouted bar reinforcement is given in Section 6.3.3.

Material	Yield Stress σ_p kN/m^2	Yield Strain ε_y $\mu\varepsilon$	Elastic Modulus E kN/m^2	NOTES
Mild Steel	393×10^3	1920	206×10^6	
Brass	105×10^3	1000	105×10^6	Values from Beer & Johnston (1981)
Cement Grout	22.7×10^3	2000	21.4×10^6	$E \approx 4.5\sqrt{\sigma_{cu}}$ where σ_{cu} has units $N/mm2$, Neville (1973).

Table 6.1 - Material Properties of Reinforcement.

6.2.3 Reinforcement surface properties

A series of interface tests was performed to measure the limiting shear strength between different reinforcement surface textures and Leighton Buzzard 14/25 sand, in order to predict

the pullout resistance of the reinforcement. The tests were performed by preparing a specimen of the interface material in the lower half of the Medium Direct Shear Apparatus (see Chapter 3) with a surface texture as close as possible to that of the reinforcement being modelled. The upper half of the shearbox was filled with the test sand and the interface test was carried out in a similar manner to a direct shear test.
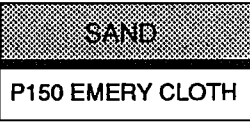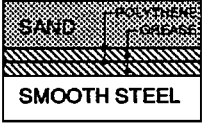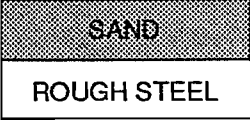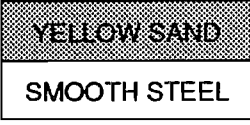
Test	Interface	Vertical Stress σ'_v kN/m^2	Mobilised Stress $(\tau/\sigma)_{max}$	Friction Angle $\phi'_i{}^\circ$	NOTES
I1	SAND / GROUT	64.8	.695	34.8°	
I2	SAND / P150 EMERY CLOTH	64.9	.620	31.8°	
I3	SAND / POLYTHENE GREASE / SMOOTH STEEL	64.9	.009	0.5°	
I4	SAND / ROUGH STEEL	64.9	.422	22.9°	
I5	SAND / SMOOTH STEEL	64.9	.298	16.6°	
I6	YELLOW SAND / SMOOTH STEEL	64.9	.346	19.1°	Yellow sand

Table 6.2 - Summary of interfaces tested in the MDSA.

The interfaces tested are summarised in Table 6.2 with details of the applied vertical stress σ'_v, the maximum measured stress ratio $(\tau/\sigma'_v)_{max}$ and the interface friction angle ϕ'_i, where

$$\phi'_i = \tan^{-1}\left(\frac{\tau}{\sigma'_v}\right)_{max} \qquad \dots(6.1)$$

The rate of increase in mobilised interface friction angle ϕ'_i with shear displacement is shown in Figure 6.4. Several interesting points arise from the data:
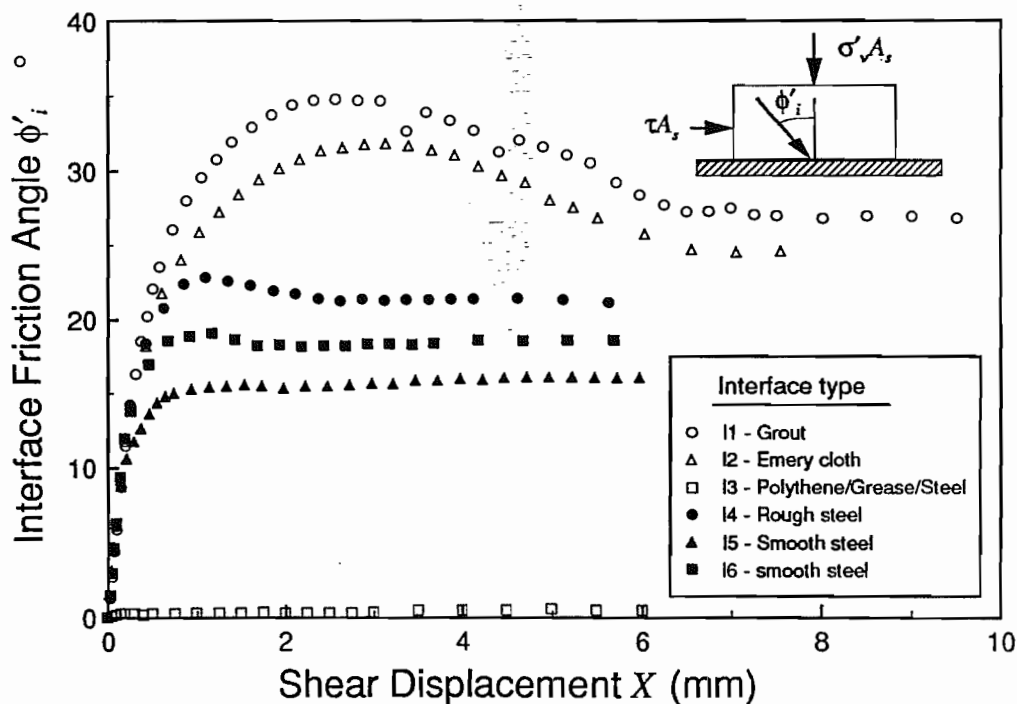
Figure 6.4 - Interface tests modelling typical reinforcement surface characteristics.

(i)   the rougher the reinforcement surface the greater the interface friction angle. The greatest interface friction angle was obtained for the interface prepared by raining the sand onto the grout immediately after its initial set. The lowest was for steel lubricated with a grease and polythene sandwich. The interface friction angles

for grout of 35° and steel of 17° – 23° agree well with typical values quoted in the literature, for example Potyondi (1961), Simons and Menzies (1977) and Tomlinson (1986).

(ii)   the interface friction angle increased quite markedly from 17° to 23° by roughening the surface of smooth steel by grit blasting; similar observations have been reported by Kishida and Uesugi (1987). An increase in ϕ'_i of 2° was obtained for the smooth steel specimen when the white Leighton Buzzard sand was substituted by the more angular yellow sand.

(iii)   friction was more or less eliminated when the sand was separated from smooth steel by a grease-polythene-grease-polythene layer. For this interface the value of ϕ'_i is likely to be highly sensitive to the applied vertical stress σ'_v and to the rate of shear (0.02 $mm/$ min was used) owing to viscous nature of the grease in the interface (Shell Barbatia).

6.3 Reinforced Tests on Medium Dense Sand

6.3.1 Description of tests

Out of the total of 29 reinforced direct shear tests, 9 were performed on medium dense ($I_d = 55\%$) white Leighton Buzzard 14/25 sand. The reinforcement was of length $L = 920mm$ and placed vertically in the shearbox (i.e. $\theta = 0°$) at the time of sample preparation; the applied vertical stress was $\sigma'_v = 100kN/m^2 \pm 2kN/m^2$. Resistance strain gauges were fixed to the reinforcement to allow measurement of the axial and bending strains occurring during shear. Specific details are given in Table 6.3.

Anchor plates were fixed to the ends of the reinforcing bars to increase the axial force P_{ax} in the reinforcement in three tests (MD7, MD8 and MD9). The anchor dimensions and thickness t are given in Table 6.4. Test MD8 was a repeat of test MD7.

Test	Vertical Stress σ'_v kN/m^2	D mm	D_i mm	Material	N° Bars	Interface Type (Table 6.2)	Strain Gauge Type & Length
MD1	99.9	15.88	13.19	Brass	1	-	linear/2mm
MD2	100.1	25.40	22.36	M. steel	2	I2	linear/5mm
MD3	102.2	15.88	-	M. steel	2	I4	linear/5mm
MD4	98.3	25.40	-	M. steel	2	I4	linear/5mm
MD5	99.3	15.88	-	M. steel	2	I3	post yield/5mm
MD6	99.5	25.40	-	M. steel	2	I3	linear/5mm
MD7	99.7	15.88	-	M. steel	2	I2	linear/5mm
MD8	99.6	15.88	-	M. steel	2	I2	linear/5mm
MD9	99.6	15.88	-	M. steel	2	I2	post yield/5mm

Table 6.3 - Details of reinforced direct shear tests on medium dense sand.

Test	Description of Anchor
MD7 MD8	$100mm \times 100mm$ mild steel plate, $t = 6.2mm$
MD9	$900mm \times 32mm$ mild steel rectangular bar, $t = 6.2mm$ connected to both reinforcing bars.

Table 6.4 - Description of anchors used for tests MD7, MD8 and MD9.
(t equals the thickness of the anchor).

6.3.2 Boundary measurements

The variation of measured shearing resistance (τ/σ'_v) with shear displacement X is shown in Figure 6.5 for tests MD1 to MD6 (Table 6.3). The results for the unreinforced sand at same vertical stress and relative density are shown for comparison.

Many of the test data exhibit a lower initial shearing resistance than for the corresponding unreinforced test. This is a common phenomenon for stiff reinforcement and
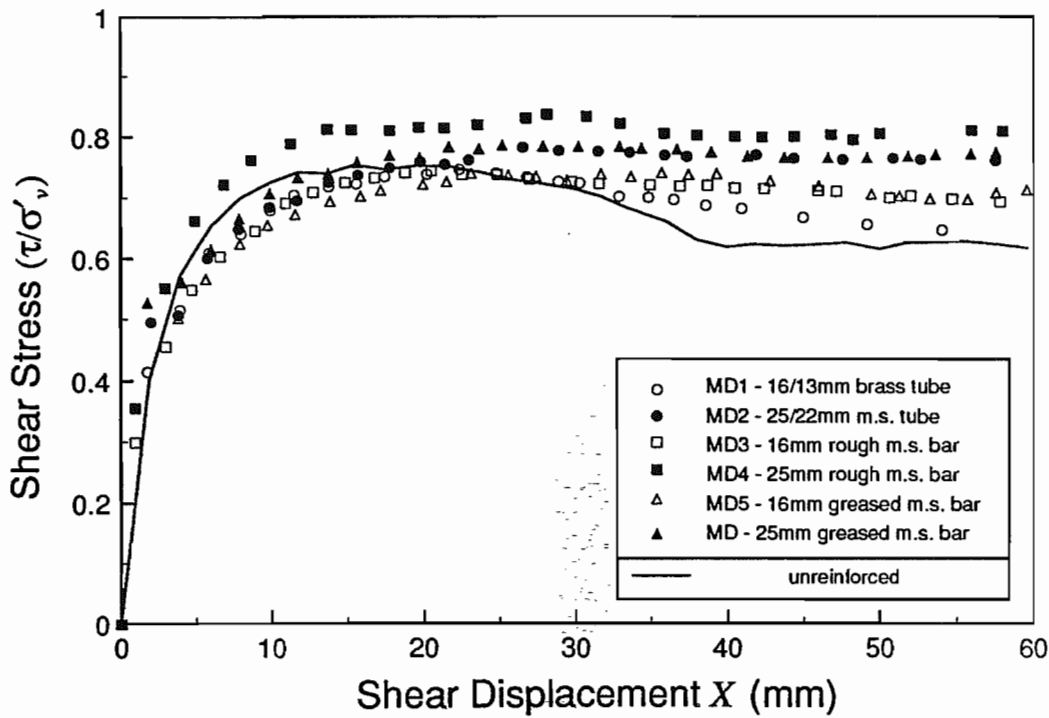
Figure 6.5 - Boundary data from reinforced direct shear tests on medium dense soil (tests MD1 to MD7).

can be for one of two reasons: (i) the reinforcement is placed in compression during application of the vertical stress, or (ii) during sample preparation the reinforcement causes local soil disturbance.

The order of the mobilised shear strengths is similar to the expected behaviour assuming that potential increases in soil shear strength are related to the reinforcement surface area and bending stiffness or moment capacity. The largest improvement was obtained from large diameter solid bar ($D = 25mm$) and the lowest from small diameter tube ($D = 16mm, D_i = 13mm$).

A relatively small difference in shear strength improvement is observed between tests on reinforcement with smooth and rough outer surfaces. This is attributed to the limited anchorage length of the reinforcement ($L_a = 460mm$).
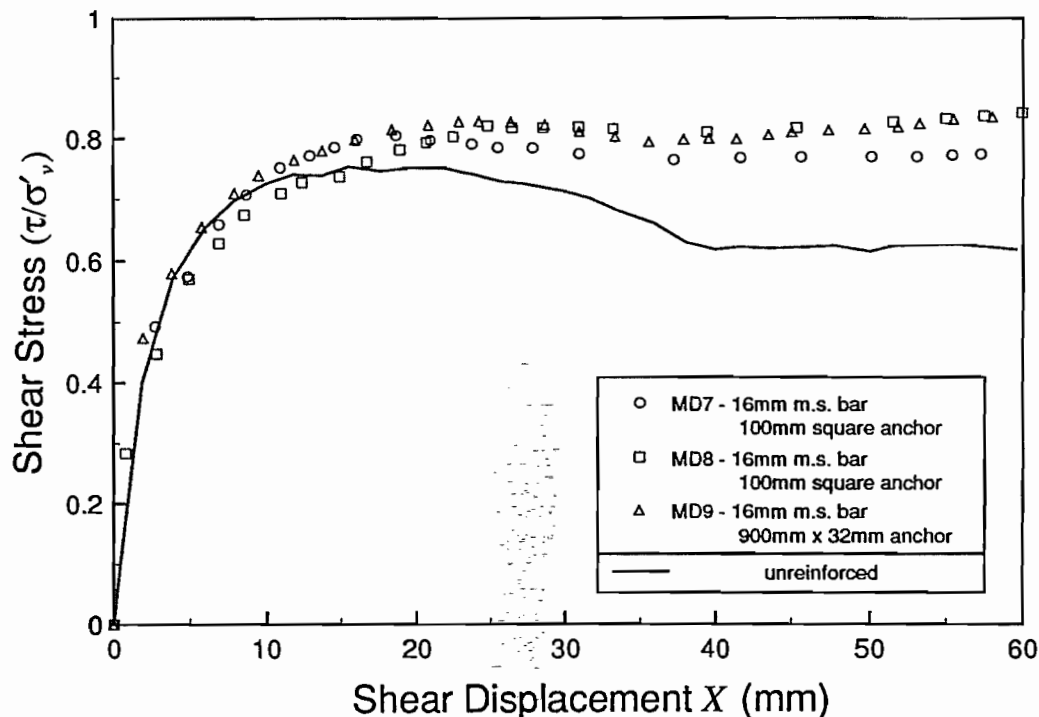
Figure 6.6 - Boundary data from tests on medium dense sand for reinforcement with anchors plates (tests MD7, MD8 & MD9).

A much greater improvement in shear strength was obtained for tests MD7, MD8 and MD9; the test data are shown in Figure 6.6. In these tests anchor plates were fitted to the reinforcement in order to increase the axial reinforcement force. The anchor plates appear to have little effect on the pre-peak shearing resistance. However, at a shear displacement of the order $X \approx 15 - 20mm$ the presence of the anchor plate allows the shear strength to increase further, and this may be attributed to a continuing increase in reinforcement axial force. This behaviour is analogous to that of a passive anchor undergoing pullout.

Despite increasing the anchor surface area by a factor of approximately two between tests MD8 and MD9 it is interesting to note that there is almost no distinguishable difference in the improvement in shear strength between the two reinforced samples. This difference may be comparable with bearing capacity theory where shape factors are employed to account for the shape of the loaded area.

Test MD8 was a repeat of test MD7 to alleviate fears of sample disturbance around the anchor plate. Sample disturbance is confirmed by the lower shearing resistance, as is the sensitivity of the improvement in soil strength to fluctuations in soil density.

6.3.3 Internal measurements

The strain gauge data for tests MD4, MD5, MD6, MD8 and MD9 were found to be in error owing to a calibration incompatibility between the data logger software and hardware. The data were found to be in error by a factor of approximately 2, and were adjusted accordingly. Therefore, it may be wise to give the strain gauge data for the above tests less credence owing to the uncertainty about the exact calibration error.

Strain gauges were used to instrument the reinforcement and monitor the maximum and minimum surface strains ε_s at different positions along the length of the reinforcement. The surface strains measured in test MD1 at five different points along the length of the reinforcement are shown in Figure 6.7, and correspond to a shear displacement $X \approx 15mm$.

A schematic illustration of the deflection of the reinforcement in the shearbox is given in Figure 6.7(a), and illustrates the sign convention for relating the surface strain to the curvature of the bar. The conventional solid mechanics definition for positive strain and axial force is adopted for the reinforcement.

The variation of the surface strains ε_{s1} and ε_{s2} normalised by the yield strain ε_y are shown in Figure 6.7(b). (ε_{s1} and ε_{s2} are measured on the face of the reinforcement closest to and furthest from the end of the shearbox to which the shear force is applied).

The reinforcement in a direct shear test undergoes deformation caused by lateral and axial loading. The surface strains are the result of axial and bending strain components, associated with the axial force P_{ax} and the bending moment M. The axial strain ε_{ax} is defined as the mean of the two measured surface strains
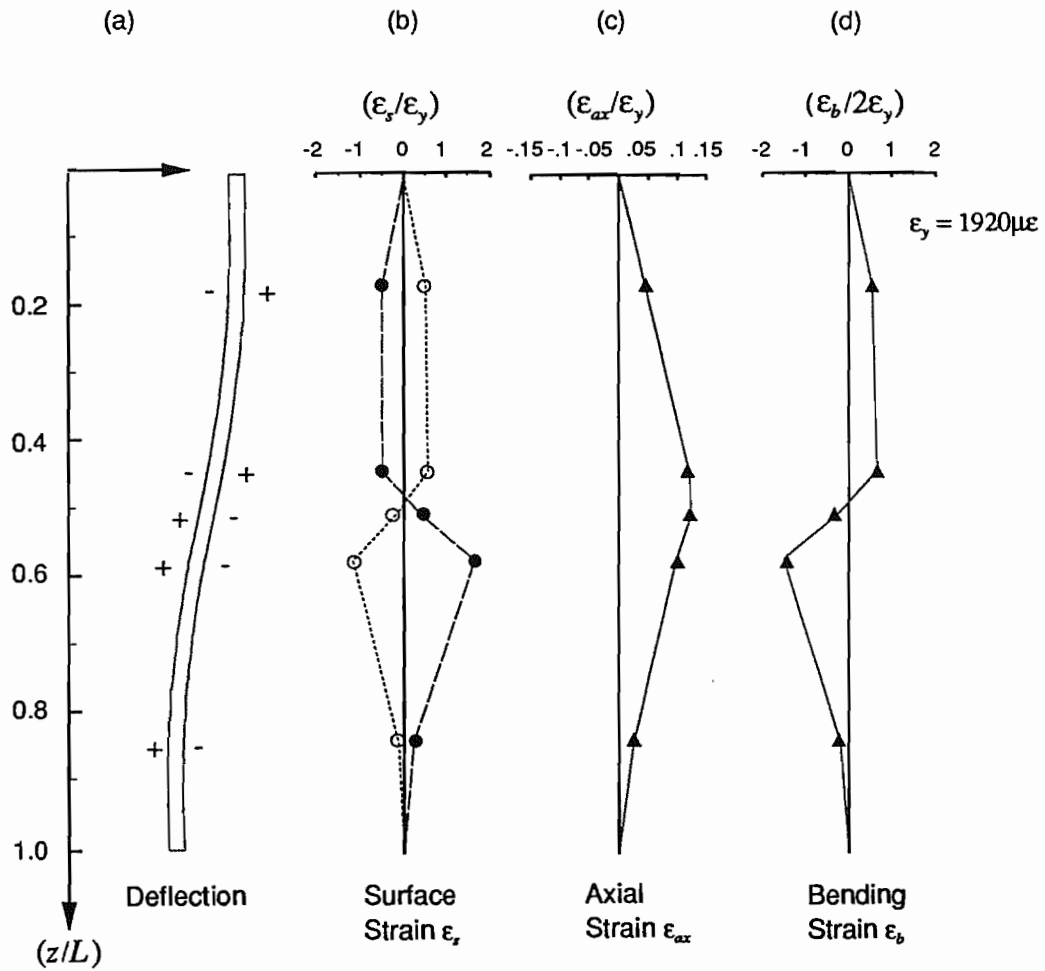
Figure 6.7 - Measured surface strains and deduced axial and bending strains at a shear displacement $X \approx 15mm$ in test MD1.

$$\varepsilon_{ax} = \frac{\varepsilon_{s1} + \varepsilon_{s2}}{2} \qquad \ldots(6.2)$$

and the bending strain ε_b as the difference between the two surface strains

$$\varepsilon_b = \varepsilon_{s1} - \varepsilon_{s2} \qquad \ldots(6.3)$$

This analysis leads to the distribution of axial and bending strain shown in Figure 6.7; note that the scales for the measured axial and bending strains in Figures 6.7(c) and (d) differ by a factor of 100, and therefore the magnitudes of these two quantities are very different.

The axial force P_{ax} in the reinforcement is

$$P_{ax} = \sigma A_r \qquad \qquad ...(6.4)$$

where A_r is the cross sectional area of the reinforcement and σ the mean axial stress in the reinforcement. It is assumed in the analysis that metallic reinforcement has an elastic-perfectly plastic stress strain behaviour. Therefore, the axial stress is

$$\sigma = \frac{\varepsilon_{ax}}{\varepsilon_y} \sigma_p \qquad \qquad ...(6.5)$$

where ε_y is the yield strain, and σ_p the yield stress of the material; the ratio $\varepsilon_{ax}/\varepsilon_y$ is always less than or equal to unity. The axial force may therefore be expressed as, equation (6.4) and equation (6.5)

$$P_{ax} = \frac{\varepsilon_{ax}}{\varepsilon_y} \sigma_p A_r \qquad \qquad ...(6.6)$$

Defining the plastic axial capacity of the reinforcement bar as $P_p = \sigma_p A_r$, then equation (6.6) can be expressed in non-dimensionalised form as

$$\frac{P_{ax}}{P_p} = \frac{\varepsilon_{ax}}{\varepsilon_y} \qquad \qquad ...(6.7)$$

The bending moment M at a given cross section in the reinforcement may be calculated assuming: (i) plane sections remain plain during bending, (ii) the bending strain varies linearly across the cross section, and (iii) the material is elastic-perfectly plastic. Consider the cross section through a circular bar, Figure 6.8, subjected to the stress and strain distributions, as shown, for the case when the maximum bending strain $\varepsilon_b > 2\varepsilon_y$; in other words the bar is subject to elastic-plastic bending.

When the maximum bending strain $\varepsilon_b \leq 2\varepsilon_y$ the bending is purely elastic, and the bending moment M is
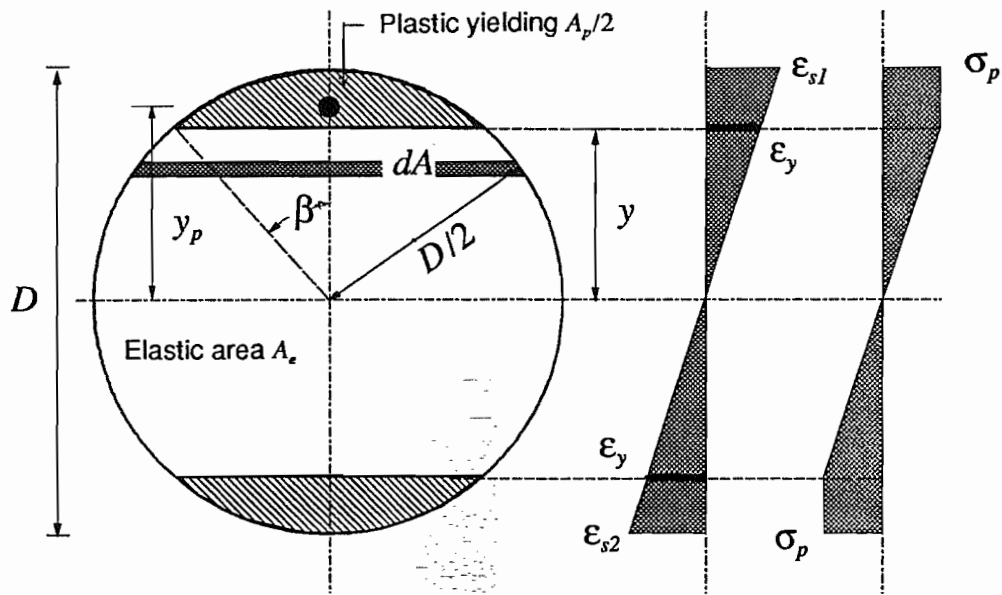
Figure 6.8 - Cross section through reinforcement subjected to an elastic-plastic bending moment and corresponding strain and stress blocks.

$$M = \frac{I\sigma}{y} = \frac{\pi D^3}{32}\sigma \qquad \ldots(6.8)$$

where I is the second moment of area of the cross section $(I = \pi D^4/64)$, y the distance between the point of maximum stress and the neutral axis $(y = D/2)$, σ is the maximum stress in the bar and D the reinforcement diameter. The ultimate bending moment that the cross section can sustain is the fully plastic moment M_p which develops when the yield stress σ_p is mobilised over the entire area of the cross section

$$M_p = \frac{D^3}{6}\sigma_p \qquad \ldots(6.9)$$

In some cases the bending moment in the cross section may be elastic-plastic, therefore one can write

$$M = m_p + m_e = \sigma_p A_p y_p + \frac{\sigma}{y}I' \qquad \ldots(6.10)$$

where A_p is the area of the cross section which has yielded plastically (and is assumed to be split equally either side of the neutral axis in this analysis), y_p is the distance between the neutral axis and the centroid of area $A_p/2$, y is the distance between the neutral axis and the point where the bending strain $\varepsilon_b/2 = \varepsilon_y$, and I' is the second moment of area of the elastic portion of the cross section (area A_e in Figure 6.8). From trigonometry the depth of plastic yielding y is

$$y = \frac{D}{2}\cos\beta \qquad\qquad \text{...(6.11)}$$

where β is defined in the figure. From geometry the total area A_p is

$$A_p = \frac{D^2}{2}(\beta - \cos\beta\sin\beta)$$

and the lever arm y_p

$$y_p = \frac{D}{3}\left(\frac{\sin^3\beta}{\beta - \cos\beta\sin\beta}\right)$$

giving the plastic portion of the bending moment as

$$m_p = \frac{D^3}{6}\sigma_p\sin^3\beta \qquad\qquad \text{...(6.12)}$$

The second moment of area I' of the elastic portion, from calculus, is

$$I' = \int_A y^2\,dA = \frac{D^4}{32}\left(\frac{\pi}{2} + \frac{1}{4}\sin4\beta - \beta\right)$$

giving the elastic portion of the bending moment as

$$m_e = \frac{D^3}{16}\left(\frac{\pi/2 + \sin4\beta/4 \mp \beta}{\cos\beta}\right)\sigma \qquad\qquad \text{...(6.13)}$$

Substituting for m_p and m_e in equation (6.10) gives the total moment in the cross section as

$$M = D^3 \left\{ \left(\frac{\sin^3 \beta}{6} \right) \sigma_p + \left(\frac{2\pi + \sin 4\beta - 4\beta}{64 \cos \beta} \right) \sigma \right\} \qquad \ldots (6.14)$$

where the values for σ and β are defined by:

if $\varepsilon_b < 2\varepsilon_y$ then

$$\sigma/\sigma_p = \varepsilon_b/2\varepsilon_y \qquad \text{and} \qquad \beta = 0$$

if $\varepsilon_b \geq 2\varepsilon_y$ then

$$\sigma = \sigma_p \qquad \text{and} \qquad \beta = \cos^{-1}(2\varepsilon_y/\varepsilon_b)$$

Normalising equation (6.14) by the fully plastic moment M_p, equation (6.9), yields

$$\frac{M}{M_p} = \sin^3 \beta + \left(\frac{6\pi + 3 \sin 4\beta - 12\beta}{32 \cos \beta} \right) \left(\frac{\sigma}{\sigma_p} \right) \qquad \ldots (6.15)$$

allowing comparison of the bending moment between tests on different diameter reinforcement.

Simplifying assumptions were made to obtain equation (6.15), and potentially these affect the accuracy of the calculation, they are: (i) the assumption of superposition in order to obtain the axial and bending strains ignores the effect of axial force on the position of the neutral axis for elastic-plastic bending, and (ii) the assumption of elastic-perfectly plastic reinforcement material behaviour ignores the influence of strain hardening.

The effect of the first assumption was checked by comparing the bending moment obtained from equation (6.15) with that from a more rigorous analysis accounting for a shift in position of the neutral axis. This showed that for small values of axial force (P_{ax}/P_p) the error was a small percentage.

For example, consider the case of a reinforcing bar of diameter $D = 15.9mm$ and with material properties equal those for mild steel in Table 6.1. If the surface strains are $\varepsilon_{s1} = 4000\mu\varepsilon$ and $\varepsilon_{s2} = -3200\mu\varepsilon$, equation (6.7) gives an axial force $(P_{ax}/P_p) = 0.20$, and equation (6.15) gives a bending moment $(M/M_p) = 0.865$. With a method similar to that used to obtain equation (6.15), but allowing for the shift in the position of the neutral axis,

and unequal areas of plastic yielding, the bending moment was $(M/M_p) = 0.876$; an error of approximately 2%. Therefore, for low ratios of (P_{ax}/P_p) equation (6.15) is theoretically sufficiently accurate.

The second assumption of elastic-perfectly plastic material behaviour leads to a larger error in M. However, as the ratio of the ultimate failure stress σ_{ult} to the yield stress σ_p for the reinforcement material was of the order 1.3, the error in the calculation is unlikely to be sufficient to merit a more sophisticated analysis.

The development of normalised axial force (P_{ax}/P_p) with shear displacement X for tests MD2 to MD9 is shown in Figure 6.9.
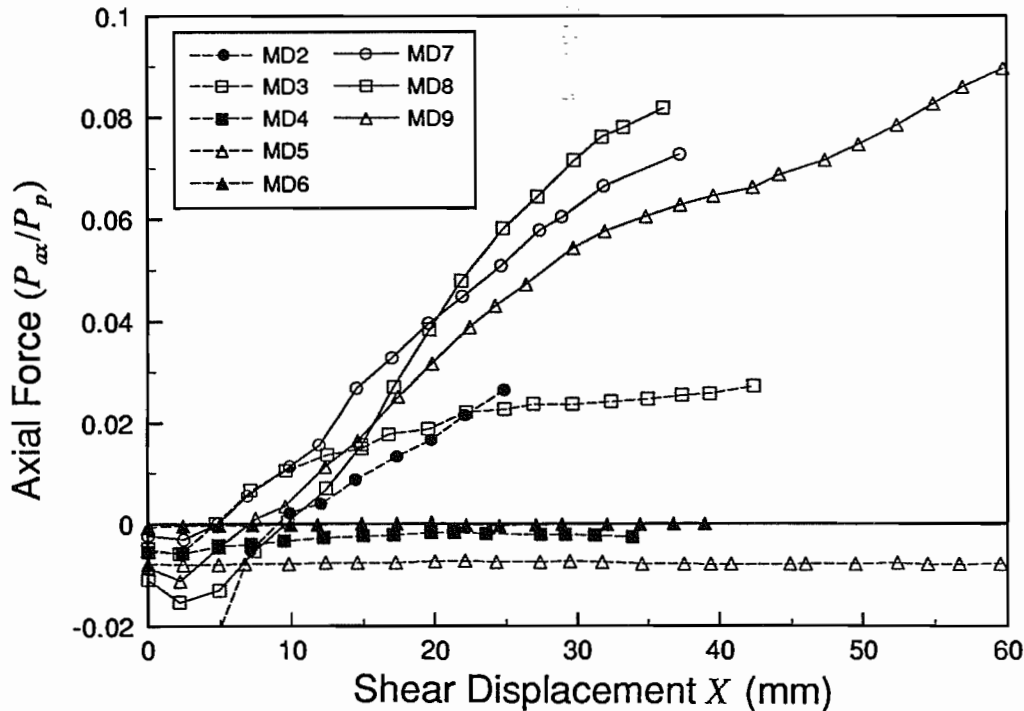
Figure 6.9 - Development of axial force (P_{ax}/P_p) with shear displacement X for tests on medium dense sand.

The reinforcement is initially in compression at the beginning of all tests. This compressive force resulted from an induced compressive strain as the vertical stress σ'_v was

applied. For reinforcement with a rough outer surface, or fitted with anchor plates the compressive force increases slightly with shear displacement as sample contraction occurs. The response of the axial force beyond this point is dependent on the reinforcement.

For tests on reinforcement fitted with anchor plates the axial force (P_{ax}/P_p) increases quasi-linearly with shear displacement X until the end of the test. For tests on reinforcement with a rough outer surface the axial force also increases linearly, but reaches a limiting value at a shear displacement $X \approx 25 - 30mm$. However, in the case of test MD4 the axial force is reduced but still remains compressive at the end of the test. The reinforcement fitted with the polythene-grease coating, interface type I3, was unable to mobilise any surface friction and consequently maintained a constant compressive axial force independent of the shear displacement. This compressive load is a result of end loading of the reinforcement.

The low axial reinforcement force, of $(P_{ax}/P_p) \approx -0.02 \rightarrow +0.08$ observed in all of the tests is attributed to the short anchorage length of the reinforcement $(L_a = 460mm)$; the higher value is for reinforcement with anchor plates, and the lower value for reinforcement with a friction reducing sleeve.

Figure 6.10 presents the normalised bending moment profiles (M/M_p) for the tests described in Table 6.3. The profiles were calculated from the surface strains measured at a shear displacement $X \approx 20mm$ using equation (6.15). Owing to the limited number of strain gauges the bending moment profiles are somewhat coarse, but show that the maximum moment is developed at between $0.1L$ and $0.2L$ from the centre of the shearbox. The central plane of the shearbox $(z/L \approx 0.5)$ is seen to be a point of symmetry of loading as the bending moment is tending to zero at this level. Therefore, the reinforcement shear force will be a maximum at this level.

The maximum mobilised bending moment in the reinforcement varies between $(M/M_p) \approx 0.20 - 0.60$. The lower value of bending moment is for the larger diameter $D = 25mm$ solid bar reinforcement, and the higher value for tubular reinforcement of the
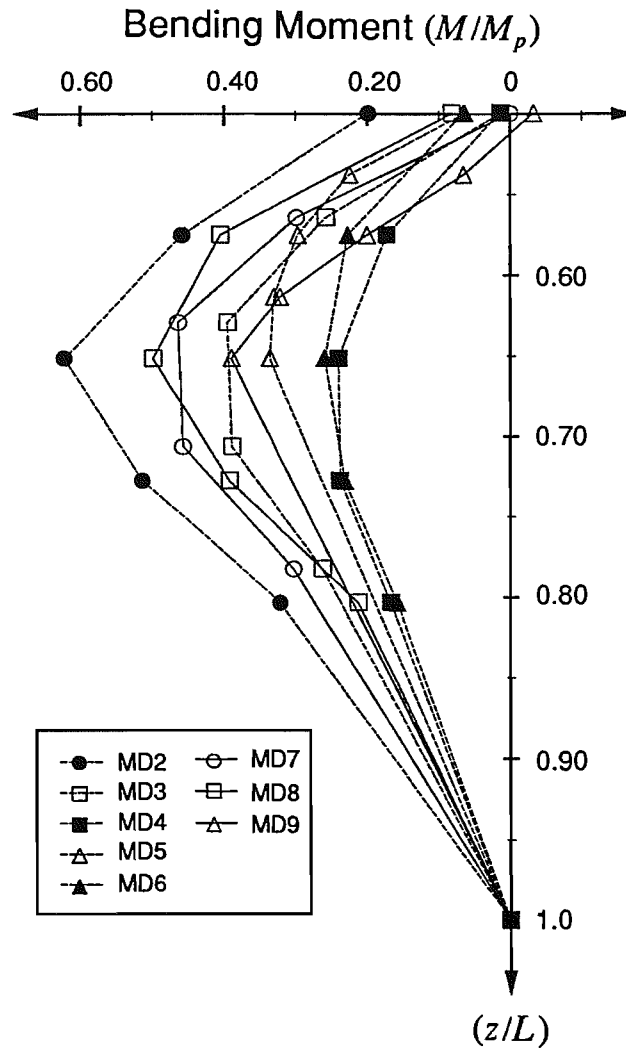
Figure 6.10 - Bending moment (M/M_p) distribution measured at a shear displacement $X \approx 20mm$ for tests on medium dense sand.

same external diameter. The latter has exceeded the elastic yield moment of the cross section $M/M_p = 0.59$. All of the bending moment profiles for the $D = 16mm$ reinforcement fall within a very small range, with the maximum bending moment approaching the elastic yield moment.

As a result of the development of plasticity within the reinforcement at very small shear displacements the strain gauges failed at an early stage of the test; for this reason post yield strain gauges were used in later tests.

6.4 Reinforced Tests on Dense Sand

6.4.1 Description of tests

In common with the tests on medium dense samples the reinforcement consisted of 2 $N°$ mild steel bars of length $L = 920mm$ placed symmetrically in the shearbox at some angle θ to the vertical. The relative density of the soil was $I_d \approx 90\%$; the method used to prepare samples with this density was described in Chapter 3. The effect of anchor plates led to an axial force-displacement relationship too far removed from that of a soil nail undergoing pullout, therefore they were not used for tests on dense sand.

The reinforced tests on dense sand may be divided into four categories:

(i)   a study of reinforcement orientation θ.

(ii)   a study of reinforcement bending stiffness EI and plastic moment capacity M_p.

(iii)   a study of the soil bearing capacity σ'_b (by varying σ'_v).

(iv)   and a study of different methods of reinforcement installation.

Each of these categories is now discussed in further detail and the experimental results presented.

6.4.2 Reinforcement orientation

The effect of reinforcement orientation on soil shear strength improvement was investigated by testing two bar diameters of reinforcement D:$16mm$ and $25mm$, at three angles of inclination θ: $0°, 15°$ and $25°$. Solid bars were used for this test series and each bar had a total of 20 strain gauges attached; 19 were placed on one side of the reinforcement, and one on the opposite side at a distance $(z/L) = 0.5$ along the length of the reinforcement. This was to allow calculation of the maximum axial force (see Figure 6.7). The bending strain ε_b at each of the gauge points was calculated assuming a linear variation of axial force,

with a maximum at $(z/L) = 0.5$ and a minimum at $(z/L) = 0$ and 1. Each of the reinforcement bars was sheathed with emery cloth. This corresponds with the surface texture of interface type I2. Details of each test are summarised in Table 6.5.

Test	Vertical Stress σ'_v kN/m^2	D mm	$\theta°$	Material	N° Bars	Interface Type (Table 6.2)	Strain Gauge Type & Length
O1	103.3	15.88	0°	M. steel	2	I2	post yield/5mm
O2	103.6	15.88	15°	M. steel	2	I2	post yield/5mm
O3	103.7	15.88	25°	M. steel	2	I2	post yield/5mm
O4	100.2	25.40	0°	M. steel	2	I2	post yield/5mm
O5	103.2	25.40	15°	M. steel	2	I2	post yield/5mm
O6	104.6	25.40	25°	M. steel	2	I2	post yield/5mm

Table 6.5 - Reinforcement details for a study of reinforcement inclination.

The shearing resistance (τ/σ'_v) mobilised in these tests with shear displacement X is shown in Figure 6.11.

For each reinforcement orientation and bar diameter an increase in soil shear strength is observed throughout the test, therefore differing from the tests on medium dense sand shown in Figure 6.5. At a shear displacement $X \approx 25mm$ the data separates into two distinct groups. The largest increase in shear strength is observed for the tests on $D = 25mm$ reinforcement and the lowest for tests on $D = 16mm$ reinforcement. The effect of reinforcement orientation appears to have little effect on the mobilised shear strength for a given bar diameter D.

The development of reinforcement axial force (P_{ax}/P_p) with shear displacement X is shown in Figure 6.12. For some of the tests an initial compression is observed, however, this force rapidly becomes positive as the shear displacement increases. As the reinforcement is oriented away from the vertical $(\theta = 0°)$ the induced axial force is observed to increase.
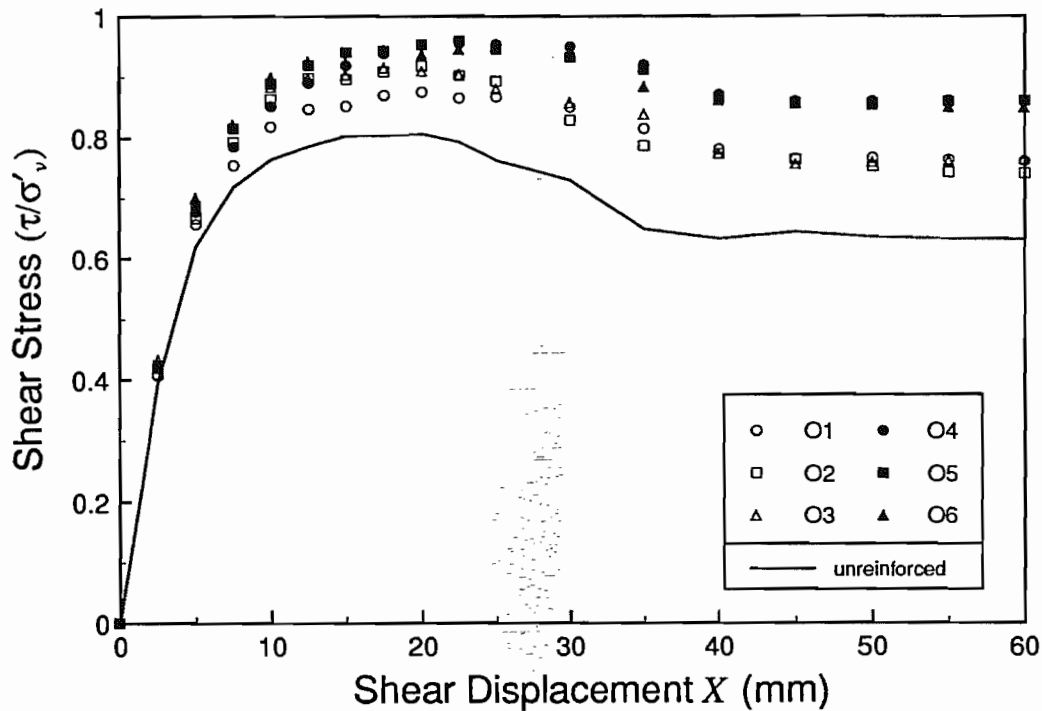
Figure 6.11 - Boundary data from the study of reinforcement orientation.

This is consistent with the findings of Jewell (1980) who observed that as reinforcement was oriented towards the direction of the principal tensile strain increment in the soil the magnitude of the axial force was increased.

By a shear displacement of approximately $X \approx 25 - 30mm$ a large percentage of the limiting axial force, measured at the end of the test, has been mobilised. This suggests the limiting pullout force for bar reinforcement is mobilised at small relative soil-reinforcement displacements. However, as the reinforcement was inclined the displacement required to mobilise the limiting axial force was increased. A larger proportion of the plastic axial force capacity P_p was mobilised in the $16mm$ reinforcement than for the $25mm$ reinforcement. This is consistent with the ratio of reinforcement surface area to the cross sectional area (A_c/A_r) for the two diameters (where A_c is the circumferential area per unit length).
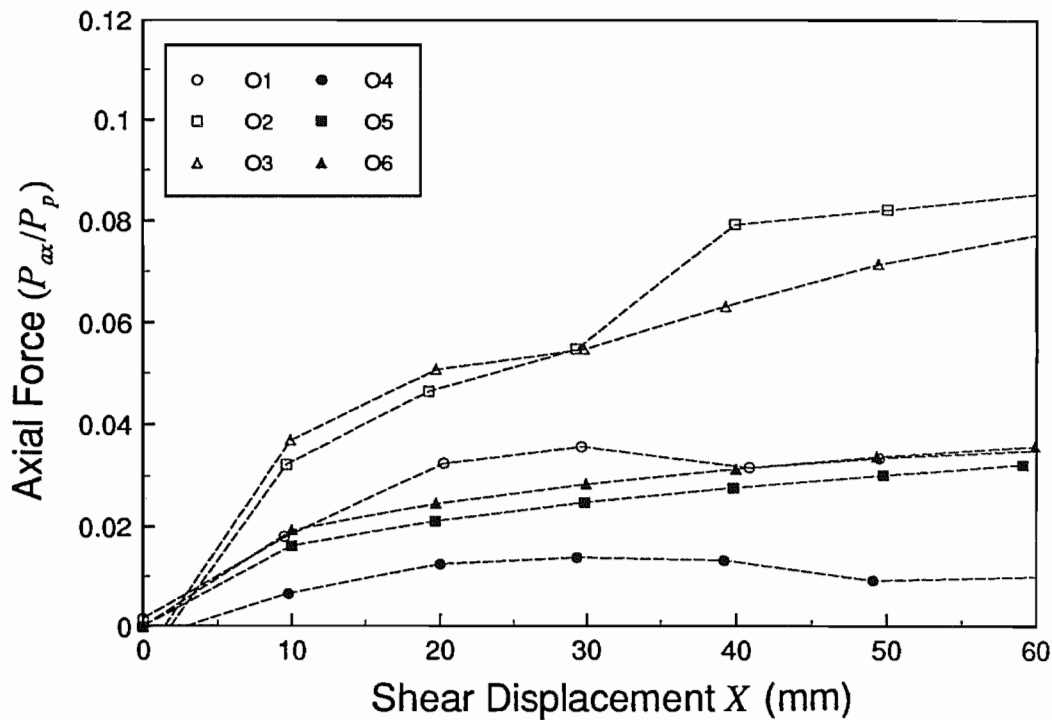
Figure 6.12 - Development of axial force (P_{ax}/P_p) with shear displacement X.

Figure 6.13(a) and 6.14(a) show the reinforcement bending moment (M/M_p) profiles

for shear displacements of $X = 20mm$ and $X = 60mm$ respectively.

For both shear displacements the bending moments are effectively symmetrical about

the central shear plane of the shearbox ($(z/L) = 0.5$); the limited asymmetry is explained by

the variation in soil strength with depth. The bending moment profile shows that the smaller

diameter reinforcement mobilises more of its plastic moment capacity (M/M_p) than the larger

diameter reinforcement; this is confirmed by the greater post test plastic deformation of the

$D = 16mm$ reinforcement.

As the reinforcement is oriented away from the vertical the maximum moment in the

reinforcement is reduced. The post test reinforcement deformation for tests on $D = 16mm$

reinforcement is shown in Plate 6.1, where diminishing plastic deformation is observed

with increasing θ.
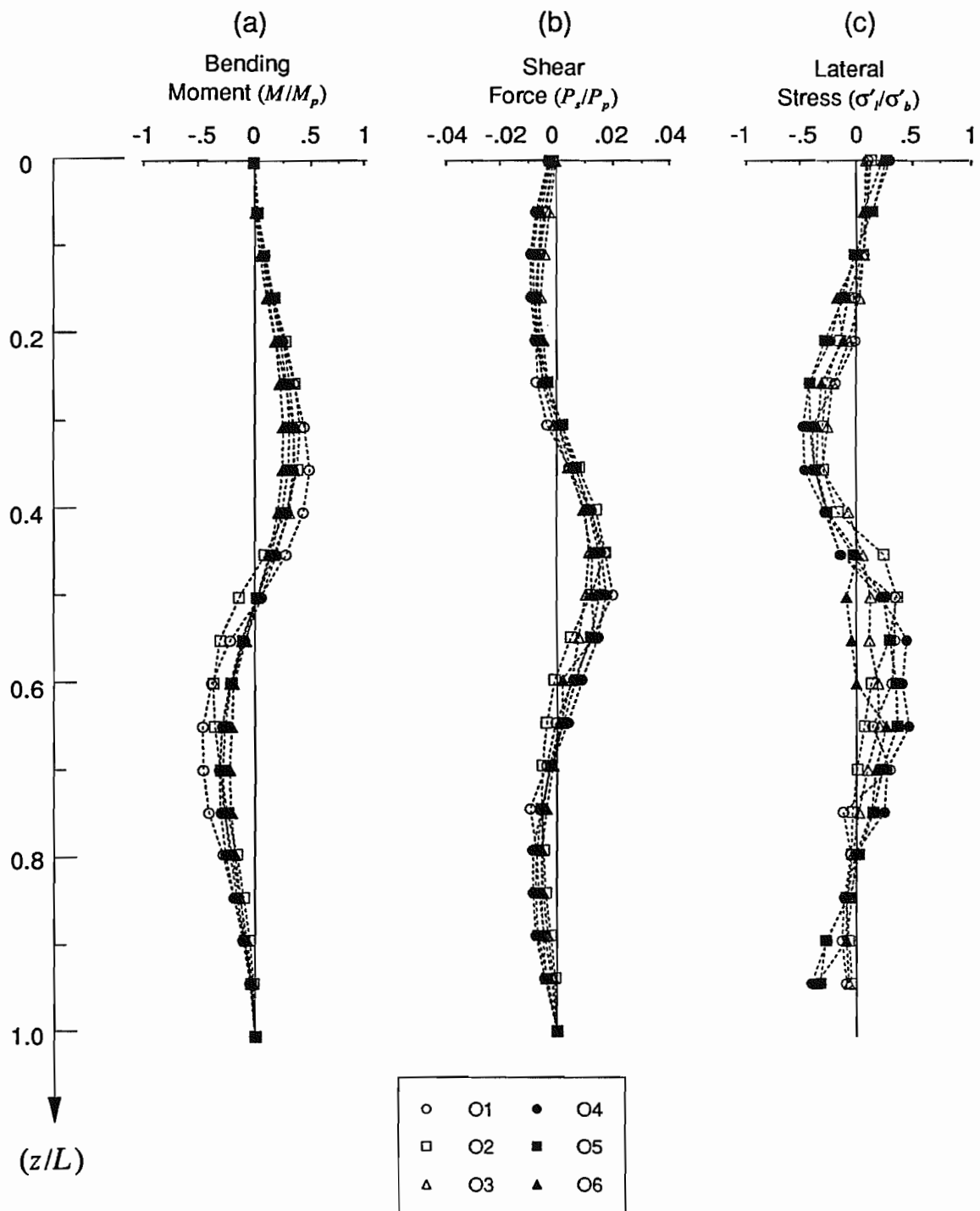
Figure 6.13 - Profiles of (a) bending moment (M/M_p), (b) shear force (P_s/P_p) and (c) lateral stress (σ'_l/σ'_b) at a shear displacement $X = 20mm$.
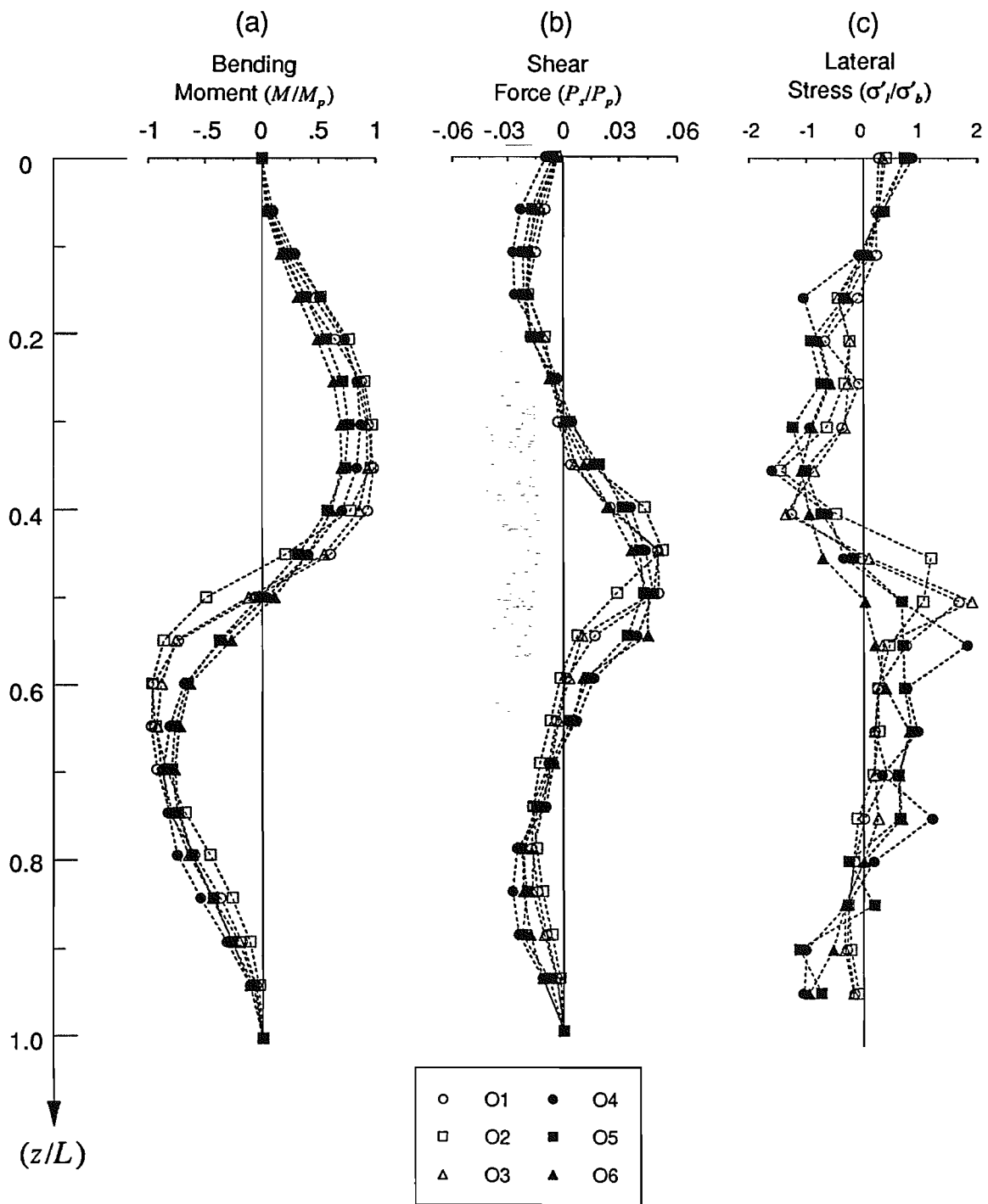
Figure 6.14 - Profiles of (a) bending moment (M/M_p), (b) shear force (P_s/P_p) and (c) lateral stress (σ'_l/σ'_b) at a shear displacement $X = 60mm$.

The normalised shear force (P_s/P_p) distributions at shear displacements of $X = 20mm$ and $X = 60mm$ are shown in Figures 6.13(b) and 6.14(b) respectively. These shear force profiles were obtained by differentiating the respective bending moment profiles. The differential equation relating the shear force (P_s/P_p) at some distance z along the reinforcement to the bending moment (M/M_p) is

$$\frac{P_s}{P_p} = \left(\frac{M_p}{P_p}\right)\frac{d}{dz}(M/M_p) = \left(\frac{2D}{3\pi}\right)\frac{d}{dz}(M/M_p) \qquad \ldots(6.16)$$

Despite the measured bending moments being close to the fully plastic moment $(M/M_p \approx 1)$ in all tests the maximum shear force (P_s/P_p) in the reinforcement is less than 6% of the plastic axial capacity P_p of the reinforcement. The maximum shear force is observed to be located at the level of the central plane of the shearbox.

The normalised lateral stress (σ'_l/σ'_b) against the reinforcement is shown in Figures 6.13(c) and 6.14(c) at shear displacements of $X = 20mm$ and $X = 60mm$ respectively. The lateral stress (σ'_l/σ'_b) at some point z along the reinforcement is related to the bending moment profile (M/M_p) by the differential equation

$$\frac{\sigma'_l}{\sigma'_b} = \left(\frac{M_p}{\sigma'_b}\right)\frac{d^2}{dz^2}(M/M_p) = \left(\frac{D^3\sigma_y}{6\sigma'_b}\right)\frac{d^2}{dz^2}(M/M_p) \qquad \ldots(6.17)$$

where σ'_b is the theoretical bearing stress. For the case of punching shear failure around a bar Jewell et al. (1984) derived the value of the bearing stress as

$$\left(\frac{\sigma'_b}{\sigma'_n}\right) = \tan\left(\frac{\pi}{4}+\frac{\phi'}{2}\right)\exp\left\{\left(\frac{\pi}{2}+\phi'\right)\tan\phi'\right\} \qquad \ldots(6.18)$$

in which σ'_n is the normal stress in the soil governing bearing failure around the bar. In the direct shear apparatus σ'_n is taken as equal to the intermediate principal stress σ'_2 acting perpendicular to the applied vertical and horizontal stresses. Based on the experimental measurements on sand by Stroud (1971) the normal stress can be related to the applied vertical stress σ'_v by

$$\sigma'_n = \sigma'_2 \approx 0.75\sigma'_v \qquad\qquad ...(6.19)$$

For a measured peak soil strength of $\phi' = 46°$ and a vertical stress $\sigma'_v \approx 100kN/m^2$

equation (6.18) yields a bearing stress of $\sigma'_b \approx 2170kN/m^2$. This value was used to normalise

the lateral stresses σ'_l in Figures 6.13 and 6.14.
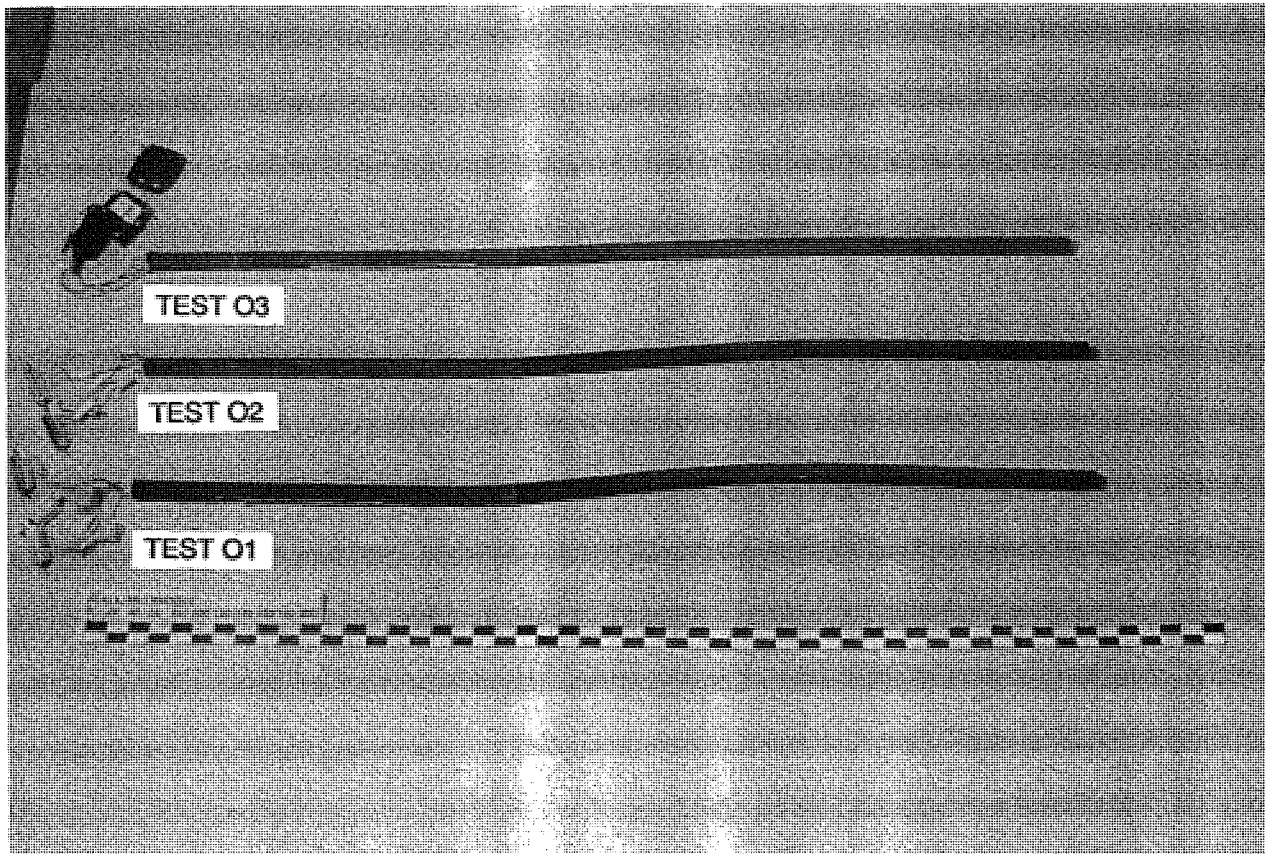
Plate 6.1 - Post test deformation of $D = 16mm$ reinforcement tested at different orientatioïs θ to the vertical.

The lateral stresses (σ'_l/σ'_b) shown in Figures 6.13 and 6.14 suggest a well defined

loading distribution against the reinforcement. At the larger shear displacement of

$X = 60mm$ the lateral stress is more less equal to the theoretical bearing capacity of the soil

over the entire length of the reinforcement. As the ratio $(\sigma'_l/\sigma'_b) \approx 1$ it is inferred equation

(6.18) is suitable for analysing the maximum soil pressure against reinforcement in the direct shear apparatus. Palmeira and Milligan (1989) found other test data to support equation (6.18).

As stated earlier the large diameter $D = 25mm$ bars suffered much less permanent deformation than the smaller $D = 16mm$, bars indicating a different failure mode. An observation of the lateral stress acting on the reinforcement for tests on $D = 25mm$ shows that the limiting bearing stress was mobilised over most of the reinforcement. Therefore, it appears the mode of failure for the large diameter reinforcement was that of rigid body, whereas for the smaller diameter reinforcement failure occurred by plastic hinge formation. Further analysis of these tests is given in Chapter 8.

6.4.3 Reinforcement bending stiffness

A study of the effect of reinforcement bending stiffness on soil shearing resistance was performed by varying the reinforcement diameter D. Mild steel bars were used in all tests, except for two on grouted bars. Details of each test are given in Table 6.6. Although tests O1 and O4 were reported in the previous section they are included here as they form an integral part of this study. A range of bending stiffness of the reinforcement EI from $0.02kNm^2$ to $67kNm^2$ was examined, representing a factor of approximately 3500 between the stiffest and least stiff reinforcements.

The intention of using grouted bars was not only to model a typical method of installing soil nails, but also to investigate its influence on the shear strength of the soil. Grouted bar reinforcement was formed in the shearbox after the preparation of the unreinforced sand sample using the following steps:

(i)   an open ended, thin walled brass tube of external diameter $51mm$ and length $1.2m$ was driven vertically into the soil sample through holes in the top plate of the shearbox. The sand was removed from within the tube at various intervals during

Test	Vertical Stress σ'_v kN/m^2	D mm	D_g mm	Material	N^o Bars	Interface Type (Table 6.2)	Bending Stiffness EI kNm^2
D1	104.3	6.47	-	M. steel	2	I5	0.018
O1	103.3	15.88	-	M. steel	2	I2	0.642
O4	100.2	25.40	-	M. steel	2	I2	4.203
D2	103.0	50.80	-	M. steel	2	I4	67.24
D3	104.6	50.80	6.47	Grout/ M. steel	2	I1	N/a
D4	108.2	50.80	15.88	Grout/ M. steel	2	I1	N/a

Table 6.6 - Study of reinforcement bending stiffness

the driving process by vacuuming. Care was taken not to remove or disturb the sand below the end of the tube. This technique was continued until the tube had been driven to the bottom of the shearbox. The process was then repeated for the second reinforcement.

(ii) the inner reinforcing bar of diameter D was then placed in the tube, and centred by means of wire spacers.

(iii) the grout mix, consisting of the water-cement ratio and proportions of Ordinary Portland and High Alumina cement given in Section 6.2.2 was prepared and poured into the brass tubes to the level of the top of the shearbox. To ensure adequate compaction of the grout a compressed air vibrator was applied to the top of the brass tube for approximately 1 minute.

(iv) the initial set of the grout occurred approximately 17 minutes after mixing. When this initial set was detected the brass tubes were winched out of the shearbox by an overhead hoist, leaving the grouted bars in the sand sample. If any slumping of the sand around the reinforcement occurred the test was repeated.

(v)   the vertical stress was then applied to the soil sample and the grout left to cure for

24 hours before testing.

Only two grouted bar tests were performed as is indicated in Table 6.6. Figure 6.15

presents data from the tests summarised in the table.
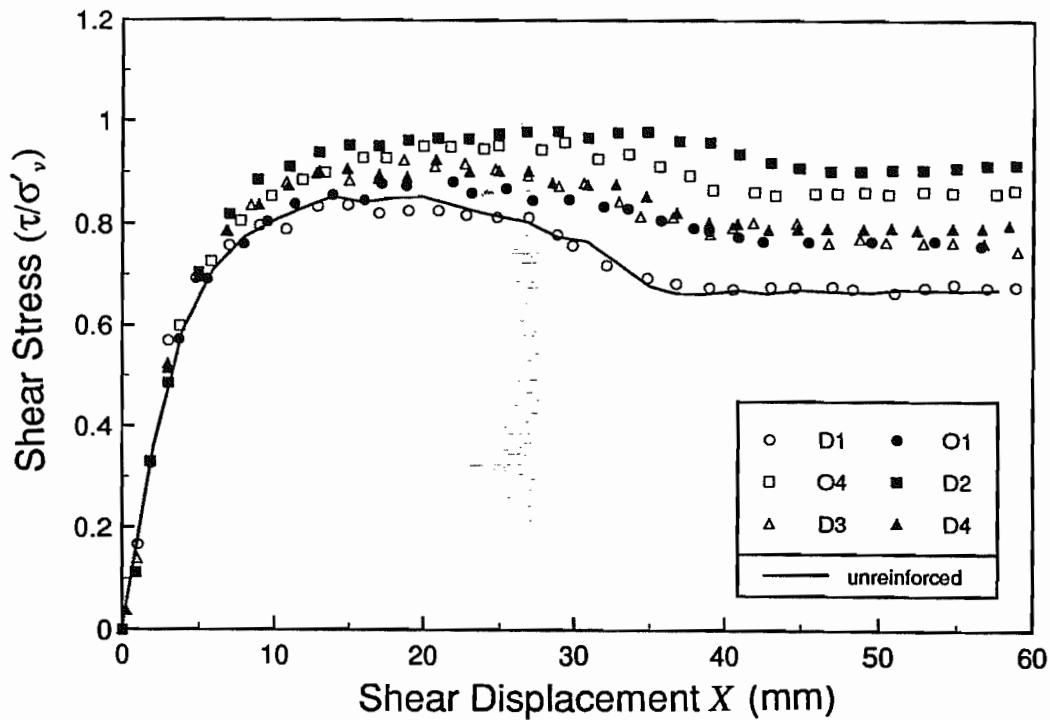
Figure 6.15 - Boundary data for a study of reinforcement bending stiffness.

Ignoring tests D3 and D4 on grouted reinforcement, the general trend is that as the

reinforcement diameter increases so does the shear strength (τ/σ'_v) of the soil. This trend

was previously observed for tests on medium dense sand. The smallest diameter

reinforcement $D = 6.5mm$ resulted in a negligible increase in shear strength, whereas the

largest diameter reinforcement $D = 51mm$ had a more significant effect of the order six

times greater. This sixfold increase in improvement is small when compared with the three

thousandfold increase in reinforcement bending stiffness EI or five hundredfold increase in

plastic moment capacity M_p.

The post test deformation of the reinforcement showed different failure modes as the reinforcement diameter changed; with smaller diameter reinforcement ($D = 6.5mm$, $16mm$) failing by plastic hinge formation and large diameter reinforcement ($D = 25mm$, $51mm$) by rigid body failure. This is seen in Plate 6.2 which shows reinforcement of varying diameters recovered from the shearbox.
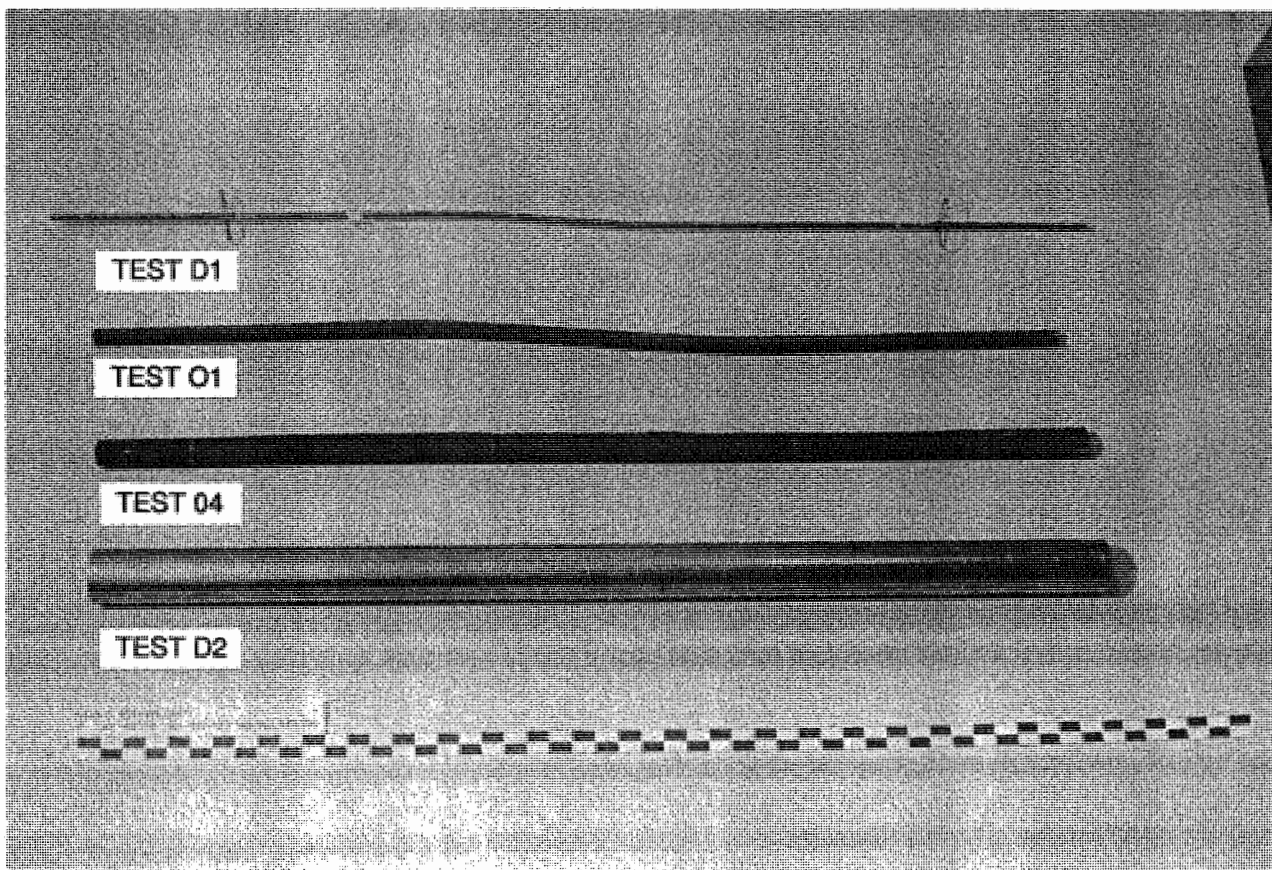
Plate 6.2 - Post test deformation of reinforcement of varying diameter D and bending stiffness EI.

Surprisingly, the soil shear strength improvement mobilised in the tests on grouted reinforcement of external diameter $D_g = 51mm$ is very similar for both tests, even though the internal bar diameter varied from $D = 6.5mm$ to $D = 16mm$.
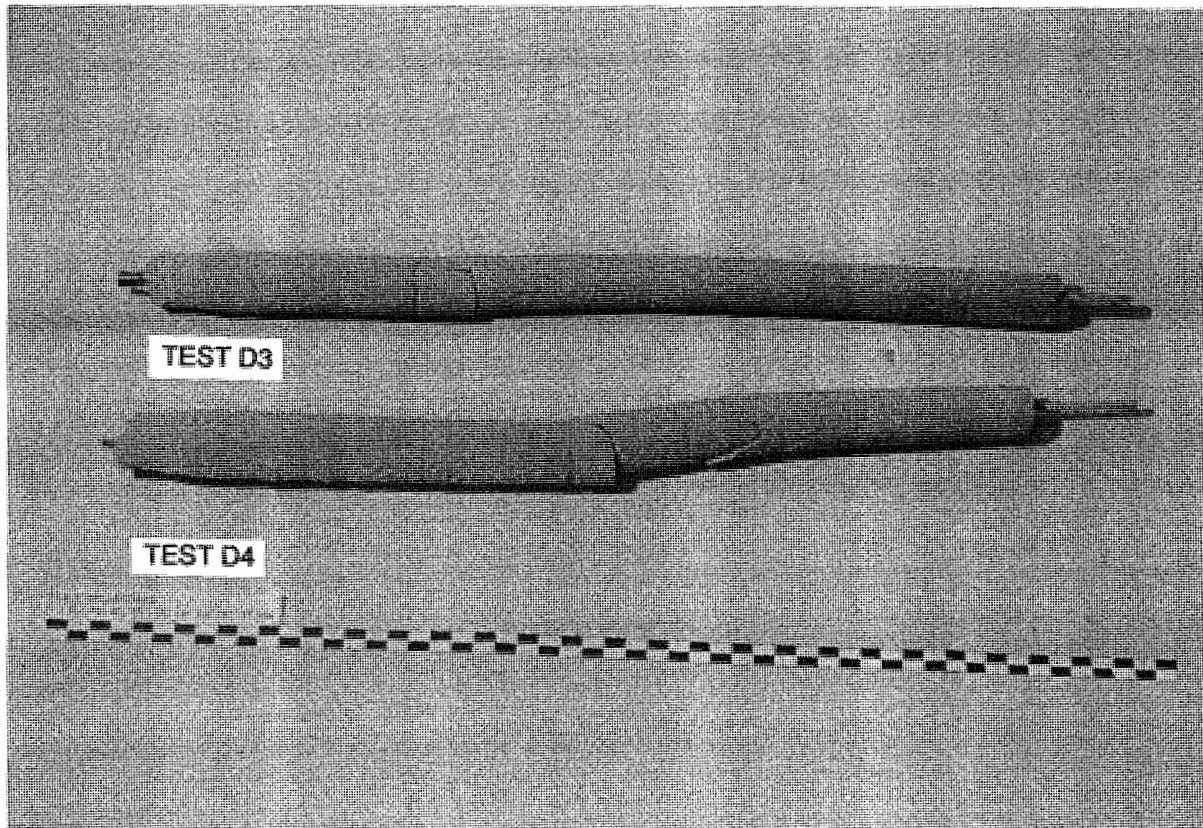
Plate 6.3 - Post test deformation of grouted reinforcement of external diameter
$D_g = 51mm$ **and internal diameter** $D = 6.5mm$ **and** $D = 16mm$**.**

The effect of grout on a bar of diameter $D = 6.5mm$ was much more significant than its effect on a bar of diameter $D = 16mm$. The additional increase in shear strength of the former was about three times that of the bar alone, at a shear displacement $X \approx 60mm$. For the larger diameter reinforcement $D = 16mm$ the effect of the grout was to increase the additional shear strength by a more modest factor of approximately 1.3.

The additional increase in shear strength observed by grouted bar over that of an ungrouted bar can be explained by the relative increase in both surface area and flexural resistance. An increase in surface area of the bar leads to an increase in reinforcement axial

force, and an increase in the cross section of the reinforcement, by the addition of grout, increases the lever arm of the reinforcement bar and consequently its flexural resistance. The post test deformation of the grouted bars is shown in Plate 6.3

6.4.4 Soil bearing capacity

The influence of soil bearing capacity on shear strength improvement was studied by testing two reinforcement bar diameters, $D = 16mm$ and $D = 25mm$, at three applied vertical stresses $\sigma'_v \approx 60kN/m^2$, $100kN/m^2$ and $150kN/m^2$. The two tests at $\sigma'_v = 100kN/m^2$ were also reported in the previous sections. In all of the tests the reinforcement was placed vertically ($\theta = 0°$). The specific details of these tests are summarised in Table 6.7 below. The final column gives the theoretical bearing stress σ'_b/σ'_v deduced from equations (6.18) and (6.19).

Test	Vertical Stress σ'_v kN/m^2	D mm	Material	N° Bars	Interface Type	Bearing Stress σ'_b/σ'_v equ^n (6.18)
S1	63.7	15.88	M. steel	2	I5	21.7
O1	103.3	15.88	M. steel	2	I2	21.7
S2	151.2	15.88	M. steel	2	I5	21.7
S3	64.1	25.40	M. steel	2	I5	21.7
O4	100.2	25.40	M. steel	2	I2	21.7
S4	151.0	25.40	M. steel	2	I5	21.7

Table 6.7 - Study of soil bearing strength

The mobilised shearing resistance (τ/σ'_v) as a function of shear displacement X for the tests described in Table 6.7 is shown in Figure 6.16..

As the applied vertical stress σ'_v increases there is an apparent reduction in the sample shear strength (τ/σ'_v) for the $D = 16mm$ reinforcement. This can be explained by the increase

in strength of the soil being much more significant than any increase in the reinforcement shear or axial force. This is supported by the observed reinforcement deformation being similar in all tests on $D = 16mm$ bars; all failed by plastic hinge formation.

The reinforcement of diameter $D = 25mm$ displays a different trend to the smaller diameter reinforcement. An examination of the post test reinforcement deformation revealed little plastic deformation of the reinforcement, suggesting rigid body failure. However, such a failure mode does not explain why the observed shear strength of the soil follows the trend in Figure 6.16. An explanation of the observed trend is offered in the following chapter.
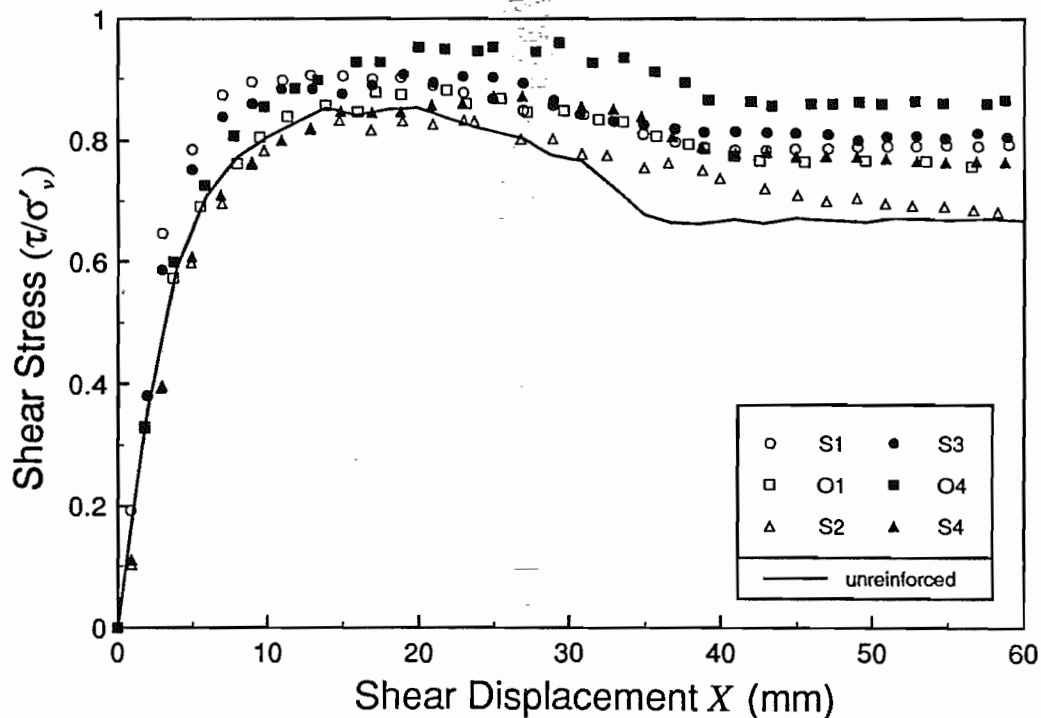
Figure 6.16 - Boundary data for a study of soil bearing strength.

6.4.5 Installation during shearing

The objective of this test series was to study the effect of reinforcing a shear surface at different stages of its development. Installing reinforcement across a pre-existing failure

surface is common to the techniques of soil dowelling, and soil nailing for slip repairs. The test procedure involved installing $D = 16mm$ reinforcement bars into the soil sample at varying shear displacements X_i, after application of a vertical stress of $\sigma'_v \approx 100kN/m^2$.

Mild steel reinforcement bars of total length $L = 960mm$ were used. A $60°$ cone was machined onto the end of each bar to aid the driving of the reinforcement. Two bars per test were driven vertically into each sample through the top plate of the shearbox.

The reinforcement driving mechanism was originally constructed for use with a piezocone and is described in detail by Nyirenda (1990). The reinforcement was driven into the soil by means of a ball screw and stepper motor mounted in a rigid frame, and fixed securely to the top plate of the shearbox. The rate of penetration of the reinforcement was $10mm/$ sec. On retrieval of the reinforcement from the sand it was observed that considerable crushing of the sand had occurred close to the reinforcement, and the surface of the reinforcement had become rougher.

The shear displacements at which reinforcement was driven are given in Table 6.8, and the experimental boundary data shown Figure 6.17.

Test	Vertical Stress σ'_v kN/m^2	D mm	Material	N° Bars	Interface Type	Installed at X_i (mm)
N1	107.7	15.88	M. steel	2	I5	0
N2	105.3	15.88	M. steel	2	I5	5.0
N3	104.9	15.88	M. steel	2	I5	10.0
N4	104.8	15.88	M. steel	2	I5	15.0
N5	105.1	15.88	M. steel	2	I5	20.0
N6	106.3	15.88	M. steel	2	I5	39.9

Table 6.7 - Study of reinforcement installation.

For reinforcement installed before application of the shear load $(X_i = 0)$ the resulting strength improvement was close to that exhibited by reinforcement placed at the time of
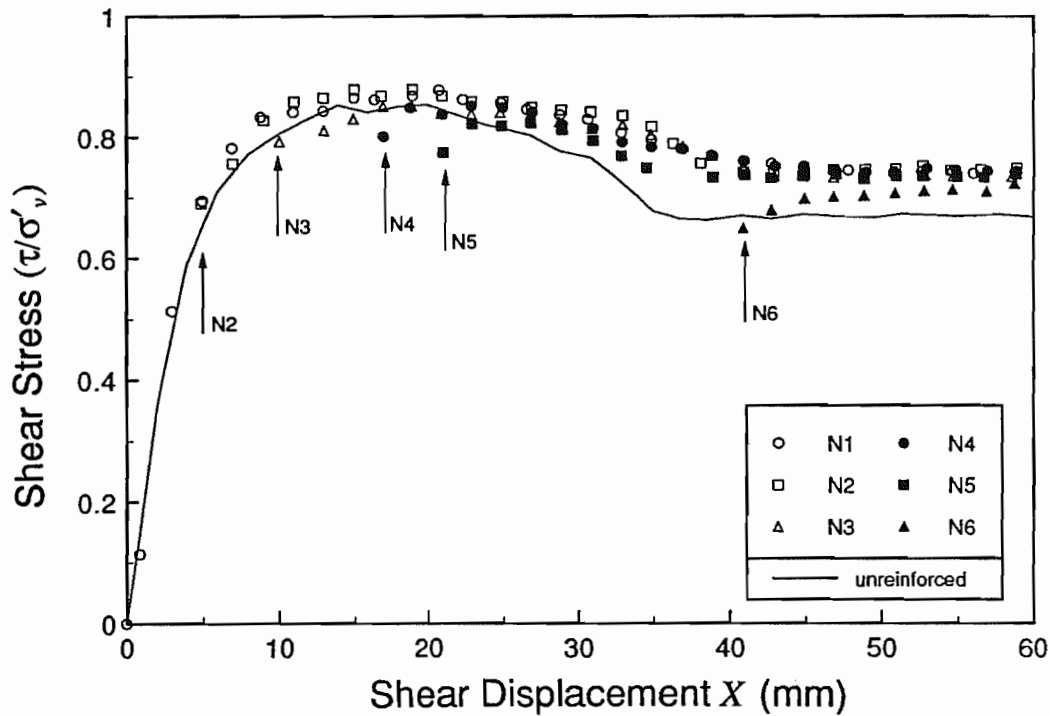
Figure 6.17 - Boundary data for a study of reinforcement installation.

sample preparation; compare test N1 with O1. This appeared also to be true for any reinforcement installed at a shear displacement X_i less than that required to mobilise the peak strength of the unreinforced sand. Reinforcement placed after mobilisation of the peak unreinforced strength resulted in an increase in soil shear strength above that of the unreinforced test, but not as great as for samples reinforced during strain hardening. The installation of reinforcement during constant volume shearing $(X_i = 40mm)$ resulted in a gradual increase in shear strength, but to a value slightly less than that of tests reinforced at an earlier stage.

Owing to the smooth reinforcement surface the increase in shear strength of the soil is attributed to reinforcement shear force and bending of the reinforcement. To mobilise shear force in the reinforcement large relative soil-reinforcement displacements were required. Therefore, the larger the shear displacement X_i at which installation occurs the
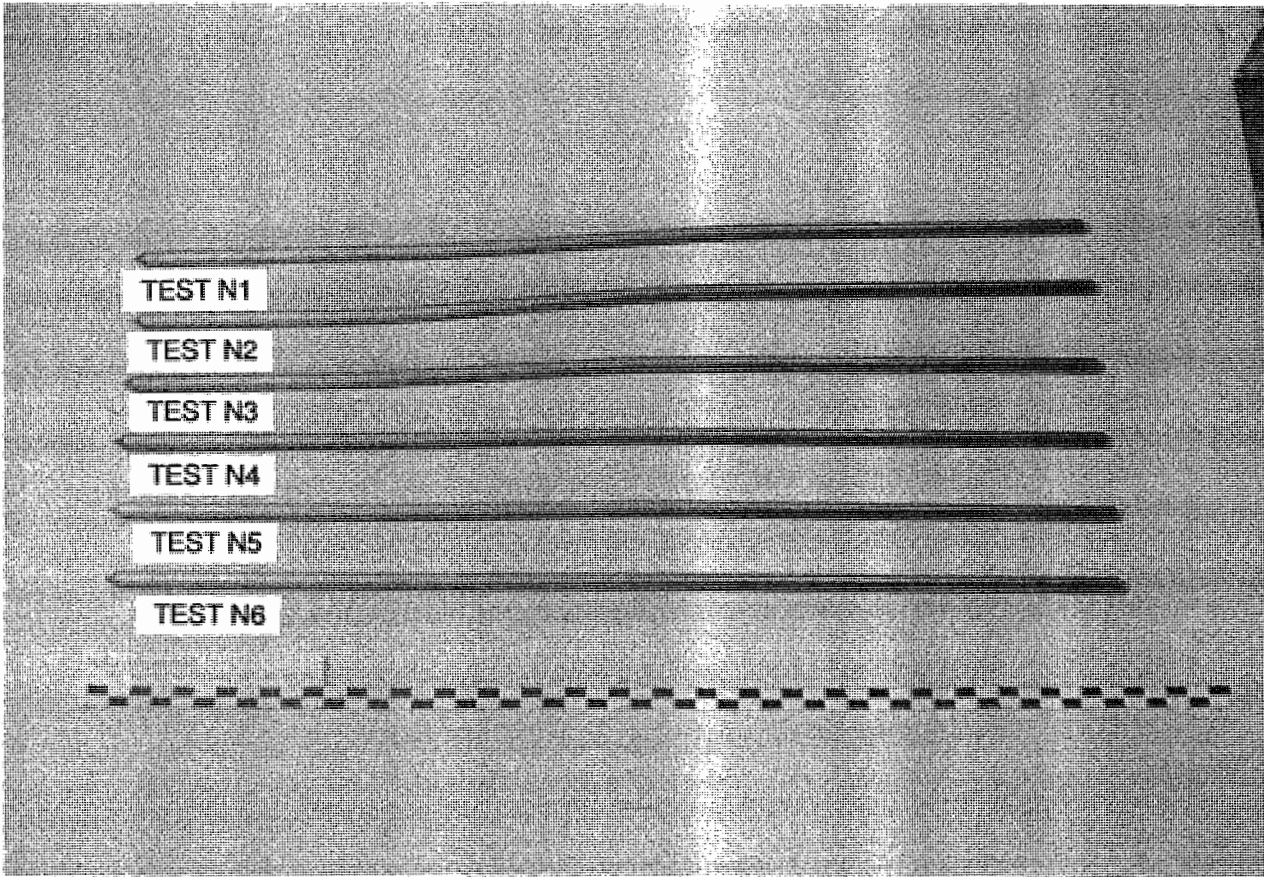
Plate 6.3 - Post test deformation of reinforcement driven into the sample at different shear displacements X.

greater will be the overall shear displacement required to increase the soil shear strength to a given value. If reinforcement is installed whilst the soil is dilating greater benefits may be obtained.

A common belief is that the action of driving reinforcement causes a local increase in the stresses acting around the reinforcement, and consequently an increase in the pullout resistance. Despite crushing of the sand around the reinforcement, indicating a local increase in stress, no perceptible increase in shear strength was observed for this method of installation. Therefore, for dense sands it appears there is very little benefit to the potential shear strength improvement by installing reinforcement by driving.

The deformed reinforcing bars recovered from this test series are shown in Plate 6.4. The deformation of the reinforcement diminishes as the installation displacement X_i increases.

6.5 Summary of Experimental Observations

The boundary and internal strain gauge data presented in this chapter lead to the following conclusions:

(i)   reinforcement crossing a failure surface in soil is loaded both by an axial force P_{ax} and a shear force P_s when a relative soil-reinforcement displacement occurs. These forces may lead to an increase or reduction in the strength of the soil. The relative soil-reinforcement displacement required to mobilise a limiting axial force is less than that required for a limiting shear force.

(ii)   the internal strain gauge data from the shearbox tests imply that provided the length of reinforcement extending either side of a shear surface is sufficient the loading of the reinforcement can be considered symmetrical; this is confirmed by the post test reinforcement deformation.

(iii)   the effect of the reinforcement surface characteristics influenced the pullout resistance of the reinforcement significantly, but showed limited effect on the reinforcement shear force. The orientation of the reinforcement also showed a similar effect on the axial and shear forces. The use of anchor plates increased the axial reinforcement force, but the axial force-displacement response is not analogous to that of a soil nail.

(iii)   an increase in the stiffness and strength of the reinforcement led to a corresponding increase in the shear strength improvement of the soil. The limiting improvement in soil shear strength is related to the relative soil-reinforcement strength, as is the failure mechanism.

(v)   the effect of driving reinforcement into dense sand had very little effect on the soil shear strength. The greatest benefit was obtained from reinforcement installed whilst the soil was dilating. The installation of reinforcement by drilling and grouting led to a significant increase in soil strength owing to the increased flexural and axial capacity.

CHAPTER 7:

THEORETICAL ANALYSIS

The objective of this Chapter is to introduce existing analyses for the prediction of reinforcement shear force and to develop a new analysis based on the experimental observations reported in Chapter 6. A review of the typical parameters required for the analyses is given. The effect of reinforcement shear force on soil shear strength is then compared with the potential benefit from reinforcement axial force.

7.1 Interaction Between Shear and Axial Force for Soil Reinforcement

7.1.1 Statement of the problem: shearbox analogy

The problem will be simplified to that of a reinforcing bar placed symmetrically across a potential failure plane in the shearbox, Figure 7.1. If at a given shear displacement X the shearing resistance of the soil alone is S, then the introduction of reinforcement will lead to a change in strength of the soil to $S + \Delta S$, at the same shear displacement. The change in strength ΔS is a direct result of the shear force P_s and axial force P_{ax} which develop in the reinforcement at the failure plane.

The reinforcement shear and axial forces result from the relative displacement between the soil and the reinforcement. A soil displacement δ across the shearing zone of soil has a shear component perpendicular to the reinforcement δ_s and an axial component parallel to the reinforcement δ_{ax}. The magnitude of these relative displacements is a function of the
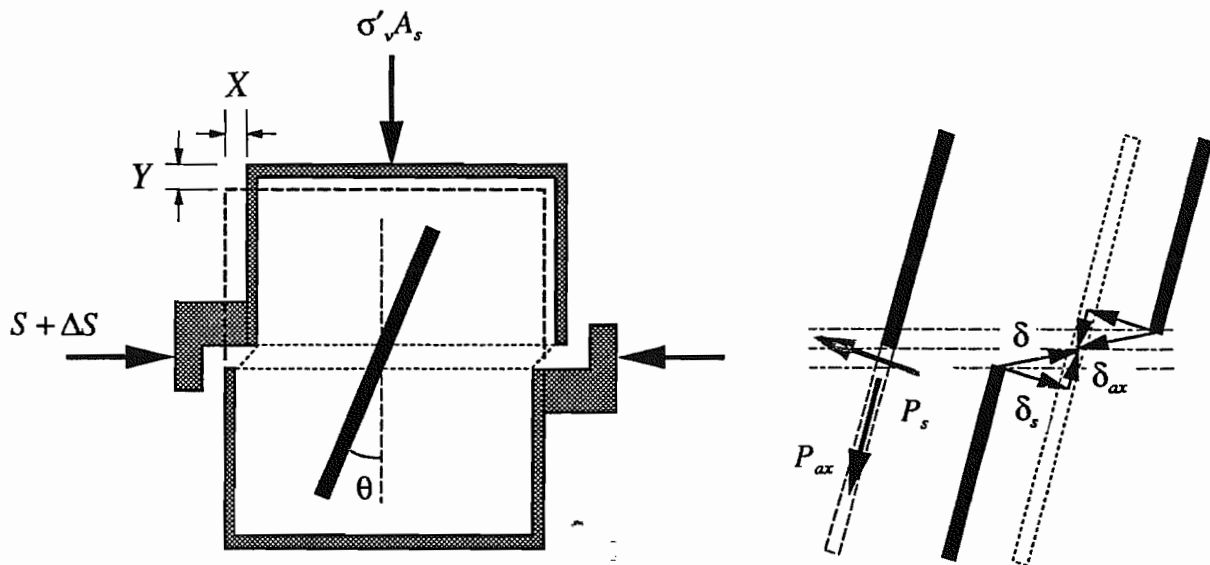
Figure 7.1 - Reinforcement crossing a potential rupture surface

reinforcement orientation. The induced shear and axial forces are a function of the lateral stiffness and strength of the soil, the bending stiffness and yield strength of the reinforcement, and the limiting shearing resistance between the soil and the reinforcement surface.

Chapter 6 showed that the forces in the reinforcement were distributed symmetrically about the central plane in the shearbox. It is therefore sufficient to consider one half of the reinforcement for analysis. This leads to a free body diagram for one half of the reinforcement, which is in some ways analogous to the problem of a laterally loaded pile.

7.1.2 Potential failure mechanisms

Three modes of failure for reinforcement in the shearbox can be identified. These are shown in Figure 7.2 for the reinforcement in the lower half of the shearbox. Failure can be due to limits on the axial load P_{ax} or the shear load P_s.

(i)   Pullout failure

This limit occurs when the reinforcement axial force P_{ax} causes the limiting bond stress to be exceeded over the entire surface area of the reinforcement,

$$P_{po} = \tau_{po} \, A_c \, L_a \qquad\qquad \dots(7.1)$$

(a) Pullout   (b) Rigid body   (c) Plastic hinge
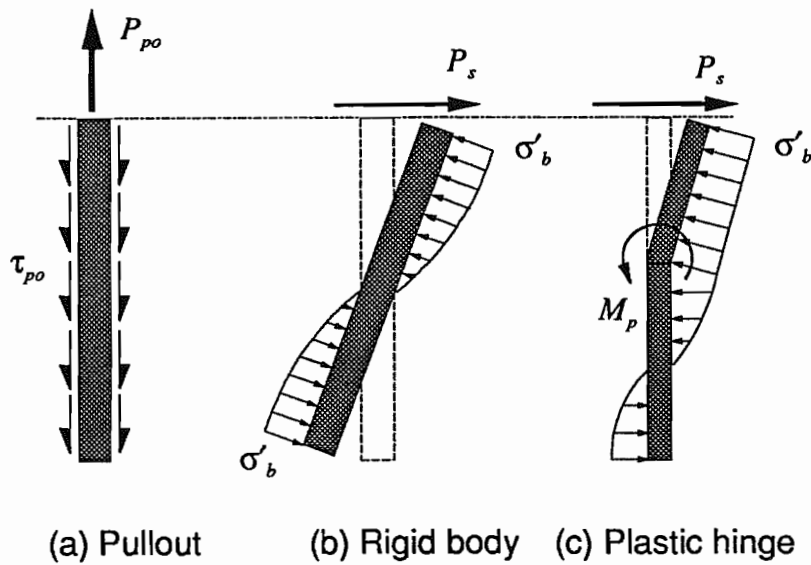
Figure 7.2 - Potential failure modes for reinforcement subjected to shear and axial force.

where τ_{po} is the limiting shear stress between the soil and reinforcement, A_c the circumferential area per unit length of reinforcement and L_a is the anchorage length of the reinforcement (which is equal to $L/2$ where L is the total length of the reinforcement in the shearbox).

To ensure the reinforcement does not fail in axial tension the pullout force must always be less than the plastic capacity of the reinforcement P_p, therefore

$$P_{po} < P_p = \sigma_p A_r \qquad \qquad ...(7.2)$$

where A_r is the cross sectional area of the reinforcement and σ_p is the reinforcement yield stress. The limit force is the lower of the axial capacity P_p and the pullout force P_{po}, Figure 7.2(a).

(ii)   **Rigid body shear failure**

This failure mode was identified by Broms (1964a) for piles subjected to a horizontal

shear load, and occurs when the lateral stress σ'_l mobilised against the reinforcement is equal to the limiting bearing stress σ'_b of the soil over the entire length of the reinforcement.

Such a failure mode can occur when the reinforcement is sufficiently strong to sustain the applied loads without forming a plastic hinge, Figure 7.2(b).

(iii)   **Plastic hinge failure**

This failure mode was also identified by Broms (1964a) for piles subjected to a horizontal shear load. This mode occurs when the bearing strength of the soil is sufficiently high to allow the formation of a plastic hinge under the applied shear load, Figure 7.2(c).

The three failure modes described above have been considered independently. In practice it is likely that a combination of axial and shear force will be mobilised at failure, so that the pullout mode will be combined with one of the shear failure modes.

7.2 Prediction of Reinforcement Shear Force

Two analyses for the prediction of reinforcement shear force are described in this section. The first model is based on elastic deformation of the soil and of the reinforcement. The second model is a plastic analysis allowing yielding of the reinforcement and of the soil. The analyses which follow consider one half of the reinforcement in the shearbox. The length of reinforcement in the model is L_a, which corresponds to half the length of the reinforcement in the shearbox i.e. $L = 2L_a$.

7.2.1 Elastic analysis

The theory of a laterally loaded pile in an elastic medium, loaded at one end by a shear force P_s can be used to predict soil reinforcement shear force, Schlosser (1983). A solution to the problem is given by considering the rate of change of shear force dP_s/dz of a beam on a Winkler medium. This yields the differential equation

$$-\frac{dP_s}{dz} = -\frac{EI}{D}\frac{d^4\delta_s}{dz^4} = K_s\delta_s = \sigma'_l \qquad \qquad \dots(7.3)$$

where z is the distance along the beam from the point of shear loading, E the Young's modulus and I the second moment of area of the reinforcement, D the width of the reinforcement, K_s the modulus of subgrade reaction of the soil, δ_s the displacement at point z and σ'_l the lateral stress acting at point z.
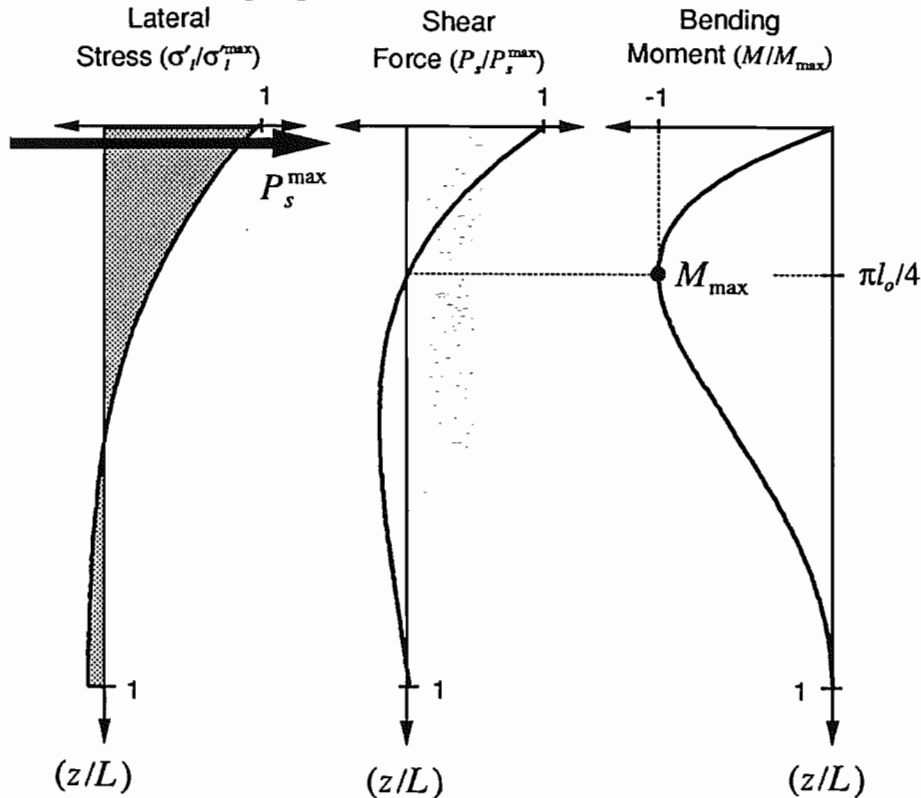
Figure 7.3 - Profiles of lateral stress (σ_l/σ_l^{max}), shear force (P_s/P_s^{max}), and bending moment (M/M_{max}) for an elastic analysis where $\eta L_a = 3$.

Solutions to equation (7.3) have been found by Hetenyi (1946), and more recently for the case of a laterally loaded pile by Poulos and Davis (1980). They give tabulated solutions for the displacement, slope, bending moment and shear along the length of the pile for a given applied shear force P_s. These solutions are expressed as a function of ηL_a, where L_a is the length of the pile and η the inverse of the *elastic length l_o*. Where l_o is

$$l_o = \frac{1}{\eta} = \sqrt[4]{\frac{4EI}{K_sD}} \qquad (\eta = \beta \ ?) \qquad \qquad \ldots(7.4)$$

For soil nails Schlosser (1982) uses $\eta L_a = 3$. This case will also be adopted in this dissertation. The Poulos and Davis (1980) solutions for the bending moment (M/M_{max}), shear force (P_s/P_s^{max}) and lateral stress[†] (σ_l/σ_l^{max}) when $\eta L_a = 3$ are shown in Figure 7.3. The maximum moment is a distance $\pi l_o/4$ from the maximum shear force P_s, which is given by

$$P_s = \frac{M_{max}}{0.318 \, l_o} \qquad \qquad \ldots(7.5)$$

In the shearbox, the loading of the reinforcement is symmetrical about the central plane and an equal and opposite bending moment is observed on either side. The length l_s is the distance between the points of maximum moment and is termed the *shear width*. Therefore, the distance between the point where the shear force is applied and the bending moment a maximum is $l_s/2 \, (= \pi l_o/4)$. In which case equation (7.5) becomes

$$P_s = \frac{4.9 M_{max}}{l_s} \qquad \qquad \ldots(7.6)$$

and equation (7.4) can be expressed as

$$l_s = \frac{\pi}{2} l_o = \frac{\pi}{2} \sqrt[4]{\frac{4EI}{K_sB}} \qquad \qquad \ldots(7.7)$$

The second moment of area I of a circular cross section is $\pi D^4/64$. If this is substituted into equation (7. 7) a non-dimensional measure of the shear width (l_s/D) is given by

$$\left(\frac{l_s}{D}\right)^e = \frac{\pi}{4} \sqrt[4]{\frac{\pi E}{K_sD}} \qquad \qquad \ldots(7. \ 8)$$

where the superscript e denotes an elastic shear width. An important feature is that the shear force P_s is limited by the shear width $(l_s/D)^e$, and this is a function of the relative stiffness of the reinforcement to the soil (E/K_sD).

[†]The lateral stress profile is identical to the displacement profile and obtained from $\sigma_l = K_s\delta_s$.

The elastic solutions quoted in this section are only valid if the maximum bending moment in the reinforcement M_{max} is less than the elastic yield moment M_e. For any structural member there is a relationship between the limiting combination of bending moment M_{max} and axial force P_{ax} causing yield. For soil nails in particular the reinforcement axial force can be significant, and it is therefore necessary to include a term in equation (7.6) to limit the maximum bending moment.

The limiting elastic bending moment of any cross section is given by $I\sigma_{bend}/y$, where y is the distance between the neutral axis and the most highly stressed fibre where the stress is σ_{bend}. For a given axial force (P_{ax}/P_p) the maximum stress available for bending is $\sigma_{bend} = (\sigma_p - \sigma_{ax})$ where $\sigma_{ax} = (P_{ax}/A_r)$. From which it is possible to express the maximum bending moment as a function of the elastic bending moment M_e and the axial force (P_{ax}/P_p)

$$\frac{M_{max}}{M_e} = 1 - \left(\frac{P_{ax}}{P_p}\right) \qquad\qquad ...(7.9)$$

Substituting for M_{max} in equation (7.6) results in

$$P_s = \frac{4.9 M_e}{l_s}\left\{1 - \left(\frac{P_{ax}}{P_p}\right)\right\} \qquad\qquad ...(7.10)$$

relating the maximum reinforcement shear force to the axial force.

The lateral stress σ'_l acting between the reinforcement and soil is a maximum at the point where the shear load is applied, and given by

$$\sigma'_l = \frac{M_{max}}{0.16\, l_o^2 D} = \frac{15.4 M_{max}}{l_s^2 D} \qquad\qquad ...(7.11)$$

and should always be less than the limiting soil bearing stress σ'_b.

In the elastic analysis the limiting shear force is governed by both the shear width l_s and the maximum moment M_{max} in the reinforcement. Therefore the maximum moment M_{max} is the lesser of

$$M_e\left\{1-\left(\frac{P_{ax}}{P_p}\right)\right\} \qquad \text{or} \qquad \sigma'_b\frac{l_s^2 D}{15.4}$$

where M_e is the elastic yield moment.

The elastic model cannot be used to define the limiting combination of shear and axial force at failure. The maximum shear force determined from this analysis simply defines the point when plasticity occurs in the reinforcement.

7.2.2 Plastic analysis

The term plastic refers to the state of stress of the soil acting against the reinforcement and not necessarily to that of the reinforcement; this may range from purely elastic to plastic.

The model proposed for estimating the shear force available from reinforcement embedded in soil is derived from an empirical fit to the experimental data presented in Figure 6.14. Figure 7.4 shows the lateral stress data for reinforcement in the lower half of the shearbox at a shear displacement of $X = 60mm$.

The shaded zone in Figure 7.4 is the model of lateral stress distribution first presented in Jewell and Pedley (1990a) as a possible mechanism for soil-nail interaction and based on this experimental data. The thick dotted line is a rigid-plastic model suggested by Brinch Hansen and Lundgren (1960), where the limiting bearing stress is mobilised over the entire length of the reinforcement. The theoretical shear force and bending moment distributions for the two models are compared with the experimental data.

The Brinch Hansen and Lundgren model shows a poorer fit to the data than the elastic-plastic Jewell and Pedley model. This can be attributed to the large rotations required by the rigid-plastic model to mobilise the soil bearing capacity over the entire length of the reinforcement. The elastic-plastic model proposed is therefore more realistic.
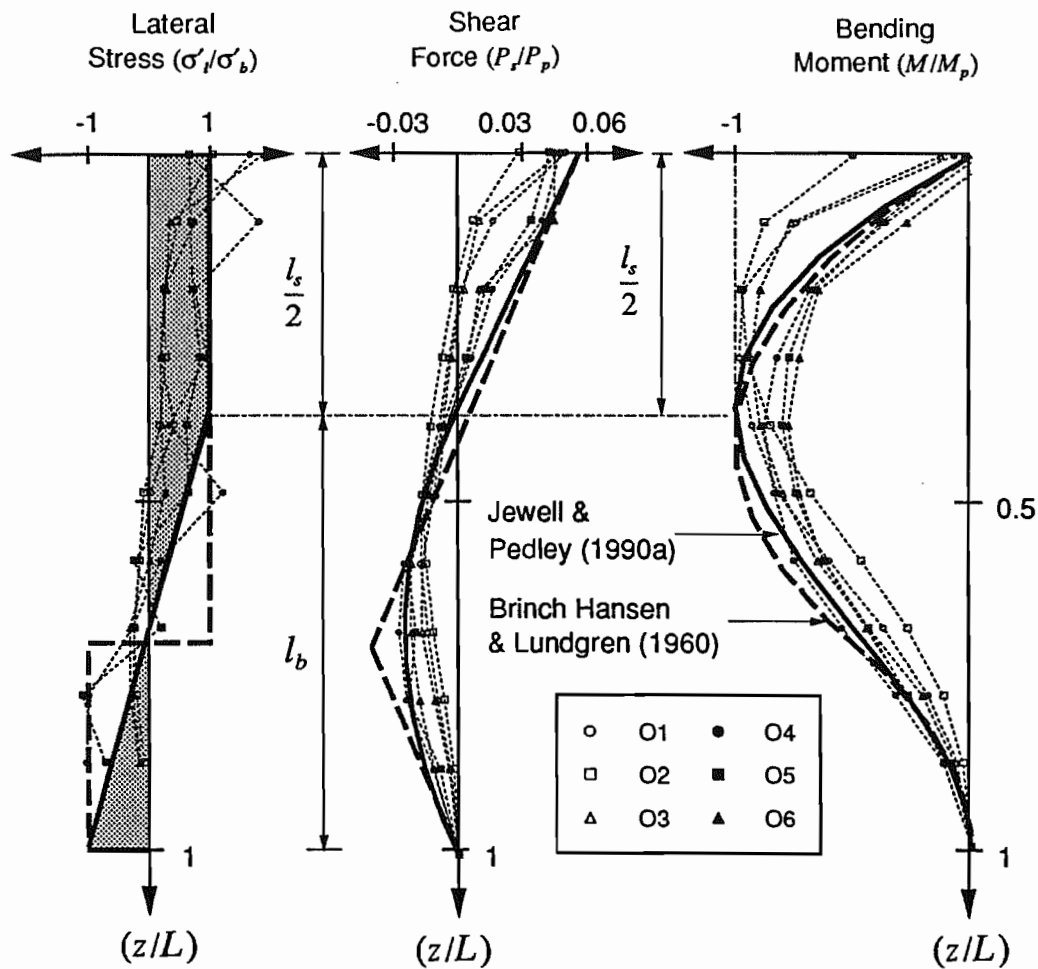
Figure 7.4 - Comparison between theoretical models of plastic soil-reinforcement interaction and experimental data at a shear displacement $X = 60mm$.

The same definition for the *shear width* l_s is defined as for the elastic model. The distance between the maximum moment M_{max} and the point of maximum shear force P_s is therefore $l_s/2$. If the distance from the maximum moment to the free end of the reinforcement is l_b, then the total length of the reinforcement is $L/2 = L_a = (l_s/2 + l_b)$.

Figure 7.4 shows that over the length $l_s/2$ the lateral stress is more or less constant. From the point of maximum moment the load decreases approximately linearly from $(\sigma'_l/\sigma'_b) = 1$ to $(\sigma'_l/\sigma'_b) = -1$ at the free end. Taking moments at M_{max} over the lengths l_s and l_b gives

$$\left\{ 2\sigma'_b \left(\frac{l_b}{2}\right)\left(\frac{2l_b}{3}\right) - \sigma'_b\left(\frac{l_b^2}{2}\right) \right\} - \left\{ \sigma'_b\left(\frac{l_s^2}{8}\right) \right\} = 0$$

which simplifies to the ratio

$$\frac{l_b}{l_s} = \frac{\sqrt{3}}{2} \qquad \qquad ...(7.12)$$

defining the geometry of loading. Resolving forces relates the shear force to the maximum bearing stress by

$$P_s = \sigma'_b D \frac{l_s}{2} \qquad \qquad ...(7.13)$$

and taking moments about the point of application of the shear force gives

$$M_{max} = \sigma'_b \frac{D l_s^2}{8} \qquad \qquad ...(7.14)$$

A relationship between the limiting shear force P_s and maximum moment M_{max} is obtained by combining equations (7.13) and (7.14),

$$P_s = 4 \frac{M_{max}}{l_s} \qquad \qquad ...(7.15)$$

A similar analysis for the Brinch Hansen and Lundgren model leads to an identical relationship between P_s and M_{max}. However, the ratio of the shear width l_s and the bearing length l_b is $(l_b/l_s) = 1/\sqrt{2}$, which gives a slightly larger shear width.

As with the elastic analysis there is a relationship between the limiting combination of bending moment M_{max} and axial force P_{ax} which causes reinforcement failure. For a plastic analysis the limiting maximum bending moment at any point is a function of the fully plastic moment M_p and the axial force (P_{ax}/P_p). Therefore, for any cross section

$$\left(\frac{M_{max}}{M_p} \right) = \rho f \left(\frac{P_{ax}}{P_p} \right) \qquad \qquad ...(7.16)$$

where ρ is a constant which depends on the cross sectional shape. This relationship between maximum bending moment M_{max} and axial force P_{ax} is now investigated for typical reinforcement cross sections.

(i) *Circular bar*
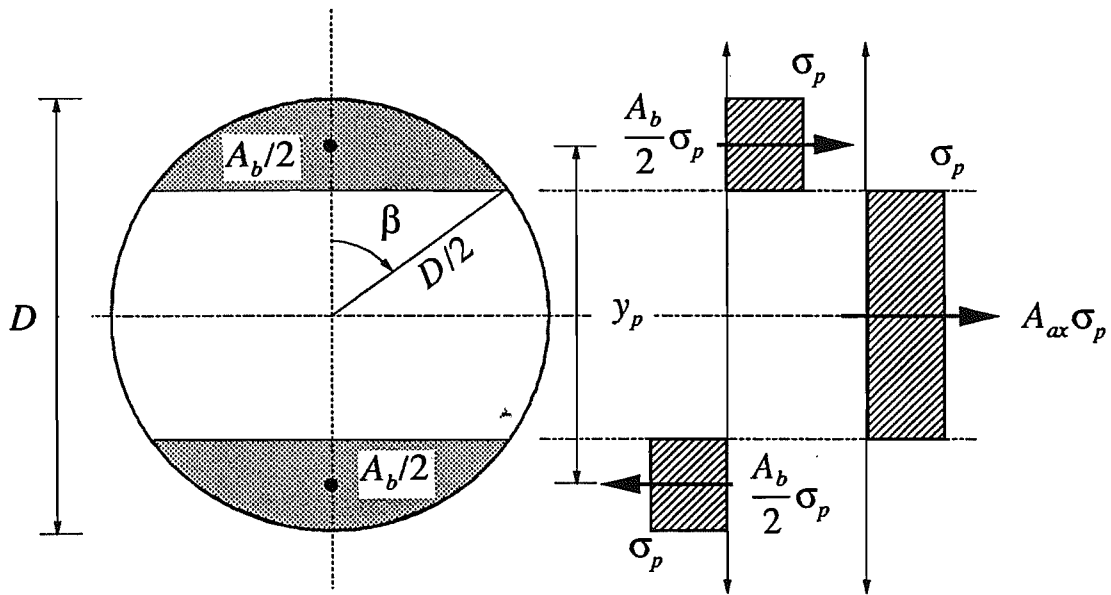
Figure 7.5 - Calculation of moment (M_{max}/M_p) axial force (P_{ax}/P_p) relationship for a circular section.

In soil nailing and dowelling the reinforcement cross section is often circular. Figure 7.5 is a cross section through a circular bar subjected to a limiting combination of bending moment M_{max} and axial force P_{ax}. The yield stress σ_p has developed over the shaded areas $A_b/2$ through reinforcement bending. These areas are assumed to be equidistant from the centroid of the section. The unshaded area A_{ax} is that which has yielded due to axial force P_{ax}. To the right of the figure the stress blocks due to the applied bending moment and axial force are shown.

If the angle β is defined as shown in Figure 7.5 the areas A_b and A_{ax} can be defined from geometry as

$$A_b = \frac{D^2}{4}\{2\beta - \sin 2\beta\} \qquad \qquad ...(7.17)$$

and

$$A_{ax} = \frac{D^2}{4} \{\pi - 2\beta + \sin 2\beta\} \qquad \ldots(7.18)$$

respectively. The moment of resistance is given by taking moments for one of the areas $A_b/2$ about the centroid of the other,

$$M_{max} = \frac{A_b}{2} \sigma_p y_p \qquad \ldots(7.19)$$

where y_p is the distance between the centroids of the two areas $A_b/2$, as shown in the figure.

Noting that the centroid of a circular sector of internal angle 2β is at distance $D \sin \beta / 3\beta$ from its apex gives y_p as

$$y_p = \frac{4D \sin^3 \beta}{3\{2\beta - \sin 2\beta\}} \qquad \ldots(7.20)$$

Substituting for y_p and A_b in equation (7.19) leads to a moment of resistance

$$M_{max} = \frac{D^3}{6} \sigma_p \sin^3 \beta \qquad \ldots(7.21)$$

which can be expressed as a fraction of the fully plastic moment M_p by,

$$\left(\frac{M_{max}}{M_p}\right) = \sin^3 \beta \qquad \ldots(7.22)$$

The axial force P_{ax} is simply the multiple of the area A_{ax}, equation (7.5), and the yield stress σ_p. Therefore the ratio of the axial force to the fully plastic axial force (P_{ax}/P_p) is given by

$$\left(\frac{P_{ax}}{P_p}\right) = \frac{\{\pi - 2\beta + \sin 2\beta\}}{\pi} \qquad \ldots(7.23)$$

The limiting combination of bending moment (M_{max}/M_p) and axial force (P_{ax}/P_p) are shown in Figure 7.6, for the angle β in the range $0 \leq \beta \leq \pi/2$.

(2) *Rectangular bar*

The limiting combination of bending moment and axial force for rectangular bar may be found in textbooks such as Todd (1981). It may also be found using the method described above for circular bar. The relationship is

$$\left(\frac{M_{max}}{M_p}\right) = 1 - \left(\frac{P_{ax}}{P_p}\right)^2 \qquad \ldots(7.24)$$

and is identical to the solution for the limiting combinations of shear force, bending moment and axial force suggested by Neal (1961) for rectangular bars, for the case when the shear force is zero. Equation (7.24) is shown in Figure 7.4.

The comparison in Figure 7.6 shows that the limiting combinations of bending moment and axial force are almost identical for rectangular and circular cross sections. For simplicity equation (7.24) is adopted for the remainder of this dissertation to derive the bending moment and axial force for both rectangular and circular cross sections.
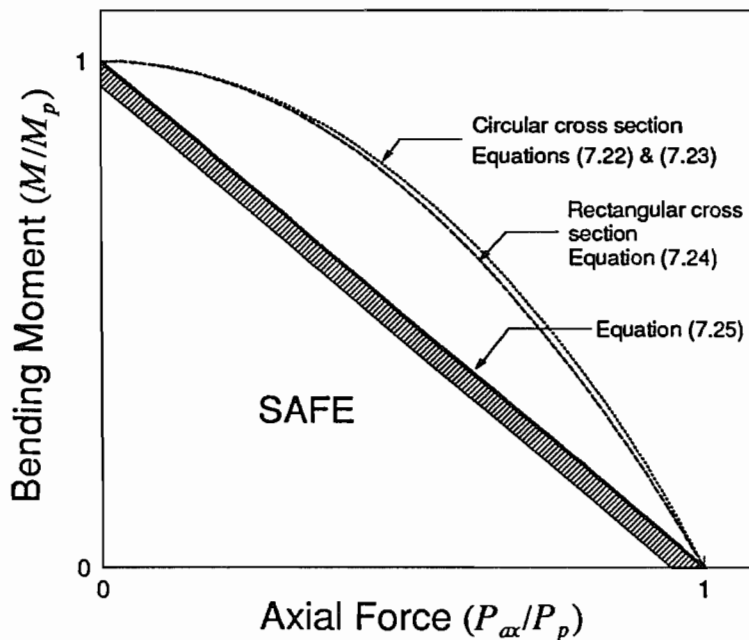
Figure 7.6 - Limiting combinations of bending moment (M_{max}/M_p) and axial force (P_{ax}/P_p).

(iii) *Safe solution*

Calladine (1985) has shown that a *lower bound* or safe solution for limiting combinations of bending moment (M_{max}/M_p) and axial force (P_{ax}/P_p) is given by the quadrilateral described by the equation

$$\left(\frac{M}{M_p}\right) = 1 - \left(\frac{P_{ax}}{P_p}\right) \qquad \qquad ...(7.25)$$

where (P_{ax}/P_p) is positive. The solution is for any cross sectional shape and is shown in Figure 7.4. This safe solution is adopted in BS5950 (1985), the British Standard code of practice for structural steelwork.

Substituting the relationship for the limiting combination of maximum moment M_{max} and axial force P_{ax} for circular bar in equation (7.15) gives

$$P_s = 4\frac{M_p}{l_s}\left\{1 - \left(\frac{P_{ax}}{P_p}\right)^2\right\} \qquad \qquad ...(7.26)$$

An expression for the non dimensional plastic shear width $(l_s/D)^p$ is given by substituting for the fully plastic moment M_p in equation (7.14). For a circular bar $M_p = D^3\sigma_p/6$, giving

$$\left(\frac{l_s}{D}\right)^p = \sqrt{\frac{4\sigma_p}{3\sigma'_b}\left\{1 - \left(\frac{P_{ax}}{P_p}\right)^2\right\}} \qquad \qquad ...(7.27)$$

and for rectangular bar of width B and thickness t the plastic moment is $M_p = Bt^2\sigma_p/4$, giving

$$\left(\frac{l_s}{t}\right)^p = \sqrt{2\frac{\sigma_p}{\sigma'_b}\left\{1 - \left(\frac{P_{ax}}{P_p}\right)^2\right\}} \qquad \qquad ...(7.28)$$

where the superscript *p* represents a plastic analysis. The analysis of the elastic shear width $(l_s/D)^e$, equation (7.8), was a function of the relative *stiffness* of the reinforcement to the soil (E/K_sD). In the plastic analysis it is seen that the shear width $(l_s/D)^p$ is a function of the relative *strength* of the reinforcement to the soil (σ_p/σ'_b), and also to the axial force (P_{ax}/P_p).

Jewell and Pedley (1990b) ignored the axial force term in equations (7.27) and (7.28) when calculating the shear width $(l_s/D)^p$. This leads to a conservative estimate of the shear force from equation (7.26) for large values of the ratio (P_{ax}/P_p); this analysis was termed a *simplified analysis*, and was suggested for design purposes.

When loaded by a shear force P_s reinforcement may fail either by the formation of a plastic hinge, or by the limiting soil bearing stress being exceeded resulting in rigid body failure, Figure 7.2. A plastic hinge occurs when

$$\left(\frac{L_a}{D}\right) \geq \left(\frac{1+\sqrt{3}}{2}\right)\left(\frac{l_s}{D}\right)^p \qquad \ldots(7.29)$$

This equation was derived from equation (7.12), which defines the minimum overall length of reinforcement for plastic hinge failure. When equation (7.29) does not hold then $(l_s/D)^p$ is given by

$$\left(\frac{l_s}{D}\right)^p = \left(\frac{L_a}{D}\right)\left(\frac{2}{1+\sqrt{3}}\right) \qquad \ldots(7.30)$$

If this value of l_s is substituted into equation (7.14) then the maximum moment in the reinforcement M_{max} during rigid body failure is given. Substitution of M_{max} and l_s into equation (7.15) gives the limiting shear force for rigid body failure.

For the case of rigid body failure (P_{ax}/P_p) is generally small, and the limiting shear force obtained from equation (7.15) can be considered independent of P_{ax}.

The plastic analysis described predicts the limiting lateral shear force which can be applied to reinforcement in soil, and the failure mode.

7.2.3 Selection of parameters for the analysis

Guidance is given in this section on typical values of the parameters used in the analyses and how they may be determined.

(i) Reinforcement material parameters

Two reinforcement material properties are used for the analysis of the limiting reinforcement shear force; the Young's modulus E and the yield stress σ_p. Steel reinforcement is commonly used and typical ranges for these parameters are $E \approx 200 \times 10^6 \ kN/m^2$ and $\sigma_p = 200\text{--}400 \times 10^3 \ kN/m^2$. Where other materials are used, such as aluminium or concrete the elastic modulus and yield stress may be obtained from standard tests or from tables, Table 6.1.

(ii) Soil parameters

In order to determine the lateral soil stress σ'_l the soil is described by either an elastic or a plastic parameter. A common elastic parameter for determining the lateral stress between soil and a beam resting on it is the modulus of subgrade reaction K_s. This parameter was introduced into soil mechanics by Winkler (1867).

The term subgrade reaction was defined by Terzaghi (1955) as *"the pressure per unit area σ'_l of surface contact between a loaded member and the subgrade on which it rests and transfers the load"* and the modulus of subgrade reaction K_s as *"the ratio between the pressure σ'_l at any given point on the surface of contact and the settlement δ produced by the load application"*, that is

$$K_s = \frac{\sigma'_l}{\delta} \qquad \qquad \text{...(7.31)}$$

Terzaghi (1955) then goes on to state that K_s is a function of the elastic properties of the subgrade and the width of the loaded area. Therefore, the modulus of subgrade reaction does not have a specific value for a given soil.

A review of some of the different methods of determining K_s that have been proposed in the literature is now given. Many of these methods are based on empirical correlations with other soil parameters or properties.

Broms (1964b) suggested using the values of K_s quoted by Terzaghi (1955) for calculating the lateral displacement of piles in cohesionless soils. These values are based on plate loading test results in sand, for a $0.30m$ square plate and an applied stress σ'_l less than half the ultimate bearing stress σ'_b. The values quoted by Terzaghi for K_s are given in Table 7.1 according the density of the sand and whether it is submerged or dry.

	K_s (kN/m^3)		
DENSITY	Loose	Medium	Dense
Dry sand	27 200	81 500	217 300
Submerged sand	15 500	54 300	131 900

Table 7.1 - Coefficients of subgrade reaction K_s for sands based on results from a $0.30m$ square plate loading test. (After Terzaghi, 1955).

Terzaghi suggests that the coefficients of subgrade K_s quoted in Table 7.1 should be modified by the factor

$$\frac{L_a + 0.5}{1.5L_a}$$

to account for differences in the shape of the reinforcement compared with the shape of the test loading plate.

Francis (1964) proposed a modified version of Vesic's (1961) expression for K_s to take into account the soil reaction on either side of a laterally loaded pile, it is of the form

$$K_s = \frac{1.3}{D} \sqrt[12]{\frac{D^4}{EI}} \frac{(E_s)^{13/12}}{1 - \mu^2} \qquad \ldots(7.32)$$

where E_s is the elastic modulus of the soil, μ the Poisson's ratio of the soil and D the loaded width.

For short term loading Francis (1964) proposes $\mu = 0.5$ and E_s as the slope of the secant passing through 50% of the ultimate undrained strength measured in a triaxial compression test. For long term loading $\mu \approx 0.4$ and $E_s = 3(1-2\mu)/m_v$, where m_v is the coefficient of volume compressibility from an oedometer test at an appropriate stress.

Menard (1975) proposed a correlation between K_s and the Menard pressuremeter modulus E_m based on an empirical settlement equation. The correlation given below is for $D \geq L_a/20$, where D is the width of the loaded area and L_a the length of the reinforcement. For $D < 0.60m$ the coefficient of subgrade reaction is related to E_m by

$$\frac{1}{K_s} = \frac{D}{E_m}\left(\frac{2}{9}2.65^\kappa + \frac{\kappa}{6}\right) \qquad \ldots(7.33)$$

For $D \geq 0.60m$

$$\frac{1}{K_s} = \frac{2D_o}{9E_m}\left(2.65\frac{D}{D_o}\right)^\kappa + \frac{\kappa D}{6E_m} \qquad \ldots(7.34)$$

where $D_o = 0.60m$ and κ is a factor dependent on the soil type, ranging between 1 for peaty soils to 0.33 for sands and gravels, Baguelin et al. (1978).

Finally, Pfister et al. (1982) have published a chart correlating K_s with the friction angle ϕ' and the cohesion intercept c' of the soil. The values presented in the chart for the case $c' = 0$ vary non linearly between $15\,000\,kN/m^3$ at a friction angle $\phi' \approx 20°$ to $100\,000\,kN/m^3$ at a friction angle $\phi' \approx 45°$. This range of K_s is similar to that given in Table 7.1 for loose sand to dense sand. However, it is important to note that Pfister et al. (1982) make no reference to the width of the loaded area or the applied stress level.

All of the methods described above for obtaining the modulus of subgrade reaction K_s are based on an empirical correlation. The methods described below for calculating the limiting lateral stress of the soil, the ultimate bearing stress σ'_b, are generally based on analytical techniques.

Two cases must be considered for the calculation of the limiting lateral stress, $\sigma'_l = \sigma'_b$: undrained loading and drained loading. For the majority of cases of soil nailing and soil dowelling the most critical loading corresponds to the drained case.

Broms (1964a) suggested that the ultimate lateral stress for undrained failure is a function of the cross section of the reinforcement and the surface roughness. For vertical piles extending to the ground surface, the ratio of the limiting lateral stress to the undrained shear strength (σ'_b/s_u) is constant with depth below three pile diameters from the ground surface. Broms quotes values for smooth piles in the range (σ'_b/s_u) = 8.3 – 11.4 for square and circular cross sections. Randolph and Houlsby (1984) give a range of (σ'_b/s_u) = 9.1 to 11.9 for plastic flow around a pile of circular cross section. The lower value is for a perfectly smooth pile and the upper value a perfectly rough pile.

Schlosser (1983) utilises the creep pressure p_f given from the Menard pressuremeter to define the limiting bearing stress for soil nailing design. He assumed $\sigma'_b \approx p_f = p_l/2$, where p_l is the Menard limit pressure. However, this analysis leads to some confusion as to whether σ'_b corresponds to the case of drained or undrained loading.

Yu (1990) derived an analytical solution from cylindrical cavity expansion theory relating the normalised limit pressure (p_l/p_o) to the friction angle of the soil ϕ', where p_o is the mean stress in the soil. For a range of soil friction angle between $\phi' = 20° – 45°$ the limit pressure (p_l/p_o) varied between 8 and 22 for a soil of stiffness $G/p_o \approx 500$, where G is the shear modulus of the soil. These results are relevant to a soil of medium density. However, (p_l/p_o) is found to be very sensitive the dilation angle of the soil ψ. Using the relationship between the limiting lateral stress stated above and assuming $\sigma_v' \approx p_o$ the typical range of limiting bearing stress might be (σ'_b/σ'_v) = 5 – 12.

Brinch Hansen (1961) proposed a lower and an upper estimate to the limiting bearing stress σ'_b for transversally loaded piles in a cohesionless soil. The lower estimate is calculated as the net difference between the passive and active earth pressure coefficients of a rough wall translated horizontally through the soil, and is given by

$$\left(\frac{\sigma'_b}{\sigma'_v}\right) = \exp\{(\pi/2 + \phi')\tan\phi'\}\cos\phi'\tan\left(\frac{\pi}{4} + \frac{\phi'}{2}\right)$$

$$- \exp\{-(\pi/2 - \phi')\tan\phi'\}\cos\phi'\tan\left(\frac{\pi}{4} - \frac{\phi'}{2}\right) \qquad \ldots(7.35)$$

The upper estimate is calculated from the passive pressure at great depth assuming that rupture lines in the soil flow around the pile, and do not extend to the ground surface, i.e. punching shear occurs. The solution is

$$\left(\frac{\sigma'_b}{\sigma'_v}\right) = \left\{\exp(\pi\tan\phi')\tan^2\left(\frac{\pi}{4} + \frac{\phi'}{2}\right) - 1\right\} \times$$

$$(1.58 + 4.09\tan^4\phi')(1 - \sin\phi') \qquad \ldots(7.36)$$

The upper and lower estimates of limiting lateral stress defined by equations (7.35) and (7.36) are plotted in Figure 7.7 for a range of friction angles $\phi' = 20° - 45°$. Also shown in the figure is the value of limiting lateral stress suggested by Broms (1964b) which is equal to

$$\left(\frac{\sigma'_b}{\sigma'_v}\right) = 3K_p = 3\left\{\frac{1 + \sin\phi'}{1 - \sin\phi'}\right\} \qquad \ldots(7.37)$$

where K_p is the Rankine passive earth pressure coefficient. Equation (7.37) is observed to lie between the upper and lower estimates of σ'_l proposed by Brinch Hansen. For lower values of friction angle ϕ' equation (7.37) is close to the upper estimate and at higher values it becomes closer to the lower estimate.

In Chapter 6, the lower estimate of limiting lateral stress proposed by Jewell et al. (1984) for a punching shear failure was adopted, equation (6.18). In a slope the normal stress σ'_n governing soil failure around the bar can be related to the vertical stress σ'_v by $\sigma'_n \approx \sigma'_v(1 + K_a)/2$, where K_a is the active earth pressure coefficient for the soil. Therefore, for this specific case equation (6.18) can be expressed as
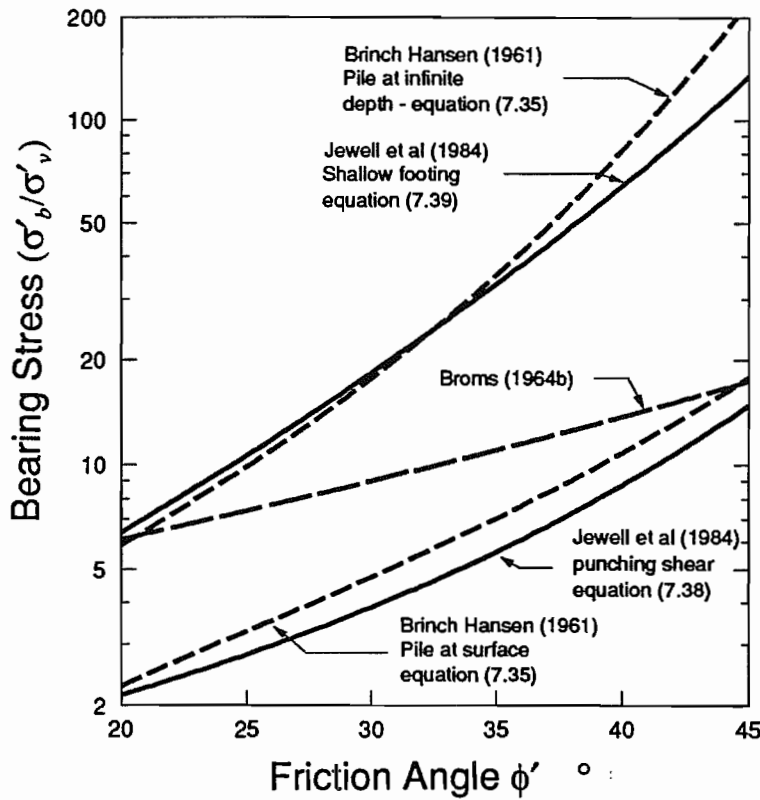
Figure 7.7 - Comparison between methods of estimating the limiting lateral stress (σ'_b/σ'_v) as a function of ϕ'.

$$\left(\frac{\sigma'_b}{\sigma'_v}\right)=\frac{(1+K_a)}{2}\tan\left(\frac{\pi}{4}+\frac{\phi'}{2}\right)\exp\left\{\tan\phi'\left(\frac{\pi}{2}+\phi'\right)\right\} \qquad \ldots(7.38)$$

Jewell et al. (1984) also proposed an upper estimate to the limiting lateral stress equal to the bearing capacity factor N_q given in Vesic (1973),

$$\left(\frac{\sigma'_b}{\sigma'_v}\right)=N_q=\tan^2\left(\frac{\pi}{4}+\frac{\phi'}{2}\right)\exp(\pi\tan\phi') \qquad \ldots(7.39)$$

The upper and lower estimates of limiting lateral stress defined by equations (7.38) and (7.39) were shown by Palmeira and Milligan (1989) to bound closely a large number of data from pullout tests reported in the literature, with equation (7.38) providing lower and safe estimate. These two bounding curves are also plotted in Figure 7.7 where it is seen that they are in close agreement with the upper and lower estimates proposed by Brinch Hansen (1961).

7.2.4 Limiting shear force for typical soil and reinforcement parameters

Typical ranges of soil and reinforcement parameters were discussed in the previous section. It will now be of interest to investigate the limiting shear force P_s that is available for typical values of these parameters.

The reinforcement will be assumed to be steel with a Young's modulus of $E = 200 \times 10^6 \ kN/m^2$ and yield stress $\sigma_p = 200 \times 10^3 \ kN/m^2$. A soil strength of the order $(\sigma'_b/\sigma'_v) = 5 - 20$ is expected to describe the majority of typical soil strengths. If the vertical stress is in the range $\sigma'_v = 50 - 500 \ kN/m^2$ then the limiting lateral stress would be of the order $250 - 10\ 000 \ kN/m^2$. The coefficient of subgrade reaction may lie within the range $K_s = 5\ 000 - 500\ 000 \ kN/m^3$ for most soils. The example studied will be for a circular bar of diameter $D = 0.10m$.

The elastic and plastic shear widths are functions of the stiffness ratio (E/K_sD) and the strength ratio (σ_p/σ'_b) respectively. For the ranges given above the stiffness ratio (E/K_sD) is in the range $4\ 000 - 400\ 000$ and the strength ratio (σ_p/σ'_b) in the range $20 - 800$. The variation in the elastic and plastic shear widths for these ranges are shown in Table 7.2 for circular bar (equations (7.8) and (7.27) with $(P_{ax}/P_p) = 0$).

ELASTIC ANALYSIS		PLASTIC ANALYSIS	
Stiffness Ratio E/K_sD	$(l_s/D)^e$ eqn (7.8)	Strength Ratio σ_p/σ'_b	$(l_s/D)^p$ equ (7.27)
4 000	8.3	20	5.2
40 000	14.8	400	23.1
400 000	26.3	800	32.7

Table 7.2 - Comparison between theoretical shear widths using the elastic and plastic lateral loading models for typical soil and reinforcement parameters.

A feature of the results in Table 7.2 is the similarity between the theoretical ranges for the plastic and elastic analyses, and the insensitivity of the shear width to changes in the stiffness or strength ratio. It is possible to conclude from these results, for typical soil and

reinforcement parameters, that the shear width is likely to be of the order 5 to 30. Table 7.2 was derived for the specific case of a circular bar with no axial force, $(P_{ax}/P_p) = 0$. However, if the second moment of area I and plastic moment M_p of non composite (e.g. Grouted bar) solid section reinforcement are substituted into equations (7.18) and (7.24) respectively, a similar range of (l_s/D) is observed, Jewell and Pedley (1990b).

Having established typical ranges for the elastic and plastic shear width (l_s/D) it is now possible to investigate the shear force available from the reinforcement. Table 7.3 gives the theoretical elastic and plastic limiting shear force P_s for circular, rectangular and tubular reinforcement. These equations have been normalised by the plastic axial capacity of the reinforcement P_p, so the limiting shear force from these equations is given as (P_s/P_p). The plastic axial capacity P_p is a good datum for comparing reinforcement shear force with axial force, as often it is considered that the soil shearing resistance is improved by axial force only.

The equations in Table 7.3 were derived by substituting for the limiting elastic and plastic bending moments in equations (7.10) and (7.26) respectively, and dividing through by the plastic capacity of the reinforcement.

CROSS SECTION	ELASTIC ANALYSIS	PLASTIC ANALYSIS
CIRCULAR diam = D	$\dfrac{1}{2(l_s/D)^z}\left\{1-\left(\dfrac{P_{ax}}{P_p}\right)\right\}$	$\dfrac{8}{3\pi(l_s/D)^p}\left\{1-\left(\dfrac{P_{ax}}{P_p}\right)^2\right\}$
RECTANGULAR width = B thickness = t	$\dfrac{2}{3(l_s/t)^z}\left\{1-\left(\dfrac{P_{ax}}{P_p}\right)\right\}$	$\dfrac{1}{(l_s/t)^p}\left\{1-\left(\dfrac{P_{ax}}{P_p}\right)^2\right\}$
TUBULAR internal diam. = D_i external diam. D	$\dfrac{1}{2(l_s/D)^z}\left[\dfrac{1-(D_i/D)^4}{1-(D_i/D)-(D_i/D)^2+(D_i/D)^3}\right]\left\{1-\left(\dfrac{P_{ax}}{P_p}\right)\right\}$	$\dfrac{8}{3\pi(l_s/D)^p}\left[\dfrac{1-(D_i/D)^3}{1-(D_i/D)^2}\right]\left\{1-\left(\dfrac{P_{ax}}{P_p}\right)^2\right\}$

Table 7.3 - Equations defining the maximum available shear force (P_s/P_p) for various cross sections.

For typical shear widths (l_s/D) in the range 5 to 30 the plastic analysis will always give a larger shear force than the elastic analysis. For example, with a shear width $(l_s/D) = 5$

and a plastic analysis the limiting reinforcement shear force for circular bar is $(P_s/P_p) \approx 0.17$, and for rectangular bar $(P_s/P_p) \approx 0.20$. The corresponding figures for the elastic analysis are $(P_s/P_p) \approx 0.10$ and $(P_s/P_p) \approx 0.13$ for circular and rectangular bar respectively. The shear width of $(l_s/D) = 5$ in this example represents a lower limit of the shear width. Therefore, the maximum shear force available from the reinforcement will typically be less than 20% of the plastic axial capacity P_p.

Table 7.3 also gives equations for the available shear force from tubular bar reinforcement. The shear width (l_s/D) for the elastic analysis is given by substituting the 2nd moment of area I of a tube in equation (7.8), to give

$$\left(\frac{l_s}{D}\right)^e = \frac{\pi}{4} \sqrt[4]{\frac{\pi E}{K_s D}\left[1-\left(\frac{D_i}{D}\right)^4\right]} \qquad \ldots(7.40)$$

The plastic shear width of a tube is given by substituting the plastic moment of resistance M_p of a tube in equation (7.27), to give

$$\left(\frac{l_s}{D}\right)^p = \sqrt{\frac{4\sigma_p}{3\sigma'_b}\left[1-\left(\frac{D_i}{D}\right)^3\right]\left\{1-\left(\frac{P_{ax}}{P_p}\right)^2\right\}} \qquad \ldots(7.41)$$

For both plastic and elastic analyses, as the wall thickness of the tube increases, $(D_i/D) \rightarrow 0$ the shear width increases. The ratio (D_i/D) is related to the shear width (l_s/D) by a power of 3 for the plastic analysis and 4 for the elastic analysis. Therefore it is only for large values of (D_i/D) that the shear width decreases significantly. However, although the shear width decreases as $(D_i/D) \rightarrow 0$ the magnitude of the shear force increases.

Figure 7.8 shows the maximum available shear force (P_s/P_p) from the plastic analysis as a function of the strength ratio (σ_p/σ'_b) for tubular reinforcement. A range of wall thicknesses (D_i/D) are shown.

For typical soils and reinforcement materials the range for (σ_p/σ'_b) will be between 20 and 500. Steel tubular piles of the type used for soil dowelling typically have a wall
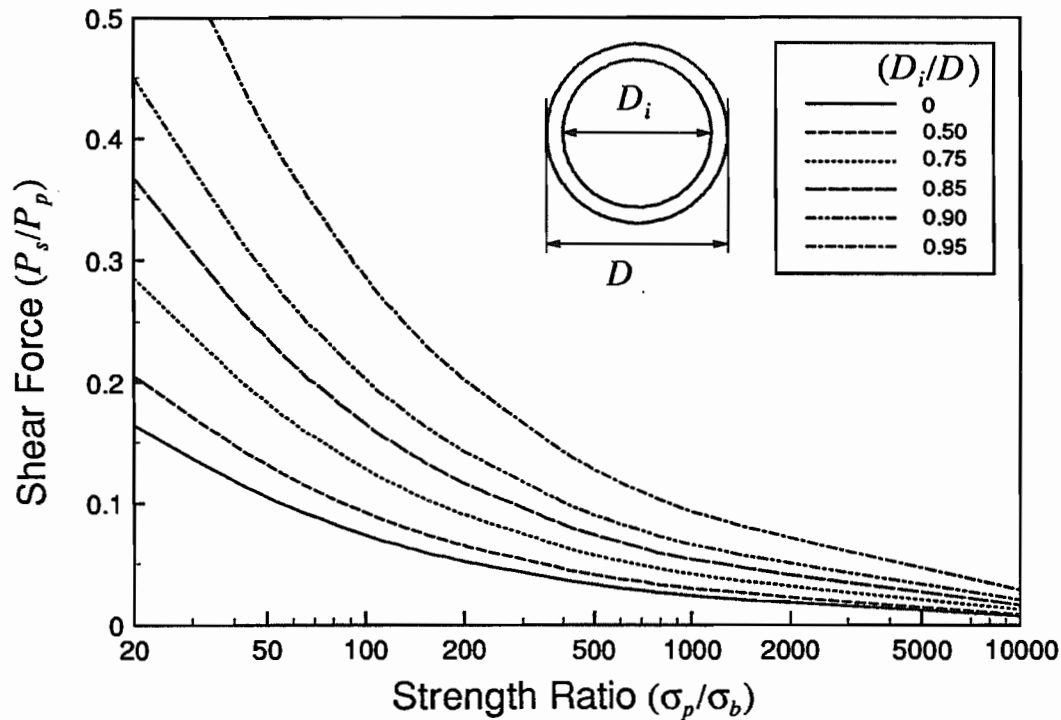
Figure 7.8 - Limiting shear force (P_s/P_p) for tubular sections as a function of the reinforcement/soil strength ratio (σ_p/σ'_b).

thickness ratio (D_i/D) $\approx 0.85 - 0.95$. Therefore, using the plastic analysis the available shear force may be as high as (P_s/P_p) = 0.40. However, this would only occur for smaller ratios of (σ_p/σ'_b) and the shear force is more likely to be of the order (P_s/P_p) = 0.15 – 0.30.

In soil nailing a commonly used cross section is a that of a steel circular bar grouted into a circular hole, see Section 6.2. The bar is of diameter is D and the hole of diameter D_g. The limiting bending moment of such a cross section is a complex function of the ratio (D/D_g) and the ratio of the yield stress of the steel to that of the grout (σ_p/σ_{cu}). No closed form solution can be obtained for either the maximum plastic moment M_p or the shear width (l_s/D). However, Jewell and Pedley (1990b) tentatively suggest that the shear width is modified to account for the increased area available for bearing due to the grout, but that any increase in flexural resistance be ignored. Therefore, the elastic analysis of the shear width is modified to give

$$\left(\frac{l_s}{D}\right)^e = \frac{\pi}{4}\sqrt[4]{\frac{\pi E}{K_s D_g}} \qquad \qquad \ldots(7.42)$$

and the plastic analysis gives

$$\left(\frac{l_s}{D}\right)^p = \sqrt{\frac{4\sigma_p}{3\sigma'_b}\left(\frac{D}{D_g}\right)\left\{1-\left(\frac{P_{ax}}{P_p}\right)^2\right\}} \qquad \qquad \ldots(7.43)$$

In soil nailing the ratio (D/D_g) is typically 0.3 to 0.4. Therefore the potential increase in reinforcement shear force owing to the presence of the grout is between 50% and 100% for the plastic analysis, (7.43). The results of test on grouted bars and the calculation of the maximum moment and available shear force are discussed further in Chapter 8.

To summarise, for typical soil and reinforcement parameters the maximum shear force obtained from reinforcement is of the order 5% to 20% of the reinforcement axial capacity P_p. If tubular or grouted bar reinforcement is used an increase in the available shear force is theoretically observed. Using the elastic analysis always leads to a conservative estimate of the maximum available shear force. All of the cases discussed do not apply when soil bearing failure occurs resulting in rigid body failure under a lower reinforcement shear force.

7.3 Prediction of Reinforcement Axial Force

The pullout force P_{po} was defined in Section 7.1.2 as a function of the limiting shear stress between the soil and the reinforcement τ_{po}, the circumferential area per unit length A_c and the anchorage length of the reinforcement L_a.

For the interpretation of pullout tests it is assumed that the limiting shear stress τ_{po} is uniform around the circumference of the reinforcement. This assumption implies that the stress acting normal to and around the circumference has a constant value, Figure 7.9(a). This is likely to be the case in a pullout test or where reinforcement is loaded axially, such that

$$\sigma'_r = \frac{P_{po}}{A_c L_a \tan \phi'_i} \qquad \ldots(7.44)$$

where $\phi'_i = \tan^{-1}(\tau_{po}/\sigma'_r)$ is the interface friction angle mobilised between the soil and the reinforcement. When reinforcement is loaded by a combination of axial force and shear force the normal stress acting around the circumference cannot be interpreted in such a simple manner.

For pullout occurring due to axial force only the most suitable method of determining the limiting shear stress is from a pullout test. Jewell (1980) developed an analysis for the specific case of pullout occurring in the shearbox. In this analysis the normal stress acting on a plane at some angle θ is deduced from a Mohr's circle of stress from the applied vertical stress σ'_v and friction angle ϕ', where θ is defined in Figure 7.1. Making an assumption about the intermediate principal stress, Jewell was able to estimate the stress acting around a circular bar lying on that plane. The stress acting around a bar σ'_r is given approximately as

$$\left(\frac{\sigma'_r}{\sigma'_v}\right) = \frac{1}{\cos^2\phi'} \{0.87 + 0.5\sin\phi'\sin(\phi'+2\theta)\} \qquad \ldots(7.45)$$

where σ'_v is the vertical stress applied to the shearbox sample.

For combined shear and pullout it is proposed that over some of the length of the reinforcement the normal stress is equal to the limiting lateral stress σ'_b in the soil. It is assumed that this stress acts over a width D equal to the reinforcement diameter, Figure 7.9(b). Using the elastic-plastic model of lateral loading of the reinforcement it will be assumed that length L_a can be divided into three sections: (i) a length $l_s/2$ determined from minimum length of reinforcement required for a plastic hinge to form, equation (7.27) for circular bar, (ii) a length l_b, the bearing length, found from the geometry of loading, equation (7.12), and (iii) a length l_p, the pullout length. Therefore, the overall length is
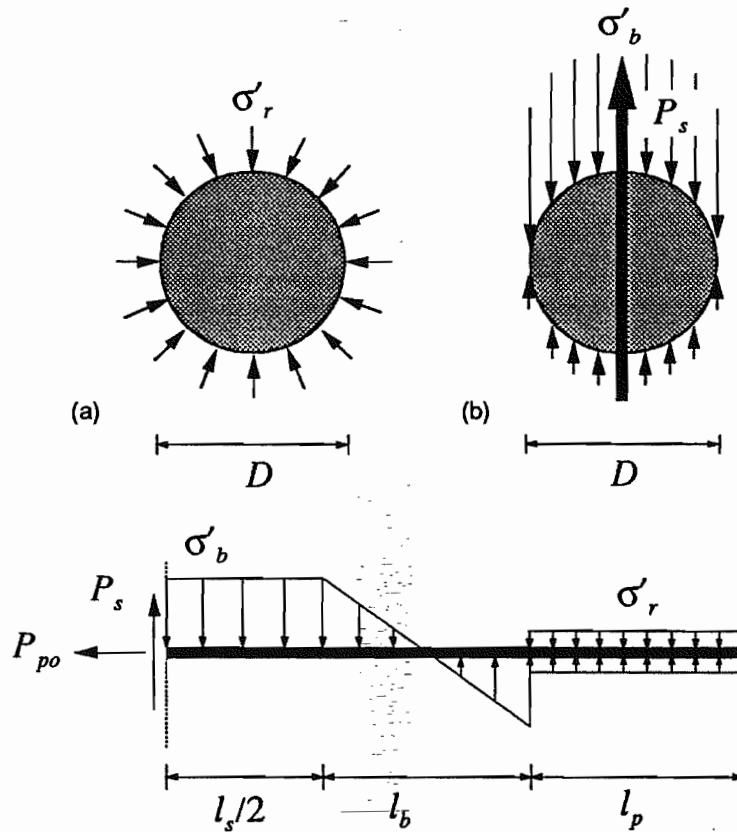
Figure 7.9 - Pullout of reinforcement undergoing shear and axial loading.

$$L_a = \frac{l_s}{2} + l_b + l_p \qquad\qquad \ldots(7.46)$$

The pullout length l_p will only be greater than zero if the overall length of the

reinforcement is sufficient for plastic hinge failure, i.e. equation (7.29) is satisfied.

The pullout resistance P_{po} is assumed to equal the sum of the forces mobilised over

lengths $l_s/2$, l_b and l_p. These forces are:

$$D\,(l_s/2)\,\sigma'_b \tan\phi'_i$$

over length $l_s/2$

$$D\,l_b\,(\sigma'_b/2)\tan\phi'_i$$

over length l_b (where the average stress is $\sigma'_b/2$ over the length) and

$$A_c\,l_p\,\sigma'_r \tan\phi'_i$$

over the length l_p, where σ'_r is either determined from pullout tests or from the shearbox analysis, equation (7.45).

The total pullout force for combined axial and shear loading for circular reinforcement is therefore

$$P_{po} = \{D\,\sigma'_b\,(l_s + l_b)/2 + \pi D\,\sigma'_r l_p\}\tan\phi'_i \qquad\qquad ...(7.47)$$

and is shown diagrammatically in Figure 7.9(c). Typical interface friction angles ϕ'_i for reinforcement materials were given in Table 6.2.
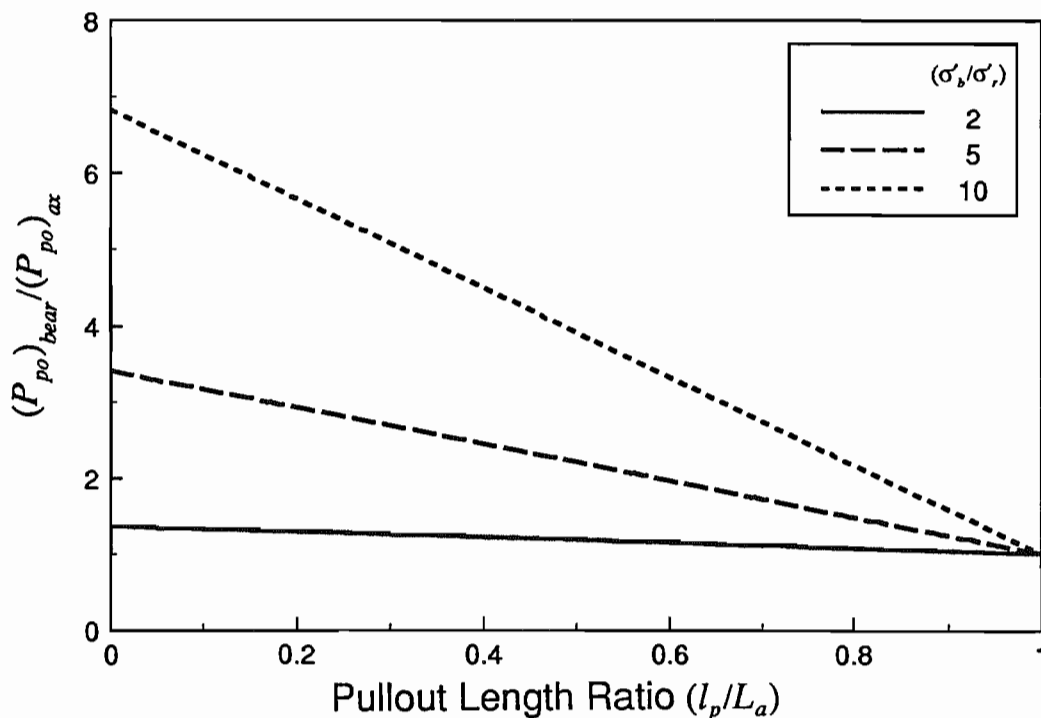
Figure 7.10 - Effect of pullout length on the increased pullout resistance from a shear load.

Figure (7.10) shows the effect of shear force on reinforcement pullout force $(P_{po})_{bear}/(P_{po})_{ax}$ for different pullout lengths (l_p/L_a) and bearing stress ratios (σ'_b/σ'_r). Where $(P_{po})_{bear}$ is the pullout force under combined shear and axial load, $(P_{po})_{ax}$ the pullout force under axial load only, σ'_b the limiting bearing stress and σ'_r the stress acting radially around the reinforcement.

Under combined shear and axial load the pullout force $(P_{po})_{bear}$ rises rapidly with increasing bearing stress (σ'_b/σ'_r) and decreasing pullout length (l_p/L_a). However, for larger values of the pullout length (l_p/L_a) the effect of shear force on the pullout force is less significant.

The theoretical conclusion derived from Figure 7.10 is that for reinforcement subjected to combined axial and shear loads the pullout resistance may be underestimated if the bearing stress acting normal to the reinforcement is ignored. The error may be significant for the case when the reinforcement is short, or if the ratio of the bearing stress to the radial stress around the reinforcement is high.

7.4 Limiting Combinations of Shear and Axial Force

Three modes of failure for reinforcement in soil were identified and equations were proposed to determine the limiting combination of forces causing failure. Schlosser (1982, 1983) proposed a multi-criteria analysis to determine the limiting combinations of shear force P_s and axial force P_{ax} for soil nails. This analysis was based on four criteria; pullout, rigid body translation, plastic hinge failure and shear failure of the reinforcement. The fourth criterion for shear failure will never occur in practice and can therefore be disregarded. This is because the ratio of (σ_p/σ'_b) between reinforcement and soil is too high in practice. A further problem with the existing multi-criteria analysis is the mixture of elastic and plastic theory.

It is proposed therefore that only three criteria define the failure envelope for reinforcement of a given cross section; pullout, rigid body failure and plastic hinge failure. All three of these criteria are described by plastic analyses. The use of an elastic analysis leads to some problems as it does not constitute a failure analysis, but more simply a boundary at which the reinforcement commences elasto-plastic behaviour.
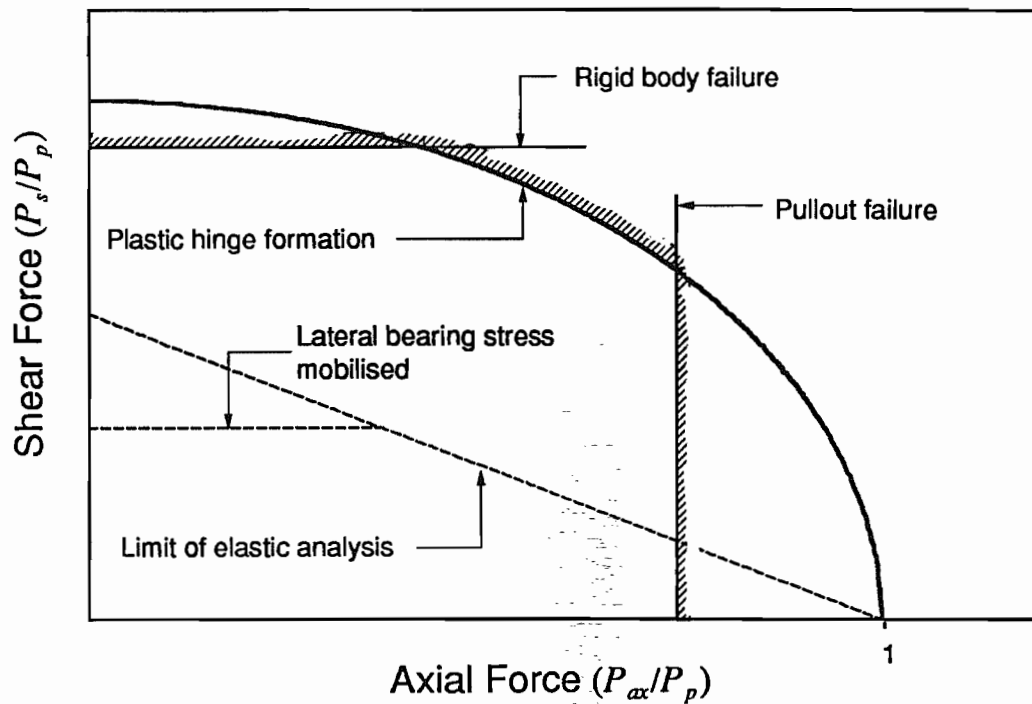
Figure 7.11 - Multi-criteria analysis limiting the combination of shear (P_s/P_p) and axial force (P_{ax}/P_p).

The criteria of pullout, rigid body and plastic hinge failure limiting the combination of shear (P_s/P_p) and axial force (P_{ax}/P_p) are presented in Figure 7.11. Also shown is the boundary at which elastic behaviour ceases. Examples of the use of the multi-criteria analysis are given in Chapter 8 where test data are analysed.

7.5 Effect of Shear and Axial Force on Soil Shear Strength

The forces resulting from displacement between the soil and reinforcement have been investigated; the effect of these forces on soil shear strength is now considered.

A simple method of analysing the influence of reinforcement shear and axial force on soil strength is to consider reinforcement crossing a potential shear surface at some angle θ. A shearbox analogy will be used for this purpose, Figure 7.12.
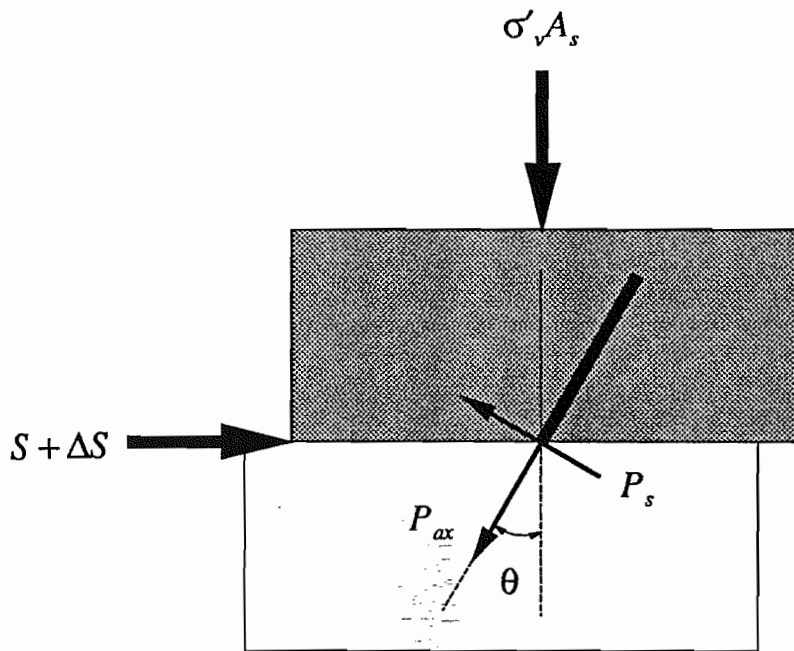
Figure 7.12 - Examination of equilibrium of forces at the point where reinforcement crosses the shear plane in the shearbox.

The net change in shear strength of the soil ΔS can be attributed to the reinforcement shear force (P_s/P_p) and to the reinforcement axial force (P_{ax}/P_p). Resolving forces parallel and perpendicular to the shear surface gives

$$\left(\frac{\Delta S}{P_p}\right) = \left(\frac{P_{ax}}{P_p}\right)(\cos\theta\tan\phi' + \sin\theta) + \left(\frac{P_s}{P_p}\right)(\cos\theta - \sin\theta\tan\phi') \qquad ...(7.48)$$

where the functions $(\cos\theta\tan\phi' + \sin\theta)$ and $(\cos\theta - \sin\theta\tan\phi')$ relate the contribution of the axial force P_{ax} and the shear force P_s respectively, to reinforcement orientation θ and soil shear strength ϕ'.

Figure 7.13 illustrates the functions describing the contribution of the axial force and the shear force to soil shear strength improvement. A range of reinforcement orientations θ and soil friction angles ϕ' are studied. For a large range of reinforcement orientation both of the functions are positive and lead to a net increase in soil shear strength. For typical orientations used in soil nailing of $(20° < \theta < 50°)$ it is observed that the contribution from the shear force function $(\Delta S/P_p)_{shear}$ is always less than that from the axial force function
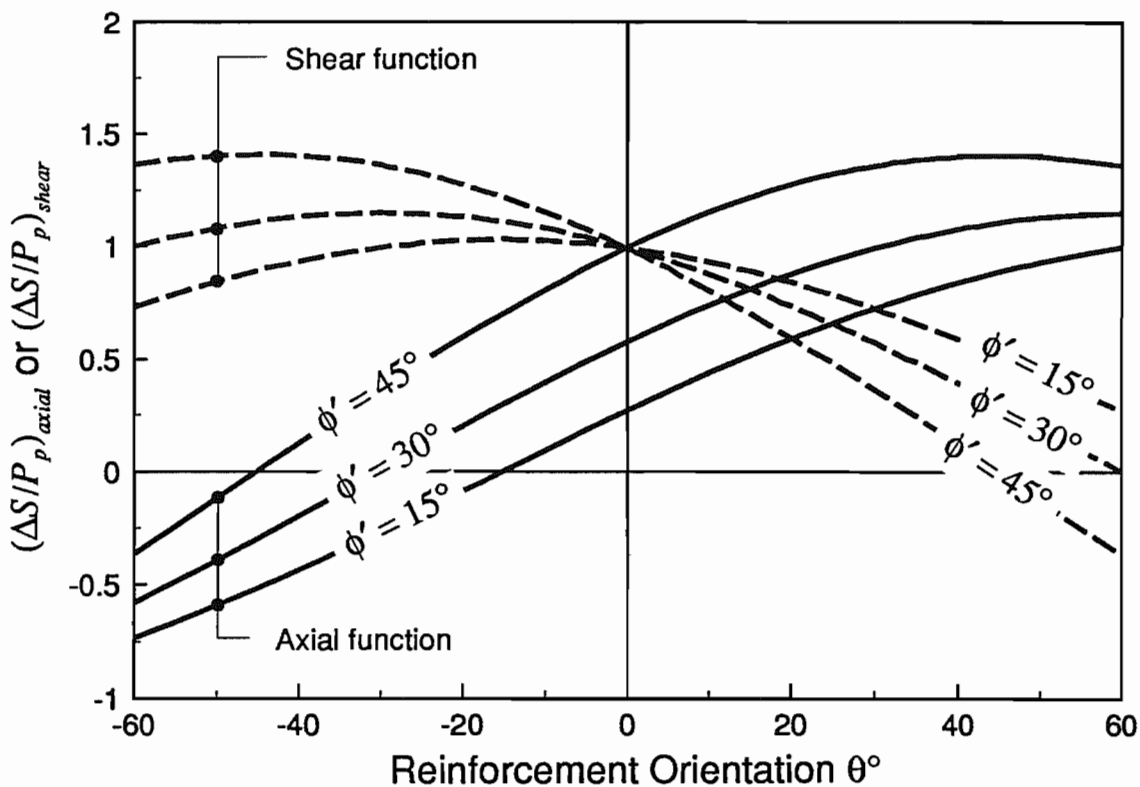
Figure 7.13 - The effect of shear and axial force on soil shear strength improvement for a range of orientations θ and friction angles ϕ'.

$(\Delta S/P_p)_{ax}$, and may lead to a reduction in strength. On the contrary, when $\theta \approx 0$, often the case for soil dowelling, the axial force function can be much less than the shear function, but is always positive.

So far only the functions relating the influence of shear and axial force on soil shear strength have been studied; the effect of the relative magnitudes of the shear and axial force on soil shear strength is now investigated.

The example considered is that of a circular bar, and a typical shear width $(l_s/D) = 10$

(a *simplified analysis* will be used). Using the equation given in Table 7.3 for the plastic analysis, it is possible to define the limiting combinations of shear force (P_s/P_p) and axial force (P_{ax}/P_p). The limiting shear force for six values of axial force have been substituted into equation (7.48) and the change in strength $(\Delta S/P_p)$ is shown in Figure 7.14. A range of reinforcement orientation θ is studied for a soil strength of $\phi' = 30°$.
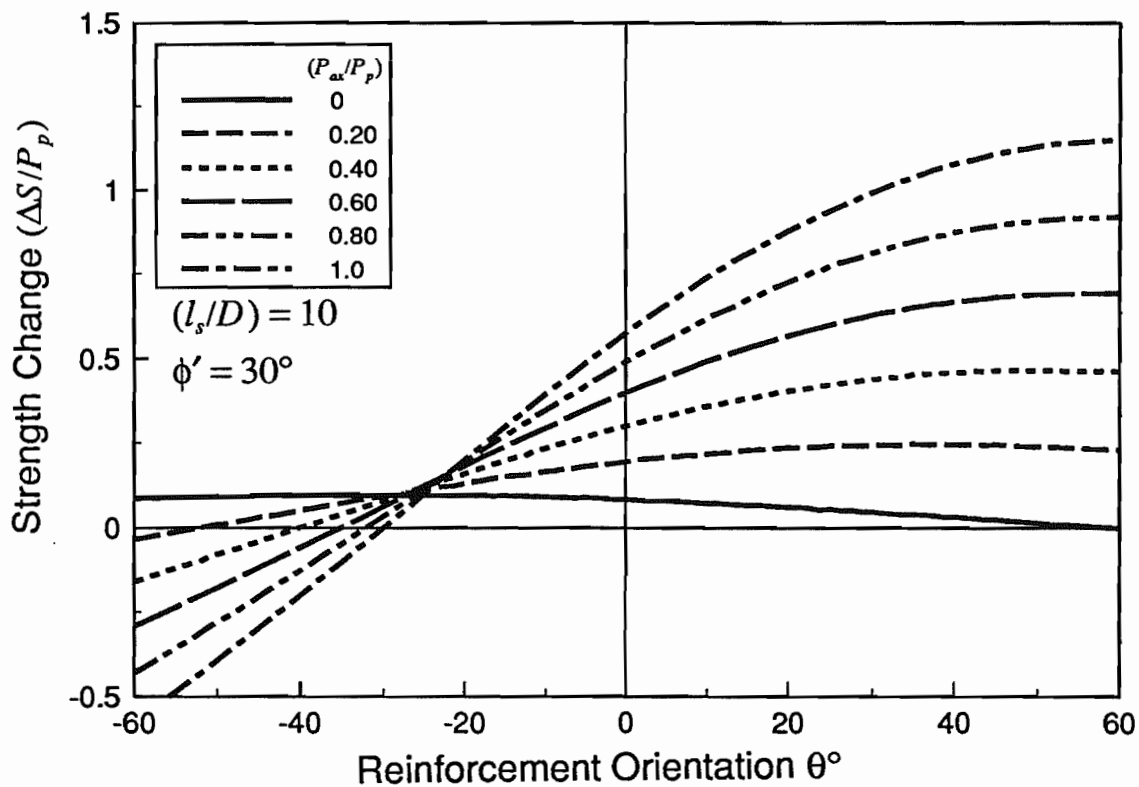
Figure 7.14 - Improvement in soil strength for limiting combinations of shear and axial force for a circular section reinforcement, $(l_s/D) = 10$, $\phi' = 30°$.

For the case of shear force only, $(P_{ax}/P_p) = 0$, the maximum increase in soil shearing resistance $(\Delta S/P_p)$ is less than 15% of the reinforcement axial capacity P_p. As the axial force in the reinforcement increases it is observed that a dramatic increase in soil shearing resistance occurs. For the case of axial force only, $(P_{ax}/P_p = 1$, $P_s/P_p = 0)$, the shear strength improvement is up to 120% of the reinforcement axial capacity. For intermediate combinations of axial and shear force it is observed that the shear strength improvement ΔS increases rapidly with increasing axial force P_{ax}.

To conclude, reinforcement when used in axial tension leads to a much greater potential increase in soil shear strength $(\Delta S/P_p)$ than can be obtained by the same reinforcement in shear for typical ranges of reinforcement orientation θ.

7.6 Summary of Theoretical Conclusions

The observations made from the theoretical analysis of soil reinforcement working in bending and shear are summarised below.

(i)   Three modes of reinforcement failure were identified for soil reinforcement subjected to combined axial and shear loading: pullout, plastic hinge formation and rigid body failure.

(ii)   Elastic and plastic analyses for the prediction of reinforcement shear force were presented. The elastic analysis led to a lower prediction of the limiting shear force than the corresponding plastic analysis. The plastic analysis was derived from the data presented in Chapter 6. The maximum shear force available from circular or rectangular steel bar reinforcement was typically found to be less than 20% of its plastic axial capacity P_p. The limiting shear force available from steel tubes increases as the wall thickness decreases, and is generally higher than for solid bar reinforcement. For both plastic and elastic analyses the limiting shear force is reduced by the axial force in the reinforcement.

(iii)   For short reinforcement under combined axial and shear loading the pullout force may be underestimated if the bearing stresses acting on the reinforcement are ignored. As the reinforcement length increases the effect of bearing on pullout force diminishes rapidly.

(iv)   A revised multi-criteria analysis for predicting the limiting combination of shear and axial force is proposed. This analysis differs from Schlosser's (1983) multi-criteria analysis as it contains three criteria only and is dependent on plastic failure modes.

(v)   For typical reinforcement orientations used in soil nailing and soil dowelling practice axial force has a much greater influence on soil shear strength improvement than shear force. This is for two reasons: firstly, reinforcement shear force has a

component reducing the normal stress in the soil, hence lowering the soil strength, and secondly the limiting shear force that can be derived from reinforcement in soil is only a small proportion of the plastic axial capacity of the reinforcement P_p.

CHAPTER 8:

ANALYSIS OF THE EXPERIMENTAL DATA

Data from Chapter 6 are now compared with the theory presented in Chapter 7 with the objective of forming conclusions about the use of reinforcement in bending and shear. The analysis which follows is divided into subsections to allow a better understanding of the factors influencing the performance of soil reinforcement. A back analysis of a test on a soil nailed wall which was loaded to failure, in which nails were instrumented, is also given.

8.1 Measured and Predicted Shear Width

The limiting shear force available from any structural member is dependent on the distance between the point where the shear load is applied and the point of maximum bending moment. The distance between points of maximum bending moment on either side of a potential shear surface was defined as the *shear width* l_s in Chapter 7. This distance can be expressed in non-dimensional form as (l_s/D), where D is the reinforcement width or diameter.

The normalised shear width (l_s/D) measured from bending moment profiles, denoted by the superscript *bm*, is given in Table 8.1 for tests MD2 to MD9 and O1 to O6. Also given in the table are ranges for the shear width deduced from post test reinforcement deformation, and denoted by the superscript *def*. The shear width from reinforcement deformation is given by

$$(l_1 + l_2)/2D > (l_s/D)^{def} > l_2/D \qquad\qquad ...(8.1)$$

where the lengths l_1 and l_2 are defined in Figure 8.1.

Predicting the shear width $(l_s/D)^{def}$ from reinforcement deformation is only possible

if significant plastic deformation has occurred. For most of the tests reported in Table 8.1

the shear widths deduced by the two methods described are in good agreement. This suggests

that the latter method can be used to predict (l_s/D) in tests where the bending moment

distribution was not measured.
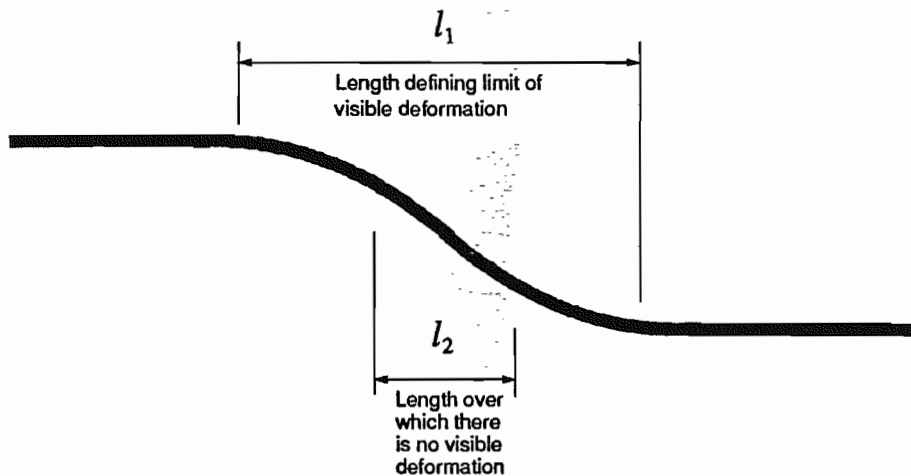
Figure 8.1 - Definition of the lengths l_1 and l_2 in deformed reinforcement.

Table 8.1 compares measured shear widths with theoretical plastic shear widths $(l_s/D)^p$

from equation (7.27) (or equation (7.41) for tubular reinforcement). The theoretical widths

were calculated assuming plane strain friction angles of $\phi' = 42°$ and $\phi' = 46°$ for medium

dense (tests MD2 to MD9) and dense sand (tests O1 to O6) respectively, and an applied

vertical stress $\sigma'_v = 100 \ kN/m^2$. Equation (6.18) gave a bearing stress of $\sigma'_b = 1340 \ kN/m^2$

for medium dense sand and $\sigma'_b = 2170 \ kN/m^2$ for dense sand. The reinforcement yield stress

was $\sigma_p = 393\ 000 \ kN/m^2$, Table 6.1.

A *simplified analysis* was used for the calculation of the shear width $(l_s/D)^p$ as in all tests $(P_{ax}/P_p) < 0.20$. This assumption leads to an error of less than 3% in the calculated shear width $(l_s/D)^p$. This may explain why the shear width was observed to be more or less constant throughout a test despite an often increasing axial force.

Test	D (mm)	Shear Width (l_s/D)			Stiffness Ratio (E/K_sD)	Strength Ratio (σ_p/σ'_b)
		Bending Moment $(l_s/D)^{bm}$	Deformation equ (8.1) $(l_s/D)^{def}$	Theoretical equ (7.27) $(l_s/D)^p$		
MD2	25.4/22.4	11.1	14.4-10.4	11.1	31 800	92
MD3	15.9	23.8	20.8-16.4	19.8	268 400	425
MD4	25.4	13.4	-	13.3	27 000	135
MD5	15.9	17.8	23.6-16.4	19.8	84 000	238
MD6	25.4	13.1	-	13.3	24 600	129
MD7	15.9	23.6	23.3-17.0	19.8	259 500	418
MD8	15.9	21.4	24.9-18.9	19.8	175 500	344
O1	15.9	16.8	21.0-17.0	15.5	66 600	212
O2	15.9	17.0	23.0-15.7	15.5	69 900	217
O3	15.9	16.9	20.5-17.6	15.5	68 200	214
O4	25.4	14.2	15.0-11.8	13.3	34 000	151
O5	25.4	14.2	-	13.3	34 000	151
O6	25.4	12.3	-	13.3	19 200	114

Table 8.1 - Comparison between predicted and measured shear widths and back calculated stiffness and strength ratios.

Agreement between theoretical and measured shear widths is generally very good. For the tests on solid bar reinforcement of diameter $D = 25mm$ equation (7.29) was not satisfied because the reinforcement was of insufficient length for a plastic hinge to form. For this reason the shear width was predicted using equation (7.30). The failure mode was confirmed as rigid body failure by the limited plastic deformation of the reinforcement, and the measured bending moments.

As noted earlier, the shear width was observed to remain more or less constant throughout a test. Therefore, the *elastic* stiffness ratio (E/K_sD) and the *plastic* strength ratio (σ_p/σ'_b) can be back calculated from the measured shear width $(l_s/D)^{bm}$. Table 8.1 gives back calculated stiffness and strength ratios, which are observed to be in good agreement with the ranges proposed in Section 7.2.4.

Although the stiffness and strength ratios are given for $D = 25mm$ reinforcement bars the values should be treated with caution because the failure mode in these tests was that of rigid body. Therefore the shear width is a function of the reinforcement geometry and not the strength or stiffness ratio of the soil. Ignoring the values for $D = 25mm$ reinforcement the stiffness ratio (E/K_sD) for dense sand is of the order $66\ 000 - 70\ 000$, and the strength ratio (σ_p/σ'_b) in the range $210 - 220$. For medium dense sand the respective ranges are $175\ 000 - 270\ 000$ and $340 - 430$, excluding test MD5.

The moduli of subgrade reaction K_s given in Table 7.1 for dry sand, modified to take into account the shape of the reinforcement, give a stiffness ratio of (E/K_sD) $\approx 115\ 000$ for medium dense sand and (E/K_sD) $\approx 43\ 000$ for dense sand for $E = 206 \times 10^6\ kN/m^2$. These theoretical stiffness ratios are about 50% lower than the back calculated values. This suggests the moduli of subgrade reaction given in Table 7.1 may be a suitable starting point for estimating the shear width with the elastic analysis. Especially when considering the general insensitivity of $(l_s/D)^e$ to changes in K_s.

The theoretical bearing stress for dense and for medium dense sand is $\sigma'_b = 2170\ kN/m^2$ and $1340\ kN/m^2$ respectively, giving stress ratios of $(\sigma_p/\sigma'_b) = 180$ and 290. These ratios are similar to the back analysed values, explaining the good agreement between measured and theoretical shear widths. Therefore, the plastic analysis is proposed as it does not require recourse to empirical correlations for the soil strength or stiffness, as with the elastic analysis.

With the plastic analysis of the shear width it is also possible to predict the failure mode. Table 8.2 gives the shear width $(l_s/D)^p$ and failure mode for a combination of three applied vertical stresses σ'_b and six bar diameters. The predicted failure mode is indicated

by (H) for plastic hinge failure and (R) for rigid body failure. Also given is the shear width for two ratios of (D/D_g) for grouted bar reinforcement. In all cases the length of the reinforcement was $L_a = 460mm$.

D (mm)	Shear Width $(l_s/D)^p$		
	$\sigma'_v = 60\ kN/m^2$	$\sigma'_v = 100\ kN/m^2$	$\sigma'_v = 150\ kN/m^2$
6.5	20.1 (H)	15.5 (H)	12.7 (H)
15.9	20.1 (H)	15.5 (H)	12.7 (H)
25.4	13.3 (R)	13.3 (R)	12.7 (H)
50.8	6.6 (R)	6.6 (R)	6.6 (R)
$D = 6.5mm$ $D_g = 50.8mm$	7.7 (H)	5.6 (H)	4.5 (H)
$D = 15.9mm$ $D_g = 50.8mm$	11.2 (H)	8.7 (H)	7.1 (H)

Table 8.2 - Effect of σ'_v on the shear width $(l_s/D)^p$ for different diameters D.

A shear width $(l_s/D) = 16$ was predicted for $D = 6.5mm$ bar and an applied vertical stress $\sigma'_b = 100\ kN/m^2$. The measured shear width in test D1 at the same applied vertical stress and on reinforcement of the same diameter was $(l_s/D)^{def} = 19 - 28$. It is believed that the observed shear width is greater than the predicted width because of the existence of a zone of deforming sand in the central region of the shearbox rather than a discrete slip surface. The proposed model of soil reinforcement interaction assumes a discrete failure surface and will therefore always give the minimum shear width.

Tests S1 and S2 were on $D = 16mm$ bars and at vertical stresses of $\sigma'_v \approx 64\ kN/m^2$ and $150\ kN/m^2$ respectively. The measured shear widths for these two tests were $(l_s/D)^{def} \approx 18 - 21$ for test S1 and $(l_s/D)^{def} \approx 16 - 20$ for test S2. The agreement between the measured and predicted shear widths for these tests is good, although the predicted width for test S2 is an underestimate as might be expected.

For tests on bars of diameter $D = 25mm$ and $D = 50mm$ the deformation of the reinforcement was too limited to be able to estimate the shear width from equation (8.1). Therefore, no comparisons can be made with Table 8.2. Despite the theoretical failure mode for test S4 on $D = 25mm$ bar and with $\sigma'_v \approx 150kN/m^2$ being plastic hinge formation no post test deformation was observed.

Two tests were carried out on grouted bar reinforcement. The shear width given by equation (7.43) for test D3 was $(l_s/D)^p = 6$ and for test D4 was $(l_s/D)^p = 9$. The ratios of bar to grout diameter (D/D_g) for these tests were 0.13 for test D3 and 0.31 for test D4. Measured shear widths from failure cracks in the grout were $(l_s/D)^{def} = 17 - 28$ for test D3 and $(l_s/D)^{def} = 9 - 14$ for test D4. Of interest is that the measured shear widths are close to those for bars of the same diameter with no grout, suggesting that the grout has little effect. Two test results are insufficient to verify the validity of equation (7.43). However, for small ratios of (D/D_g) it appears that equation (7.43) underestimates the shear width by a large margin. For this case it may be necessary to analyse the bending resistance of the section as a reinforced concrete beam.

To summarise, the majority of the predicted and measured shear widths were in good agreement, although the predicted shear widths tended to be lower. This suggests that the equations put forward for the prediction of both the shear width and the failure mode are valid for bar type reinforcement. A more sophisticated analysis is required for grouted bar reinforcement.

8.2 Measured and Predicted Shear Force

The shear force P_s in the reinforcement was observed to be a maximum where it crossed the central plane of the shearbox. Figures 8.2 and 8.3 give the normalised shear force (P_s/P_p) against shear displacement X for tests on medium dense sand. The shear force (P_s/P_p) initially increases linearly with shear displacement and then appears to levels off to a more or less constant value. In many of the tests the strain gauges failed before a maximum shear

force was reached. In tests where a maximum shear force was reached the limiting value was less than 5% of plastic axial capacity P_p of the reinforcement. The rate of increase of shear force with shear displacement is observed to be more or less constant over a large range of shear displacement, and independent of the bar diameter, excluding test MD2 on tubular bar. However, the absolute magnitude of the shear force at a given shear displacement increases with increasing bar diameter.
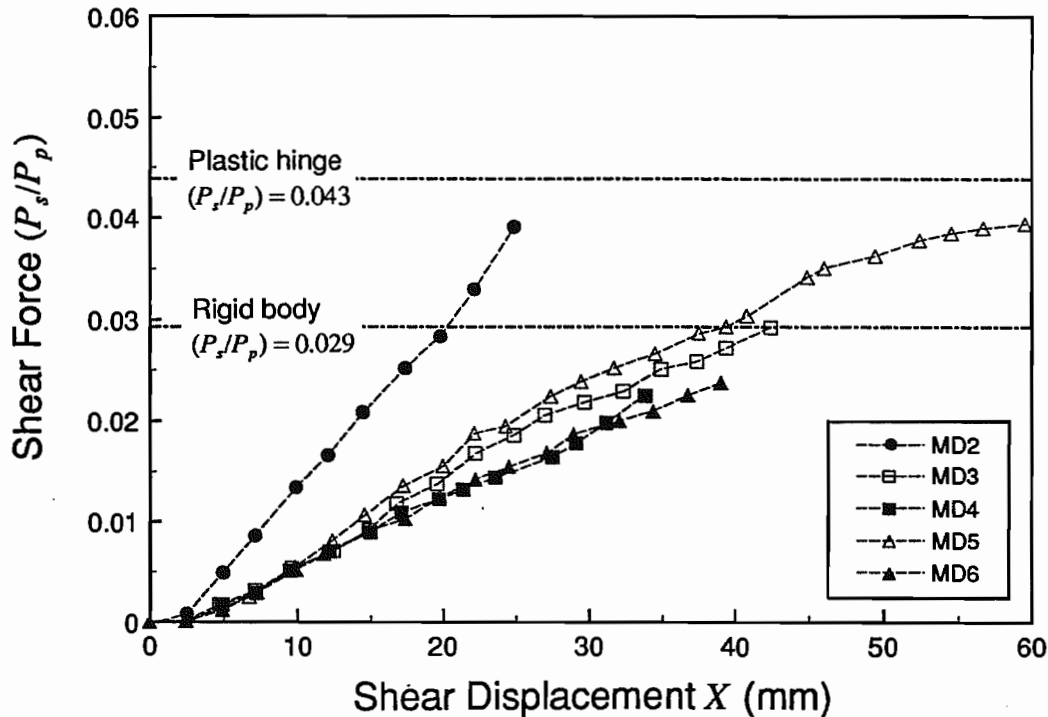
Figure 8.2 - Development of reinforcement shear force (P_s/P_p) with shear displacement X in medium dense sand.

Figure 8.3 shows the development of shear force with shear displacement for reinforcement fitted with anchor plates. Comparing Figures 8.2 and 8.3 it is observed that both the magnitude and the rate of increase of shear force with shear displacement are unaffected by axial reinforcement force. The surface texture of the reinforcement also has little effect.
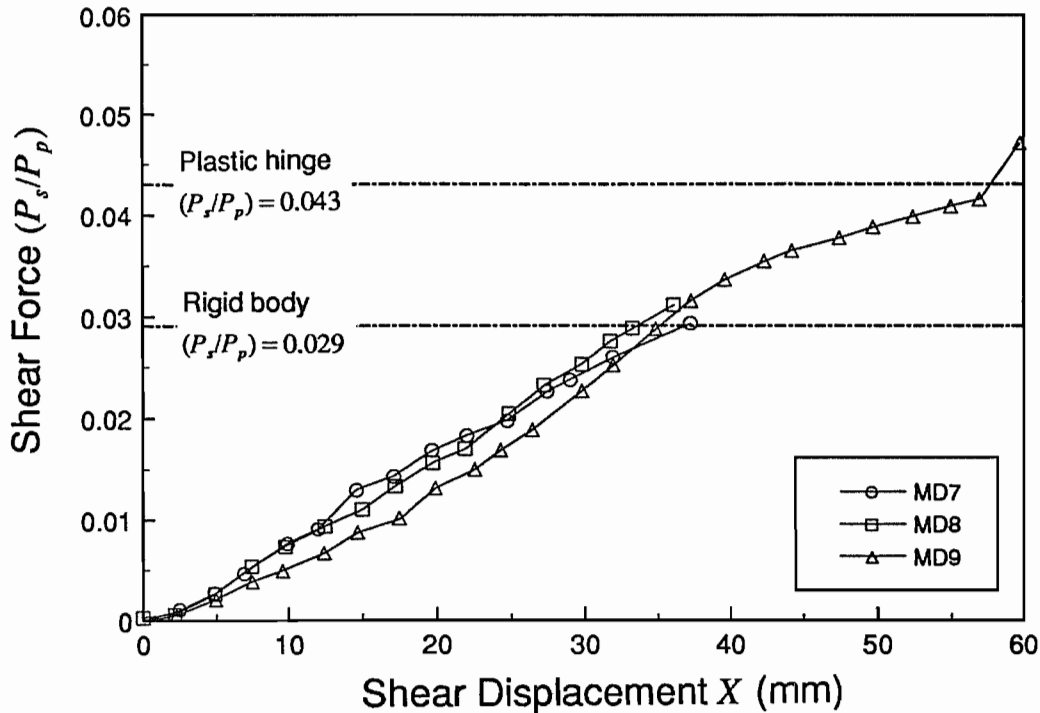
Figure 8.3 - Development of reinforcement shear force (P_s/P_p) with shear displacement X in medium dense sand for reinforcement with anchor plates.

A much higher rate of increase of shear force was observed for tubular bar reinforcement, test MD2, than for solid bar reinforcement, Figure 8.2. This can be attributed to the tubular bar reaching a higher ratio of (M/M_p) than solid bar at a given shear displacement because of the smaller cross sectional area available for bending.

Figure 8.4 shows the development of shear force (P_s/P_p) with shear displacement X for six tests on dense sand. In these tests the reinforcement bars were placed at orientations of $0°$ (O1 & O4), $15°$ (O2 & O5) and $25°$ (O3 & O6) to the vertical.

The trends exhibited in these tests are similar to those observed for tests on medium dense sand. However, as the reinforcement was oriented away from the vertical the shear displacement required to reach a limiting shear force was increased. Even at a shear displacement $X = 60mm$ the shear force observed in inclined reinforcement was less than the limiting value attained for vertical reinforcement at $X \approx 45 - 50mm$.
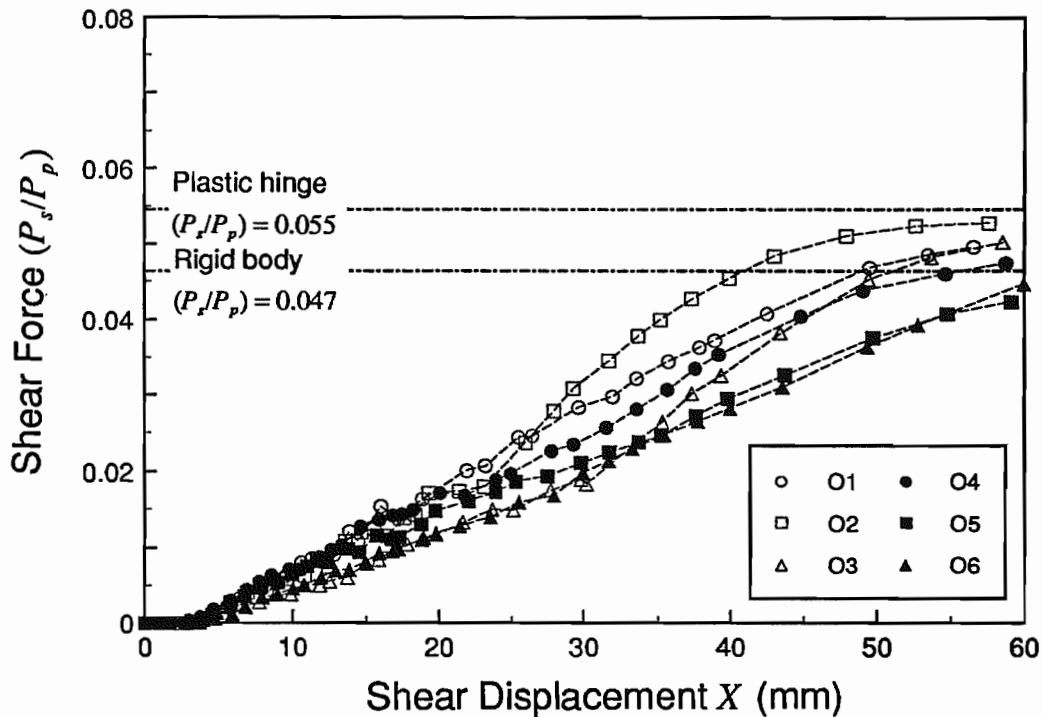
Figure 8.4 - Development of reinforcement shear force (P_s/P_p) with shear displacement X in dense sand.

The equation given in Table 7.3 for the limiting plastic shear force for circular bar and plastic hinge failure is

$$\left(\frac{P_s}{P_p}\right) = \frac{8}{3\pi(l_s/D)}\left\{1 - \left(\frac{P_{ax}}{P_p}\right)^2\right\} \qquad \ldots(8.2)$$

For rigid body failure the maximum moment can be calculated from equation (7.14) and the shear width from equation (7.30). If these are substituted into equation (7.15), the limiting shear force for circular bar is

$$\left(\frac{P_s}{P_p}\right) = \left(\frac{2\sigma'_b}{\pi\sigma_p}\right)(l_s/D) \qquad \ldots(8.3)$$

For tests on medium dense sand and $D = 16mm$ reinforcement the shear width for plastic hinge failure was $(l_s/D) = 20$, giving a limiting shear force $(P_s/P_p) = 0.043$ from equation (8.2). The shear width for $D = 25mm$ reinforcement given by equation (7.30) is

$(l_s/D) = 13$ for rigid body failure. For a bearing stress of $\sigma'_b = 1340 \ kN/m^2$ the limiting shear force from equation (8.3) is $(P_s/P_p) = 0.029$. These values of limiting shear force, shown in Figures 8.2 and 8.3, are good upper estimates of the observed maximum shear forces.

For test MD2 on tubular reinforcement the theoretical limiting shear force is $(P_s/P_p) = 0.108$. This is much higher than the observed maximum due strain gauge failure at an early stage of the test.

For the tests on dense sand the shear widths for plastic hinge and rigid body failure were $(l_s/D) = 15.5$ and 13.3 respectively. A limiting shear force $(P_s/P_p) = 0.055$ is given by equation (8.2) for plastic hinge failure, and $(P_s/P_p) = 0.047$ is given by equation (8.3) for rigid body shear failure, remembering $\sigma'_b = 2170 \ kN/m^2$. These limiting shear forces are shown in Figure 8.4. The agreement between theoretical and measured shear force at the end of the test is very good.

The term (P_{ax}/P_p) in equation (8.2) was ignored when calculating the limiting shear forces given above for plastic hinge failure. This can be justified for the test data presented owing to small magnitudes of the axial force in the reinforcement.

For many of the tests the reinforcement was not instrumented, consequently the shear force (P_s/P_p) was not measured. The excellent agreement of the data presented above with the plastic analysis described in Chapter 7 suggests that it can be used to predict the shear force in these tests.

For grouted bar reinforcement the limiting shear force may be increased due to the presence of the grout. The moment of resistance M_R of a bar of diameter D centred in an annulus of grout of diameter D_g can be calculated from composite beam theory. No closed form solution exists to this problem, but the ultimate bending resistance can be found using the following steps:

(i)   assuming that the grout is unable to withstand tensile stress or strain the plastic neutral axis is located by taking equilibrium of forces for the grout and steel.

(ii)   from the position of the plastic neutral axis the areas of grout in compression, steel in compression and steel in tension, and the location of their centroids can be calculated.

(iii)   the moment of resistance M_R is given by taking moments of the areas calculated in

(ii) about the plastic neutral axis, assuming the full yield stress has developed over them.

The above method leads to a simplified solution. For the case of an actual design the grout and steel yield stresses would require factoring, according to typical reinforced concrete practice, BS8110 (1985).

Using the method described above, the moment of resistance (M_R/M_p) of circular grouted bar has been calculated and is shown in Table 8.3, where M_p is the plastic moment of the bar alone. A range of diameter ratios (D/D_g) and yield stress ratios $\lambda = (\sigma_p/\sigma_{cu})$ are studied.

D/D_g	Moment of resistance M_R/M_p			
	$\lambda = 5$	$\lambda = 10$	$\lambda = 15$	$\lambda = 20$
1.00	1.000	1.000	1.000	1.000
0.80	1.092	1.047	1.031	1.024
0.60	1.336	1.174	1.118	1.089
0.40	2.236	1.672	1.460	1.350
0.30	3.813	2.588	2.103	1.845
0.20	8.250	6.026	4.598	3.793
0.15	12.542	10.598	8.906	7.375
0.10	20.827	19.181	17.776	16.501

Table 8.3 - Theoretical moments of resistance (M_R/M_p) for circular bar grouted reinforcement for varying strengths of steel and grout, λ and diameter ratios (D/D_g).

The moment of resistance of a grouted bar increases dramatically with decreasing (D/D_g). However, if the ratio (D/D_g) becomes too small the internal bar will fail in axial tension before the grout has mobilised its compressive strength.

In Chapter 7, the maximum moment was expressed as a function of the axial force (P_{ax}/P_p) in the reinforcement. The bending moment - axial force relationship was investigated for the simpler case of square bar in a square section of grout. This showed theoretically that for a given axial force the moment of resistance M_R of the grouted section was always greater than the moment of resistance M_p of the bar alone. For the case $(P_{ax}/P_p) = 0$ the analysis gave moments of resistance close to those for circular bar shown in Table 8.3. Although it is possible to repeat such an analysis for a circular grouted cross section the complexity of the calculation cannot be justified as it is unlikely that the results quantify what happens in practice.

A range of $(D/D_g) = 0.3 - 0.4$ is often used in practice. For this range the moment of resistance is theoretically increased by a factor 1.5 to 4, depending on λ. The moment of resistance for the reinforcement of test D3, with $(D/D_g) = 0.127$, is theoretically $(M_R/M_p) = 11.47$. For test D4 with $(D/D_g) = 0.313$ it is $(M_R/M_p) = 1.71$. In both cases $\lambda = 17.3$, Table 6.1. If these moments of resistance and the measured ranges of shear widths of $(l_s/D) \approx 17 - 28$ for test D3 and $(l_s/D) \approx 9 - 14$ for test D4 are substituted into equation (7.15), the potential limiting shear force is $(P_s/P_p) = 0.35 - 0.57$ for test D3 and $(P_s/P_p) = 0.10 - 0.16$ for test D4. Therefore, some additional benefit is theoretically possible due to the grout. However, as the grouted bars were not instrumented it was not possible to establish the magnitude of the reinforcement shear force in tests D3 and D4.

To conclude, the agreement between theoretical and measured shear force is very good. Therefore, it is proposed that the theory presented in Chapter 7 be used for the prediction of the limiting shear force available from circular bar reinforcement in soil.

8.3 Measured and Predicted Axial Force

Figures 6.9 and 6.12 show the mobilisation of reinforcement axial force (P_{ax}/P_p) with shear displacement X for tests on medium dense and dense sand respectively. For many of these tests (ignoring those which had anchor plates attached) the maximum axial force is

mobilised at a shear displacement of the order $X \approx 20 - 30mm$. To allow comparison between tests the limiting pullout force will be taken as the value of (P_{ax}/P_p) mobilised at $X = 25mm$. This assumption is consistent with the behaviour of inextensible reinforcement in pullout tests, where the peak pullout force is mobilised at small relative soil-bar displacements. The behaviour of reinforcement under pullout is different to its behaviour under shear loading, where large displacements are required to mobilise the limiting shear force. Therefore, the pullout mode   is likely to govern the start of collapse of a structure for cases where reinforcement is loaded in tension and shear.

Tests on sleeved reinforcement worked successfully, with no change in axial force with shear displacement being observed (tests MD5 and MD6). During these tests a compressive force was present at all times in the reinforcement. It is suggested that this is due to the soil loading the end of the reinforcement. A simple back calculation of the stress acting on the end of the reinforcement from the measured axial force reveals that the stress is proportional to the cross sectional area of the reinforcement, but much higher than that expected from σ'_v. This may be due to the reinforcement attracting loading from the surrounding soil as was observed by Dyer (1985).

Two models for analysing the pullout capacity of bars were described in Chapter 7. One of these assumed that the stress around the reinforcement (σ'_r/σ'_v) was radial, and for the case of reinforcement in the shearbox could be calculated from equation (7.45). Equation (7.44) relating the stress σ'_r to the pullout force P_{ax} can be rearranged to give

$$\left(\frac{\sigma'_r}{\sigma'_v}\right) = \frac{D\sigma_p}{4L_a\sigma'_v\tan\phi'_i}(P_{ax}/P_p) \qquad \qquad ...(8.4)$$

Table 8.4 shows the measured limiting pullout force from tests on instrumented reinforcement in dense sand. These data were substituted into equation (8.4) to back analyse the radial stress σ'_r around the reinforcement. For this back analysis the anchorage length was $L_a = 460mm$, the interface friction angle $\phi'_i = 32°$ and the vertical stress σ'_v was taken from Table 6.5.

Table 8.4 compares the back analysed radial stress from equation (8.4) with the theoretical value from equation (7.45). Equation (7.45) is observed to overestimate the radial stress, with the largest error observed for vertical reinforcement. The difference between the measured and theoretical values may be due to: (i) the short anchorage length of the reinforcement, (ii) combined shear and pullout loading affecting the stresses around the bar, or (iii) the initial assumptions for deriving equation (7.45) about the stress state around a circular bar were incorrect.

Test	Measured Force (P_{ax}/P_p)	Radial Stress (σ'_r/σ'_v)		Pullout Force (P_{ax}/P_p)	
		Measured equ (8.4)	Predicted equ (7.45)	Radial Stress equ (8.4)	Bearing Stress equ (7.47)
O1	0.0363	1.91	2.34	0.0445	0.0875
O2	0.0499	2.61	2.53	0.0483	0.0895
O3	0.0533	2.79	2.54	0.0485	0.0896
O4	0.0126	1.09	2.33	0.0269	0.0543
O5	0.0231	1.94	2.53	0.0301	0.0543
O6	0.0267	2.22	2.54	0.0306	0.0543

Table 8.4 - Comparison between theoretical and measured reinforcement pullout forces.

Assuming the stress acts radially around the reinforcement equation (8.4) can be rearranged to calculate the theoretical limiting pullout force (P_{ax}/P_p). As equation (7.45) overpredicts the radial stress σ'_r, the pullout force will also be overestimated. This is observed when comparing the measured and predicted pullout forces shown in Table 8.4.

Equation (7.47) is an alternative prediction of the pullout force, and is relevant for combined shear and axial loading. This leads to an upper estimate of the pullout force by accounting for the lateral bearing stress σ'_b acting on the reinforcement. Table 8.4 gives the pullout force predicted with equation (7.47) for tests O1 to O6.

The lengths l_s, l_b and l_p were calculated using the elastic-plastic interaction model and equation (7.46). This gave values of $l_s = 0.247m$, $l_b = 0.214m$ and $l_p = 0.245m$ for $D = 16mm$

reinforcement, and of $l_s = 0.336m$, $l_b = 0.292m$ and $l_p = 0$ for $D = 25mm$ reinforcement. The theoretical bearing stress was $\sigma'_b = 2170 \, kN/m^2$ and the radial stress calculated from equation (7.45).

For the particular tests examined equation (7.47) overestimated the limiting pullout force, as did equation (8.4). For bar reinforcement there are very few analytical methods available for estimating pullout resistance. This explains why the pullout resistance is often estimated using empirical methods, e.g. Schlosser and Guilloux (1981).

8.4 Limiting Combination of Shear and Axial Force

Equations defining limiting combinations of shear force (P_s/P_p) and axial force (P_{ax}/P_p) were given in Chapter 7. These are now compared with measured shear and axial force data.

Figure 8.5 compares the theoretical limiting combination of shear and axial force with experimental data for tests on circular bar reinforcement in medium dense sand. In many of the tests the data fall short of the theoretically predicted limiting envelope. This is a result of strain gauge failure at an early stage of the test. For the two tests where gauge failure did not occur, the measured combination of shear and axial force at the end of the test is close to the theoretically predicted value.

The shaded zone shown in Figure 8.5 is the approximate range for the shear and axial force, measured when the soil mobilises its peak strength. At this stage of a test the limiting axial force has generally been attained, but the shear force is still observed to be increasing.

Figure 8.6 is similar to Figure 8.5, but is for tests carried out on dense sand and with reinforcement at different orientations to the vertical. The data points shown in the figure are taken at approximately $10mm$ intervals of shear displacement X. In these tests strain gauge failure did not occur allowing the axial and shear forces to be followed to the end of the test, where the data points all lie very close to the theoretical limiting combination of shear and axial force. The predicted rigid body failure strength shown in the figure also
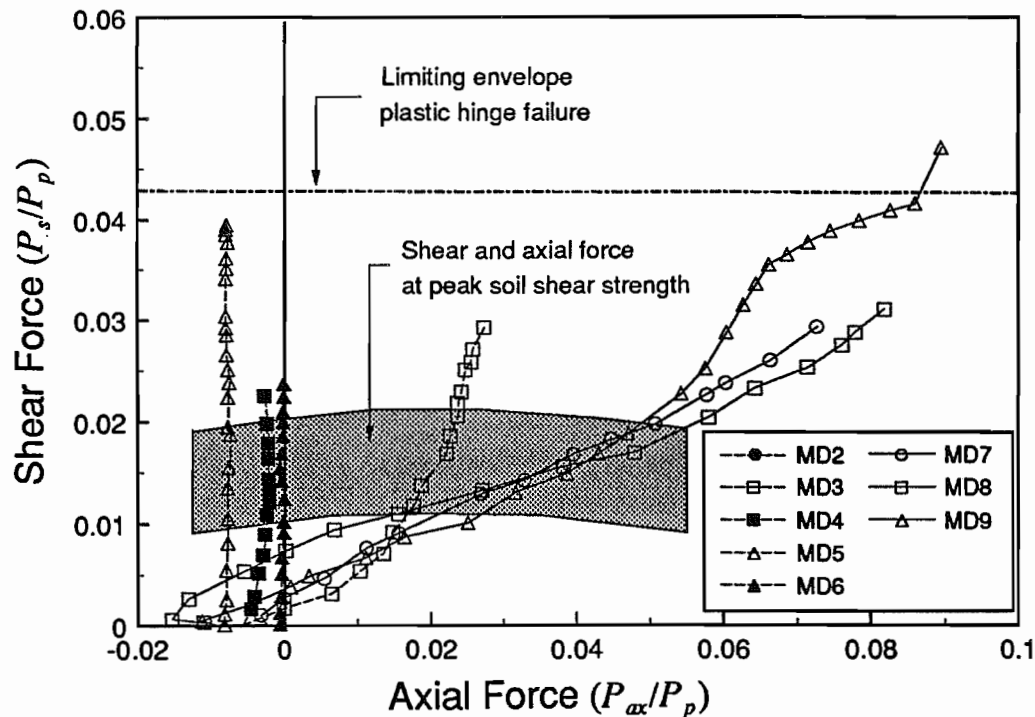
Figure 8.5 - Limiting envelope of shear and axial force compared with data from tests on medium dense sand.

agrees closely with the data presented. As with Figure 8.5 the shaded zone represents the range of shear and axial force measured during mobilisation of the peak shear strength of the soil. At the mobilisation of the peak soil strength it is apparent that at best only 50% of the available shear force has developed. However, for the majority of tests the limiting pullout force has already been mobilised.

As the model used to predict the limiting combinations of axial and shear force was essentially derived from the experimental data presented in this dissertation, it is important to illustrate that the theory agrees with other test data in the literature. Very few sources of experimental or laboratory data exist of this type in which the shear and axial forces have been measured. Examples are reported in Marchal (1984), Marchal (1986) and also Juran et al. (1981).

Marchal (1984) presents the data from tests in a circular shearbox of internal diameter $590mm$ by Quinnet and Thonnard (1984). The reinforcement was of a non standard cross section, but approximating to a rectangular section of width $B = 50mm$, thickness $t = 8.8mm$
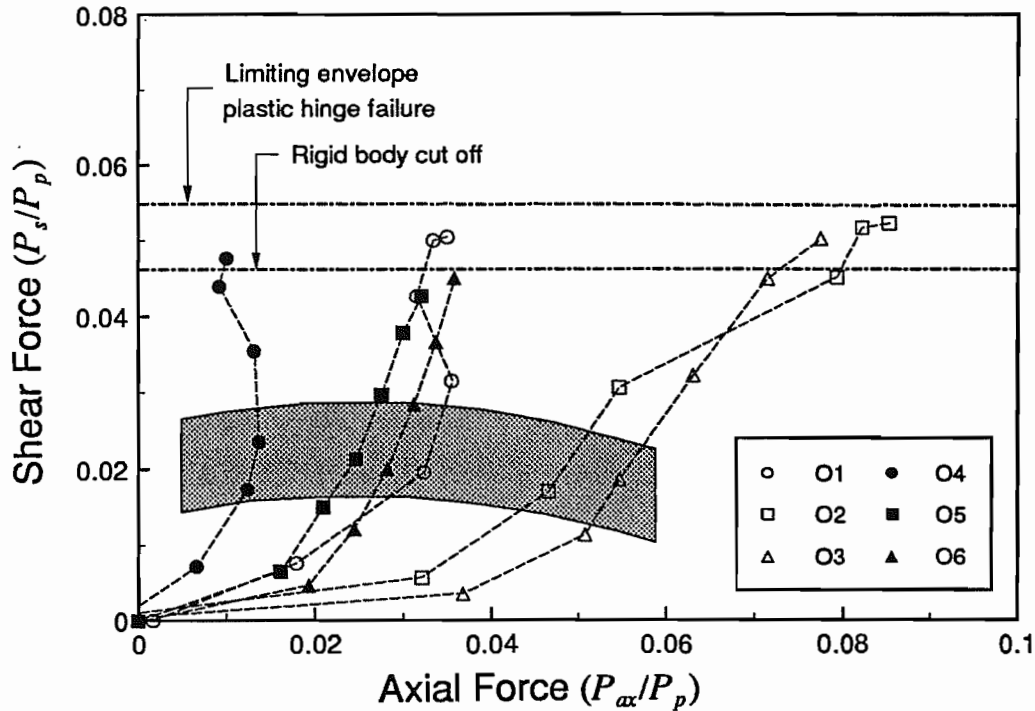
Figure 8.6 - Limiting envelope of shear and axial force compared with data from tests on dense sand.

and a yield stress $\sigma'_y = 337 \times 10^3 \, kN/m^2$. The soil was a medium dense sand with a secant friction angle $\phi' = 37°$ at an applied vertical stress $\sigma'_v = 350 \, kN/m^2$. Four angles of inclination θ with respect to the vertical were studied: $-19°, 0°, +12°$ and $+19°$. The data are shown in Figure 8.7 and compared with the theoretically predicted range for the limiting combination of shear force (P_s/P_p) and axial force (P_{ax}/P_p). A range for the limiting combination of forces is given because the unusual shape of the shearbox leads to uncertainty about the normal stress σ'_n governing bearing failure of the soil. It has been assumed that the normal stress is in the range

$$\sigma'_v < \sigma'_n < K_o\sigma'_v$$

where K_o is the *at rest* earth pressure coefficient of the soil, and is equal to $(1 - \sin\phi')$, Jaky (1944). This assumption gives a range $\sigma'_b = 1455 - 3604 \, kN/m^2$, from equation (6.18).

Figure 8.7 - Theoretical prediction of limiting shear and axial forces compared with shearbox data from Quinnet and Thonnard (1984).

The data shows that either the predicted range for the limiting shear force is too high, in which case the limiting shear force is as low as $(P_s/P_p) \approx 0.04$, or that gauge failure occurred before the end of the test. The maximum reinforcement shear force attained is less than 6% of the reinforcement axial capacity P_p. This is in agreement with previous observations of the limiting shear force of reinforcement in soil. The reinforcement axial force, which is mobilised very rapidly, is also observed to be influenced by the reinforcement orientation.

A further series of tests was carried out in the same apparatus by Moutaouakkil and Niang (1985) and are reported by Marchal (1986). Aluminium reinforcement of rectangular cross section of width $B = 20mm$, thickness $t = 2mm$ and yield strength $\sigma_p = 190 \times 10^3 \, kN/m^2$ was used. Five inclinations θ were studied: $-40°$, $-20°$, $0°$, $+20°$ and $+40°$. To increase the axial reinforcement force transverse members were attached to the reinforcement bars. The soil in these tests was a dense sand with a secant friction angle $\phi' = 43°$ at an applied vertical stress $\sigma'_v = 100 \, kN/m^2$.

Data from these tests are shown in Figure 8.8, and compared with the predicted range of the limiting combination of shear and axial force. Several of the data fall short of the predicted range. An examination of the source data revealed that strain gauge failure had occurred at an early stage of the test. For two of the tests the measured shear force lies above the predicted range, indicating that the assumptions made to predict the limiting range may have been conservative. However, the magnitude of the measured shear force is only a small fraction of the available axial capacity. The shear displacement required to attain this shear force was in excess of $X = 50mm$.
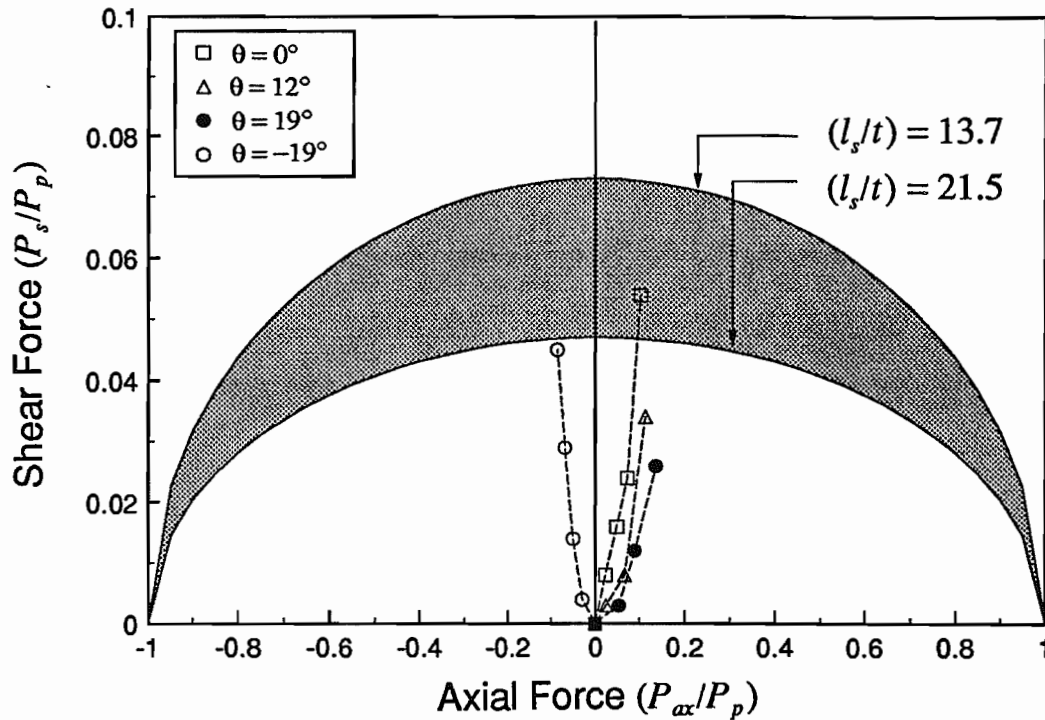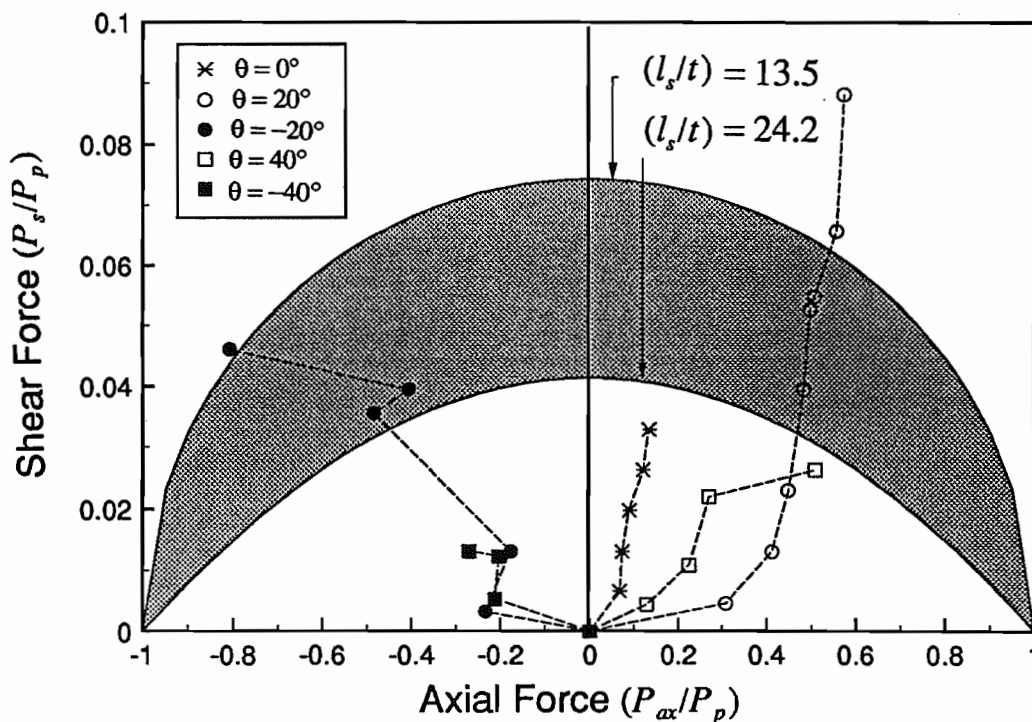

Figure 8.8 - Theoretical prediction of limiting shear and axial forces compared with shearbox data from Moutouakkil and Niang (1984).

Analysis of the data in Juran et al. (1981) leads to similar trends and observations as reported here. This infers that the multi-criteria analysis proposed provides an accurate estimate of the limiting shear force available from reinforcement in soil.

An important and general observation of all of the data is that the limiting axial force is mobilised rapidly, with a much slower mobilisation of the limiting shear force. For designs where the displacement of a reinforced structure is critical, it appears that the more important

stabilising force is axial force, as large displacements are required to mobilise the limited shear capacity of the reinforcement. The latter occurs after the soil has exceeded its peak shear strength.

Figures 8.5 to 8.8 show that the rate of increase of shear force with axial force (dP_s/dP_{ax}) decreases with increasing reinforcement orientation θ. An analysis of the ratio of the shear to axial force of reinforcement crossing a potential shear surface was proposed by Beech and Juran (1984), and is expressed by

$$\left(\frac{P_s}{P_{ax}}\right) = \frac{1}{2\tan 2\theta} \qquad\qquad ...(8.5)$$

This expression was derived by constructing a Mohr's circle of stress for the bar at the point at which it cuts the potential shear surface. To derive this relationship the assumption that a bar could be represented by a single state of stress was made. Such an assumption does not satisfy the boundary conditions existing for a bar in soil and this point is discussed further in Jewell (1990).
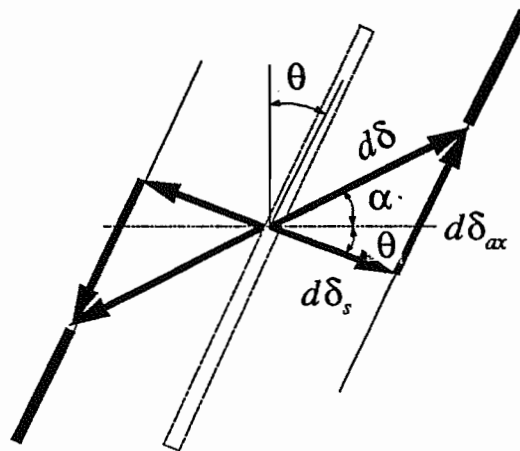
Figure 8.9 - Displacement increments for a bar crossing a potential failure surface.

Consider a reinforcing bar crossing a failure surface at some angle θ. A relative soil-reinforcement displacement $d\delta$ induces shear and axial forces in the reinforcement. The increment of displacement $d\delta$ can be considered as the resultant of a shear displacement

increment $d\delta_s$ perpendicular to the reinforcement and an axial displacement increment $d\delta_{ax}$ parallel to the reinforcement. This is shown diagrammatically in Figure 8.9. The orientation of the incremental displacement $d\delta$ with respect to the shear surface α is assumed to be between zero and the angle of dilation of the soil ψ. Resolving parallel and perpendicular to the reinforcement for the displacements leads to the following relationship between the shear and axial displacement increments

$$\frac{d\delta_{ax}}{d\delta_s} = \tan(\theta + \alpha) \qquad \ldots(8.6)$$

An increment of shear displacement $d\delta_s$ will induce an increment of shear load dP_s.

Using the elastic solution for the displacement of a laterally loaded pile from Poulos and Davis (1980), the following relationship between an increment of shear displacement $d\delta_s$ and increment of shear load dP_s is obtained

$$\frac{dP_s}{d\delta_s} = \frac{K_s D}{2.13} \sqrt[4]{\frac{4EI}{K_s D}} \qquad \ldots(8.7)$$

which for circular bar simplifies to

$$\frac{dP_s}{d\delta_s} = \frac{K_s D^2}{4.26} \sqrt[4]{\frac{\pi E}{K_s D}} \qquad \ldots(8.8)$$

An increment of axial displacement $d\delta_{ax}$ will induce an increment of axial load dP_{ax}.

The load displacement relationship for the pullout of a bar can be approximated by an elastic-plastic model. If the limiting pullout force is $(P_{ax}/P_p)_{\lim}$ and the relative soil bar displacement when this force is mobilised is δ_{po} then the relationship between and increment of pullout displacement and pullout force is

$$\frac{dP_{ax}}{d\delta_{ax}} = \frac{(P_{ax}/P_p)_{\lim}}{\delta_{po}} P_p \qquad \ldots(8.9)$$

Pullout tests on circular bars of diameter D in sand by Jewell (1980) suggested that $\delta_{po} \approx 0.22D$.

Combining equations (8.6), (8.8) and (8.9) and eliminating the incremental shear and axial displacements leads to an expression for the relationship between increments of shear and axial force,

$$\frac{dP_s}{dP_{ax}} = \frac{K_s D \sqrt[4]{\pi E / K_s D}}{15.2 (P_{ax}/P_p)_{\lim} \sigma_p \tan(\theta + \alpha)} \qquad \qquad ...(8.10)$$

for circular bar and assuming $\delta_{po} = 0.22D$. The relationship between axial and shear force is therefore not a simple function of the orientation of the reinforcement, Beech and Juran (1984), but a much more complex function of the soil and reinforcement stiffnesses, the limiting soil-reinforcement friction and the orientation of the reinforcement.

Theoretical rates of increase of shear and axial force dP_s/dP_{ax} are compared with test data in Figure 8.10. The theoretical rates were calculated using the back analysed soil stiffness ratio $(E/K_s D) \approx 70\,000^\dagger$, the limiting pullout forces given in Table 8.4 and assuming that $\alpha = \psi = 13°$.

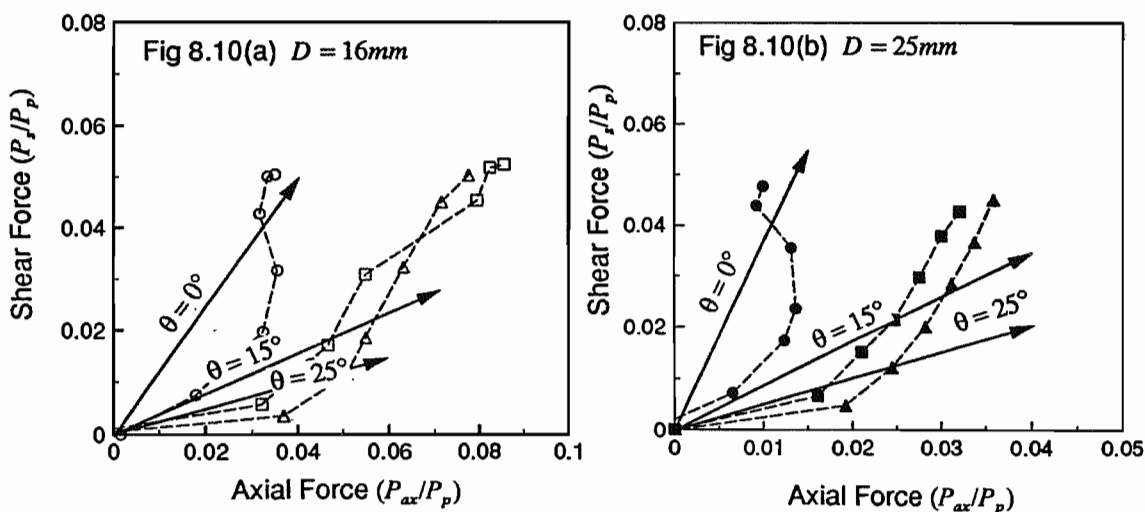**Figure 8.10 - Measured and theoretical rate of development of shear and axial force, (a) bar diameter $D = 15.9mm$ and (b) bar diameter $D = 25.4mm$.**

†The stiffness ratio of $(E/K_s D) = 70000$ was back analysed from tests on $D = 15.9mm$ reinforcement, however, the same ratio will also be applied to the tests on $D = 25mm$ reinforcement for reasons explained in Section 8.1.

The fit of the theoretical rate of increase of shear force with axial force to the experimental data can be described as encouraging, bearing in mind the number of parameters used in the analysis. In general the rate of increase of the shear force with respect to axial force appears to intersect the data at a point corresponding to the mobilisation of the maximum shear strength of the soil. Combining equation (8.10) with a theoretical estimate of the pullout resistance and the multi-criteria analysis defines theoretically not only the limiting combination of shear and axial force but also the loading path followed.

The multi-criteria analysis has been shown to provide a good estimate of the theoretical limiting combination of shear and axial force for a large number of data. It has also been shown that the available shear force from reinforcement subject to rigid body shear failure can be predicted, as can the rate of increase of shear force with axial force. The latter analysis is very sensitive to the parameters chosen.

·8.5 Limit Equilibrium Analysis and Boundary Forces

The effect of the reinforcement shear and axial forces on the soil strength will now be discussed, and the shear and axial forces measured during shearbox tests are compared with the change in soil shear strength measured at the boundary using equation (7.48).

The change in soil shear strength ΔS will be considered to be equal to the change in soil shearing resistance associated with each reinforcing bar (i.e. total change is $n\Delta S$, where n is the number of reinforcing bars). This change in shear strength is normalised by the reinforcement axial capacity P_p, providing a useful measure of how efficiently the reinforcement is being used.

Figure 8.11 shows the measured difference in strength per reinforcing bar for tests on medium dense sand. The largest change in strength is brought about by tubular section reinforcement. The fixing anchor plates to the reinforcement of diameter $D = 16mm$ (compare tests MD7, 8 & 9 with MD3 & 5) had a significant effect on strength which is attributed to the additional axial reinforcement force. Table 8.5 compares the measured
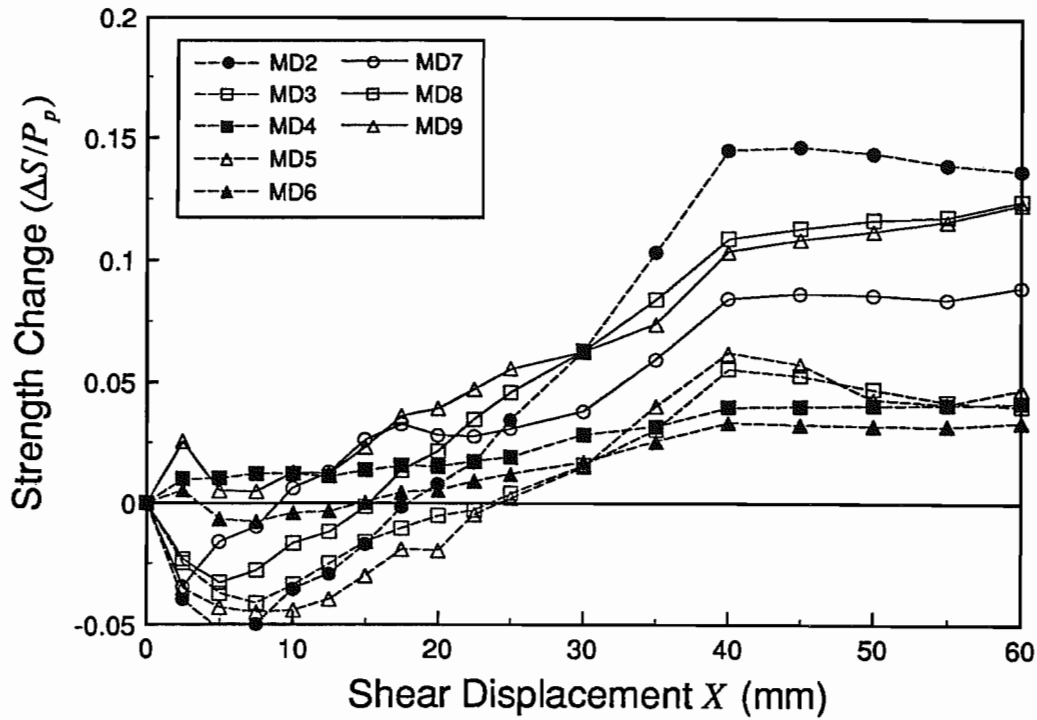
Figure 8.11 - Shear strength change per bar ($\Delta S/P_p$) with shear displacement X for reinforcement in medium dense sand.

change in soil strength per reinforcing bar with that calculated using equation (7.48) by substitution of the measured shear and axial forces at a shear displacement of $X = 25mm$. It has been assumed that the peak strength of the soil $\phi' = 42°$.

Test	$D(mm)$	Axial Force (P_{ax}/P_p)	Shear Force (P_s/P_p)	$(\Delta S/P_p)$ Equ (7.48)	$(\Delta S/P_p)$ Measured
MD2	25.4/22.4	0.0266	0.0391	0.0631	0.0344
MD3	15.9	0.0227	0.0186	0.0390	0.0040
MD4	25.4	-0.0020	0.0144	0.0126	0.0187
MD5	15.9	-0.0076	0.0194	0.0126	0.0021
MD6	25.4	-0.0005	0.0155	0.0151	0.0118
MD7	15.9	0.0508	0.0197	0.0654	0.0308
MD8	15.9	0.0581	0.0204	0.0727	0.0460
MD9	15.9	0.0431	0.0169	0.0557	0.0557

Table 8.5 - Limit equilibrium analysis of the strength change ($\Delta S/P_p$) per bar for tests on medium dense sand at a shear displacement $X = 25mm$.

The agreement between the measured boundary change in strength and that calculated with equation (7.48) is variable. The boundary strength change ($\Delta S/P_p$) was calculated as the difference in strength at a given shear displacement X between the reinforced test and a standard unreinforced test. Generally the magnitude of ($\Delta S/P_p$) was small compared with the strength measured in the unreinforced test. Any small fluctuation in the strength of the unreinforced test compared with the reinforced test led to a large error in ($\Delta S/P_p$), which explains the variable agreement. The repeatability of medium dense samples was not as good as for dense samples owing to the larger range of reinforcement types tested.
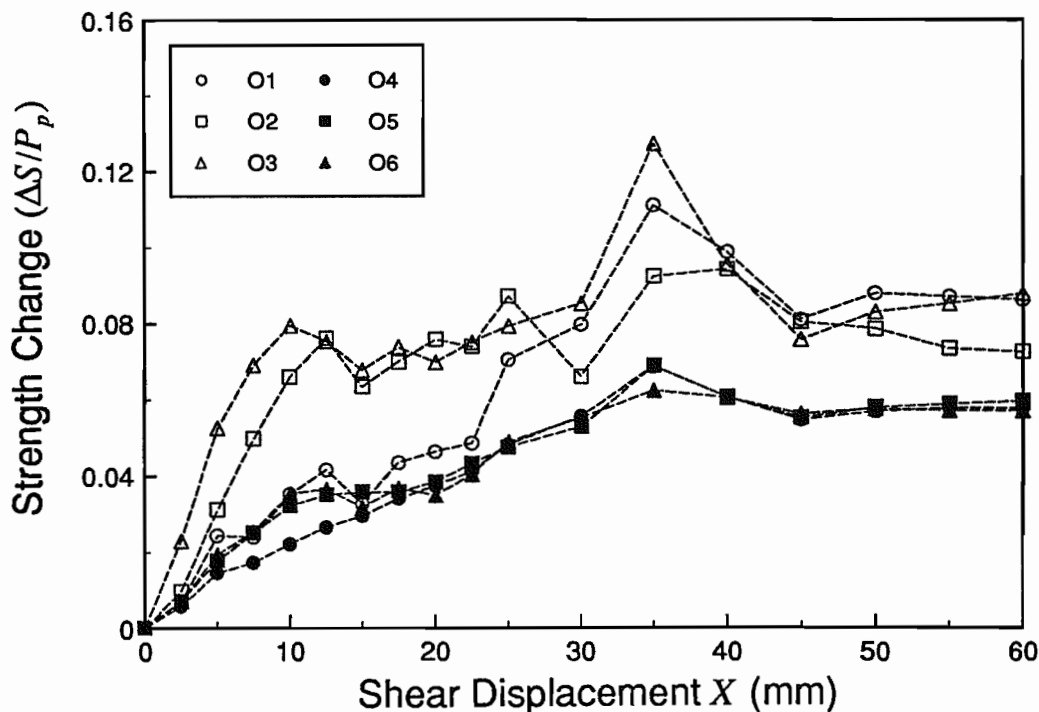
Figure 8.12 - Shear strength change per bar ($\Delta S/P_p$) with shear displacement X for reinforcement in dense sand.

Further ($\Delta S/P_p$) data are presented in Figure 8.12 for reinforced tests on dense sand in which the reinforcement orientation was varied. In the later stages of the test it is observed that the improvement in strength is fairly independent of the reinforcement orientation, but dependent on the bar diameter. This is in contrast to the data in the earlier stages of the test

where the improvement in strength is much more rapid as the reinforcement is inclined with respect to the vertical, confirming the observation that axial reinforcement force is mobilised at small relative soil reinforcement displacements. Table 8.6 compares the measured difference in strength with that deduced from equation (7.48) at shear displacements $X = 25mm$ and $X = 60mm$.

Test	$D\,(mm)$	Axial Force (P_{ax}/P_p)	Shear Force (P_s/P_p)	$(\Delta S/P_p)$ Equ (7.48)	$(\Delta S/P_p)$ Measured
Shear displacement $X = 25mm$					
O1	15.9	0.0363	0.0244	0.0620	0.0701
O2	15.9	0.0499	0.0237	0.0794	0.0866
O3	15.9	0.0533	0.0149	0.0795	0.0789
O4	25.4	0.0126	0.0196	0.0326	0.0482
O5	25.4	0.0231	0.0186	0.0421	0.0475
O6	25.4	0.0267	0.0160	0.0438	0.0489
Shear displacement $X = 60mm$					
O1	15.9	0.0333	0.0496	0.0841	0.0859
O2	15.9	0.0828	0.0528	0.1411	0.0723
O3	15.9	0.0767	0.0502	0.1279	0.0875
O4	25.4	0.0092	0.0474	0.0569	0.0577
O5	25.4	0.0321	0.0423	0.0697	0.0595
O6	25.4	0.0360	0.0447	0.0700	0.0570

Table 8.6 - Limit equilibrium analysis of the strength change $(\Delta S/P_p)$ per bar for tests on dense sand at a shear displacements $X = 25mm$ and $X = 60mm$.

The agreement between the predicted and measured shear strength difference is generally very good, although there is some discrepancy for the tests O2 and O3 on inclined reinforcement at $X = 60mm$. This disparity may be the result of an error in the axial strain measurement owing to the extreme bending of the reinforcement (see Figure 6.12).

The agreement of the data in Table 8.6 with the predictions from equation (7.48) support the conclusions of other researchers. That is the limit equilibrium approach can be used accurately to calculate the soil shear strength improvement brought about by reinforcement crossing a potential failure surface.

Theoretical analyses of tests on uninstrumented reinforcement are compared with measured strength changes in Tables 8.7 and 8.8. The shear widths (l_s/D) given in the tables are calculated from reinforcement deformation, equation (8.1) where possible, or theoretically if insufficient deformation occurred. The corresponding boundary measurements of the change in strength, plotted against shear displacement X are given in Figures 8.13 and 8.14 respectively. Also shown for comparison are the data from tests O1 and O4.

Test	D (mm)	Applied Stress $\sigma'_v(kN/m^2)$	Shear Width (l_s/D)	Axial Force (P_{ax}/P_p)	Shear Force (P_s/P_p)	$(\Delta S/P_p)$ Predicted Equ (7.48)	$(\Delta S/P_p)$ Measured
S1	15.9	64	19.0	0.0161	0.0447	0.0644	0.0403
S2	15.9	151	17.9	0.0379	0.0474	0.0866	0.0524
S3	25.4	64	13.3†	0.0100	0.0299	0.0403	0.0191
S4	25.4	151	12.7†	0.0237	0.0669	0.0914	0.0551
† Calculated from equ (7.27)							

Table 8.7 - Theoretical prediction of the change in soil strength for tests in which the applied vertical stress σ'_v was varied.

As might be expected the theoretical predictions of $(\Delta S/P_p)$ are overestimates. The prediction of (P_s/P_p) in the previous sections has generally proved to be quite accurate and it is proposed that the major source of error lies in the calculation of the axial force (P_{ax}/P_p). The observation that even a small overestimate of the axial force (P_{ax}/P_p) can have such a large effect on $(\Delta S/P_p)$ demonstrates that reinforcement placed so that it works in axial tension instead of shear is much more efficient.

The test data for the grouted bar reinforcement shows that the addition of grout to a reinforcing bar can increase quite dramatically the shear strength of the soil. This is undoubtedly attributed to the increase in surface area of the reinforcement as well as the enhanced flexural strength; the latter only becoming very significant for small ratios of (D/D_g) and large shear displacements.

Test	D (mm)	Shear Width (l_s/D)	Axial Force (P_{ax}/P_p)	Shear Force (P_s/P_p)	($\Delta S/P_p$) Predicted Equ (7.48)	($\Delta S/P_p$) Measured
D1	6.5	18.5	0.0741	0.0458	0.1225	0.1639
D2	50.8	6.6†	0.0078	0.0232	0.0313	0.0187
D3	6.5/50.8	27.8	0.7080	0.3502	1.0830	0.5219
D4	15.9/50.8	14.0	0.1209	0.1037	0.2289	0.1082
† Calculated from equ (7.27)						

Table 8.7 - Theoretical prediction of the change in soil strength for tests in which the bar diameter was varied.

Figure 8.13 - Shear strength change per bar ($\Delta S/P_p$) with shear displacement X for reinforcement in dense sand with varying applied vertical stress σ'_v.

Concerning the method of reinforcement installation it is interesting to look at the data from tests in which the reinforcement was driven into the soil sample. The first point to note is that the shear displacement at which the reinforcement is driven appears to have little
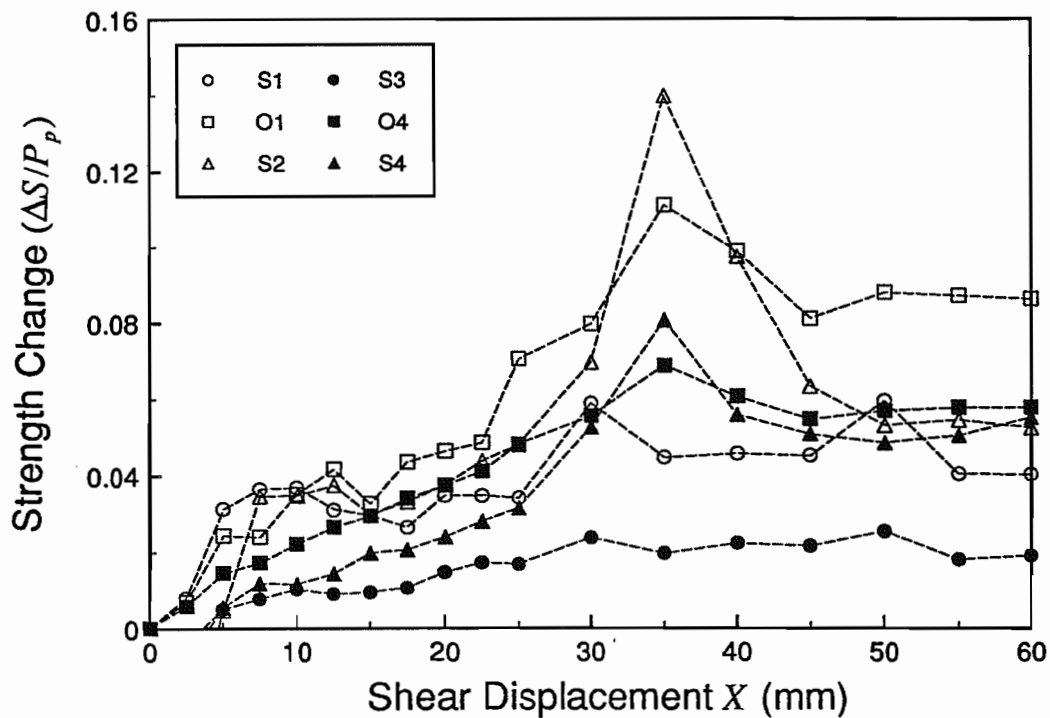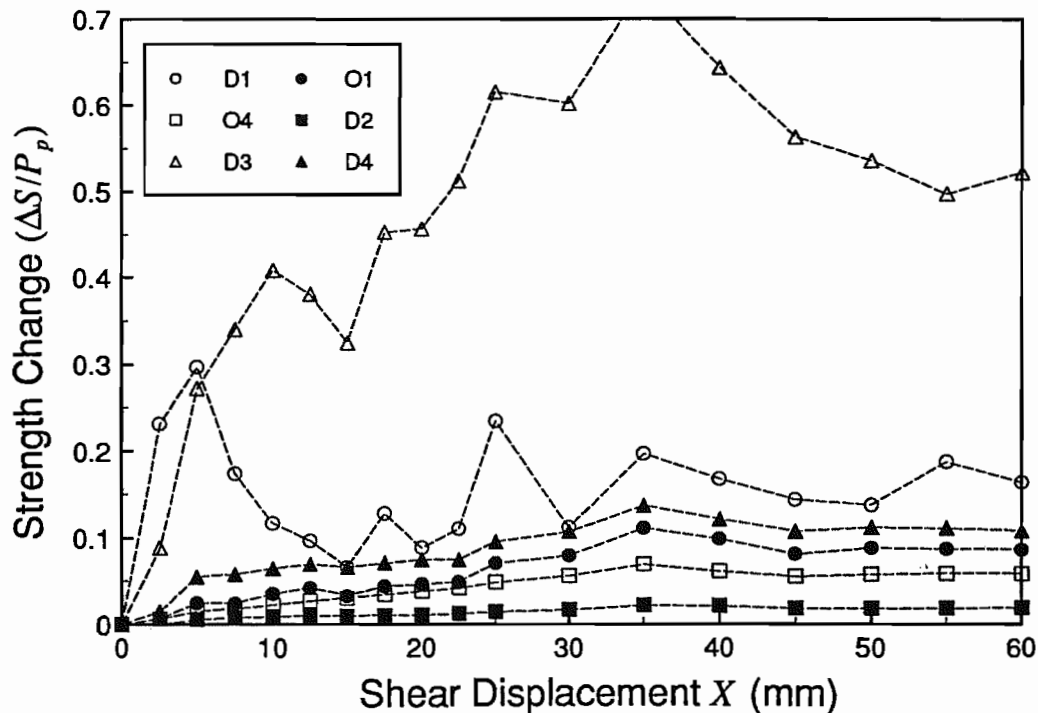
Figure 8.14 - Shear strength change per bar ($\Delta S/P_p$) with shear displacement X for reinforcement of varying diameter in dense sand.

effect on the final shear improvement. The improvement appears to require a shear displacement of the order $30mm$ to reach a maximum. This is because it is derived principally from the bending of the reinforcement.

To conclude, the limit equilibrium analysis of soil strength improvement has been shown to predict the change in strength due to an axial and a shear load. Previously this has only been shown to be correct for reinforcement under axial load, Jewell, 1980, Dyer, 1985 & Palmeira, 1987. For reinforcement where the axial force is approximately equal to, or greater than the shear force then its contribution to the shear improvement of the soil can be quite significant. However, as the magnitude of the axial force increases the shear force becomes less significant; this is the case for previous researchers who used grid reinforcement leading to large relative axial forces. For reinforcement working entirely in shear the mobilised shear force has little effect on soil shear strength. The maximum shear force available is dependent on the relative soil reinforcement displacement. The method
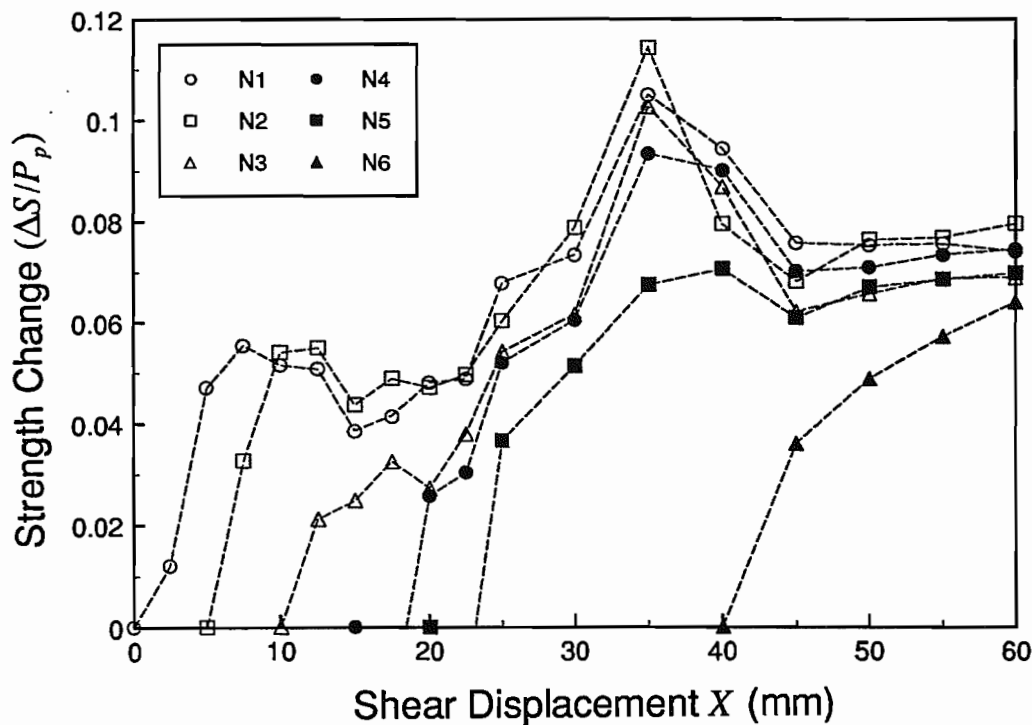
Figure 8.15 - ($\Delta S/P_p$) for reinforcement installed at different shear displacements X_i.

of reinforcement installation had little effect on shear strength improvement for the soil used in the tests. However, the reinforcement cross section does. In general the ratio of the reinforcement surface area to that of the cross section has the largest effect.

8.6 Case History - Soil Nailed Wall in Germany

The instrumented nailed wall described below is one of the few cases where bending moment distributions have been measured in the nails, and is reported fully by Gassler (1987). The instrumented slope was a 6m high cut inclined at 10° to the vertical into which 5 rows of instrumented nails of between $3m$ and $3.5m$ in length were placed. The nails were of the drilled and grouted type with an external (hole) diameter, $D_g = 55mm$ and with a bar diameter $D = 22mm$. The reinforcement was disposed as shown in Figure 8.16. The measured friction angle in the soil was $\phi' = 40.5°$ and the unit weight of the soil $\gamma = 15.6 \ kN/m^3$. The yield stress for the high yield steel bars was $\sigma_p = 420 \times 10^3 \ kN/m^2$ ($P_p = 160 \ kN$, $M_p = 0.745 \ kNm$).

$$
\begin{array}{ll}
D = 22mm & \phi' = 40.5° \\
D_g = 55mm & \gamma = 15.6kN/m^3 \\
\sigma_y = 420MN/m^2 & p = 110kN/m^2
\end{array}
$$
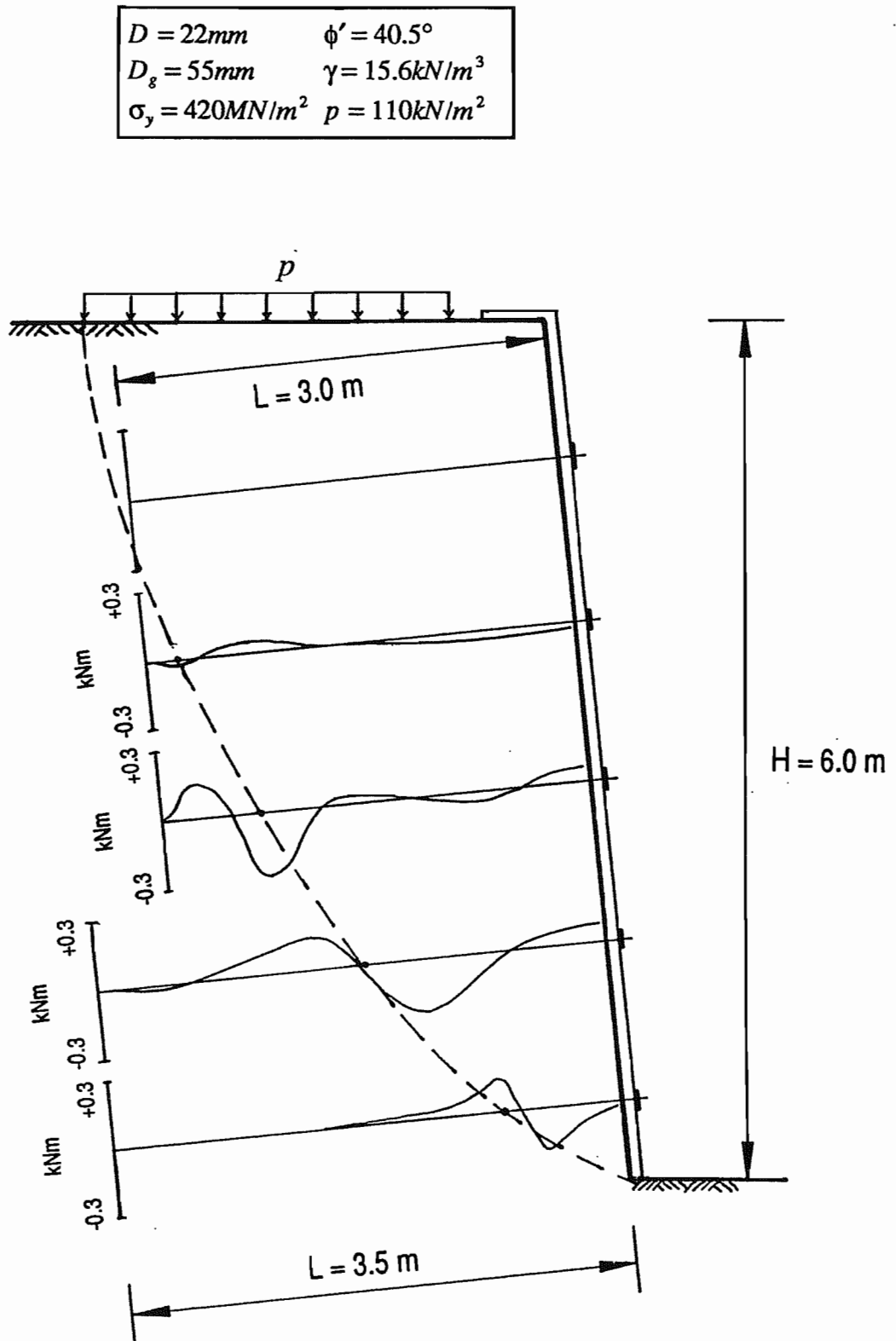
Figure 8.16 - Bending moment distribution at collapse of soil nailed wall, after Gassler (1987).

8.31

$$
\begin{array}{ll}
D = 22mm & \phi' = 40.5° \\
D_g = 55mm & \gamma = 15.6kN/m^3 \\
\sigma_y = 420MN/m^2 & p = 110kN/m^2
\end{array}
$$

Figure 8.17 - Axial force distribution at collapse of soil nailed wall, after Gassler (1987).

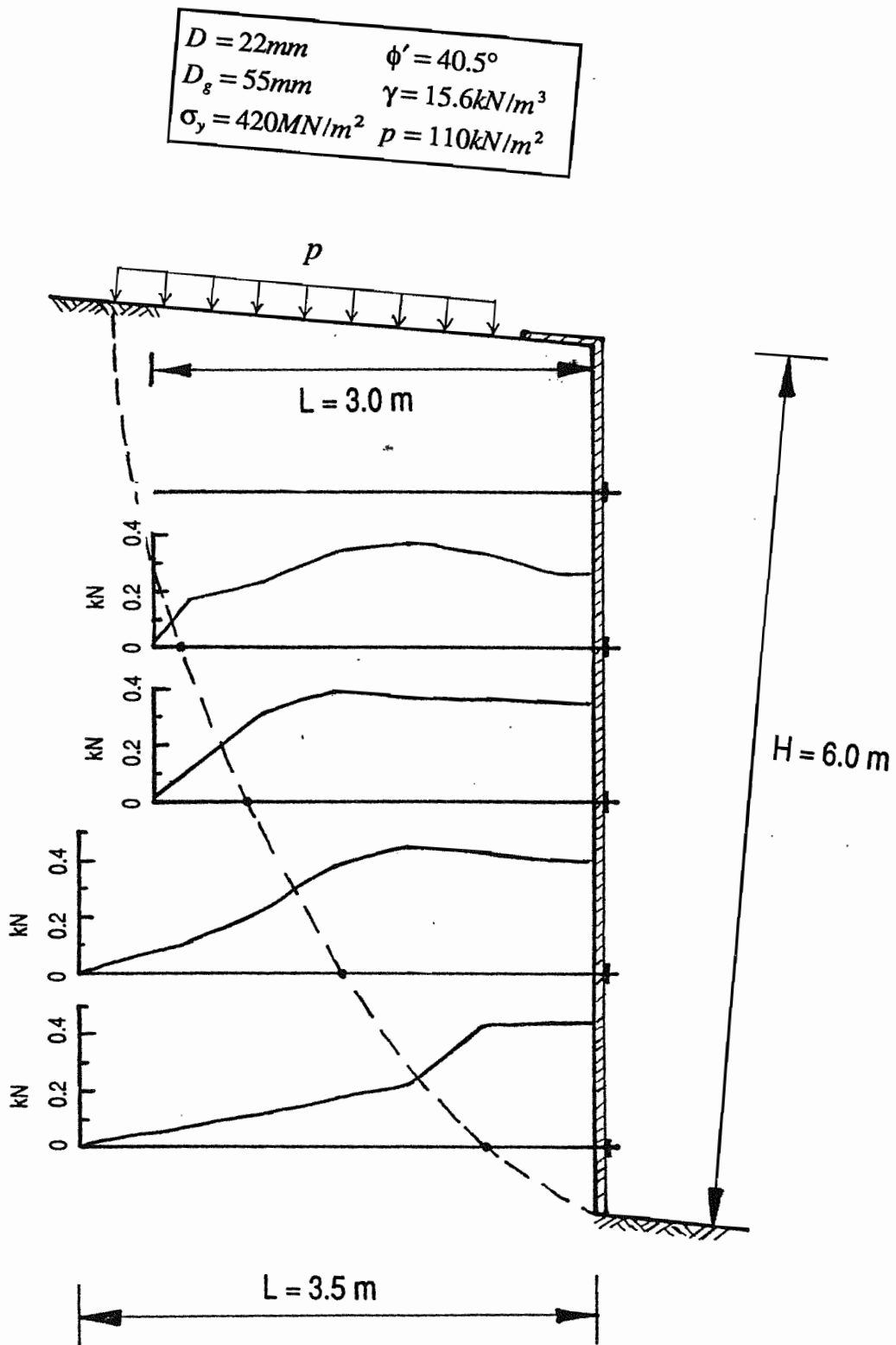A uniform surcharge, p, was applied at the top of the slope, and achieved a value $p = 110 \, kN/m^2$ when the wall collapsed. The bending moments in the reinforcement were observed to be a maximum at failure, even though a higher surcharge of $p = 150 \, kN/m^2$ at an earlier stage of the tests had been achieved. The measured values at failure are shown in Figure 8.16, together with the trace of the critical failure surface. It is interesting to note that there is an oscillation of the bending moment distribution along the bars and this can be explained by the presence of a whole series of similar failure surfaces passing through the failure zone. Figure 8.17, similar to Figure 8.16 shows the axial force distribution in the nails occurring at collapse.

Summarised in Table 8.8 for the three lowest nails intersected by the rupture surface are the measured maximum bending moments (M_{max}/M_p), the observed shear width (l_s/D), the measured axial force (P_{ax}/P_p), the shear force (P_s/P_p), and the inclination of the reinforcement to the normal to the shear surface θ.

Nail Row	Depth Z (m)	Moment[†] M_{max}/M_p (kNm)	Shear Width (l_s/D)	Axial Force (P_{ax}/P_p)	Shear[‡] Force (P_s/P_p)	Inclination $\theta°$
3	3.44	0.280	20.7	0.125	0.0101	28
4	4.53	0.243	32.0	0.243	0.0048	37
5	5.54	0.215	12.4	0.273	0.0090	47
[†] $M_{max} = (M_{max}^+ - M_{max}^-)/2$ where M_{max}^+ and M_{max}^- are measured on either side of the shear surface.						
[‡] $P_s = (dM/dX)$ at $M = 0$, X is measured along the nail.						

Table 8.8 - Observed data from soil nailed wall reported by Gassler (1987).

The theoretical model described in Chapter 7 predicts the minimum shear width (l_s/D) as would apply across a single shear surface. A wider and less precise zone of shearing soil would be more likely under field loading, as opposed to in the shearbox, so that a greater shear width would be expected than the minimum predicted value.

Recorded in Table 8.9 are the measured and predicted values for the shear width. For the calculation of the bearing stress it has been assumed that the lateral stress σ'_n governing

the bearing failure around the nail is related to the vertical stress by $\sigma'_n = (1 + K_a)\sigma'_v/2$, where K_a is the active earth pressure coefficient for the soil (Figure 7.7). The additional bearing area of the grout surrounding the bar has been taken into account using equation (7.43).

As shown in Table 8.9 the measured values for the shear width (l_s/D) are indeed greater than the minimum possible values which would apply across a well defined single rupture surface.

Nail Row	Measured Shear Width (l_s/D)	Vertical Stress $\sigma'_v = \gamma Z + p$ (kN/m²)	Bearing Stress σ'_b (kN/m²)	Predicted Shear Width (l_s/D)
3	20.7	153	1407	12.6
4	32.0	171	1572	11.9
5	12.4	186	1710	11.4

Table 8.9 - Comparison between the measured and theoretical shear widths.

The comparison in Table 8.10 is for the maximum shear forces in the nails at the intersection with the failure surface. The first check is on the basic equation relating moment to maximum shear force

$$P_s = 4\frac{M_{max}}{l_s} \qquad ...(7.15)$$

Substitution of the measured values (l_s/D) and M_{max} into equation (7.15) gives predicted shear forces which agree reasonably with the values deduced from the measured moments in the nails (columns 2 and 3 in Table 8.10).

It is interesting to determine the absolute maximum shear force that could have been developed if the nails had become fully plastic before failure of the structure. The measurements in Table 8.8 show that less than 30% of the plastic moment capacity of the nails was developed when failure occurred with the nails pulling out. The final column in

Nail Row	Shear Force (P_s/P_p)		
	Measured	Predicted[†]	Limiting[‡]
3	0.0101	0.0115	0.0664
4	0.0048	0.0064	0.0672
5	0.0090	0.0147	0.0690

† Measured (l_s/D) and M_{max} in equation (7.15).

‡ Predicted (l_s/D) and measured (P_{ax}/P_p) in equation (8.2).

Table 8.10 - Comparison between measured, predicted and limiting shear forces.

Table 8.10 records the limiting shear force calculated using the minimum predicted shear width, and allowing for the maximum plastic moment that would correspond with the measured axial force.

The important point illustrated by the results in Table 8.10 is that the structure collapsed with the nails pulling out well before sufficient shear displacement could occur to mobilise the available moment capacity, and hence shear force, in the reinforcement. In other words, while it is possible in a displacement controlled direct shear apparatus to test to large shear deformations so as to eventually reach the plastic capacity of the reinforcement, the loading in a field structure is stress controlled. Thus failure in the field, or in a stress controlled shear apparatus, occurs as soon as the overall shearing resistance starts to reduce, which would be at about $X = 25mm$ in the direct shear test (see in Figure 6.12 for example). At the point of failure in direct shear tests less than 30% of the available plastic resistance was mobilised in the reinforcement, $(P_s/P_p) < 0.02$ or 2%, corresponding closely to that observed in the field structure.

Finally, the measured values of axial and shear force can be substituted into the limit equilibrium equation (7.48) to determine the improvement in soil shearing resistance from the axial and shear forces, as shown in Table 8.11. Expressed as a percentage of the improvement due to the axial force alone, the measured shear force is seen to provide less than 3% additional improvement at failure.

Nail Row	Axial Force (P_{ax}/P_p)	Shear Force (P_s/P_p)	Shear Improvement $\Delta S/P_p$		$\Delta S_{shear}/\Delta S_{axial}$ (%)
			Axial Force	Shear Force	
3	0.125	0.0101	0.153	0.0049	2.2
4	0.243	0.0048	0.312	0.0014	0.5
5	0.273	0.0090	0.359	0.0005	0.1

Table 8.11 - Improvement in soil shearing resistance due to axial and shear force in the reinforcement.

8.7 Conclusions

An analysis of the test data from a series of reinforced direct shear tests in the large direct shear apparatus, has resulted in the following observations and conclusions:

(i)   The equations predicting the shear width (l_s/D) were generally found to be in agreement with the experimental data, from both bending moment profiles and reinforcement deformation. The shear width, which is a fundamental parameter governing the shear force P_s in reinforcement crossing a potential shear surface typically lies in the range 5 to 30, for a large variety of soil types and reinforcement cross sections.

(ii)   The maximum shear force available from reinforcement in soil is a function of the relative reinforcement to soil strength (σ_p/σ'_b), the shape of the cross section and also the length of reinforcement embedment L_a. Typically, for solid section reinforcement the maximum shear force available P_s will be less than $5-10\%$ of the reinforcement axial capacity P_p. For reinforcement of hollow cross section, or whose section area has been increased by grout the shear force is usefully increased.

(iii)   The maximum or limiting shear force available from reinforcement in soil generally requires large relative soil-reinforcement displacements to be mobilised, especially when compared with the relative soil-reinforcement displacement to mobilise the limiting pullout capacity. In the direct shear test it was observed that before

mobilisation of the limiting shear capacity the soil had fully strain softened; the corollary of which is that for structures in which displacements are critical the shear force cannot be counted on to stabilise the structure.

(iv)   The theoretical predictions of axial force proposed both led to an over prediction of the pullout capacity of the reinforcement. This particular aspect still requires further investigation.

(v)   The proposed multi-criteria analysis allowed the prediction of the limiting combination of shear and axial forces and bounded the test data very well. An elastic equation was proposed which defines the initial rate of increase of shear force with axial force and fitted the data well.

(vi)   The limit equilibrium analysis to estimate the increase in shear strength of the soil has been shown to hold for the case when reinforcement is undergoing both shear and axial loading. The agreement between the measured shear strength improvement and that deduced using the limit equilibrium analysis was variable. This was due to the magnitude of the strength of the unreinforced soil being great compared with the magnitude of the improvement. It was noted that the potential benefit of using reinforcement in axial tension is much greater than using it in shear.

(vii)   Observations made during the collapse of a soil nailed wall showed that bending of the reinforcement did not happen until excessive displacements had occurred. At collapse, a back analysis of the structure discovered that the highest contribution of shear force to the reinforcement soil strength improvement was less than 3% of that due to the axial force.

CHAPTER 9:

CONCLUDING COMMENTS

A summary of the overall conclusions resulting from this experimental study is given below. This is followed by suggestions for future research into soil reinforcement interaction.

9.1 Large Direct Shear Apparatus

The performance of the Large Direct Shear Apparatus was enhanced by making the upper and lower boundaries symmetrical. This was done by fixing the top platen to the upper half of the shearbox and by changing the method of applying the vertical load. The modifications led to reduced rotation of the upper half of the shearbox, an improvement in the measurement of sample dilation at the boundaries, and a more uniform shear strain distribution across the central plane. Before carrying out future testing in the LDSA modifications to be contemplated might include a mechanism to reduce the eccentricity between the applied shear load and the centroid of the sample, independent load control for each vertical loading jack, and a general stiffening of the shearbox to allow testing of soils at higher vertical stresses. For the majority of soils and reinforcements the width of the shearbox could be made smaller to reduce the time and effort required for sample preparation.

Data recorded from tests in the modified LDSA were comparable with those from a smaller shearbox with similar symmetrical boundary conditions.

9.2 Unreinforced Tests

The direct shear apparatus overestimates the simple or direct shear resistance of the soil by about 5%; this phenomenon appears to be indigenous to the test. Data from unreinforced tests was analysed using both Mohr's circle and flow rule methods of analyses, with good agreement between the two techniques for plane strain strengths. Using the two methods in parallel allowed any sources of error in the boundary shear stress or dilation measurements to be identified and by-passed.

Methods of analysing the critical state friction angle of the soil from test data were investigated. Owing to the overestimation of the shear stress on the central plane in the direct shear test the critical state strength obtained was generally higher than the expected range for the sand tested.

A comparison between direct shear test data for two sands of similar mineralogy, particle size and distribution led to the conclusion that the dilation and peak strength at low stress levels are significantly affected by particle angularity. This data, and additional data from the literature, were compared with the strength predicted using Bolton's (1986) stress-dilatancy index; the trend observed suggested that Bolton's prediction for the plane strain strength was an overestimate. For design purposes it is recommended to apply his prediction of triaxial strength to both plane strain and axisymmetric problems.

9.3 Reinforced Tests

The limiting shear force available from soil reinforcement is a function of the maximum moment in the reinforcement and its distance from the point of shear load application. This maximum moment is dependent on the reinforcement cross section and yield strength, the lever arm is a function of the soil bearing strength. As the bearing strength of the soil rises with respect to that of the reinforcement the limiting shear force increases. Other factors influencing the limiting shear force are the axial force in the reinforcement, the length of reinforcement, the orientation of the reinforcement, and the thickness shear surface or zone.

A plastic analysis was proposed to predict the limiting combination of shear and axial force. When combined with pullout and rigid body failure criteria the analysis allowed the multi-criteria analysis proposed by Schlosser (1983) to be redefined. A similar elastic analysis, based on lateral pile loading theory, leads to an underestimate of the limiting shear force and is not recommended owing to its dependence on the modulus of subgrade reaction.

The effect of reinforcement shear and axial force on soil strength was calculated successfully using a limit equilibrium analysis based on reinforcement spanning a potential failure surface in the soil. For a large range of reinforcement orientations the effect of reinforcement axial force on soil shear strength is greater than the effect of a shear force of equivalent magnitude. Typical orientations of soil nails and soil dowels are such that where possible axial reinforcement force should be used. In soil nailed structures it is wise to preclude the reinforcement shear force in stability calculations as the displacements required to mobilise them renders the structure unserviceable. Also, the strength of the soil reduces to a residual or critical state strength before the maximum reinforcement shear force develops. In soil dowelling the most efficient reinforcement is likely to be a thin walled tube.

The effect of reinforcement installation appeared to have little effect on the shear force available from the reinforcement. However, the method of installation had a more significant effect on axial force as this influenced the reinforcement surface properties. The greatest benefit from the reinforcement was obtained if it was installed before mobilisation of the peak strength of the soil.

9.4 Suggestions For Future Research

In all of the reinforced tests described the reinforcement axial force was very low. The multi-criteria analysis should be investigated further by increasing the magnitude of the reinforcement axial force. The multi-criteria analysis should also be investigated for a larger range of soils.

Problems exist in predicting the limiting pullout capacity of bars in sand owing to uncertainty about the radial stress around the reinforcement; both empirical studies with common soil parameters and high quality pullout tests from calibration chambers are required.

Further investigations should be made into soil dowelling. Particular aspects to be researched are the effect of different soil properties either side of the failure surface, the limiting lateral soil stress against the dowel, the effect of several rows of dowels and linking them at the surface. The model for estimating the limiting reinforcement shear force should be extrapolated to the problem of the lateral resistance of piles and the effect of a compressive load in the pile should be introduced.

REFERENCES

Airey, D.W. (1987). *Some observations on the interpretation of shearbox test results.* Internal report CUED/D - SOILS/TR 196, University of Cambridge.

Baguelin, F., Jezequel, J.F. and Shields, D.H. (1978). *The Pressuremeter and Foundation Engineering*, Transtech Publications, Switzerland.

Beech, J. and Juran, I. (1984). *Analyse theorique du comportement d'un soutenement en sol cloue.*, Proc. Symposium In-situ Soil and Rock Reinforcement, Press ENPC, Paris.

Beer, F.P. and Johnston, E.R. (1981). *Mechanics of Materials*, McGraw Hill, New York.

Bolton, M.D. (1986). *The strength and dilatancy of sands.* Géotechnique, Vol.36, N°.1, pp65-78.

Bolton, M.D. (1987). Discussion of *The strength and dilatancy of sands.* (Géotechnique, Vol.36, N°.1, pp65-78), Géotechnique, Vol.36, N°.2, pp219-226.

Bolton, M.D. and Pang, P.L.R. (1982). *Collapse limit states of reinforced earth retaining walls.* Géotechnique, Vol.32, N°.4, pp349-367.

Bridle, R.J. (1989). *Soil nailing - analysis and design.* Ground Engineering, September, pp52-56.

Brinch Hansen, J. (1961). *The ultimate resistance of rigid piles against transversal forces*, Danish Geotechnical Institute, Bulletin N°.12, Copenhagen.

Brinch Hansen, J. and Lundgren, H. (1960). *Hautprobleme der Bodenmechanik*, Springer-Verlag, Berlin.

Broms, B.B. (1964a). *Lateral resistance of piles in cohesive soils*, J. Soil Mechanics & Foundations Division ASCE, Vol.90, N°.SM2, pp27-63.

Broms, B.B. (1964b). *Lateral resistance of piles in cohesionless soils*, J. Soil Mechanics & Foundations Division ASCE, Vol.90, N°.SM3, pp123-155.

Bruce and Jewell (1986/7). *Soil Nailing: Application and Practice.* Ground Engineering (Part 1 - November 1986, pp10-15. Part 2 - January 1987, pp21-38).

BS1377 (1975). *Methods of test for soils for Civil Engineering purposes.* British Standards Institute, London.

BS5950 (1985). *Structural Use of Steelwork in Buildings.* Part 4, British Standards Institute, London.

BS8110 (1985). *Structural Use of Concrete*, British Standards Institute, London.

Calladine, C.R. (1985). *Plasticity for Engineers*, Ellis Horwood.

Cartier, G. (1986). *La stabilisation des pentes instables par clouage.* Bulletin de Liaison LCPC, N°.141, pp45-56.

Cartier, G., Delmas, P., Gestin, F. and Morbois, A. (1984). *Renforcement de talus de remblais instables par clouage.* Proc. Conf. In-situ Soil and Rock Reinforcement, Paris, pp237-242.

Cartier, G. and Gigan, J.P. (1983) *Experiments and observations on soil nailing structures.* Proc. 8th European Conf. Soil Mech. & Found. Eng., Helsinki, Vol.2, pp473-476.

Cole, E.R. (1967). *The behaviour of soils in the simple shear apparatus.* PhD. Thesis, University of Cambridge.

De Josselin de Jong, G. (1976). *Rowe's stress-dilatancy relation based on friction.* Géotechnique, Vol.26, N°.3, pp527-534.

Delmas, P., Berche, J.C., Cartier, G. and Abdelhedi, A. (1986). *Une nouvelle methode de dimensionnement du clouage des pentes: programme PROSPER.* Bulletin de Liaison LCPC, N°.141, pp57-66.

Dyer, M.R. (1985). *Observation of the stress distribution in crushed glass with applications to soil reinforcement.* DPhil. thesis, University of Oxford.

Francis, A.J. (1964). *Analysis of pile groups with flexural resistance*, J. Soil Mechanics & Foundations Division ASCE, Vol.90, N°.SM3, pp1-32.

Gassler, G. (1987). *Vernagelte Gelandesprunge-Tragverhalten und Standsicherheit.* PhD thesis, University of Karlsruhe.

Gassler, G. (1990). *In-situ techniques of reinforced soil.* Proc. International Reinforced Soil Conference, Glasgow.

Gassler, G. and Gudehus, G. (1981). *Soil nailing - some aspects of a new technique.* Proc. 10th Int. Conf. Soil Mech. & Found. Eng., Stockholm, Vol.3, pp665-670.

Gigan, J.P. and Delmas P. (1987). *Mobilisation des efforts dans les ouvrages cloues.* Bulletin de Liaison LCPC, N°.147, pp49-58.

Gudehus, G. and Schwarz, W. (1985). *Stabilisation of creeping slopes by dowels.* Proc. 11th Int. Conf. Soil Mech. & Found. Eng., San Fransisco, Vol.3, pp1697-1700.

Haussmann, M.R. and Lee, L.L. (1978). *Rigid model wall with soil reinforcement.* Symposium on Earth Reinforcement, Pittsburgh, pp400-427.

Hetenyi, M. (1946). *Beams on Elastic Foundations.* Ann Arbor, University of Michigan Press.

Hill, R. (1950). *The Mathematical Theory of Plasticity.* Oxford University Press, London.

Institut fur Bautechnik (1986). *Bodenvernagelung System Bauer.* Zulassungs-Nr.Z20.1-101, Berlin.

Ito, T. and Matsui, T. (1975). *Method to estimate lateral force acting on stabilising piles.* Soils and Foundations, Vol.15, N°.4, pp43-59.

Jaky, J. (1944). *The coefficient of earth pressure at rest.*, Journal of the Society of Hungarian Architects and Engineers, pp355-358.

Jewell, R.A. (1980). *Some effects of reinforcement on the mechanical behaviour of soils* PhD. Thesis, University of Cambridge.

Jewell, R.A. (1989). *Direct shear tests in sand.* Géotechnique, Vol.39, N°.2, pp309-322.

Jewell, R.A. (1990). *Soil Nailing - General Report,* Proc. International Reinforced Soil Conference, Glasgow.

Jewell, R.A., Milligan, G.W.E., Sarsby, R.W. and Dubois, D. (1984). *Interaction between soil and geogrids,* Proc. Symposium Polymer Grid Reinforcement, Thomas Telford Ltd., London.

Jewell, R.A. and Pedley, M.J. (1990a). *Soil nailing design - The role of bending stiffness,* Ground Engineering, March, pp30-36.

Jewell, R.A. and Pedley, M.J. (1990b). *Analysis for soil reinforcement with bending stiffness,* Internal Report OUEL 1821/90, University of Oxford. (Submitted to J. Soil Mechanics & Foundations Division ASCE for publication)

Jewell, R.A. and Wroth, C.P. (1987). *Direct shear tests on reinforced sands.* Géotechnique, Vol.37, N°.1, pp53-68.

Jones, C.J.F.P. (1985). *Earth Reinforcement and Soil Structures.* Butterworths, London.

Juran, I., Baudrand,G., Farag, K. and Elias, V. (1988). *Kinematical limit analysis approach for the design of nailed soil retaining structures.* Proc. International Symposium on Theory and Practice of Earth Reinforcement, Fukuoka, Japan. pp301-306.

Juran, I., Schlosser, F., Louis, C., Kernoa, M. and Eckmann, B. (1981). *Le renforcement des sols par barres passives.* Proc 10th Int Conf Soil Mech and Found Engng, Stockholm, pp713-716.

Kakurai, M. and Hori, J. (1990). *Soil-reinforcement with steel bars on a cut slope.* Proc. International Reinforced Soil Conference, Glasgow.

Kishida, H. and Uesugi, M. (1987). *Tests on the interface between sand and steel in the simple shear apparatus.* Géotechnique, Vol.37, N°.1, pp45-52.

Kolbuszewki, J.J. (1965). *Sand particles and their density.* Symposium on Densification of Particulate Materials, Materials Science Club, London.

Long, N.T., Legeay, G. and Madani, C. (1983). *Soil-reinforcement friction in a triaxial test.* Proc. 8th European Conf. Soil Mech. & Found. Eng., Helsinki, Vol.1, pp381-384.

Louis, C. (1984). *New method of sinking/grouting ground anchors.* French Patent 84 02742.

Marchal, J. (1984). *Renforcement des sols par clouage - Etude experimentale en laboratoire.* Proc Int Conf on in-situ soil and rock reinforcement, Paris, pp275-278

Marchal, J. (1986). *Clouage des sols - Etude experimentale en laboratoire de l'interaction sol-clou.* Bulletin de liaison des LCPC, N°.143, pp41-49.

McGown, A., Andrawes, K.Z. and Al Hassani, M.M. (1978) *The effect of inclusion properties on the behaviour of sand.* Géotechnique, Vol.28, N°.3., pp327-346.

Menard, L. (1975). *The interpretation of pressuremeter test results,* Sols-soils, No.26.

Mitchell, J.K. and Villet, W.C.B. (1987). *Reinforcement of earth slopes and embankments.* NCHRP Report 290, USA Transportation Research Board, National Research Council, Washington D.C.

Moutaouakkil, L. and Niang, E.M. (1985). *Renforcement d'un sol par clouage - etude experimental en laboratoire,* Travail fin d'etudes, Ecole Nationale des Travaux Publics de l'Etat, Lyon.

Neal, B.G. (1961). *The effect of shear and normal forces on the fully plastic moment of a beam of rectangular cross section,* Journal of Applied Mechanics, Transaction of the A.S.M.E., Vol.28, pp269-274.

Neville, A.M. (1973). *Properties of Concrete,* 2nd Edition, Pitman Publishing, London.

Nyirenda, Z.M. (1990). *The piezocone in lightly overconsolidated clay,* D.Phil Thesis, University of Oxford.

Palmeira, E.M.(1987). *The study of soil-reinforcement interaction by means of large scale laboratory tests* D.Phil Thesis, University of Oxford.

Palmeira, E.M. and Milligan, G.W.E. (1989). *Scale and other factors influencing the results of pullout tests of grids buried in sand*, Géotechnique, Vol.39., No.3., pp511-524.

Pfister, P., Evers, G., Guillaud, M. and Davidson, R. (1982). *Permanent ground anchors: Soletanche design criteria*, Report No. RD-81/150, Federal Highway Administration, Washington.

Plumelle, C., Schlosser, F., Delage, P. and Knochenmus, G. (1990). *French national research project on soil nailing: Clouterre*. Proc. ASCE Conference Design and Performance of Earth Retaining Structures, ASCE Geotechnical Special Publication N°.25, pp660-675.

Potts, D.M., Dounias, G.T. and Vaughan, P.R. (1987). *Finite element analysis of the direct shearbox test*. Géotechnique, Vol.37, N°.1, pp11-23.

Potyondi, J.G. (1961). *Skin friction between various soils and construction materials*, Géotechnique, Vol.11, pp339-353.

Poulos, H.G. and Davis, R.A. (1980). *Pile Foundation Analysis and Design.*, John Wiley.

Quinnet and Thonnard (1984). *Renforcement d'un sol par clouage - etude experimental en laboratoire*, Travail fin d'etudes, Ecole Nationale des Travaux Publics de l'Etat, Lyon.

Rabejac, S. and Toudic, P. (1974). *Construction d'un mur de soutenement entre Versailles-Chantiers et Versailles-Matelots*. Revue Generale des Chemins de Fers, 93eme Annee, April, pp399-413.

Randolph, M.F. and Houlsby, G.T. (1984). *The limiting pressure on a circular pile loaded laterally in cohesive soil*, Géotechnique, Vol.34, N°.4, pp613-624.

Roscoe, K.H. (1970). *The influence of strains in soil mechanics*. Géotechnique, Vol.20, N°.2, pp129-170.

Rowe, P.W. (1962). *The stress-dilatancy relation for static equilibrium of an assembly of particles in contact.* Proc. R. Soc. 269A, pp500-527.

Rowe, P.W. (1969). *The relation between shear strength of sands in triaxial compression, plane strain and direct shear.* Géotechnique, Vol.19, N°.1, pp75-86.

Schlosser, F. (1982). *Behaviour and design of soil nailing,* Proc. Symposium Recent Developments in Ground Improvement Techniques, Bangkok, pp399-413.

Schlosser, F. (1983). *Analogies et diferences dans le comportement et le calcul des ouvrages de soutenement en terre armee et par clouage du sol,* Sols et Fondations, N°.418, pp8-23.

Schlosser, F. and Guilloux, A. (1981). *Le frottement dans le renforcement des sols,* Revue Francaise de Geotechnique, N°16, pp65-77.

Shaffiée, S. (1986). *Simulation numerique du comportement des sols cloues; interaction sol-renforcement et comportement de l'ouvrage,* PhD. Thesis, Ecole Nationale des Ponts et Chaussees.

Shen, C.K., Herrmann, L.R., Romstad, K.M., Bang, S., Kim, Y.S. and Denatale, J.S. (1981). *In-situ earth reinforcement lateral support system.* Report 81-03, Dept. of Civil Engineering, University of California, Davis.

Simons, N.E. and Menzies, B.K. (1977). *A Short Course in Foundation Engineering,* Butterworths.

Sommer, H. (1979). *Stabilisation of a creeping slope in clay with stiff elements.* Proc. 7th European Conf. Soil Mech. & Found. Eng., Brighton, Vol.3, pp269-274.

Stocker, M.F. and Reidinger, G. (1990). *The bearing behaviour of nailed retaining structures.* Proc. ASCE Conference Design and Performance of Earth Retaining Structures, ASCE Geotechnical Special Publication N°.25, pp676-91.

Stroud, M.A. (1971). *The behaviour of sand at low stress levels in the simple shear apparatus.* PhD thesis, University of Cambridge.

Tatsuoka, F. (1987). Discussion of *The strength and dilatancy of sands*. (Géotechnique, Vol.36, N°.1, pp65-78), Géotechnique, Vol.36, N°.2, pp219-226.

Taylor, D.W. (1948). *Fundamentals of Soil Mechanics*. Wiley, New York.

Terzaghi, K. (1955). *Evaluation of coefficients of subgrade reaction*, Géotechnique, Vol.5., pp297-326.

Todd, J.D. (1981). *Structural Theory and Analysis*, 2nd Edition, Macmillan Publishers Ltd.

Tomlinson, M.J. (1986). *Foundation Design and Construction*, 5th Edition, Longman Scientific and Technical.

Vesic, A.S. (1961). *Bending of beams resting on isotropic elastic solid*, J. of the Engineering Mechanics Division ASCE, Vol.87, N°.EM2, pp35-53.

Vesic, A.S. (1973). *Analysis of ultimate loads of shallow foundations*, J. Soil Mechanics & Foundations Division ASCE, Vol.99, N°.SM1, pp45-73.

Vidal, H. (1969). *La Terra Armée*. Annales de l'Institut Technique du Batiment et des Travaux Publics, Series Materials (38) N°.259-260.

Wang, W.L. and Yen, B.C. (1974). *Soil arching in slopes*. J. Soil Mechanics & Foundations Division ASCE, Vol.100, N°.GT1, pp61-78.

Winkler, E. (1867). *Die lehre von elastizitat un festigkeit*, Prague, pp182.

Winter, H., Schwarz, W. and Gudehus, G. (1983). *Stabilisation of clay slopes by piles*. Proc. 8th European Conf. Soil Mech. & Found. Eng., Helsinki, Vol.2, pp545-550.

Yu, H.S. (1990). *Personal communication*, University of Oxford.